INFORMATION TO USERS

This manuscript has been reproduced from the microfilm master. UMI films the text directly from the original or copy submitted. Thus, some thesis and dissertation copies are in typewriter face, while others may be from any type of computer printer.

The quality of this reproduction is dependent upon the quality of the copy submitted. Broken or indistinct print, colored or poor quality illustrations and photographs, print bleedthrough, substandard margins, and improper alignment can adversely affect reproduction.

In the unlikely event that the author did not send UMI a complete manuscript and there are missing pages, these will be noted. Also, if unauthorized copyright material had to be removed, a note will indicate the deletion.

Oversize materials (e.g., maps, drawings, charts) are reproduced by sectioning the original, beginning at the upper left-hand corner and continuing from left to right in equal sections with small overlaps.

Photographs included in the original manuscript have been reproduced xerographically in this copy. Higher quality 6" x 9" black and white photographic prints are available for any photographs or illustrations appearing in this copy for an additional charge. Contact UMI directly to order.

Bell & Howell Information and Learning
300 North Zeeb Road, Ann Arbor, MI 48106-1346 USA
800-521-0600

A STUDY OF A VARIABLE SPEED 3-IN KNELSON CONCENTRATOR

Jinghong Ling

A thesis submitted to the Faculty of Graduate Studies and research in partial fulfilment of the requirements of the Degree of Philosophy

Department of Mining and Metallurgical Engineering

McGill University, Montréal

ABSTRACT

The distribution of fluidization flow of a variable speed 3-in (7.5 cm) Knelson centrifugal concentrator was first studied. Its performance was then investigated for different types of synthetic ores, and the effect of rotation speed, fluidizing water, gangue density and size distribution, and feed rate determined. To obtain some fundamental information relative to the recovery mechanisms of the Knelson Concentrator, the percolation or migration of dense particles in a gangue bed was investigated in the gravitational field, using a fluidization column. The equations for determining the instantaneous radial settling velocity of a spherical particle in the dilute zone of the inner bowl were derived for the Stokes' Law region.

Recovery of tungsten from magnetite and silica gangues and recovery of magnetite from silica gangue were studied. Results indicate that rotating speed of the Knelson Concentrator affected both the movement of mineral particles and fluidization of the separation zone, which in turn affected KC performance. For all types of feeds studied, the fluidizing water flow rate needed to achieve a maximum recovery increased with increasing rotating speed. The study of capture kinetics showed that tungsten recovery from silica decreased gradually and almost linearly as the feed rate increased from 0.5 to 5 kg/min; this decrease became smaller with increasing Gs. However, the recovery drop (or the corresponding capture rate constant) was small for coarse (>106 μm) tungsten and moderate for fine (<106 μm) tungsten, suggesting that for typical

applications of gold recovery from the circulating load of a grinding circuit, feed rate should be maximized. Further, accelerations of 30 to 60 Gs were adequate for very good recovery of tungsten above 25 μm. The recovery of magnetite from a -425 μm silica gangue was limited to a d_{50c} of 40 μm. Rotation velocity had little impact on how fine magnetite could be recovered, especially above the velocity corresponding to 60 Gs.

At 1 Gs (i.e. in the gravitational field), an optimum fluidization flow was also observed for all systems studied. High density gangue, especially when coarse, had a detrimental effect on percolation and migration. Particles of high density percolated or migrated faster than those of lower density. When the gangue bed was well fluidized, the migration rate of coarse particles was higher than the percolation rate of fines. These observations are basically consistent with the effect of fluidization water, gangue size distribution and density on Knelson performance.

RÉSUMÉ

Nous avons d'abord étudié l'effet de la vitesse de rotation d'un concentrateur Knelson de 3 pouces sur la distribution de l'eau de fluidification. La performance du Knelson en fonction de sa vitesse de rotation, du débit d'eau de fluidification et du taux d'alimentation a par la suite été étudiée à l'aide de minerais synthétiques de densité et granulométrie différentes. Pour comprendre les mécanismes de récupération, nous avons étudié l'infiltration et la migration des particules denses dans un lit de gangue contenu dans une colonne fluidifiée. Nous avons également dérivé les équations décrivant la sédimentation radiale de particules sphériques dans la zone diluée du rotor interne du Knelson, dans le régime de Stokes.

La récupération de particules de tungstène de gangues de magnétite et silice et de magnétite de gangue de silice a été étudiée. La vitesse de rotation du concentrateur Knelson a un impact et sur le niveau de fluidification de la zone où s'effectue la séparation, et sur la vitesse de sédimentation des particules denses; la récupération de celles-ci dépend de l'interaction des ces deux phénomènes. De façon générale, la récupération maximale est obtenue à débit de fluidification intermédiaire, qui augmente lorsque la vitesse de rotation augmente. La récupération des particules de tungstène diminue lorsque le taux d'alimentation augmente de 0,5 à 5 kg/min; cette baisse de récupération diminue lorsqu'on augmente la vitesse de rotation du Knelson. Cette diminution est limitée aux particules de tungstène inférieure à 105 μm, et même pour

ces particules plus fines, elle est moins prononcée que l'augmentation du taux d'alimentation, ce qui permet de conclure qu'un Knelson utilisé au sein d'un circuit de broyage devrait être alimenté à taux maximum. Généralement, une vitesse de rotation donnant des accélérations de 30 à 60 Gs est suffisante pour très bien récupérer du tungstène de taille supérieure à 25 μm. De plus, la récupération de la magnétite d'une gangue de silice plus fine que 300 μm est généralement limitée aux particules de taille supérieure à 40 μm (D_{50}); augmenter la vitesse de rotation du Knelson n'a que très peu d'effet sur la récupération de particules plus fines, surtout au-dessus d'une vitesse de rotation correspondant à une accélération de 60 Gs.

Le travail en colonne fluidifiée a également identifié un débit de fluidification optimum qui varie selon la granulométrie et densité de la gangue et de la phase dense. La vitesse de percolation des particules denses diminue de façon très marquée si la densité de la gangue augmente, surtout si celle-ci est grossière. Les particules de densité élevée s'infiltrent plus rapidement que celles de densité plus faible. Lorsque le lit de gangue est bien fluidifié, le taux de percolation des particules denses grossières est plus élevé que celui des fines. Ces observations sont en bon accord avec l'effet du débit d'eau de fluidification et du type de particules denses et de gangue sur le fonctionnement du concentrateur Knelson de 3 pouces.

ACKNOWLEDGEMENTS

I offer my sincerest thanks to my supervisor, Professor and Dr. André R. Laplante, whose high scientific standards never failed to bring out the best in me and my research. Indeed, I can never thank him enough for all the kindness and concern which he has generously offered me during my stay at McGill University. I am very grateful to Professor J.A. Finch for his constructive advice for my fundamental study on the percolation and migration of dense particles in the gravitational field. Special thanks also goes to Professor M. E. Weber for his invaluable critical advice and comments on my theoretical study of centrifugal separation. I want to thank Dr. L. Huang gratefully for insightful discussions and productive help. A special thank is owed to Mr. R. Langlois for his effective help in setting up the Knelson Concentrator and his supply of essential experimental equipment for the research. Useful discussions and kindly help was also received from my colleague Mr. A. Farzanegan, a Ph.D. candidate. Finally, but most importantly, I wish to thank my wife Meilian Li, and my son, Guozhi, for their gifts of time, patience, understanding, support, and love, which allowed me to complete this dissertation.

This project has been made possible only through the financial support of the Natural Science and Engineering Research Council of Canada (NSERC) and other relative contributors, to whom I should like to express my great appreciation.

TABLE OF CONTENTS

NOMENCLATURE

a_n	constant coefficient (the subscript n can be any number.)
b_n	constant coefficient
C_n	constant coefficient
C_D	drag coefficient of a solid particle
C_L	dynamic coefficient of friction
conc.	concentrate
C_P	total coefficient (in Equation 3.33)
d	distance between the centres of two particles
d_b	average diameter of bulk particles
d_i	characteristic size of particle size class
d_p	diameter of a moving solid particle
d'	maximum size of a particle that can pass between a certain voidage (in Equation 2.5)
d_{50c}	corrected cut size
D_{80}	80% mass passing aperture
f	collision frequency of a particle in the separation zone, 1/second
f_b, $\vec{f}_b$	buoyancy force in the gravitational field
F_b, $\vec{F}_b$	buoyancy force in a centrifugal field
F_c, $\vec{F}_c$	centrifugal force
F_d, $\vec{F}_d$	drag force

F_{dx}, $\vec{F}_{dx}$	X-component of drag force
F_{dy}, $\vec{F}_{dy}$	Y-component of drag force
F_{dz}, $\vec{F}_{dz}$	Z-component of drag force
f_g, $\vec{f}_g$	gravity force
F_L, $\vec{F}_L$	dynamic friction force
F_{Lx}, $\vec{F}_{Lx}$	X-component of dynamic friction force
F_{Lz}, $\vec{F}_{Lz}$	Z-component of dynamic friction force
g, $\vec{g}$	gravitational acceleration, 981 cm/s^2 or 9.8 m/s^2
Gs	ratio of centrifugal to gravitational accelerations
GRG	gravity recoverable gold
H	height of the inner bowl
h	Z-component of displacement $\vec{r}$
h'	Z'-component of displacement $\vec{r}$
h_1	h when t = 0
h'_1	h' when t = 0
i	the number of a ring (in Equation 8.4)
$\vec{i}$	unit vector in X-direction
$\vec{j}$	unit vector in Y-direction
$\vec{k}$	unit vector in Z-direction
k	constant coefficient (in Equation 2.1)
K'	rate constant (in Equation 8.3)
K	dimensionless rate constant (in Equation 8.4)

KC	Knelson Concentrator
k_n	constant coefficients
k_p	dimensionless correction factor (in Equation 3.32)
k_r	constant, min/kg (in Equation 8.1)
LKC	laboratory Knelson Concentrator
m	mass of a solid particle
m	sharpness of separation coefficient
M'	total mass of an accelerating particle
MLS	Mozley laboratory separator
M_h	hydrodynamic mass (or added mass) of an accelerating particle
n	subscript number
n_d	rotating speed of the drive motor, rpm (in Equation 5.1)
n_v	number of bulk particles per unit volume
p_i	mass fraction of particles of a given size and density which will be directed to the concentrate as a result of the classifying action
Q	fluid flow rate, L/min or ml/s
q_1	constant coefficient (in Equation 3.19)
Q_s	feed rate, kg/min (in Equation 8.1)
$\vec{r}$	displacement of a solid particle from a point of rotation axis
r	X-component of displacement $\vec{r}$
r_1	X-component of displacement $\vec{r}$ when t = 0, or inside radius of rotating tube (in Equation 2.1)

r_d	radius of the motor pulley, cm
r_i	fraction of particle i in the concentrator feed which reports to the concentrate by short circuit (Equation 7.2)
R_1	radius of the air cone at the bottom ring with water fluidization, cm (in Equation 5.6)
R_5	radius of the air cone at the top ring with water fluidization, cm (in Equation 5.6)
R	fractional recovery (in Equation 8.2)
Re	fluid Reynolds number
Re_p	particle Reynolds number
R_o	radius of the outer bowl, cm
R_t	radius of the inner surface of the top rib, cm (in Equation 5.1)
R_w	tungsten recovery, % (in Equation 8.1)
SEM	scanning electron microscope
STD	standard deviation
t	time, second
t_b	time for a particle to move up from the bottom to the top of the inner bowl (in Equation 3.26), second
u_0	terminal velocity of particle (in Equation 2.4)
U_F	superficial fluid velocity of fluidization (flowrate divided by lateral area of the rings of inner bowl), cm/s
u_f, $\bar{u}_f$	fluid velocity, cm/s

u_{fx}, $\bar{u}_{fx}$	X-component of fluid velocity $\bar{u}_f$
u_{fy}, $\bar{u}_{fy}$	Y-component of fluid velocity $\bar{u}_f$
u_{fz}, $\bar{u}_{fz}$	Y-component of fluid velocity $\bar{u}_f$
$\bar{u}$	average fluid velocity, cm/s (in Equation 5.5)
u_i	interstitial velocity of fluidization flow (superficial velocity of fluidization/voidage of the separation zone), cm/s
U_{max}	optimum fluidization velocity, cm/s (in Equation 7.1)
U_{mf}	minimum fluidization velocity, cm/s
u_p, $\bar{u}_p$	particle velocity, cm/s
u_{px}, $\bar{u}_{px}$	X-component of particle velocity $\bar{u}_p$
u_{py}, $\bar{u}_{py}$	Y-component of particle velocity $\bar{u}_p$
u_{pz}, $\bar{u}_{pz}$	Y-component of particle velocity $\bar{u}_p$
u_r, $\bar{u}_r$	relative velocity of fluid to a particle, cm/s
u_{rx}, $\bar{u}_{rx}$	X-component of relative velocity $\bar{u}_r$
u_{ry}, $\bar{u}_{ry}$	Y-component of relative velocity $\bar{u}_r$
u_{rz}, $\bar{u}_{rz}$	Y-component of relative velocity $\bar{u}_r$
v	particle velocity (in Equation 2.1)
V	volumetric holdup of fluid flow in the inner bowl (in Equation 5.3)
V_0	volume of the air cone of the inner bowl without water, 57.43 cm^3
V_b	volume of a particle bed
V_l	volume of the bed not occupied by solid material
V_s	volume of solid material

v_{max}	terminal velocity of particle in Equation 2.2
V_T	volume of separation zone

Greek Letters

α	angle between Z- and Z'-directions, radian
δ	thickness of the flowing film, cm (in Equation 5.2)
ϵ	fractional voidage
ρ	fluid density, g/cm^3
ρ_s	density of a moving solid particle, g/cm^3
μ	fluid viscosity, g/(cm.s)
τ	retention time of the flowing film in the inner bowl
ψ	non-spherical coefficient of particle (in Equation 2.1)
ω	angular speed of inner bowl, radian

LIST OF FIGURES

LIST OF TABLES

CHAPTER 1 INTRODUCTION

1.1 The Knelson Concentrator

The Knelson Concentrator (KC) is an innovative centrifugal separator which was patented by Byron Knelson in Canada in the early 1980's. It has since received industrial acceptance worldwide, and exhibited excellent performance for both gold vein and alluvial applications (Laplante et al, 1990; Knelson et al, 1990; Darnton et al, 1995; Poulter et al, 1994; Cloutt, 1995; Hart et al, 1995; Mesa et al, 1994; and Suttill, 1990). It combines the advantages of a simple structure, a high capacity, a wide size range of recoverability and the ability to yield very high enrichment ratios. It is used in over 70 countries and accounts for more than 1200 separate installations. A new generation of Knelson Concentrators, including the Centre Discharge model, have since been commercialized; a continuous prototype is also under developed (Laplante et al, 1997; Brewis, 1995).

Despite widespread acceptance, the Knelson Concentrator is still undergoing intensive research and development. So far, a number of research projects on its effective use have been carried out at McGill University. Efforts have focused on the characterization of ore types (Laplante, 1993; Laplante et al, 1997, 1995, Woodcock et al, 1993), the evaluation of plant performance (Laplante et al, 1994, and 1992; Putz et al, 1993; Zhang, 1998), and the study of concentration mechanisms with a laboratory

KC (Laplante et al, 1996a, 1996b, 1995, 1994, and 1992; Huang, 1996). Some attempt at modifying its bowl geometry have been made, and results, though inconclusive, have shed additional light on how the units works (Laplante at al, 1998).

The separation principle of the KC, for all models, is based on the difference in centrifugal forces exerted upon gold and gangue particles and on fluidization of the concentrate bed. The standard KC is designed as a roughing concentrator for gold ores, working at a constant rotating speed that generates an average centrifugal acceleration of 60 Gs.[1] Since the magnitude of centrifugal force applied on a particle depends on the rotating speed of the inner bowl of the KC, it is important to investigate thoroughly the effect of rotating speed. However, very little information on this subject has been published so far (Knelson, 1985), which means that the relationship between rotating speed and unit performance remains as yet unprobed. As some users of the KC are wondering, why does the KC have to work at 60 Gs? Could it be possible for the KC to work at 30 Gs so as to reduce power and water consumptions? Can the KC run at 120 Gs or even faster in order to increase its capacity and gold recovery, or recover other, lower density, minerals? Practical questions such as these are obviously related to the rotating speed of the KC. Answers are not trivial. Recovery is achieved when particles can radially move to the concentrate bed before being rejected with the tails

[1]60 Gs, or 588.6 m/s^2, is sixty times 9.81 m/s^2, the acceleration of falling objects in earth's gravitational field at sea level. It is both average and theoretical because (i) the rotating radius increases as the feed flows upwards from the bottom of the Knelson inner bowl, and (ii) it is assumed that the slurry has reached the same rotating velocity as the bowl itself.

stream. Particle radial movement can take place either by percolation or by migration after radial settling (to be defined in Section 3.4.1). Further, particles already recovered must not be rejected by concentrate bed erosion before the end of the recovery cycle. All these mechanisms are affected by fundamental operating variables such as feed rate, rotation velocity and fluidizing water flow rate, but in different ways. The responses are very dependent on particle size and density, and are also significantly affected by the size distribution and density of the gangue.

This project will attempt to develop a phenomenological understanding of how these variables interplay, using a variable speed centrifuge, in this case a 3" (7.5 cm) laboratory concentrator (LKC), a unit which has been extensively studied at its normal centrifugal acceleration of 60 Gs. The study was deemed worthwhile because it would lead to a better understanding of fundamentals relating to the recovery mechanisms of the KC, and it might provide useful information for the development and application of industrial centrifuge concentrators.

1.2 Objectives of the Study

In this research work, a series of experiments and necessary theoretical analysis of the fundamentals and performance of the variable speed centrifuge was conducted. The research work was designed to:

a. study the percolation behaviour of dense particles in a fluidized bed in the gravitational field, and investigate the effects of fluidizing water, gangue density and particle size on the percolation and migration process.

b. study the effect of rotating speed on the flow rate and pressure of fluidizing water.

c. investigate the effect of rotating speed on separation of dense particles from gangue.

d. investigate the interactions of fluidization water, gangue density, particle size distribution and feed grade on the performance of the variable speed KC at different rotating speeds.

e. study the effect of rotating speed and feed rate on ring-by-ring recovery of the KC.

f. explore mathematically the effect of centrifugal acceleration and water fluidization on particle settling velocity.

1.3 Structure of the Thesis

This thesis consists of nine chapters. Chapter 1, as seen above, introduces briefly the background, rationale and objectives of the research project and then outlines the structure of the thesis. Chapter 2 reviews the prior application and research on centrifugal concentrators, including the Knelson Concentrator, and on the fundamentals of this field. Chapter 3 deals with theoretical considerations, stressing the analysis of

the settling of dense particles under the influence of both centrifugal acceleration and water fluidization.

Chapter 4 describes the percolation behaviour of dense particles in a fluidized bed in the gravitational field on the basis of laboratory measurements, and discusses the implication of the micromodel of percolation in the study of the Knelson recovery mechanisms.

Chapter 5 shows first the experimental set-up for the variable speed centrifuge concentrator and then presents some characteristics of the unit which are essentially related to its operation, followed by a discussion on the effect of rotating speed on the fluidization flow rate.

Chapters 6 and 7 report on a series of gravity concentration tests on a number of synthetic ores with the Knelson. Chapter 6 mainly deals with separation of tungsten from silica and magnetite gangues, while Chapter 7 focuses on separation of magnetite from silica gangue. These three systems represent separations of increasing difficulty. Both chapters discuss the effect of acceleration on the optimum fluidization and the particle size distribution in the concentrates.

Chapter 8 demonstrates how feed rate affects the performance of the Knelson and how the mass and particle size of the concentrate are distributed in each ring of the inner

bowl. A 9-test program was conducted to determine tungsten recovery from silica at different retention time and rotating speed, and a set of rubber stoppers was used to extract concentrate from each individual ring.

In Chapter 9, conclusions based on the thesis experiments are drawn, and claims to original knowledge and suggestions for future work are also presented.

CHAPTER 2 LITERATURE REVIEW

2.1 History of Centrifuge Concentrators

The early centrifuge technology was described by LEONARDO DA VINCI (1452-1519) who suggested the idea of using centrifugal force for lifting liquids. The first centrifugal device known in the history of engineering was a centrifugal pump which had operated in a copper mine in Portugal in the fifth century (Lazarkiewicz, 1965). In the field of mineral processing engineering, centrifuge concentrators for gold recovery predate this century, as crude early versions were developed when the industrial revolution was spreading from Great Britain to the rest of Western countries.

The Hendy Concentrator was one of the earliest forms of centrifugal concentrators employed in California, patented in 1868 (Rose, 1898; Louis, 1894). It is shown in section and in plan in Figure 2-1 (Louis, 1894). It consisted of a shallow cast-iron pan, 1.2 m or 1.8 m (4 feet or 6 feet) in diameter, supported on a vertical shaft in the centre, and rotated by bevel gear. The pulp was fed into the pan near the periphery, and then, as a consequence of a rapid oscillating motion given by the revolution of a crank shaft, the heavy particles moved outwards by centrifugal force and accumulated in the peripheral gutter, while the lighter particles were discharged into the central circular basin and were removed by opening discharge gates at intervals. A somewhat similar machine was the Duncan Concentrator, which was made of wrought

iron instead of cast iron (Rose, 1898; Louis, 1894). The pan revolved at a speed of 8½ rpm, while the pulp was supposed to make about 3 revolutions in the pan. Both the Hendy and the Duncan Concentrators were used to a certain extent in California, and were capable of doing very fair work in the recovery of sulphides, except on fine slime (owing to their insufficient rotating speed). These two types of crude centrifugal concentrator were later replaced to a great extent by conventional gravity devices of some form or other.

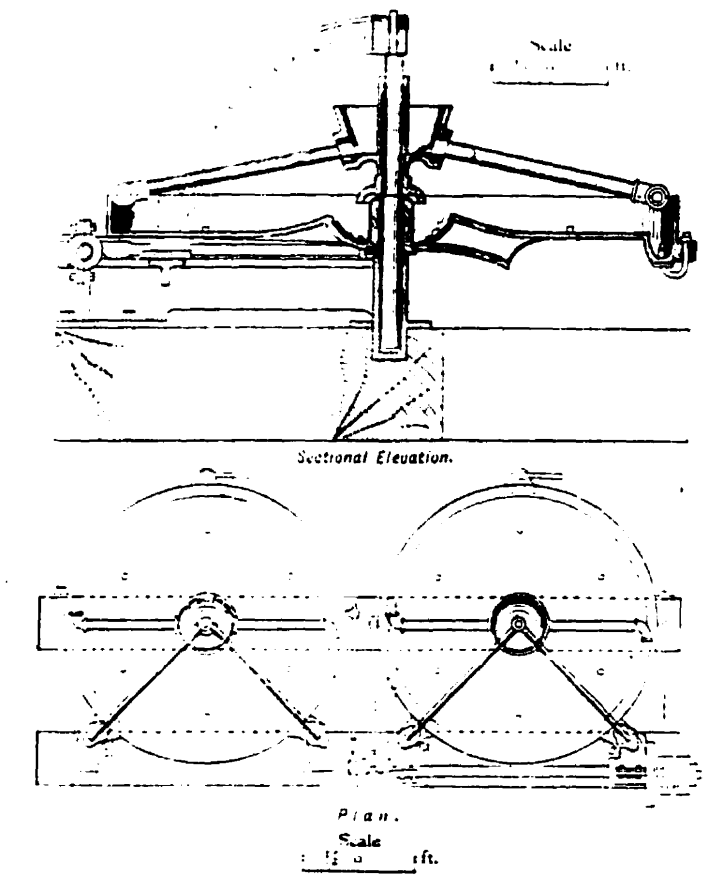

Figure 2-1 Hendy Concentrator (after Louis, 1894)

It should be mentioned that the principle of centrifugal concentration was also employed in the early pan amalgamation in America and Australia. The Baux and Guiod Amalgamator (Phillips, 1867) might be a typical example. This machine, which is shown in Figure 2-2, was occasionally used for the extraction of gold from tailings. As described briefly by Phillips (1867), water and ores were introduced at the bottom of the pan, through a hopper bolted on its side (at A). The substances being ground were thrown by centrifugal action upon a bed of mercury lying in a groove around the internal circumference, whilst the tailings was discharged from the centre of the lid to the spout B.

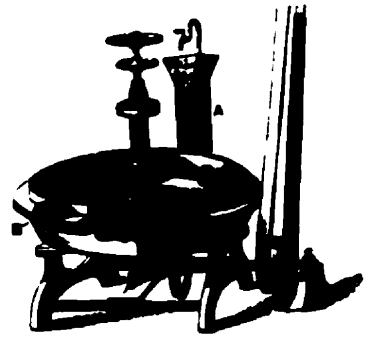

Figure 2-2 Baux and Guiod's Amalgamator (Phillips, 1867)

Perhaps the Ainlay bowl (Taggart, 1945), which had been used to a limited extent on doodlebugs and small placers operations in the years prior to 1945, was an embryonic form of some contemporary advanced centrifugal concentrators. This device

was a vertical bowl-shaped basin, 30 to 90 cm (12- to 36-in.) diameter at the rim, rubber-riffled on the inner surface. The peripheral speed at the bowl rim could be up to about 300 m (1000 feet) per minute. The slurry was fed into the bowl and moved around upward toward the bowl periphery under the influence of centrifugal force; gold was caught between the riffles, and the overlying lighter sand passed on upward and over the rim. The gold concentrate was washed out of the bowl at intervals by shutting off feed. It was claimed that capacities were 0.38 to 1.15 m^3 of <5 mesh gravel per hour for the 30 cm bowl and 3.8 to 7.6 m^3 of <9 mm material per hour for the 90 cm unit.

In addition, the following types of centrifuges, which have been tried or designed, may be recognized as a contribution to the evolution of centrifugal concentrators.

In the period of 1910-1912, the Peck Centrifugal Separator was tried at Anaconda, Montana, U.S.A., producing a commercial concentrates (Truscott, 1923). This device consisted of two pans, which were rotated independently in the same direction. The pulp passed through the bottom of the inner and smaller pan into the space between the two pans. The heavy mineral particles could then form a bed upon the inner wall of the outer pan, which would be removed after each concentration cycle, while the gangue was rejected to the overflow through appropriate nozzles around the lip.

In 1913-1914, the Laist Centrifugal Separator was tried at Anaconda as a continuous separator of granular slime from colloidal material and excess water (Truscott, 1923). This machine consisted of a number of radial chambers which were used to collect the settled material during rotation. The design of this centrifuge boosted some of the features of the prototypes of the nozzle-bowl and the ejecting disc centrifuges (Loggio et al, 1994) for solid-liquid separation of today.

In 1912, the Trent Centrifugal Separator worked to separate mineral particles from gangue or separate solids from water (Truscott, 1923). Its structure appears complex because of the embodying of a number of features such as the feeding by a centrifugal pump and the discharging by a narrow aperture.

In 1935, Mr. MacNicol patented a centrifuge of novel construction in Australia, which is supposed to resemble to some modern centrifuges, including the KC (Napier-Munn, 1997). For example, the rotating bowl was equipped with grooves, and fluidization water was added at their bottoms. Unfortunately, this device was not adopted by the mining industry. An obstacle in its commercialization was the lack of necessary wear-resistant materials for the bowl and moving parts.

2.2 Recent and Contemporary Development and Application of Centrifugal Concentrators

2.2.1 Introduction

With the rapid development of technology and science, many new centrifugal concentrators have come into being, either in the stage of development or in full commercialization. The advent of new materials and electric and electronic technology has made possible centrifugal concentrators with features such as high centrifugal acceleration and capacity, acceptable wear rates, and high efficiency and automatic operation. As a result, centrifugal concentration has been increasingly used for the processing of various materials in particular ores, and instilled a renewed interest in this field. Basically, the centrifuges already used or potentially suitable for a variety of industrial applications may all be divided into two types: the mono-centrifuge and the multi-gravity concentrators. The former can be sub-divided into the ordinary centrifuge and the water-injection centrifuge. Among them, the Knelson Concentrator, one of the water-injection type, will be introduced in more detail latter on, since it is the focus of this research.

2.2.2 The mono-centrifugal concentrators

Mono-centrifugal concentrators may be defined as gravity concentrators that separate heavy material from lighter gangue mainly by the mechanism of centrifugal separation. They may be sub-divided, according to whether or not there is a back-

injection water system, into two types: the ordinary (single wall) centrifuges and the back-injection centrifuges.

The ordinary concentrator

The batch (B) or continuous (C) Falcon Concentrator is a vertical centrifuge consisting of a concentration rotor. The rotor is actually a cone plus cylinder-shaped bowl with a length equal to approximately twice its diameter. The processing (inner) surface is covered by a wall of wear-resistant material such as rubber and urethane. Figure 2-3 shows B6 Falcon Concentrator.

Feed material enters to the base of the high speed rotor mechanism in a slurry form through a central downcomer. The impeller at the very base of the rotor evenly

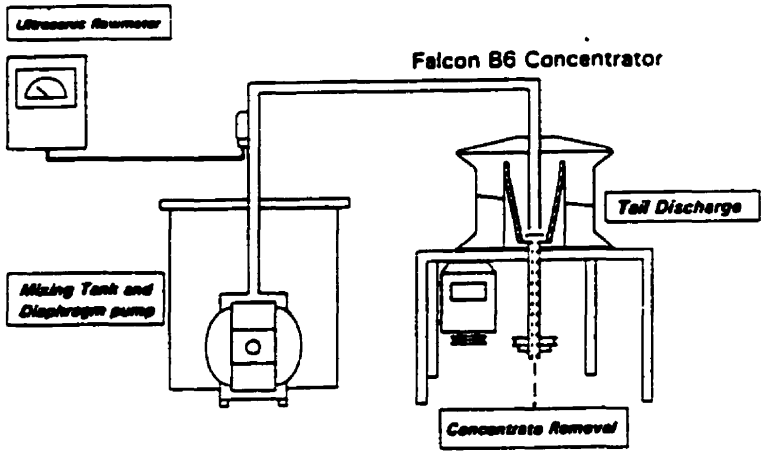

Figure 2-3 Experimental Set-up for the B6 Falcon Concentrator (Laplante et al, 1994)

distributes the slurry to the internal wall and provides an initial acceleration. Under the action of the centrifugal force, heavy particles settle down over a bed of material which has already accumulated closest to the wall at the very beginning of the feeding cycle, layering as a concentrate, and lighter particles are rejected out the rotor top with the water flow to report as tailings. The concentrate is discharged either at intervals or continuously depending upon the design of the rotor. Thus, as described by Falcon Concentrators Inc. (1997 a), the Falcon Model 'B' units rinse out periodically the concentrate through the hollow drive shaft at predetermined "batch" intervals; the 'Falcon Model 'C' units bleed the concentrate off at a controlled variable rate through a series of plane mass flow hoppers, pinch valves and discharge orifices. The rotating speed of both models can generate up to 300 Gs centrifugal field. The largest unit built to date, the model C40, is claimed to have a maximum solids capacity of 200 tons (180 tonnes) per hour for a feed particle size below 850 μm (20 mesh) (Falcon Concentrators Inc., 1997a). It is also claimed by the manufacturer that the Model 'B' units are suitable for fine feed applications requiring very low weight recoveries, such as fine free gold recovery and tailings scavenging, while the Model 'C' units are suitable for a wide range of minerals and fine feed applications requiring low to high weight recoveries, such as fine gold primary recovery, fine coal cleaning, and fine iron and tin recovery. However, applications of the Model 'B' units might be limited since barren gangue material pinned to the rotor at the beginning of the recovery cycle makes up most of the concentrate.

Laplante (1993) compared the performance of the Falcon concentrators with that of the Knelson concentrator and pointed out that the batch Falcon is typically effective for gold finer than 37 μm, for short recovery cycle. For the B6 Falcon, Laplante et al (1994) demonstrated that gold recovery from a fine gold-pyrite-silica flotation tail with characteristics of a low sulphide content and a fine size ranged from 30 to 70% at upgrading ratios of 5 to 15, but results with a massive sulphide ore were very poor due to the characteristics of high density feed, with gold recoveries typically around 10 to 20% at very low upgrading ratios. In a study conducted by Lins et al (1992), the results of pilot plant tests using the Falcon B6 and B12 to recover gold from a hydrocyclone overflow showed that gold recovery was between 24% and 44% at 15-30 minute operation cycles. This performance is reasonably fair since the results of amalgamation analysis suggested that only 25% of total gold in the feed was gravity recoverable. In processing ultrafine tantalum for bench scale testwork, the Falcon B unit was shown to be capable of recovering very fine tantalum and superior to the Knelson Concentrator and the Kelsey Jig, though its performance was not as good as that of the Mozley Multi Gravity Separator (Burt et al. 1995). A fundamental and practical study of the Falcon B unit was carried out by Buonvino (1993), who used a synthetic ore (5% magnetite, 95% silica) and two natural gold ores of different gangue densities (a massive gold-copper sulphide ore and a fine gold-pyrite-silica flotation tails) to investigate the relationship between the performance of the centrifuge and major operating parameters. The results of his study showed that the recovery of mid-size particles (53 to 150 μm) was poorer than that of finer size ($<$ 53 μm). Regarding the recovery mechanisms of

the Falcon B unit, he suggested that particles were captured into the concentrate bed in two different ways: either by burying of coarse particles in the bed (migration) or by lodging of finer particles in the interstices between the coarse particles (percolation).

Recent research work has shown the potential of the continuous Falcon for fine coal cleaning. Honaker et al (1996) conducted a series of cleaning tests of fine coal from the Illinois No. 5 seam, using a C10 Falcon as the principal separator and comparing its performance to that of a Knelson Concentrator, a MDL LD-9 spiral and a Pack-flotation Column. Their results showed that owing to its relatively high centrifugal acceleration (300 Gs) the C10 Falcon was the most effective in rejecting the coal pyrite and ash-bearing particles from a 210 x 37 μm size feed. For the feed below 37 μm, however, their results indicated that the ash rejection values achieved by the Falcon were not significant probably due to an insufficient centrifugal force. Besides the effect of particle size, Honaker et al (1995) also discovered that the performance of the Falcon Model 'C" was a function of bowl geometry, feed solids content and feed rate. Based on the testing above and various stages of successful pilot scale testing, Honaker et al have carried out an industrial scale testing using the C40 Falcon to clean fine coal streams (Falcon Concentrator Inc., 1997b). Over a one year period of full production good metallurgical results were confirmed.

The Yunxi Centrifuge originated in China and has become a popular gravity device in the Chinese mineral industry since its development in the early 1960's. Its

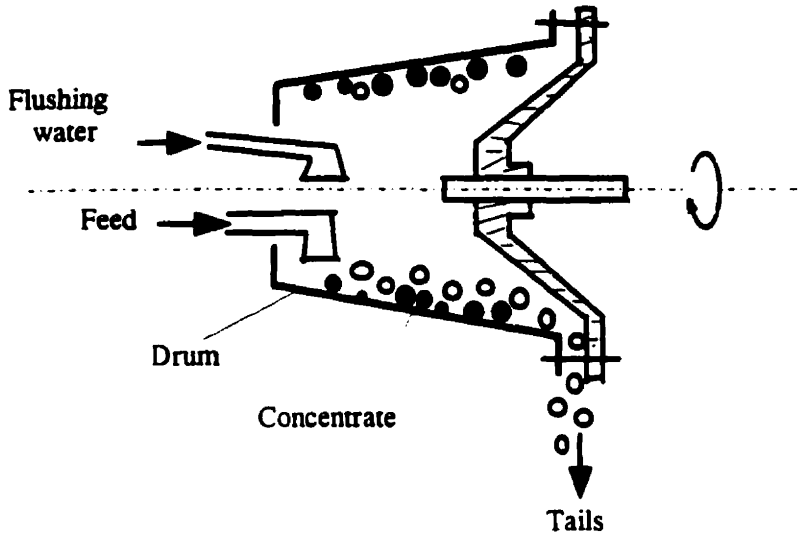

Figure 2-4 Schematic illustration of the Yunxi Centrifuge

principal concentration component is a rotating tapered drum which in most cases is horizontally aligned (Sun,1982), and may be vertically aligned for some models (Li et al, 1984). Figure 2-4 shows a simple schematic illustration of the horizontal Yunxi Centrifuge. The pulp is fed into the small end of the rotating drum by nozzles and the tailings is discharged from the large end of the drum. The concentrate is also discharged to the large end of the rotating drum by flushing water, once the feed is stopped or transferred to another centrifuge, at regular time intervals, as frequently as every 3 to 5 minutes. All operations, including feeding and discharging of the concentrate, are electronically controlled.

The size of the commercial Yunxi centrifuge is designated by both the diameter of the small end and the length of the drum. The centrifugal acceleration generated inside the drum can be varied from 20 to 172 Gs by varying the rotating speed of the drum (Teaching and Research Divisions of Mineral Processing, 1978). Normally, the low Gs unit is used for roughing, while the high Gs unit is employed for cleaning. The centrifuge is used mainly for the recovery of cassiterite, wolframite and hematite (Li et al, 1984; Liu et al, 1984; Sun et al, 1984; Burt et al, 1984). Its throughput is low: for instance, the ϕ800x600 rougher unit has a throughput of 30 tonnes per day, a water consumption of 50 m^3/day, an enrichment ratio of 2.5 to 3.0, and a recoverable size of 10 to 74 μm for tin slime treatment (Li et al, 1984).

The SL-type Separator is a continuous discharge centrifuge patented in 1985 and used for the fine and ultrafine cassiterite recovery in China (Lu, 1985; Ren et al, 1994a, 1994b). Figure 2-5 illustrates schematically this centrifuge, whose working components

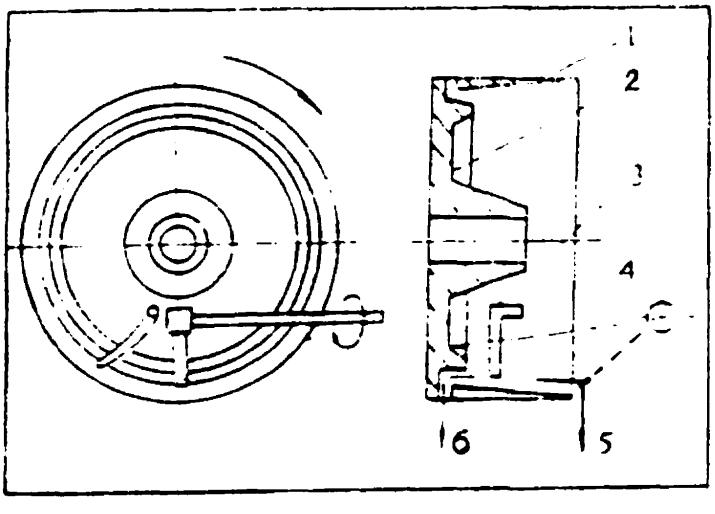

Figure 2-5 The schematic illustration of the SL-type Separator (Ren et al, 1994)

consist essentially of a horizontal drum and a water jet. The pulp is fed onto the inner wall of the rotating drum through a pipe (3); due to a very high centrifugal acceleration, heavy particles settle down close to the wall of the drum and are flushed away as concentrate continuously (6) by the impact of a water jet (4) acting against the longitudinal flow, which results in a "hydraulic weir" (Ren et al, 1994a) to prevent heavy particles from travelling to the tailings stream. Lighter particles are spun with water flow off the drum as the tailings (5).

There are three models of the SL-type separator available, which are designated by the drum diameter. The SL-300 model is a laboratory unit which can generate a 1500 Gs acceleration; the SL-600 and the SL-1200 models are the industrial scale units generating 660 and 330 Gs forces, respectively (Ren et al, 1994b). The throughput of the centrifuge is between 110 and 2000 kg/hour for -10 μm slimes, depending upon the drum size. It is claimed that the SL-type is capable of treating 10-74 μm cassiterite with high recoveries, provided operating parameters are properly adjusted.

The DTsS Refining Centrifuge, and another similar unit, the TsBS unit, were developed in the former Soviet Union and used for the treatment of auriferous marine sands with a gold recovery of over 90% in less than 0.01% of the bulk (Burt, 1984). They are unfluidized and vertical riffled cone type units. When the feed slurry flows into the rotating cone, heavy particles in the feed are centrifuged and trapped between

the riffle rings, from which they are removed at intervals, while lighter particles flow up and out of the cone as the tailings.

The sorting centrifuge was developed and being tested on plant-scale in Germany for sorting of plastics waste into different sorts (Hoberg, 1993). It is a horizontal double-cone centrifuge with a screw conveyor and can generate up to 1500 Gs centrifugal acceleration. When operating, the centrifuge uses either water or a sodium chloride solution (specific gravity: 1.1) as the separating liquid. Three plastics products of different specific gravity can be continuously recovered from a waste plastic mixture sized at 8 - 10 mm.

The Rotating Tube, developed by Ferrara (1960), is an experimental scale device consisting of a horizontal Perspex tube, 1100 mm in length and 20 mm in diameter, capable of rotating at up to 2200 rpm. Separation in the rotating tube is achieved with the help of centrifugal acceleration, which enables heavy particles to remain in the rotating tube while lighter particles are spiralled towards the other end of the tube and then discharged. Batch tests on cassiterite and cinnabar ores showed that the tube could achieve good recoveries, but at enrichment ratios lower than 9 (Ferrara, 1974).

The back-injection centrifuge

The distinctive feature of this type of centrifuge is the use of injection water to fluidize the concentrate bed from behind. Two of the back-injection centrifuges that

have been commercialized will be discussed, the Knelson Concentrator (to be described in 2.3) and SuperBowl. Other separators are also available, such as the Hy-G.

The SuperBowl is a batch centrifuge for gold and precious metals, recently developed and manufactured by the Falcon Concentrators Inc (Plummer, 1995). Figure 2-6 (Falcon Concentrators Inc., 1997) shows the Model SB4 laboratory SuperBowl. The heart of the centrifuge is a vertical plastic rotor bowl; its lower part is inward tapered and smooth walled so as to provide a migration zone for centrifuged mineral particles, and its upper part is composed of by two concentration grooves and riffles. The grooves are evenly perforated for back-injection water to fluidize the concentrate bed.

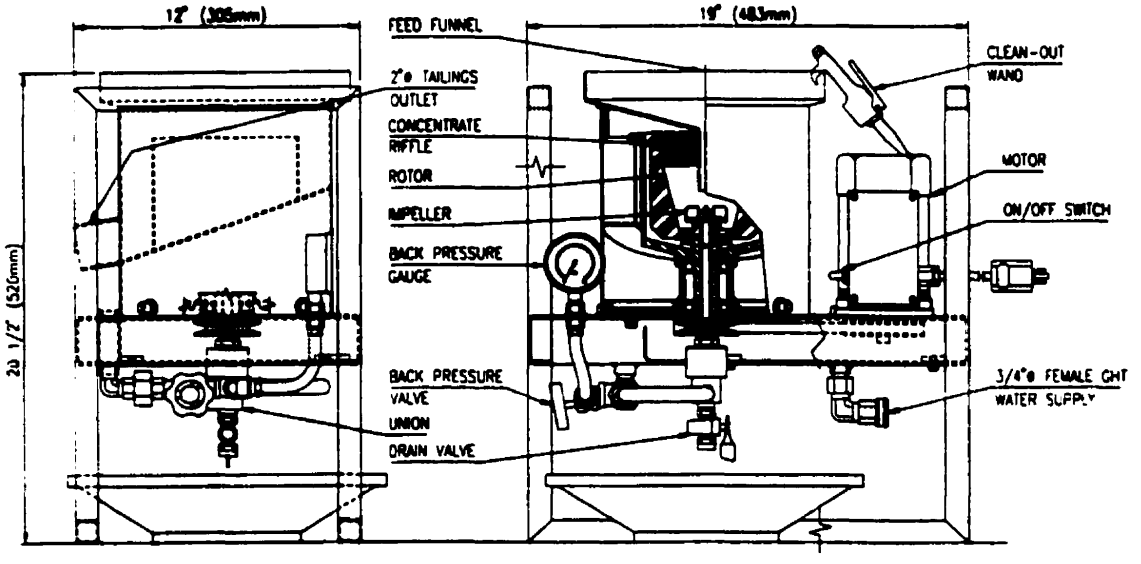

Figure 2-6 The Model SB4 laboratory SuperBowl (Falcon Concentrators Inc., 1997)

Feed slurry is directed into the rotating rotor bowl and then imparted an acceleration of up to 200 Gs acceleration. Thus, heavy particles settle rapidly on the lower wall of the rotor and most of them migrate into the riffles, where the concentrate is fluidized and cleaned by back-injection water. Lighter particles are washed out of the bowl due to their lower specific gravity or small size. When a concentration cycle is finished and the centrifuge and injection water are shut down, the concentrate inside the bowl is rinsed into a pan after removing the rotor bowl. For the larger scale SuperBowls, the concentrate is rinsed by a built-in spray manifold.

SuperBowls are currently manufactured in four sizes, from laboratory scale to high capacity models, either automated or manual (Sutter, 1997a). Since the unit works at higher G fields than the Knelsons and employs back-injection water technology, it is claimed that it will capture a significant part of the market. Recent statistical information shows that SuperBowls are found in 12 countries and used for alluvial-primary recovery, concentrate cleaning, recovery in grinding circuits, and metallurgical testwork, etc. (Sutter, 1997b).

2.2.3 The multi-gravity concentrators

Compared with the mono-centrifugal concentrator (i.e. the concentrators that achieve separation mainly by centrifugation), the multi-gravity concentrator may be defined as gravity concentrators that separate heavy material from lighter gangue by the combined mechanisms of centrifugal separation and other conventional gravity

separation. Examples of this type of concentrators include the Kelsey Centrifugal Jig, the Mozley Multi-Gravity Separator (MGS), and the Rotating Spiral.

The centrifugal jig works by combining jigging and centrifuging. At least there are two types of centrifugal jig available from different manufacturers: the Kelsey Centrifugal Jig (Brewis, 1995) and the Altair's Centrifugal Jig (Altair International, 1997), also known as the Campbell Centrifugal Jig (Environmental Management of the U.S., 1997).

The Kelsey Jig was invented in Australia and is manufactured by the Geologics Pty. Ltd. (Brewis, 1995). The basic operating principle of the Kelsey centrifugal jig,

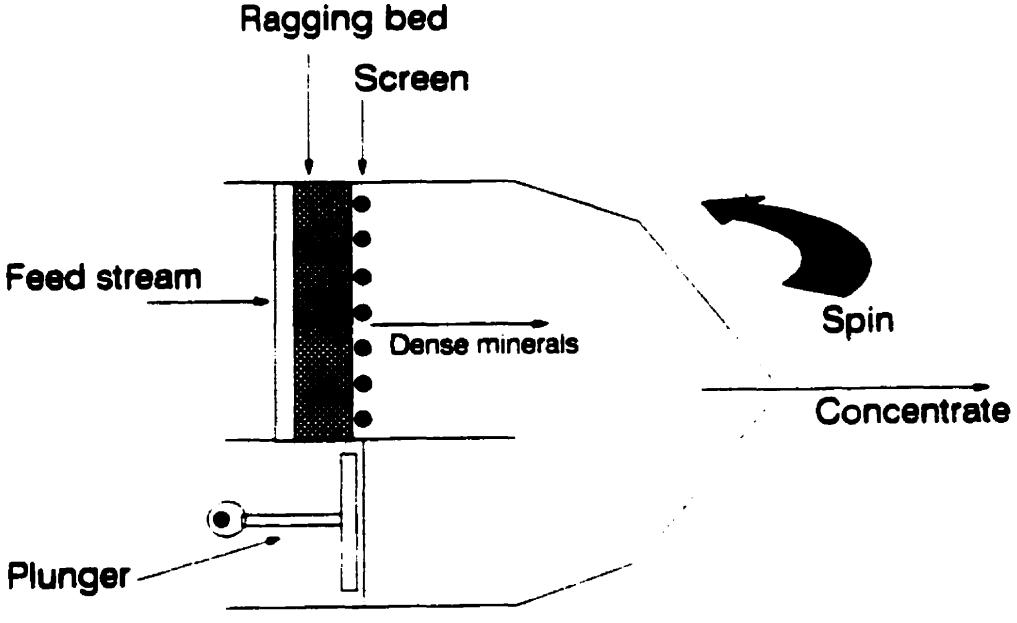

Figure 2-7 The spinning Harz Jig - Vertical orientation (Beniuk et al, 1994)

as illustrated in Figure 2-7, can be concisely demonstrated by a spinning Harz jig (Beniuk et al, 1994). In Figure 2-7, the hutch of the Harz jig is turned from a conventionally horizontal to a vertical orientation and spun about an axis. Feed enters the rotating jig and is then distributed onto the ragging bed by centrifugal force. Pulsation of water generated by the plunger causes the ragging to dilate and contract, thus resulting in differential acceleration of the feed and ragging particles according to their specific gravity and eventually allowing the centrifugally settled dense particles in the feed to move through the screen and be discharged through a spigot. Lighter particles are displaced over the surface of the ragging layer by the incoming feed and carried away to tailing.

The commercial Kelsey Centrifugal Jig has a number of concentrate hutches and incorporates a side pulsing mechanism, rotated by a spin drive (Beniuk et al, 1994). The centrifugal acceleration generated by the centrifugal jig can be as high as 100 times gravity (Brewis, 1995), thereby leading to increased particle separation efficiency, particularly at fine sizes below 40 μm that cannot be effectively recovered by conventional jigs. Another key feature of the unit is its ability for continuous operation since both concentrate and tailing are continuously discharged. Consequently, the Kelsey has found applications in the treatment of mineral sands, and the recovery of fine cassiterite and tantalite (Brewis, 1995; Wyslouzil, 1990). It has and still is being tested for fine hematite recovery (Laplante, 1998). In addition, an empirical model of the Kelsey has been developed by using a laboratory-scale jig to process tungsten slime

tailing and by considering the effects of the main operation parameters such as g-force, ragging characteristics and stroke length (Tucker, 1995).

The Altair's Centrifugal Jig is similar to the Kelsey Centrifugal Jig in many ways. It has several potential commercial applications, including the development of gold and heavy mineral sand deposits; coal cleaning and preparation; and environmental remediation (Altair International, 1997). However, because little technical information is available, and no industrial application has reached a commercial development, it is very difficult to assess the efficiency of the unit. Because water is injected as a pulse without negative flow (i.e. the minimum flow is zero), its water consumption is high and the average flow being higher than that of the Kelsey jig, fine heavy particle recovery is likely to suffer.

The Mozley Multi-Gravity Separator (MGS) achieves very fine mineral separation through a combined action of both the conventional shaking table and the centrifuge. In other words, it is a type of drum-shaped shaking table which rotates at speeds variable enabling a centrifugal acceleration equal to 5.5 to 15.1 Gs to be generated at the drum surface while shaking in the axial direction. Figure 2-8 illustrates a general arrangement of C900 MGS. The drum is tapered at one degree with the smaller diameter at the concentrate end, the axis of which can be inclined to about 10 degrees.

On operating, feed slurry enters the rotating and shaking drum about half way and wash water is added via a perforated ring near the open end of the drum. Under the influence of both centrifugal acceleration and a sinusoidal shaking, heavy particles settle radially through the slurry film and form a layer of concentrate bed pinned to the inner wall of the drum. The concentrate is then moved counter-current to the flow by scrapers which are assembled inside the drum and rotate at a slightly higher speed than

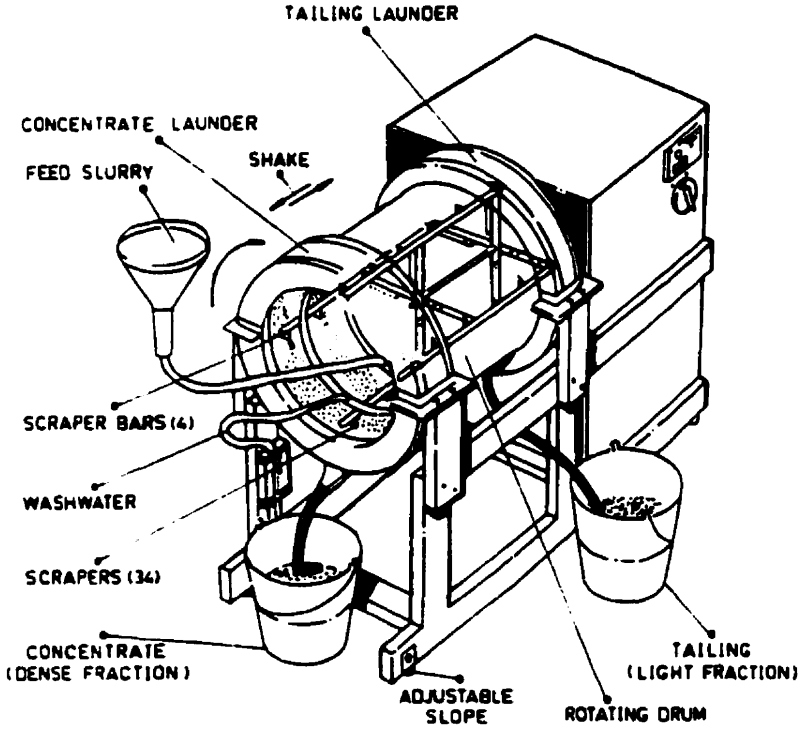

Figure 2-8 The laboratory/pilot plant MGS general arrangement

(Traore et al, 1995)

the drum, and discharged from the smaller end of the drum into the concentrate launder. Lighter particles are conveyed down the drum by water flow and discharge into the tailing launder.

The MGS has been experimentally proven to be a highly effective gravity device for the recovery of fine and ultrafine particles. Chan et al (1991) conducted gravity testwork with a plant scale MGS to treat tin, chromite, celestite and magnetite fine, comparing performance with that of conventional devices such as the shaking table and spiral. Their experimental results demonstrated that the MGS could deliver a superior performance in treatment of very fine materials. Recently, Traore et al (1995) used a synthetic ore made up of ferrosilicon and quartz and a natural tungsten ore to carry out a comparative performance study between the MGS and a fine table. They pointed out that the MGS appeared to obtain better results than the fine table, especially for particles below 20 μm. When experimentally compared with other three new types of centrifugal concentrators, including the Falcon B and the Knelson centrifuges, Burt et al (1995) reported that the performance of the Mozley MGS was superior in treatment of tantalum slime with a size typically 45% below 12 μm. In testwork on fine chromite slime and table tailings, Özdag et al (1994) demonstrated that it was possible for the MGS to upgrade the slime and table tailings to 56.8% and 53.8% Cr_2O_3 in the concentrate with 60.0% and 48.5% Cr_2O_3 recovery, respectively. In addition, research work showed that the MGS could reject some 75-85% of the pyritic sulphur from seam coal in Virginia

(Brewis, 1995). (The MGS is commercially used to recover fine cassiterite in Australia and Russia.)

In industrial applications, the MGS has largely duplicated its laboratory performance. At the Bristol Mineral Company in UK, treating a cyclone underflow with a particle size ranging between 75 and 5 μm grading 67% celestite, the MGS was able to achieve the 94% grade required at a recovery of 65% thereby successfully making a saleable product (Chan et al, 1991). Also, as reported by Brewis (1995), the MGS has found its applications in ultrafine cassiterite recovery, at the Wheal Jane plant in Cornwall; wolframite recovery from the plant tailings at Mineral Regina SA in Peru; upgrading graphite flotation concentrates in South Australia; the separation of gold from flotation concentrates in the Czech Republic, etc. Recently, the capacity of the unit has been increased to 4 t/hr for the C902 MGS and 60 t/hr for the MeGaSep (Richard Mozley Limited, 1998). The Mozley Double Drum MGS, which is constructed with two identical units, has been used in a number of countries.

The Rotating Spiral was developed in 1978 by the Sinkiang Institute of Metallurgy, China, its first commercial application being on tantalite and columbite ores (Hou, 1983). It is composed of a spiral and a rotating device driven by a motor so as to enable the spiral to spin around the vertical shaft. Another feature is that there are many riffles built radially on the spiral surface, which are similar to those on the deck

of the conventional shaking table. Therefore, it is claimed that this device combines the features of the conventional spiral, the centrifuge and the shaking table.

Practice in treatments of tantalum, columbium, tin and gold ores has shown that the Rotating Spiral is a highly effective gravity concentrator since it has a high throughput and a high enrichment ratio (up to 100).

The centrifugal magnetofluid separator was developed and being tested in Russia and it is claimed that this device was able to accurately divide fine non-magnetic particles of raw materials based on density (Lepekhin et al, 1995). The device is a multi-gravity centrifuge that works not only by combining techniques of centrifugal separation and separation in magnetic fluids, but also by means of magnetic separation (when there is a magnetic component in the feed). As described by Lepekhin et al (1995), the vertical concentrating rotor of the device consists of a storage space for a heavy fraction, and of a row of rectilinear Nd-Fe-B permanent magnets placed in a circle to generate a magnetic field. At the beginning of operation, a ferromagnetic fluid is fed to the rotor and fills the heavy fraction storage space and the gaps between magnets up to a certain level. Then, the raw material slurried with water is fed to the rotor rotating at about 50 Gs. Under influence of centrifugal acceleration, heavy particles overcome the buoyancy force of the magnetic fluid and settle down in the storage vessel of the heavy fraction, while lighter particles flow away through the discharge tube. After a certain processing period, the accumulated heavy fraction is

discharged from the rotor. The device was tested to recover fine copper or gold from quartz, having achieved a recovery exceeding 90%. A similar unit, the MAGSTREAM, is marketed by the Intermagnetics General Corp., Guilderland, New York, USA. Low capacites, the cost of the magnetic fluid, and poor performance below 75 μm limit its industrial potential.

2.3 Development and Applications of the Knelson Concentrator

2.3.1 Development of the Knelson Concentrator

The first and very crude Knelson Concentrator (KC) was commercialized in 1980 in Canada by Byron Knelson, whose inspiration of the Knelson design arose from a desire to "scientifically increase efficiency and reduce gold loss" in placer processing after his seven-day visit to Yukon placer mining sites in the early 1970s (Knelson, 1992, and 1985; Knelson et al, 1990). This early stage of the KC was a vertical back-injection centrifuge with two concentric bowls. The inner bowl was a concentration cone which had a straight perforated wall outwardly inclined at approximately 30 degrees with 5 cm flat metal rings spaced 5 cm apart. This first machine, which had a variable speed by virtue of a mechanical belt system, led to the selection of a rotating speed of about 240 rpm to achieve a centrifugal acceleration of 60 Gs (Knelson, 1985). Fluidization of the concentrate bed in the inner bowl was achieved by utilizing a hollow drive shaft to deliver pressured water to a jacket between the outer and inner bowls, which enables the water enter the concentrate bed through the perforated wall. Because of a water

pressure imbalance in the rings, the manufacturing of the first concentrator design came to a stop after a number of these machines were used.

In order to overcome the problem of pressure imbalance in the ring and retain a greater volume of concentrate, the second Knelson Concentrator design was made by using a cylindrical shaped inner bowl, by increasing ring depth from the bottom to the top to form a cone shape, and by introducing tangential back pressure water injection. However, due to the excessive volume of the bottom ring, a problem of imbalance became apparent when building a large machine, as the water pressure required to fluidize the bottom ring was much higher than the top ring.

The third generation of the KC was designed in 1984 with a 'V' shaped profile to the rings of the conical inner bowl, which is claimed to allow even greater depth of concentration. This improvement has resulted in a number of benefits including the ability to mould rings and much greater bowl life due to abrasion resistance of polyurethane or special rubber (used in tropical countries).

Presently there are six different sizes of the KC ranging from 3" (7.5 cm) to 48" (122 cm), or from laboratory scale to high capacity production models, which are capable of processing up to 100 tonnes of minus 6 mm solids per hour. According to how the concentrate is discharged, they may be classified into three models. The first is the standard model, which requires manual flushing of the concentrate after each

recovery cycle. The second model is the Centre Discharge unit or the CD model, only available for 12-in to 48-in units. Its concentrate removal can be achieved automatically in about two to four minutes by mechanically flushing the concentrate to the concentrate launder through the multi-port hub after diversion of the feed and reduction of fluidizing water pressure and rotation speed. The third and latest model is the experimental variable discharge concentrator, which removes the concentrate by means of variable extraction manifolds mounted to the inner bowl. Figure 2-9 shows a schematic drawing of the 12" (30 cm) Knelson Variable Discharge Concentrator.

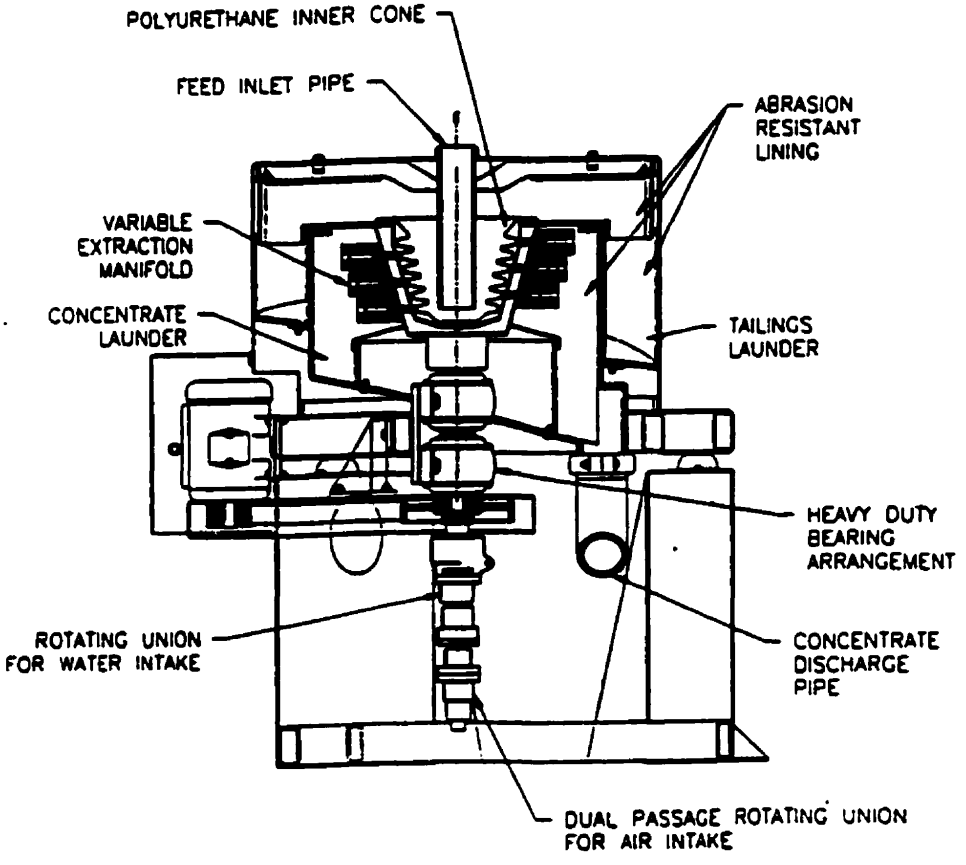

Figure 2-9 12-in Knelson Variable Discharge Concentrator (Knelson et al, 1994)

Owing to its excellent performance, KC-based gold gravity recovery has become a common practice in new and existing gold mills throughout the mining industry. In fact, the Knelson Concentrator can be found in over 70 countries and accounts for more than 1200 separate installations (Laplante et al, 1997; Brewis, 1995), as will now be detailed.

2.3.2 Industrial applications

2.3.2.1 The recovery of gold in grinding circuits

In Canada, the processing plant of Les Mines Camchib, which originally used a flotation - cyanidation circuit to treat a copper-gold ore, was the first one that applied the KC in a non-placer gold operation (Laplante et al, 1990). In the early 1980's, a gravity circuit consisting of a pinched sluice, two KCs and a home made table was developed in the grinding circuit in order to recover gravity recoverable gold in the circulating load. The overall gold recovery to the gravity concentrate was progressively improved from 20 to 40% and the overall mill recovery of gold increased by 1 to 3%. This successful installation was then followed by a similar one at the Belmoral Mine near Val d'Or (Knelson, 1992). An installation of an automated KC followed by a single stage of tabling in the grinding circuit prior to cyanidation at the Golden Giant mine in Ontario, operated by Hemlo Gold Mines Inc, could be able to account for approximately 25% of the site gold production, producing total cost savings estimated to reach $250,000 annually in reduced stripping costs (Honan et al, 1996).

In mid-1990, a 30-in KC was used to replace the jig in the grinding circuit at the Est Malartic mill, Canada, where a massive copper sulphide/gold ore was treated to produce a gravity gold product, a copper flotation concentrate and a gold precipitate (Hope et al, 1993). This improvement (the use of the Knelson-based gravity circuit) yielded a significant economic benefit, increasing total gold recovery from original 10.8% (with the jig-based circuit) to approximately 40%. The higher upgrading ratio (1000:1) of the KC also solved the overload problem of the cleaning table which was caused by the jig high yield.

In 1995, the Campbell gold mill at Balmertown of Ontario, one of the gold mills of Placer Dome Canada Ltd, installed two Knelson CD 76 cm concentrators to replace the existing jigs in a rod/ball mill grinding circuit (Folinsbee et al, 1997). Since then, this change has increased gravity recovery from 35% to 50%, which translates into economic value through a reduced gold inventory in the plant process (particularly in the pressure oxidation autoclave circuit), an ability to increase mill throughput, and reduction in security risks and manpower requirements in the gravity area.

In Australia, the Basement Plant of the Boddington Gold Mine is one of the hard rock processing plants that have successfully used the KC in the grinding circuit (Hart et al, 1995). The feed grade of this plant is quite high, averaging about 12 g/t after blending, and research showed that up to 30% of gold in plant feed could be recovered by gravity concentration. Originally, there had been a conventional gravity separation

circuit consisting of spirals and tables to recover gravity recoverable gold (GRG) from cyclone underflow bleed which was split from the recirculating load of the grinding circuit. Since the spirals could not efficiently recover coarse liberated gold, a 50 cm fully automated CD Knelson Concentrator was retrofitted into the existing gravity circuit to process the 1.5-3 mm material (which contains the majority of coarse gold) and the minus 1.5 mm concentrate and middlings from the rougher spirals in October 1992. This improved gravity circuit operated well above initial design expectations, and a further development of the circuit, which would exclude the spirals for security's sake, was proposed. Another example in Australia is the Paddington Gold Mine, where the gravity circuit (within the grinding circuit) was modified by replacing the plane table and installing two 75 cm KCs with pre-scalping of the feed with a 2 mm DSM screen (Owen, 1991). Gravity gold recovery improved from 3.2% (original gravity circuit) to 33% (after installation of the KCs), which corresponded to an improvement in overall plant recovery of 2%. Furthermore, the KC installation at Paddington resulted in improved leach kinetics due to the lowered grade to the leach circuit, thus saving $206,000 p.a. in chemical reagents.

Among the recent installations in Australia is that at Pasminco Mining Group's EZ Rosebery base metal mine in Tasmania, which led to the decommissioning of the conventional gravity jig circuit and, since then, the recovery of gold to doré has doubled to 30% (Brewis, 1995). Installations of the KC inside the grinding circuit in Australia were also made in the St Ives Gold Plant (Cloutt, 1995), where three 75 cm KCs are

used to treat the cyclone underflow with a gold recovery of 37% of the feed, and the Sundowner plant of the Darlot Gold Project (Beer, 1991), where a gravity circuit including a 50 cm KC complemented the CIP circuit to produce in excess of 15% of the total gold in the ore.

In the U.S.A., the Montana Tunnels mill installed a gravity circuit to recover coarse gold from the circulating load of the grinding circuit in 1991 (Darnton et al, 1992). Essentially, the circuit consisted of a pinched sluice to upgrade cyclone underflow, two 75 cm Knelson concentrators for roughing and cleaning of the sluice concentrate, and a Wilfley table to produce final concentrate for final melting. Production data, including those for leach and flotation, indicated that average overall gold recovery for the period since gravity start up was 2.7% higher than 1990 without the gravity circuit, and a projected gravity circuit expansion and relocation project would yield an estimated 50% increase in gravity gold production (Darnton et al, 1995). Another American plant, the Leadville Unit of the ASARCO Incorporated, also installed a 75 cm Knelson Concentrator in the primary grind circuit in early 1991; the early stage of operation has resulted in an increased gold recovery, producing a gravity gold concentrate of 36 oz/ton (Lloyd, 1991).

It is well known that separating gold from a complex sulphide ore may be one of the most difficult applications of conventional gravity concentration, since the specific gravity of the gangue (sulphides) is high and the occurrence of gold is usually

complicated. Installation of a Knelson within the grinding circuit can improve gold recovery, but it is seldom over a level of 30%, as it has happened in the Pasminco Mining's Rosebery concentrator (Poulter et al, 1994). In many cases, this natural problem of high sulphide ores, i.e., poor liberation and fine gold particle size, will possibly result in another two problems in separation: high concentrate bed erosion rates and low percolation rates (Laplante et al, 1997). In order to enhance the unit recovery, promising solutions have been recently proposed for these three problems (Laplante et al, 1997, 1998, 1996b; Zhang, 1998). For the first problem, it is necessary to conduct careful and simple GRG characterization test to study the feasibility of a gravity circuit (Laplante et al, 1996b). If a gravity circuit is adopted, careful removal of oversize from the gravity unit feed, such as by pre-screening, can be an effective approach to minimize the erosion rates (the second problem). A study conducted by Zhang (1998) on the table tails (the Knelson feed) of Barrick's Est Malartic's gravity circuit (within the grinding operation) is a case in point. The results of Zhang's testwork showed that gold recovery for the -850 μm feed with a lab KC was 76% at a fluidization water pressure 28 kPa, whilst for the -212 μm feed, i.e., the feed prepared by removing the +212 μm fraction, the highest gold recovery, 91%, was achieved at the same pressure and same feed grade (around 560 g/t Au). The third problem, i.e., low gold percolation rates through the slurry, seems to require much more effort to overcome. One of the possible alternatives is to increase the retention time for specific applications (Laplante et al, 1997). If the finest gold accounts for only a small portion in the feed or can be recovered in the subsequent leaching operation, the second option can be to increase fluidization water

flow to minimize the collapse of the flowing film to the intermediate sizes (Laplante et al, 1998).

2.3.2.2 Treatment of low grade alluvial gold ores

As the mineralogy is usually simple and the difference in specific gravity between gold and most gangue minerals is considerable in the case of alluvial gold ores, the KC offers a high recovery. The 20" (50 cm) and 30" (75 cm) models are the most common sizes used.

Bateman Engineering Inc., Lakewood, Colorado of the U.S.A., was one of the first mining companies that used the KC for recovery of fine gold from placer deposits in the early commercial stage of the KC (Anon., 1983). The first separation stage of the gravity circuit operated by Bateman Engineering Inc. was conducted by six large KCs working in parallel, and then a smaller unit was used for the second stage to clean the rough concentrate of the first stage so as to produce a final concentrate for refining. Another example is the Metana Minerals N.L. treatment plant in Australia (Knelson et al, 1990). This plant was first commenced with a typical trommel-jig gravity circuit to treat a sandy ore in 1986. Because of clay balls forming within the trommel and failing to break up, fine gold was locked within the clay balls which floated over the jigs and into the tailings dam, or were ejected with dirty oversize from the trommel, thus causing considerable recovery losses. In order to improve the gravity circuit, the plant commissioned a new gravity circuit consisting of a trommel, 30" (75 cm) Knelson

Concentrators and jigs in 1989. The minus 6 mm trommel product, which contains about 80% of the recoverable gold in the feed, is processed by the 30" KCs, while the plus 6 mm minus 20 mm material is blended with the minus 6 mm tailings from the KC and treated by the jigs. Production results showed that the KCs completely broke up the clay; gold recoveries increased by about 35%.

Recently, the installation of the largest Knelson-based gravity circuit in North America was completed at the Dome Mine, Ontario, owned and operated by Placer Dome Canada Ltd (Brewis, 1995). The design of this new circuit was based on the results of an intensive pilot project conducted to compare the performance of the KC with the existing jig-based circuit. It was reported from the project that a single fully-automated Knelson concentrator treating only 10-12% of the jig feed could recover more gold than the jig circuit.

2.3.2.3 Treatment of flash flotation concentrate

Flash flotation has become one of the recognized approaches to recover gold bearing sulphide minerals from hard-rock ores mainly because it can recover gold from the circulating load of grinding circuits and improve overall recovery. In Canada, this approach is currently being applied in a number of gold mines, such as the Lucien Béliveau (Putz, 1994), Est Malartic, Macrea, and Chimo mines (Laplante et al, 1998). Since there is frequently a significant amount of GRG in the concentrates of flash flotation, gravity recovery of the GRG from these products before smelting (to maximize

economic return) has been increasingly accepted. The Lucien Bélveau mill is a gold plant who used Knelsons to treat its flash flotation concentrate (Putz et al, 1993; Putz, 1994). Recently, the mill was moved to the Chimo mine, and recovery from the flash flotation concentrate was supplemented by Knelson recovery from the cyclone underflow, for coarser gold (+300 μm) that would not readily float in the flash cell.

The Merro De Ouro Gold Mine in Brazil ranks as one of the lowest grade (0.65 g/t gold) gold mines in the world (Suttill, 1990). Most of the orebody is weathered and native gold is associated with the quartz boudins, and graphitic and sulphide pockets. The basic plant flowsheet consists of crushing, grinding, flotation, cyanidation of flotation concentrate followed by CIP. Before cyanidation, the flotation concentrate (grading up to 600 g/t Au) is centrifuged in a 30" Knelson Concentrator to collect coarse gold. It is reported that the concentrate of the KC accounts for about 50% of gold production.

2.3.2.4 Other applications

The KC can be occasionally used to recover free gold from plant final tailings. Le Bourneix gold mine in France is a case in point, where the grade of the flotation tailings varied from 0.3 to 1 g/t, 90% of which was coarser than 106 μm (Meia, 1993). The mine installed a 50 cm (20") KC to recover free gold from >106 μm fraction of flotation tailings, and production showed that gold in the KC concentrate graded more than 1800 g/t and accounted for 1.5% of the total gold recovery. At the Leadville mill

in Colorado, operated by ASARCO Inc., a 76 cm KC was projected to recover gold from the mill final tails so as to produce a 120-180 g/t gold concentrate (Lloyd, 1991).

2.3.3 Laboratory applications

The small Knelson Concentrator units (3- and 7.5-in) have found four applications in mineral processing applied research. As seen below, the first two applications are as conventional as other gravity devices, while the last two, developed at McGill University, are quite novel.

2.3.3.1 Feasibility studies of the KC based gravity approach

Patchejieff et al (1994) carried out gravity experiments at a copper flotation mill aimed at the characterisation of gold occurrences and a feasibility study of KC-based gravity recovery. Tests with final flotation tailings and flotation concentrates indicated that some gold in the copper ore was gravity recoverable, and could be easily upgraded up to a 1000 times by a 7.5" (19 cm) KC. Thus, these researchers concluded that additional extensive pilot and plant testing had to be pursued in order to determine in more detail the feasibility of a large scale implementation of the gravity module and the subsequent flow sheet arrangement.

The Noranda Technology Centre has investigated the potential of gravity concentration of gold from Noranda's base metal flotation mills by means of a 7.5" KC (Ounpuu, 1992). Testwork on samples from Westmin Myra Falls, Bell Copper and

Heath Steele mines showed that fine (-150 μm) free gold/electrum, some of which could not be recovered successfully by flotation, could be recovered by gravity techniques from the grinding circuits of base metal flotation mills. Among the testwork mentioned above, perhaps the testwork on Heath Steele ore sample was the most interesting, because the geologists had never seen any visible gold in the ore and microscopy had never indicated any free gold in mill products even though the mill feed averaged 0.5 g/t Au. The 7.5" KC circuit obtained up to 20% unit recovery and produced a concentrate assaying 500 ppm Au from a cyclone underflow bleed.

Meza et al (1994) used 7.5 cm and 19 cm Knelson Concentrators to study the recovery of alluvial gold from four types of placer sand in Colombia. A number of operating variables were investigated during their study, and it was observed that the fluidizing water pressure was the most important variable affecting recoveries. Gold recoveries of over 98% were obtained from three-stage tests under optimum operating conditions.

It should be mentioned that a 15 cm (6") KC of the second earlier bowl design ("deep ring straight wall" design) had been used for pilot-scale tests by Forssberg et al in Sweden (1987). Tests on an artificial ore containing 1% of milled lead shot (to mimic free gold) demonstrated that feed rate and water pressure were decisive parameters for the performance of the KC. Tests on natural auriferous sulphide ores yielded gold recoveries of 70% to 75% with enrichment ratios of 20 to 25 :1.

For research related to the recovery of lower high density minerals rather than gold, the Iron Ore Company of Canada (IOCC) had used a continuous discharged early Knelson prototype to separate iron minerals from silica gangue in the -74 μm fraction (Penney, 1996). However, testing halted in the summer of 1992, as the early Knelson prototype could not be operated satisfactorily. Testing of a second prototype is taking place at Montana tunnels (Laplante, 1998).

2.3.3.2. Evaluating plant gravity circuits

The use of a laboratory KC to study the performance of plant recovery units has been reported by a number of researchers. Laplante et al (1992) conducted a study focusing on the performance of a 30" plant KC operated at 25 t/h and 80 kPa of back-water pressure by using a 3" laboratory KC. As a higher recovery of fine gold could be achieved by the laboratory KC than the plant KC, they suggested that two plant KCs of Les Mine Camchib Inc. be operated in parallel, rather than operating with one on, one off. They also recommended that recovering fine gold below 300 μm be further favoured by finer screening of the plant KC feed to yield a higher grade and more tightly sized feed.

Putz et al (1993) used a 3-in Knelson to evaluate two gravity circuit configurations treating a flash flotation concentrate at the Lucien Béliveau mill. Their experimental result showed that gold recovery in the 30-in Knelson averaged 45% in the KC and Deister table circuit and decreased to less than 32% when using a

hydroseparator, a spiral and a 20-in Knelson. Mineralogical changes were partly responsible for the decrease, but the ore itself had a GRG (gravity recoverable gold) content in excess of 84% (Woodcock et al, 1993). This is a good indication that the use of the gravity circuit after flotation was not entirely satisfactory. Their further investigation of the free gold content in the ball mill products and the cyclone underflow indicated that much of the gold in the ball mill recirculating load was too coarse for significant recovery in the flash flotation cell and should be recovered by gravity from the cyclone underflow or ball mill discharge. This was subsequently implemented in the Chimo mill.

2.3.3.3. Determining gold content and GRG

(1) Measuring gold content

Determining the correct gold content in an ore can be a particularly difficult task. Obviously, this involves the statistical problem of measuring the concentration of gold particles occurring with a very low frequency. Some mineral processing studies (Laplante et al, 1992; Banisi et al, 1991) have shown that this problem becomes particularly acute with increasing particle size. This had long been recognized by geologists (Clifton et al, 1969; Griffith, 1960; Giusti, 1986).

Physical processing, either by laboratory flotation or gravity separation, is a better route to determine gold content in a sample, since it is easier, safer, more cost-effective and less harmful than chemical processing. Compared with flotation, which

has a low reproducibility due to the difficulty of floating coarse gold (Graham, 1989), laboratory gravity separation provide more reproducible results and can handle larger samples. The laboratory Knelson concentrator has been proved to be a legitimate tool to estimate gold content in samples, and a 3-in Knelson based procedure which can yield reliable estimates of overall gold assays in 5 to 70 kg samples, usually finer than 850 μm, has been successfully used at McGill University (Laplante et al, 1992, 1993b, and Putz et al, 1993; Zhang, 1998). This procedure concentrates GRG into subsamples of 100 to 150 grams, which can be fully assayed size-by-size, thus eliminating any nugget effects.

(2) Measuring GRG (gravity recoverable gold) in an ore

The definition of GRG (gravity recoverable gold) is gold that can be recovered gravimetrically as 'free gold' under optimum conditions of gravity separation (Laplante et al, 1995b). The amount of GRG in a given ore is an important criterion for circuit design and separator selection.

A 3-in Knelson base procedure has been developed to characterize the GRG content in a gold ore (Woodcock, 1994; Laplante et al, 1996b). This procedure is a three stage process: a representative ore sample (from 40 to 120 kg) crushed and rod milled to 100% -850 μm is first processed with a 3-in Knelson, the entire concentrate is assayed and tail samples taken; about 27 kg of the tails of this step is then ground to a finer size (45-55 % -75 μm) to achieve further gold liberation, and processed with the

KC; the third step repeats the above process with a tail sample from the second step (usually 25 kg) ground at 75-80% -75 μm. A wide variety of ores were tested; three basic responses (represented by the cumulative percent GRG retained for all the three stages) were deserved, ranging from very poor (below 30% GRG) to the exceptionally amenable (up to 97% GRG); most samples returned between 60 and 70% GRG (Laplante et al, 1996b).

2.3.3.4. Predicting gold recovery

A novel methodology to predict gold recovery in industrial gravity circuits has been developed by Laplante et al (1995). As described by the authors, this methodology, which is designed for gravity circuits located in the circulating load of secondary grinding mills, makes use of a population balance model which represents gold liberation, breakage and classification behaviour and applies GRG pre-concentration and recovery data to predict overall recovery. The GRG content of the ore is estimated from the test presented in the previous section. Case studies on three gravity circuits with greenfield, retrofit and optimization applications indicated that the above methodology predicted the very large circulating loads observed in an actual plant with acceptable accuracy; predictions of gold recovery were also in good agreement with plant performance.

2.4 Theoretical Studies of Centrifugal Separation and Interstitial Trickling

2.4.1 Theoretical studies of centrifugal separation

2.4.1.1 The equations of motion of a solid particle in the centrifugal field

In the field of mineral processing, the early (perhaps the first) attempt to unfold the physical principles of centrifugal separation process was made by Ferrara (1960), who intended to ascertain the reasonable prospects of separating particles of different specific gravity by means of a rotating tube and to gain an idea of some parameters which might be useful in the design of experimental centrifuges. After making several simplifications, this author derived an equation for the motion of a particle sliding along the wall of a rotating cylindrical tube under viscous fluid flow conditions:

$$\frac{4}{3}\pi\left(\frac{d_p}{2}\right)^3\rho_s\frac{dv}{dt}=-\frac{4}{3}\pi\left(\frac{d_p}{2}\right)^3(\rho_s-\rho)\psi\omega^2\left(r_1-\frac{d_p}{2}\right)-18k\mu\frac{1}{r_1^4}Q\left(\frac{d_p}{2}\right)^2$$

$$+\ 24k\mu\frac{1}{r_1^3}Q\left(\frac{d_p}{2}\right)^2-6\pi k\mu v\left(\frac{d_p}{2}\right) \qquad (2.1)$$

where r_1 is the inside radius of the tube; ω is its angular velocity; d_p is the diameter of the particle; ρ_s and ρ are the densities of the particle and the fluid; ψ is the non-sphericity coefficient of the particle; μ is the viscosity of the fluid; Q is the flow of the

fluid in the tube; v is the velocity of the particle along the tube wall; k is the coefficient of the non-sphericity of the particle.

On the right hand side of Equation (2.1), the first term represents the frictional force between the particle and the tube wall; the second, third and fourth terms express the thrust of the fluid.

When dv/dt = 0, Ferrara further derived the expression of the terminal velocity of the particle travelling along the tube wall, i.e. V_{max}, as follows.

$$v_{max} = -\frac{1}{36k\mu}(\rho_s-\rho)\psi\omega^2 d_p^2(2r_1-d_p) + \frac{1}{4\pi}Q\frac{d_p}{r_1^4}(8r_1-3d_p) \qquad (2.2)$$

Admittedly, Ferrara's equations described above only deal with the axial movement of a particle along a horizontal cylindrical tube. In other words, these equations describe merely the transportation behaviour of a particle in a rotating centrifuge. For the radial movement of a particle in a single wall centrifuge, a detailed and reasonable analysis of centrifugal settling process can be found in Coulson et al (1990). In brief, for the Stokes' Law region, the equation describing the settling velocity of a spherical particle in the radial direction under the influence of a centrifugal field can be expressed in the following form:

$$\frac{dr}{dt} = \frac{d_p^2(\rho_s - \rho)r\omega^2}{18\mu} \qquad (2.3)$$

$$= \frac{d_p^2(\rho_s - \rho)g}{18\mu}\,\frac{r\omega^2}{g} = u_0\frac{r\omega^2}{g} \qquad (2.4)$$

where r is the radial position of a particle; dr/dt is its instantaneous velocity; and u_0 is the terminal velocity of the same particle in the gravitational field.

Thus, the instantaneous velocity (dr/dt) is equal to the terminal velocity u_0 in the gravitational field, increased by a factor of $r\omega^2/g$ (Coulson et al, 1990). It should be pointed out that Equation 2.3 is derived for the motion of a rigid spherical particle only in the Stokes' law region (or the creeping flow region). This means that the drag coefficient for this particle is equal to $24/Re_p$, where Re_p is the particle Reynolds number. Since particles may move in different flow regimes in the centrifugal field, different relationships for drag coefficient must be considered for different particle Reynolds numbers. Clift et al (1978) have reviewed and compared many expressions for the drag coefficients, which may be useful for this work to make theoretical consideration of particle movement in the Knelson Concentrator. Other authors discussed the drag coefficient with similar expressions, such as Dallavelle (1948) and Madhav et al (1995).

For separations in a rotating ferrofluid, Svoboda (1996) has recently developed a similar general model of the balance of forces acting on a particle in a rotating

ferrofluid separator, which includes the hydrodynamic drag and magnetic traction force. This study showed that the model allows, to some extent, to determine more precisely the cut-point density and to improve the selectivity of separation than another older model.

2.4.1.2 The configuration and structure of the slurry stream in a centrifuge

With respect to the configuration and structure of the slurry stream inside a single wall centrifuge, Sun (1982) proposed that the slurry flowing along the inclined surface of the rotating drum of the Yunxi Centrifuge is a weak turbulent flow, and that this flow could be divided into four layers from the top to the bottom of its intersection: 1) the dilute layer, which is the top flow with lower turbulence intensity and containing very few particles; 2) the suspended layer, where small vortices (or swirls) are well developed and a great amount of light particles are suspended under diffusive turbulent fluctuations; 3) the rheological layer, in which there is weak turbulence and the slurry flows slowly along the bottom layer; 4) the sedimentary layer, which is formed by settled heavy particles. Thus, separation takes place within the rheological layer, where particles are subjected to the Bagnold effect and well stratified, heavy particles settling down into the lower layer while lighter particles are suspended up to the upper layer.

As to the basic configuration for the flow-field in the centrifuge, Ungarish (1993) has proposed an interesting fundamental model for fluid in a rotating cylindrical container. As described for the spin-up of the fluid from rest, the resulting velocity

field consists of three regions: a shrinking non-rotating inner region (I), an expanding partially spun-up outer region (III), and Ekman shear layers (II) which suck fluid from (I) and feed it into the spinning region (III). Ungarish's fundamental model might implicate a general separation principle of centrifuges, which shows how heavy particles centrifugally settle down from the non-rotating region to the spinning region. Another flow field associated with the centrifugal separation of polydispersed suspensions, i.e. suspensions of particles which differ significantly in size or density, was recently investigated by Ungarish (1995). He analyzed mathematically the configurations in long and finite rotating cylinders, and obtained the formulation and solution of polydispersed rotating flow problems in the framework of the "mixture model".

2.4.2 Theoretical studies of interstitial trickling

Since separation in back-injection centrifuges involves also an interstitial trickling process, which may also be called percolation, it is necessary to review some references that might present pertinent information for the present work. Unfortunately, little is known about interstitial trickling in centrifugal fields. However, much progress has been made in the understanding of interstitial trickling in the gravitational field. In view of many obvious analogies to centrifugal trickling, it is believed that the fundamental knowledge in the gravity field will offer useful insight in understanding and interpreting the centrifugal trickling process, and in enhancing pertinent research so as to close the major gap of knowledge between gravity and centrifugal systems. The following presents a brief review on this subject.

2.4.2.1 Interstitial trickling in a jig

In the case of jigging, interstitial trickling, or consolidation trickling, is one of the three important mechanisms for the ideal jigging process which were proposed by Gaudin (1939). It takes place at the end of each pulsion stroke in the jig when the jig bed begins to compact and the larger particles interlock. Under the influence of gravity and of the fluid stream, smaller particles continue to move downwards through the interstices of the larger ones, thus completing the interstitial trickling process. However, this process is complex and the trickling velocity of fine particles depends a number of variables such as the size of the fine particles and of the interstices. In spite of this complexity, great efforts have been made by research workers to indicate or estimate the maximum relative size of particle that can trickle interstitially. For instance, the maximum size d_p' of a particle that can pass between four equisized light spheres of diameter d_p can be easily estimated (Burt, 1984):

$$d_p' = (2d_p^2)^{0.5} - d_p = 0.41\ d_p \qquad (2.5)$$

A recent research was conducted by Witteveen (1995), who predicted mathematically and measured experimentally the porosity (a parameter relative to interstices) distribution in a jig bed as a function of time and location in the bed during operation. This author first proved a qualitative relationship between transmission and porosity, and then measured transmission in a transparent laboratory jig and in a transparent laboratory fluidized bed by means of an optical bench with a laser source. Based on the similarity between the transmission values measured and the porosity

values calculated by a mathematical model, Witteveen concluded that the calculated porosity distribution in a uniform jig bed is comparable in a qualitative way with the porosity distribution in reality.

2.4.2.2 Particle percolation in a centrifuge

A more recent research which includes a study on the distribution of concentrate in the Knelson concentrator rings has been completed by Huang (1996) at McGill University. At the beginning of this study, he used a 3-in KC with an inner bowl that is vertically separable in two halves to recover tungsten (used to mimic of gold) concentrates from synthetic ores. He then removed the concentrate cakes ring-by-ring from each half of the inner bowl after freezing it. The photographs of the concentrate cakes demonstrate that most tungsten was recovered on the surface of the concentrate bed due to partial fluidization. Huang came to the conclusion that the separation of tungsten particles from the gangue took place at the surface of the rings and depended mainly on competing forces and on acceleration of the consolidation trickling of tungsten and the high density of the separation zone.

For the Falcon Model 'B' units, Buonvino (1993) proposed two different recovery mechanisms: i) coarse particles are captured by burying themselves in the concentrate bed; ii) fine particles are captured by lodging themselves between the interstices on the surface of the bed. Obviously, these two mechanisms can be regarded as particle migration and percolation, and they may take place in a two step process

(Laplante et al, 1994). As suggested by Laplante et al (1994), the first step is migration and percolation of dense particles to the slurry interface and concentrate bed, which is a function of feed rate; the second step is actual capture of dense particles in the concentrate bed, which is relatively unaffected by feed rate. A mathematical model of the Falcon's performance was also constructed in three different phases by these authors.

2.4.2.3 Particle percolation and migration in the gravitational field

In the case of dry and cohesionless particles, Bridgwater and his co-workers (1969, 1971, 1978, 1983; Masliyah et al, 1974; Stephens et al, 1978a, 1978b) have published many technical and academic papers involving interparticle trickling in the gravity field since the 1960's. As classified by Bridgwater et al (1983), particle percolation consists of strain induced interparticle percolation, defined as the drainage of one species through a shearing particle array, and spontaneous interparticle percolation, defined as the drainage of one species through a particle array in the absence of strain. On the other hand, the motion of large particles through an array of smaller ones was termed "particle migration" (Bridgwater et al, 1983; Stephens et al, 1978b).

Strain induced percolation is considered a process of particle release and capture. Bulk particle motion in a shearing particle array may be described as that of a number of blocks between which are found failure zones several particle diameters across (Bridgwater et al, 1983, 1978; Stephens et al, 1978a, 1978b). From the movement of

percolating particles in a simple shear apparatus which contained a cell of bulk particles and was sheared manually, it was observed that the bulk particles were shuffled with respect to each other due to the strain applied across the failure zone (Bridgwater et al, 1983). If the strain rate in the failure zone is high enough, sufficient space will eventually be provided into which a smaller particle may drop. Should the space be insufficient for the smaller particle to pass through, it is not likely to be projected back to its original location since a ratchet mechanism may then operate.

Regarding the interstitial trickling behaviour of large particles, it was considered that they move towards the region of maximum strain rate, the movement being controlled by the strain rate gradient rather than the strain rate as for percolation of smaller particles (Stephens et al, 1978).

In an early study of percolation conducted by Masliyah and Bridgwater (1974), a numerical procedure was used to gain some insight into the motion of a particle when it was undergoing spontaneous interparticle percolation. These authors pointed out that a particle rapidly attains a mean downwards velocity upon entering the array, and that the mean downwards drift velocity is insensitive to packing voidage fraction.

As further shown by Bridgwater et al (1983), basically, the dimensionless percolation velocity is inversely proportional to the ratio of the percolating particle diameter, d_p, to the bulk particle diameter, d_b. This means that the percolating velocity

of a smaller particle is higher than that of a larger one under the same bulk material conditions. Bridgwater et al also found that particle shape has a marked influence on percolation velocity, and that increases in percolating particle density give a small but significant increase in percolation velocity. On the other hand, Bridgwater et al pointed out that the effect of fluid flow on percolation would be to produce an apparent change in the magnitude and direction of g.

In another research, Donsi et al (1988) investigated experimentally the contribution to segregation given by percolation of fine particles through the voids of the coarse bed material which was fluidized by compressed air. They observed that the volumetric concentration of fines (lead spheres) contained by the coarse bed (glass beads) depended on the gas velocity and also on their terminal velocity and size. They also discovered that a floating layer at the top of the bed formed above a defined value of the fluidizing gas velocity. This means that the percolation velocity of the fines had been greatly reduced.

2.4.2.4 Measurement of percolation velocity in the gravitational field

There is a typical methodology for measuring percolation velocity and studying the movement of fines in a fluidized or packed bed of coarse in the gravity field (Morooka et al, 1989; Kusakabe et al, 1991). In the case of a fluidized bed, a fluorescent tracer technique was used by Morooka et al (1989) to measure the movement of fine porous catalyst particles of 60 -65 μm through a fluidized bed of 1.54 mm silica

of fine porous catalyst particles of 60 -65 μm through a fluidized bed of 1.54 mm silica gel spheres. In this study, the fine catalyst particles were coated with a fluorescent dye so as to be the tracers, and the fluidized bed was formed in a transparent acrylic fluidized column, underneath which ambient air was introduced to fluidize the silica gel bed. The flow pattern of the tracers was detected by means of an array of bifurcated optical fibre probes when they were passing through the fluidized bed. The results of this study showed that in the presence of gas bubbles percolation of fines increased with increasing gas velocity and height from the gas distributor. In the case of a packed bed, a methodology similar to the above was employed by the same research team (Kusakabe et al, 1991), but the percolating fines were not coated with a fluorescent dye. The results of this study also demonstrated that the percolation velocity of fines increased with increasing gas velocity and size of packed particles, and that the measured percolation velocity agreed with the value calculated from a flow model of fines. However, even though Kusakabe et al (1991) claimed that the model was based on the successive collisions of fines with coarse particles, they simply used the free settling velocity of a particle, rather than the hindered settling velocity of a particle, to derive their model.

CHAPTER 3 THEORETICAL CONSIDERATIONS

3.1 Introduction

3.1.1 Structure of the flowing slurry in the KC

The movement of the slurry in the Knelson centrifugal concentrator (KC) is three dimensional. As soon as the slurry is fed on the bottom of the conical inner bowl, it is accelerated radially, axially and tangentially. It flows upward in a spiral motion along the near vertical sides of the inner bowl (75^0 to the horizontal), until it is discharged at the top. As the result of the tangential acceleration, most solid particles are centrifuged out of the inner layer[1] of the flowing slurry, causing this layer to be highly diluted. The remaining particles then concentrate themselves near the surface of the concentrate bed, forming the second zone where the slurry comes in contact with a radial (and tangential) inward fluidization flow and thus both the motion of the fluid and individual particles is much more difficult to describe. Some particles will eventually percolate or migrate to the surface of the concentrate bed. Whether or not this is successfully achieved will depend on their density, size and shape, as well as the extent of fluidization in this second zone.

Hence, according to the previous literature review (Laplante et al. 1994; Sun, 1982; Ungarish, 1993), it is expected that the structure of the flowing slurry inside the

---

[1]Inner layer: the layer of slurry closest to the rotation axis. It is in fact the surface of the flowing slurry.

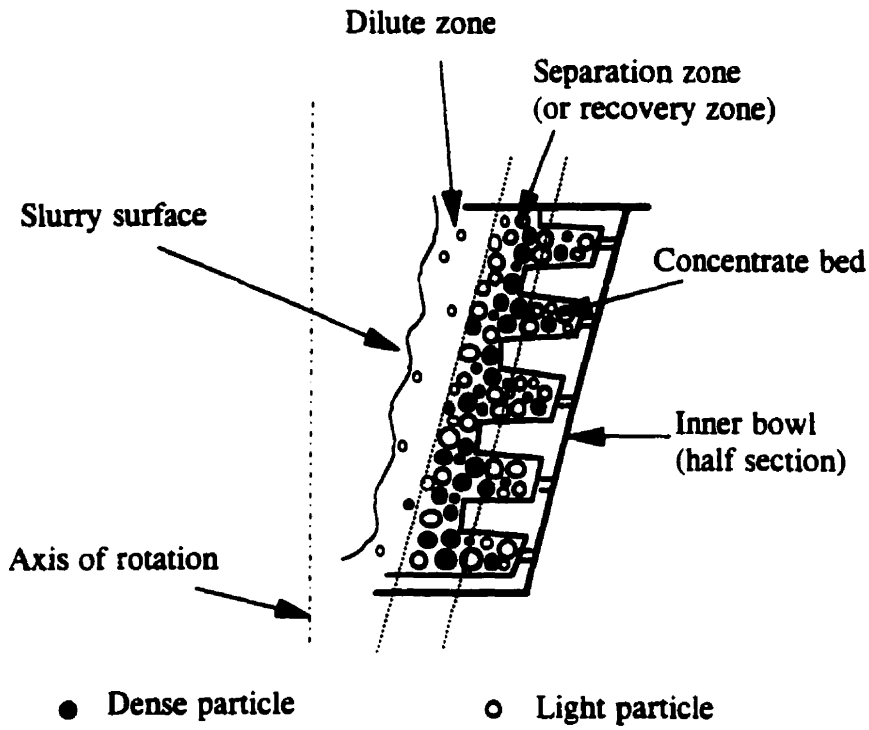

Figure 3.1 Schematic illustration of the structure of the slurry in the inner bowl

inner bowl consists of two zones in the radial direction. As illustrated schematically in Figure 3.1, near the central axis of the inner bowl is the dilute zone, which generally contains only very fine light (gangue) particles. Between the dilute zone and the middle section (Huang, 1996, p.98) of the concentrate bed is the separation zone (or recovery zone), where solid particles already centrifuged are highly concentrated and partially fluidized due to the action of the fluidization flow. In fact, the separation zone consists of the outer layer of the flowing slurry and the inner section (Huang, 1996, p.98) of the concentrate bed.

3.1.2 Movement of a solid particle in the KC

Centrifugal separation of minerals in the KC is a complex process, during which mineral particles are subjected to a number of forces including centrifugal, drag (or thrust), buoyancy, and shock resulting from inter-particle collision. Based on the structure of the flowing slurry, the movement of a particle in the inner bowl of the KC can be divided into two stages: 1) a centrifugal accelerating motion through the dilute zone of the inner bowl, and 2) percolation or migration through the separation zone towards the concentrate bed.

3.2 Accelerating Motion of a Spherical Solid Particle in the Dilute Zone in a Knelson

3.2.1 The major forces on a spherical solid particle accelerating in the dilute zone

Considering the motion of a smooth spherical solid particle of mass m in the dilute zone of the flowing slurry inside inner bowl of a Knelson, at some time t the particle will be moving with a velocity $\bar{u}_p$. As illustrated in Figure 3.2, this velocity vector $\bar{u}_p$ can then be resolved into three components in the positive directions of the cartesian coordinate system: the radial velocity $\bar{u}_{px}$, the axial (vertical) velocity $\bar{u}_{pz}$, and the tangential velocity $\bar{u}_{py}$.

Figure 3.3 illustrates the movement of the particle towards a ring of the KC inner bowl. The major forces acting on this radially settling particle are discussed as follows:

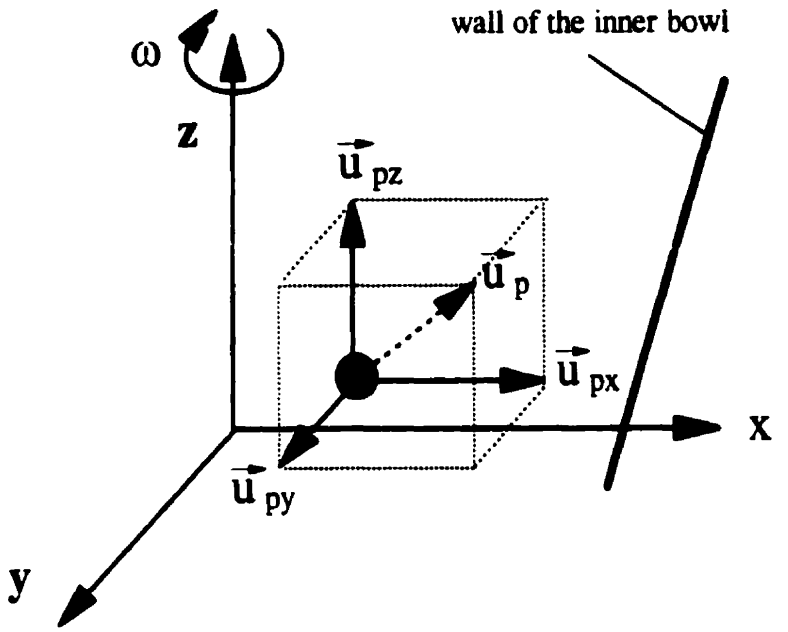

Figure 3-2 Three-dimensional motion of particle

(1) The centrifugal force $\vec{F}_c$:

$$\vec{F}_c = (\pi/6)d_p^3\rho_s\vec{r}\omega^2 \qquad (3.1)$$

where $\vec{r}$ is the displacement of the moving particle from the rotation axis to its present position, d_p the diameter of the particle, ρ_s its density, and ω the angular speed of the inner bowl.

(2) The drag force $\vec{F}_d$ (Weber, 1998; Odar et al, 1964):

$$\vec{F}_d = \frac{\pi d_p^2}{4}\frac{C_D}{2}\rho|u_r|\vec{u}_r \qquad (3.2)$$

where C_D is the drag coefficient of a sphere; ρ is fluid density; $\vec{u}_r$ is the relative velocity of the fluid to the particle, which takes the form:

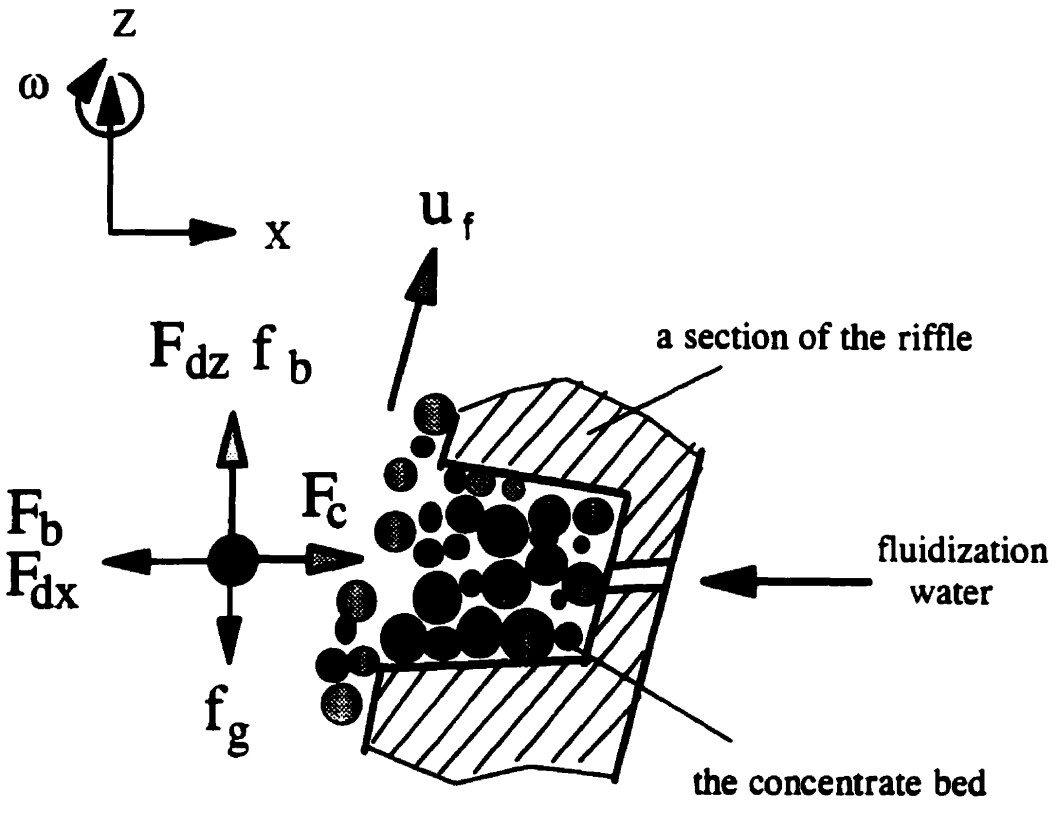

F_c = the centrifugal force
F_{dx} = the X-component of the drag force
F_{dz} = the Z-component of the drag force
F_b = the buoyancy force in the centrifugal field
f_g = the gravity of the particle
f_b = the buoyancy force in the gravity field
u_f = fluid velocity

Figure 3-3 Forces on a particle in the dilute zone

$$\vec{u}_r = \vec{u}_f - \vec{u}_p \qquad (3.3)$$

where $\vec{u}_f$ is fluid velocity; $|u_r|$ is the magnitude of $\vec{u}_r$.

The X-component of the relative velocity, u_{rx}, is equal to the algebraic sum of the X-components of $\vec{u}_f$ and $\vec{u}_p$, i.e.

$$u_{rx} = -(-u_{fx}) + u_{px} = u_{fx} + u_{px} \qquad (3.4)$$

The X-component of the drag force, F_{dx}, can be expressed as follows (Weber, 1998):

$$F_{dx} = \vec{F}_{dx} \cdot \vec{i} = \frac{\pi d_p^2}{4} \frac{C_D}{2} \rho |u_r| (u_{px} + u_{fx}) \qquad (3.5)$$

where $\vec{i}$ is the unit vector in X-direction.

Similarly, the Z-component of the drag force, F_{dz}, can be expressed as follows:

$$F_{dz} = \vec{F}_{dz} \cdot \vec{k} = \frac{\pi d_p^2}{4} \frac{C_D}{2} \rho |u_r| (u_{fz} - u_{pz}) \qquad (3.6)$$

where $\vec{k}$ is the unit vector in Z-direction.

It is noted that the drag coefficient C_D is a function of the particle Reynolds number based upon the magnitude of $\vec{u}_r$ (Weber, 1998):

$$Re_p = \frac{d_p |u_r| \rho}{\mu} \qquad (3.7)$$

where μ is the viscosity of the fluid.

(3) The gravity of the particle, $\vec{f}_g$:

$$\vec{f}_g = m\vec{g} = (\pi/6)d_p^3\rho_s\vec{g} \qquad (3.8)$$

where ρ_s is the density of the particle, m the mass of the particle.

(4) The buoyancy force in the gravitational field, $\vec{f}_b$:

$$\vec{f}_b = (\pi/6)d_p^3\rho\vec{g} \qquad (3.9)$$

(5) The buoyancy force in a centrifugal field, $\vec{F}_b$:

$$\vec{F}_b = (\pi/6)d_p^3\rho\vec{r}\omega^2 \qquad (3.10)$$

(6) The effect of the hydrodynamic mass, M_h:

Regarding the total mass of a particle accelerating in a centrifugal field, the contribution of the hydrodynamic mass (or the added mass) should be taken into account since the surrounding fluid is also accelerated if the particle is accelerated. The hydrodynamic mass of a sphere equals one-half of its displaced mass (White, 1994). Thus:

$$M' = m + M_h = (\pi/6)d_p^3\rho_s + (\pi/12)d_p^3\rho \qquad (3.11)$$

where M' is the total mass of the particle, and M_h the hydrodynamic mass of the particle.

Using Newton's Second Law of motion, the behaviour of the particle in the radial direction (X-direction) can be generally described by:

$$F_c - F_{dx} - F_b = M'(du_{px}/dt) \qquad (3.12)$$

In the axial direction (Z-direction), it can be expressed by:

$$f_b + F_{dz} - f_g = M'(du_{pz}/dt) \qquad (3.13)$$

Because the magnitude of $\overrightarrow{u}_r$, which is the square root of $(u^2_{rx} + u^2_{ry} + u^2_{rz})$, will exist in the expressions of the drag for high Reynolds number flows and make the mathematical derivation complicated, discussion of the equations of motion of a moving particle in the KC will be limited to the Stokes Law or creeping flow region. The following sections summarize this mathematical analysis, while more details are given in Appendix 1.

3.2.2 The equation of motion in the radial direction in the Stokes' Law region

In the Stokes' Law region, the drag coefficient can be expressed by (Weber, 1998):

$$C_D = \frac{24}{Re_p} = \frac{24\mu}{\rho d_p |u_r|} \qquad (3.14)$$

Combining Equations 3.5 and 3.14 gives the X-component of the drag:

$$F_{dx} = 3\pi\mu d_p (u_{px} - u_{fx}) \qquad (3.15)$$

In this work, it is assumed that the components of fluid velocity $\bar{u}_f$ are constant. The X-component of particle velocity, u_{px}, is variable with time, that is:

$$u_{px} = dr/dt \qquad (3.16)$$

where r is the X-component of the displacement $\bar{r}$. Thus, Equation 3.15 can be expressed as:

$$F_{dx} = 3\pi\mu d_p\left(\frac{dr}{dt} + u_{fx}\right) \qquad (3.17)$$

Substituting Equations 3.1, 3.16, 3.17, 3.10 and 3.11 in Equation 3.12 and then rearranging yields the equation of motion in radial direction:

$$\frac{\pi}{6}d_p^3(\rho_s - \rho)r\omega^2 - 3\pi\mu d_p\left(\frac{dr}{dt} + u_{fx}\right) = \left(\frac{\pi}{6}d_p^3\rho_s + \frac{\pi}{12}d_p^3\rho\right)\frac{d^2r}{dt^2} \qquad (3.18)$$

Since u_{fx} is assumed invariable with time, Equation 3.18 is an ordinary differential equation containing only ordinary derivatives of r.

If the particle starts (t=0) at a radius r_1 with zero radial velocity (dr/dt =0), then the solution of Equation 3.18 is given by:

$$r = e^{-a_1 t/2}(r_1 - q_1)\left[\cosh k_1 t + \frac{a_1}{2k_1}\sinh k_1 t\right] + q_1 \qquad (3.19)$$

$$\text{where} \quad a_1 = \frac{18\mu}{d_p^2(\rho_s + \frac{\rho}{2})}, \quad k_1 = \sqrt{\frac{a_1^2}{4} + \frac{(\rho_s - \rho)\omega^2}{(\rho_s + \frac{\rho}{2})}}, \quad q_1 = \frac{18\mu u_{fx}}{d_p^2\omega^2(\rho_s - \rho)}$$

If the inertial term on the right-hand side of Equation 3.18 can be neglected (or when the instantaneous velocity is close to the terminal velocity), then the expression of the instantaneous velocity of the particle is:

$$\frac{dr}{dt} = \frac{d_p^2(\rho_s - \rho)r\omega^2}{18\mu} - u_{fx} \qquad (3.20)$$

Thus, the physical meaning of Equation 3.20 is that the instantaneous radial velocity of the particle is equal to the difference between the instantaneous velocity of the particle in the static water and the radial velocity of the fluid.

3.2.3 The equation of motion in the axial direction in the Stokes' Law region

The axial movement of a spherical particle (in Z-direction) towards the top of the KC inner bowl has been shown in Figure 3.3. The drag component in the Z-direction can be expressed by:

$$F_{dz} = 3\pi\mu d_p\left(\frac{dh}{dt} - u_{fz}\right) \qquad (3.21)$$

where h is the Z-component of the displacement $\vec{r}$.

Substituting Equations 3.8, 3.9 and 3.21 in Equation 3.13 and rearranging yields the equation of motion in the axial direction:

$$\frac{d^2h}{dt^2} + \frac{18\mu}{d_p^2(\rho_s + \frac{\rho}{2})}\frac{dh}{dt} - \frac{18\mu u_{fz} - d_p^2 g(\rho_s - \rho)}{d_p^2(\rho_s + \frac{\rho}{2})} = 0 \qquad (3.22)$$

If the particle starts at t=0, h=h_1, and dh/dt=0, then the solution of Equation 3.22 is as follows:

$$h = h_1 e^{-a_2 t/2}\left[\cosh k_2 t + \frac{a_2}{2k_2}\sinh k_2 t\right] \qquad (3.23)$$

$$\text{where } a_2 = \frac{18\mu}{d_p^2(\rho_s + \frac{\rho}{2})}; \qquad k_2 = \sqrt{\frac{a_2^2}{4} + \frac{18\mu u_{fz} - d_p^2 g(\rho_s - \rho)}{d_p^2(\rho_s + \frac{\rho}{2})}}$$

If the inertial term d^2h/dt^2 on the left-hand side of Equation 3.22 is equal to zero, the particle vertical velocity can be given by:

$$\frac{dh}{dt} = u_{fz} - \frac{d_p^2 g(\rho_s - \rho)}{18\mu} \qquad (3.24)$$

The second term on the right-hand side of Equation 3.24 is the well-known expression for the terminal settling velocity of a sphere in the Stokes' Law region, thus, it can be expected that the vertical (axial) velocity of the particle in the inner bowl is

equal to the difference between the axial velocity of the fluid and the terminal settling velocity of the particle in the gravity field.

Separating variables and then integrating Equation 3.24 gives the time for a particle to move up for a vertical distance of h:

$$t = \frac{h}{u_{fz} - \frac{d_p^2 g(\rho_s - \rho)}{18\mu}} \qquad (3.25)$$

Since particles of the feed slurry starts normally at the bottom of the inner bowl, the time taken for a particle to move to the top of the inner bowl, t_b, is equal to:

$$t_b = \frac{H}{u_{fz} - \frac{d_p^2 g(\rho_s - \rho)}{18\mu}} \qquad (3.26)$$

where H is the height of the inner bowl (assuming the full motion takes place in Stokes' Law region).

3.3 Comparison of the Maximum Radial Settling Velocities of Particles

Since a particle moving in a centrifuge never reaches an equilibrium velocity (Coulson et al, 1990), comparison of the radial settling velocities of particles in the Knelson is made in terms of the maximum radial settling velocity, which is calculated with Equation 3.20. In this work, the maximum radial settling velocity of a solid

particle in the Knelson, $u_{px\text{-}max}$, can be defined as the radial instantaneous settling velocity at the surface of the largest ring of the inner bowl, i.e. dr/dt when r = R. To simplify the calculation of $u_{px\text{-}max}$ with Equation 3.20, it was assumed that the X-component of fluid velocity is equal to the superficial velocity of fluidization flow, which is the volumetric flow rate of fluidization flow divided by the total lateral area of the five rings of the inner bowl. Figure 3-4 and Table A1.1 (in Appendix 1) show the calculated maximum radial settling velocities of tungsten, magnetite and silica particles as a function of particle size at Gs and fluidization flows that were shown to yield optimal operation in actual tests.

It can be seen in Figure 3-4 that the maximum radial settling velocities of all the three types of particles are positive over most of the size range, suggesting that most particles of different size and density will be able to settle on the concentrate bed if the retention time is long enough, and if particle-particle interactions are neglected. It also shows that the difference in radial settling velocity between high and low density particles becomes smaller with decreasing particle size. As a matter of fact, as will be shown in the following chapters, dense particles can be separated from lighter particles under conditions used in Figure 3-4. Furthermore, for the same dense material such as tungsten or magnetite, the difference in the maximum settling velocity between coarse and very fine particles is extreme; nevertheless the latter can be recovered well with the Knelson. Therefore, using the theory of centrifugal settling velocity to explain the recovery process is not complete and hardly convincing. This point of view is in

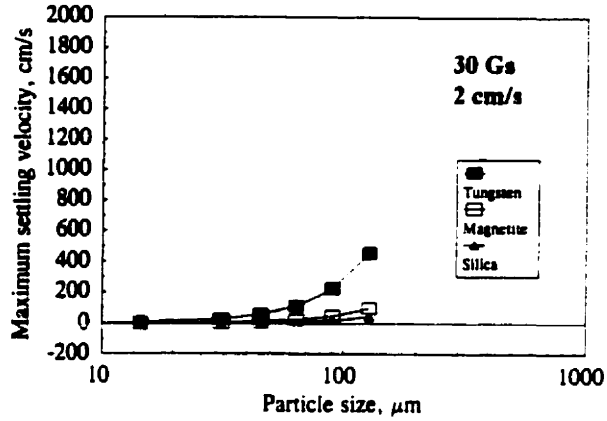

(a)

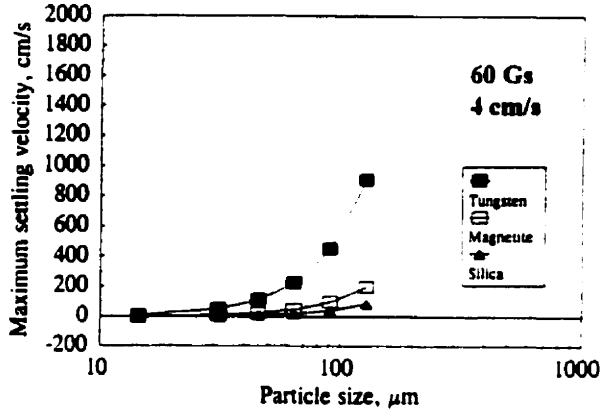

(b)

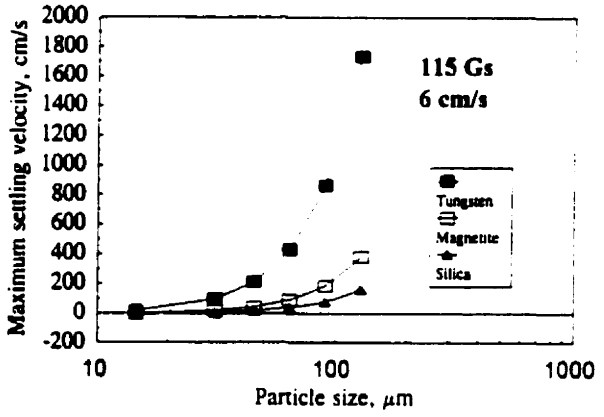

(c)

Figure 3-4 The calculated maximum radial settling velocities of particles as a function of particle size under conditions of (a) 30 Gs and a fluidization superficial velocity of 2 cm/s; (b) 60 Gs and a fluidization superficial velocity of 4 cm/s; (c) 115 Gs and a fluidization superficial velocity of 6 cm/s.

agreement with Huang's (1996), who had calculated the terminal settling velocity of particles in the absence of fluidization. As will be discussed below, another mechanism, percolation or migration of dense particles, must be invoked.

3.4 Percolation and Migration of a Dense Particle in the Separation Zone

3.4.1 Definition of particle percolation and migration

As defined by Bridgwater et al (1983), particle percolation can be defined as the drainage of small particles through a bed of coarser bulk particles, while particle migration is the passing of large particles through a bed of smaller bulk particles. Obviously, the voidage of a bulk particle bed is one of the important factors that affect particle percolation or migration since a suitable voidage is required for the particle to percolate or migrate successfully through the bulk bed. Where the bulk particles bed comes in contact with a counter-current fluid flow, the voidage is affected by the fluidization behaviour of the bed. Typically, as generalized by Davidson et al (1971), particles of low density, small size and spherical shape are more easily fluidized.

For the KC, the direction of particle percolation and/or migration is radial in the inner bowl due to the action of the centrifugal force. Percolation or migration may take place, depending on a number of variables such as the average particle size of the bed and dense particles, the voidage of the separation zone, momentum of the moving particle and the degree of fluidization.

3.4.2 The equation of motion for a particle percolating or migrating in the radial direction

3.4.2.1 Relation between the collision frequency and fractional voidage

Since the concentration of bulk particles increases as the spherical particle moves further from the dilute zone to the separation zone, a resistance or a dynamic friction force mainly due to inter-particle collision in the separation zone should be added in Equation 3.12. The collision frequency of a moving spherical particle in the separation zone of the inner bowl can be the analogy of the kinetic theory of gases (Serway, 1996), that is:

$$f = \pi d^2 \mid \overline{u}_p \mid n_v \qquad (3.27)$$

where f is the collision frequency, or the number of collisions per second; d is the distance between the centres of the moving particle and bulk particle; n_v is the number of the bulk particles per unit volume.

The fractional voidage of the separation zone, ϵ, can be expressed by:

$$\epsilon = 1 - \frac{V_T n_v \frac{\pi}{6} d_b^3}{V_T} \qquad (3.28)$$

where d_b is the average diameter of the bulk particles in the separation zone, V_T the volume of the separation zone.

Thus, the number of the bulk particles per unit volume can be expressed by:

$$n_v = \frac{6(1-\epsilon)}{\pi d_b^3} \qquad (3.29)$$

Inserting Equation 3.29 in Equation 3.27 and rearranging gives:

$$f = \frac{3|\vec{u}_p|(d_p + d_b)^2(1-\epsilon)}{2d_b^3} \qquad (3.30)$$

3.4.2.2 The expression of the dynamic friction force

The dynamic friction force $\vec{F}_L$ proposed in this work may be a function of the momentum of the percolating or migrating particle and collision frequency:

$$\vec{F}_L = C_L f m \vec{u}_p \qquad (3.31)$$

where C_L is the dynamic coefficient of friction between the bulk and percolating or migrating particles, a concept proposed in this work based on the hypothesis that percolation velocity is a function of the ratio of percolating to bulk particle densities (Bridgwater, 1983), and takes the form:

$$C_L = \frac{k_p \rho_b}{\epsilon \rho_s} \qquad (3.32)$$

where k_p is a dimensionless correction factor; ρ_b is the density of bulk particles.

If C_P is used to stand for all the constants in Equation 3.31 (the fractional voidage, ϵ, is supposed to be constant), the dynamic friction force $\vec{F}_L$ can be expressed by:

$$\vec{F}_L = C_p|\vec{u}_p|\vec{u}_p \qquad (3.33)$$

$$where \quad C_p = \frac{3k_p\rho_b(d_p+d_b)^2(1-\epsilon)}{2\epsilon\rho_s d_b^3} \qquad (3.34)$$

The X-component of $\vec{F}_L$ can be expressed by:

$$F_{Lx} = C_p\left|\frac{d\vec{r}}{dt}\right|\frac{dr}{dt} \qquad (3.35)$$

The Z-component of $\vec{F}_L$ can be expressed by:

$$F_{Lz} = C_p\left|\frac{d\vec{h}}{dt}\right|\frac{dh}{dt} \qquad (3.36)$$

3.4.2.3 The equation of motion in the radial direction in the Stokes' Law region

Since the action of fluidization flow is more significant in the separation zone than in the dilute zone, it is assumed that the X-component of fluid velocity is approximately equal to the interstitial velocity of fluidization flow with respect to the wall of the system, denoted by u_i. This interstitial velocity of fluidization flow is a function of the fractional voidage and can be expressed by (Witteveen, 1995):

$$u_i = \frac{U_F}{\epsilon} \qquad (3.37)$$

where U_F is the superficial fluid velocity, which is the fluid flow rate divided by the lateral area of the bowl rings and has units of cm/s.

The equation of motion in radial direction in the separation zone is given by:

$$\frac{\pi}{6}d_p^3(\rho_s-\rho)r\omega^2-3\pi\mu d_p\left(\frac{dr}{dt}+u_i\right)-C_p\left(\frac{dr}{dt}\right)^2=\left(\frac{\pi}{6}d_p^3\rho_s+\frac{\pi}{12}d_p^3\rho\right)\frac{d^2r}{dt^2} \qquad (3.38)$$

Assuming that the centrifugal acceleration of the particle, $r\omega^2$, is constant, the above nonlinear differential equation with constant coefficients becomes:

$$\frac{d^2r}{dt^2}+\frac{6C_p}{\pi d_p^3(\rho_s+\frac{\rho}{2})}\left(\frac{dr}{dt}\right)^2+\frac{18\mu}{d_p^2(\rho_s+\rho)}\frac{dr}{dt}+\frac{-d_p^2(\rho_s-\rho)r\omega^2+18\mu u_i}{d_p^2(\rho_s+\frac{\rho}{2})}=0 \qquad (3.39)$$

or

$$\frac{d^2r}{dt^2}+a_3\left(\frac{dr}{dt}\right)^2+b_3\frac{dr}{dt}+m_3=0 \qquad (3.40)$$

$$\text{where}\quad a_3=\frac{6C_p}{\pi d_p^3(\rho_s+\frac{\rho}{2})},\quad b_3=\frac{18\mu}{d_p^2(\rho_s+\frac{\rho}{2})},\quad m_3=\frac{-d_p^2(\rho_s+\rho)r\omega^2+18\mu u_i}{d_p^2(\rho_s+\frac{\rho}{2})}$$

When the particle starts at $t = 0$, $r = r_1$, and $dr/dt = u_{px0}$, the solution is given as follows:

$$r = \frac{b_3 + k_3}{2k_3a_3}\ln(1 - C_5e^{-k_3t}) - \frac{b_3 - k_3}{2k_3a_3}\ln\frac{1 - C_5e^{-k_3t}}{C_5e^{-k_3t}} + C_6 \qquad (3.41)$$

where $k_3 = \sqrt{b_3^2 - 4a_3m_3}$, $C_5 = \dfrac{2a_3u_{px0} + b_3 - k_3}{2a_3u_{px0} + b_3 + k_3}$,

$$C_6 = r_1 - \frac{b_3 + k_3}{2k_3a_3}\ln\frac{2k_3}{2a_3u_{px0} + b_3 + k_3} - \frac{b_3 - k_3}{2k_3a_3}\ln\frac{2k_3}{2a_3u_{px0} + b_3 - k_3} .$$

If the inertial term on the right-hand side of Equation 3.38 can be neglected (or when the instantaneous velocity is close to the terminal velocity), then the instantaneous velocity takes the form:

$$\frac{dr}{dt} = \sqrt{\left(\frac{3\pi\mu d_p}{2C_p}\right)^2 + \frac{\pi d_p^2(\rho_s - \rho)r\omega^2 - 18\pi\mu u_t}{6d_pC_p}} - \frac{3\pi\mu d_p}{2C_p} \qquad (3.42)$$

Equation 3.42 can not be confirmed at present since the dynamic coefficient of friction, C_L, is unknown. It is recommended that the correction factor k_p be determined with extensive experiments in the future.

3.4.3 The equation of motion for a particle moving up the inner bowl along the separation zone

To simplify the following discussion, the coordinates will be shifted 15 degrees (0.26 radian) so as to enable the Z-direction to be parallel to the wall of the inner bowl, which is denoted by the Z'-direction. As shown in Figure 3.5, there are five main

which is denoted by the Z'-direction. As shown in Figure 3.5, there are five main forces on the particle moving in the Z' direction in the separation zone (plus the effect of the hydrodynamic mass):

(1) The Z'-component of the centrifugal force:

$$F_c \text{ Sin } \alpha = (\pi/6)\, d_p^3 \rho_s r \omega^2 \sin \alpha \qquad (3.43)$$

where α is the slope angle of the bowl wall, equal to 15 degrees (0.26 rad).

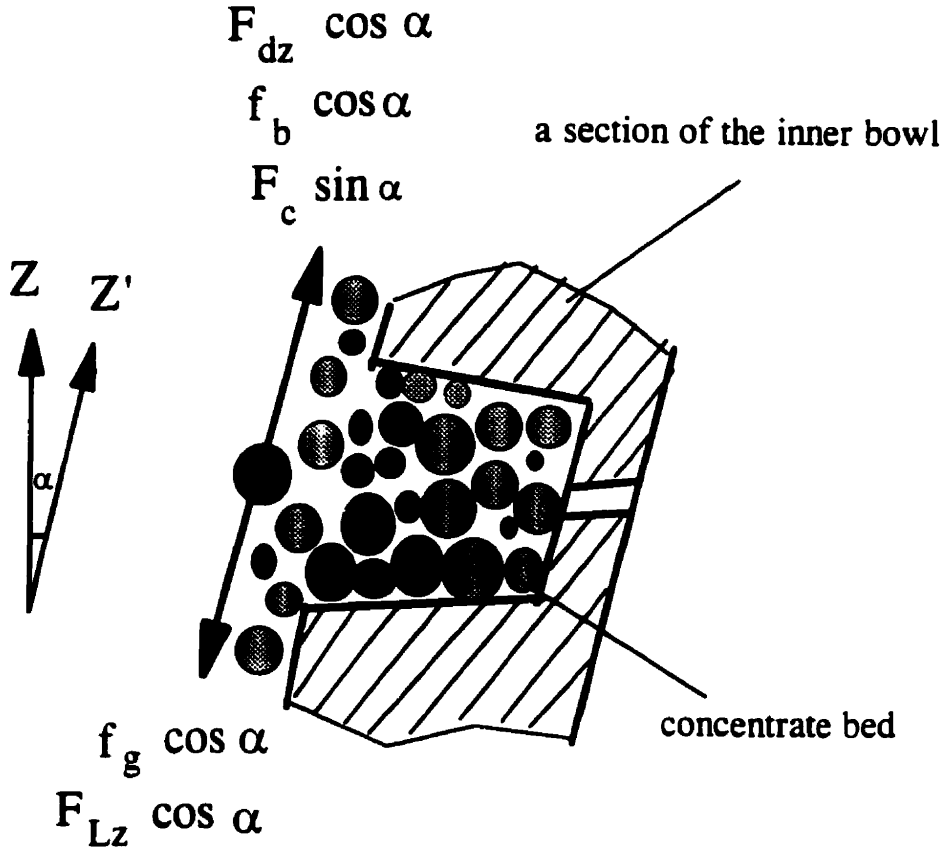

Figure 3-5 Forces on a particle in the Z'- direction

(2) The Z'-component of the gravity force:

$$f_g \cos\alpha = (\pi/6)\, d_p^3 \rho_s g \cos\alpha \qquad (3.44)$$

(3) The Z'-component of the drag:

$$F_{dz}\cos\alpha = \frac{\pi d_p^2}{4}\frac{C_D}{2}\rho |u_r|(u_{pz} - u_{fz})\cos\alpha \qquad (3.45)$$

The Z'-component of the drag in the Stokes' Law region is given by:

$$F_{dz}\cos\alpha = 3\pi\mu d_p\left(u_{fz}\cos\alpha - \frac{dh'}{dt}\right) \qquad (3.46)$$

where h' is the Z'-component of the particle displacement $\vec{r}$.

(4) The Z'-component of the buoyancy force in the gravity field:

$$f_b \cos\alpha = (\pi/6) d_p^3 \rho g \cos\alpha \qquad (3.47)$$

(5) The Z'-component of the dynamic friction force:

$$F_{Lz}\cos\alpha = C_P\left|\frac{d\vec{h}}{dt}\right|\frac{dh}{dt}\cos\alpha = \frac{C_P}{\cos\alpha}\left(\frac{dh'}{dt}\right)^2 \qquad (3.48)$$

Thus, based on Newton's Second Law of motion, the equation of motion for the particle moving up along the separation zone is expressed by:

$$\frac{\pi}{6}d_p^3\rho_s r\omega^2\sin\alpha - \frac{\pi}{6}d_p^3\rho_s g\cos\alpha + 3\pi\mu d_p\left(u_{fz}\cos\alpha - \frac{dh'}{dt}\right)$$

$$+\frac{\pi}{6}d_p^3\rho g\cos\alpha - \frac{C_P}{\cos\alpha}\left(\frac{dh'}{dt}\right)^2 = \frac{\pi}{6}d_p^3(\rho_s+\frac{\rho}{2})\frac{d^2h'}{dt^2} \qquad (3.49)$$

Assuming that the centrifugal acceleration of the particle ($r\omega^2$) is constant, and that when $t = 0$, $h' = h'_1$, and $dh'/dt = u_{pz0}$ (the initial velocity larger than zero), the solution can be obtained using the same approach as for Equation 3.38 and is expressed by:

$$h' = \frac{b_4+k_4}{2k_4a_4}\ln(1-C_7e^{-k_4t}) - \frac{b_4-k_4}{2k_4a_4}\ln\frac{1-C_7e^{-k_4t}}{C_7e^{-k_4t}} + C_8 \qquad (3.50)$$

where $C_7 = \dfrac{2a_4u_{pz0}-b_4-k_4}{2a_4u_{pz0}-b_4+k_4}$, $k_4 = \sqrt{b_4^2-4m_4a_4}$,

$$C_8 = h_1 - \frac{b_4+k_4}{2k_4a_4}\ln\frac{2k_4}{2a_4u_{pz0}+b_4+k_4} - \frac{b_4-k_4}{2k_4a_4}\ln\frac{2k_4}{2a_4u_{pz0}+b_4-k_4}.$$

where $a_4 = \dfrac{6\cos\alpha\, C_P}{\pi d_p^3(\rho_s+\frac{\rho}{2})}$, $b_4 = \dfrac{18\mu}{d_p^2(\rho_s+\frac{\rho}{2})}$,

$$m_4 = \frac{\sin\alpha d_p^2\rho_s r\omega^2 + 18\mu u_{fz}\cos\alpha - g d_p^2(\rho_s-\rho)\cos\alpha}{d_p^2(\rho_s+\rho/2)}.$$

To confirm the above solution, it is recommended that the dynamic coefficient of friction, C_L, be determined with extensive experiments in the future.

3.5 The equation of the tangential velocity of the particle

It is assumed that the tangential movement of the particle in the inner bowl is a uniform circular motion. Thus, the tangential velocity (or the velocity in the Y-direction), u_{py}, has the relationship:

$$u_{py} = r\omega \qquad (3.51)$$

3.6 Conclusion

The equations for determining the instantaneous velocities of a spherical solid particle in the Knelson centrifugal concentrator (KC) have been tentatively derived based on Newton's Second Law of motion. Since the mathematical analysis was carried out in the presence of radial fluidization flow, which made the differential equation more complex, the derivation may be considered an extension to the theory of centrifugal separation of solid particles in the presence of a static liquid described by Coulson et al (1990).

Although the solutions of the equations of motion were derived only for the Stokes' Law region, their physical meaning might be applied to the particle motion in high Reynolds number flows. It can be expected from the equations of motion for a

spherical particle in the radial direction that the instantaneous radial settling velocity and percolation (or migration) velocity of a particle moving in the inner bowl of the KC depend not only on the centrifugal acceleration, particle size and density, but also on the fluidization flow velocity. This suggests that it is possible to reduce significantly both the settling and percolation (or migration) velocities of gangue particles by controlling the rotating speed of the KC and fluidization flow so as to acquire a satisfactory recovery of dense particles from light particles.

It is also inferred from the equations of motion for the particle in the axial direction that the magnitude of the axial velocity of a particle is a function of centrifugal acceleration, the axial velocity of the following film, and the physical characteristics of the particle. Conversely, the retention time of a particle or the height of the inner bowl may be estimated if the vertical velocity of the particle is known.

As a whole, the balance between the ability of the KC to increase the radial settling and percolating velocity of dense particles and to decrease the retention time of gangue particles without unacceptably eroding dense particles already captured is quite a delicate process. Among the variables which might affect this balance, the centrifugal acceleration of the KC and appropriate fluidization of the flowing slurry are the most critical.

It was noted that the maximum radial settling velocity in the dilute zone could not explain the selectivity normally observed in Knelson concentrates. Huang (1996) had observed the same phenomenon, but he had assumed static flow, which clearly is incorrect for finest particle sizes and operating conditions. As a result, apparent settling rates (i.e. percolation and migration rates) in the zone closer to the concentrate bed, where most particles are rejected, will determine how selective the recovery is (hence this zone, as well as the inner section of the concentrate bed, is referred to as the separation zone). Unfortunately, the percolation and migration rates cannot be derived from Newton's Second Law of motion. In this work, it is proposed that a dynamic friction force can be used to aid the description of particle percolation and migration. Testwork will be conducted to determine separation performance, and then analyzed using the proposed concept.

CHAPTER 4 PERCOLATION AND MIGRATION OF DENSE PARTICLES IN THE GRAVITATIONAL FIELD

4.1 Introduction

Percolation and migration of dense particles into a bulk material bed are quite common phenomena in mineral processing. They can take place in gravity concentrators such as a jig, a sluice, a shaking table, or a centrifuge. Percolation and migration can also be observed when screening, grinding, feeding, mixing, and even transporting mineral materials, either wet or dry. For the Knelson Concentrator, centrifugal percolation and migration of gold into a concentrate bed of the inner bowl are especially important because they largely determine its performance. As mentioned in Chapter 2, the fundamentals of percolation in the gravitational field have many obvious analogies to centrifugal percolation, including the necessity for voidage of the bulk bed and the effect of solid particle properties. Moreover, gravitational percolation is more easily observed and measured than centrifugal percolation since the movement of particles in a bulk bed in the gravity field can be created in a stationary transparent tube. Percolation and migration of dense particles in the gravitational field (one g) was conducted in this work in order to gain insight into the behaviour of dense particles percolating or migrating in the inner bowl of the KC. Since the gold grade of the KC feed is usually very low (normally below 0.01%, or 100 g/t), gold particles percolate

or migrate through a material essentially made up of gangue particles. This is the system which this first phase of research sought to mimic.

Systems where gold is separated from silicates (s.g. 2.7-3) or sulphides (s.g. 5) display a significant s.g. differential. A third system with a much lower s.g. differential was also investigated: magnetite was used to mimic the dense phase, and silica the lighter one. This lower s.g. differential is very common in mineral processing, and corresponds to a large number of mineral separations, some at very large capacities (e.g. hematite-quartz, or many other oxide-silicate separations).

4.2 Experimental Methodology

4.2.1 Materials and device

Grey polyhedral tungsten particles from the Zhuzhou Cemented Carbide Work of China, with a tungsten content of $\geq 99.92\%$, and a density of 17.98 g/cm^3, were used to mimic natural gold. Three sizes of the tungsten, with the maximum size fraction between 4.8 and 1.4 mm, were purchased so as to test a wide size distribution. In Appendix 2, the natural appearance of these tungsten particles, in the 300-425 μm size fraction, is shown in Figure A2-1. SEM back-scattered images of 25-38 μm and -25 μm tungsten particles are also shown in Figures A2-2 and A2-3. It can be seen in these photographs that most of the tungsten particles are irregular in shape, with a submetallic lustre.

Magnetite (with a density of 4.78 g/cm^3) and minor amounts of coarse (>425 μm) hematite (with a density close to that of magnetite) from Iron Ore of Canada Ltd. (Carol Lake plant) were used as the dense 'desired' mineral or dense gangue, after wet cleaning with a hand magnet.

Silica sand (with a density of 2.65 g/cm^3) from Unimin Canada Ltd. was used as low density gangue; to achieve the desired size distribution, some was ground, and then combined with finer silica sand and cleaned with a LKC (Laboratory Knelson Concentrator) and a hand magnet to remove both heavy and magnetic impurities.

The three feed materials were individually screened into separate size fractions. The minus 25 μm size fraction of tungsten was further classified with a Warman cyclosizer to remove the minus 4 μm fraction.

The device used for observation and measurement of the percolation and migration of dense particles in a gangue bed was a cylindrical vertical fluidization column made of plexiglass. It was modified for this work from the design described by Couderc (1985). Figure 4-1 shows the dimensions of the modified column. Essentially, it is composed of two sections, the upper and lower sections, which are connected tightly by a pair of flanges and a rubber ring during testing. The distributor consists of an evenly perforated plexiglass plate covered by a 106 μm (150 mesh) metal screen, and is mounted inside the lower section of the column.

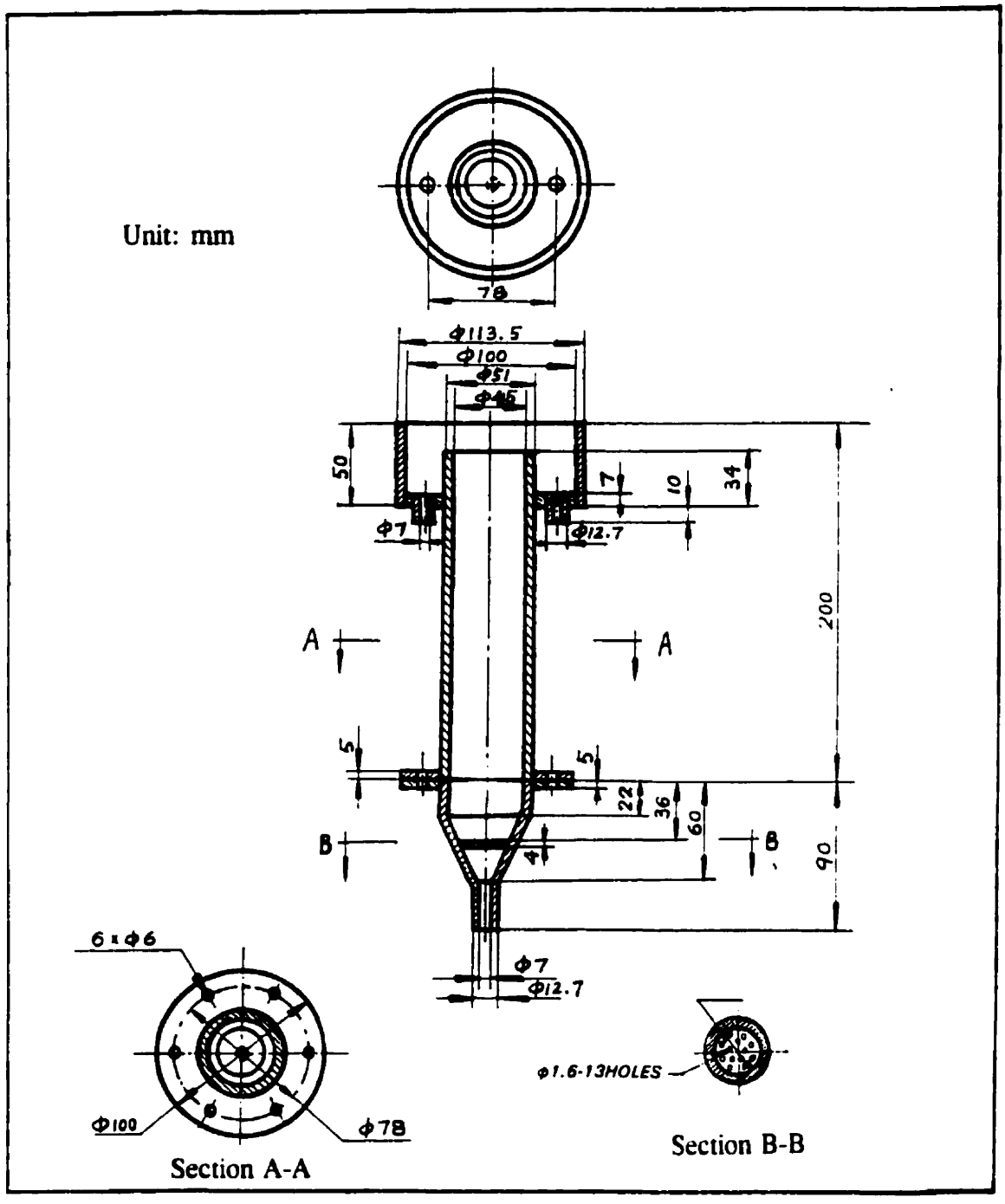

Figure 4-1 Engineering drawing of the fluidization column

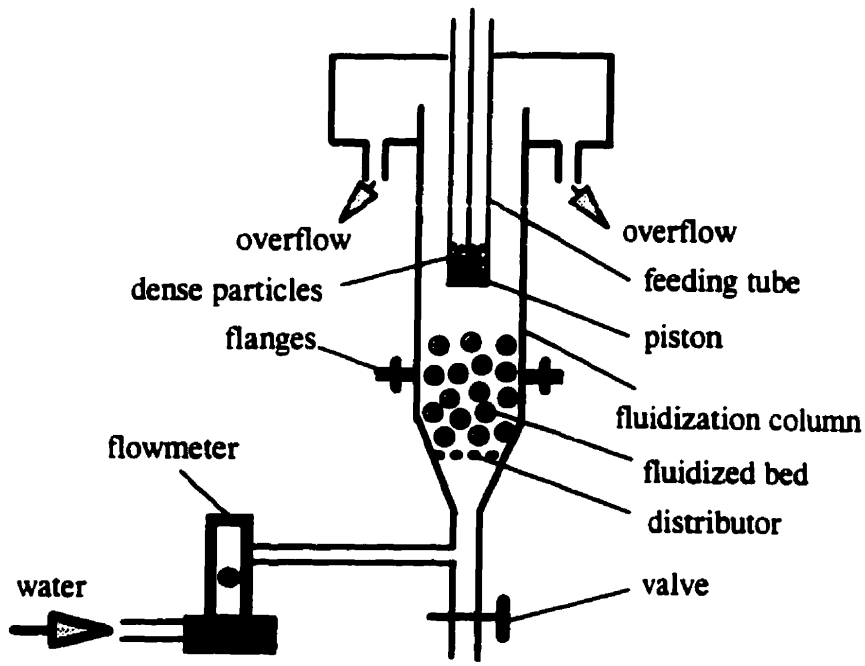

Figure 4-2 Experimental setup for percolation and migration measurement

4.2.2 Methodology

Figure 4-2 illustrates the experimental setup for percolation and migration measurement. At the beginning of each test, 80 grams of silica or 145 grams of magnetite/hematite of monosize gangue particles was added into the column and fluidization water was introduced to the bottom of the column at a high flow rate for 5 minutes so as to remove air bubbles from the system. A small amount (2 grams of tungsten or 1 gram of magnetite/hematite) of monosize dense particles was loaded in the feeding tube along with a given amount of water. The tube was shaken manually until

the dense particle surface had been wetted (in the case of dense particles of very fine size, a few drops of 0.1% Aerosol OT solution were added to the pulp inside the feeding tube to aid the wetting process). Then, fluidization flowrate was adjusted at a given reading; the feeding tube was placed and held at 4.35-4.50 cm above the surface of the gangue bed in the fluidization column. Next, the dense particles were fed by pressing the piston away from the feeding tube. Time was counted as soon as dense particles touched the gangue bed, and the test was stopped at a given time by turning off the fluidization flow. After gradually and slowly discharging water inside the column from the bottom valve, materials in the upper and lower sections of the column were cut off manually from their interface between the flanges and then flushed into two separate containers. Material inside the lower section, accounting for about two thirds of the gangue particles, was analyzed for the recovery of percolated or migrated dense particles by means of a Mozley table, a hand magnet, or by screening. (The accuracy of this approach will be discussed in Chapter 6.) Each test was repeated once, and the recovery of dense particles was averaged; the amount of dense particles that had percolated or migrated and still remained in the upper section of the gangue bed was not measured.

4.3 Results and Discussion

4.3.1 Relation between the height of the gangue bed and fluidization fluid velocity

The height of the particle bed affected by upward fluidization flow is useful for definition of the behaviour of the particle bed. To investigate the expansion

phenomenon, i.e. characteristic of fluidised beds, the height of the gangue bed was measured at different fluidization flow rates without adding dense particles. Figure 4-3 is a graph of the height of the gangue bed as a function of superficial fluid velocity[1] for four types of gangue beds with two monosizes (+212-300 μm and +600-850 μm) and two densities (2.65 and 4.78 g/cm^3). It can be seen that, as fluid velocity increased, the height of the bed increased at different rates depending on both particle size and solid density. In fact, each bed experienced expansion with increasing fluid velocity and began to fluidize at a certain fluid velocity. This incipient fluidization condition could not be identified as precisely as that of the ideal system described by Couderc (1985), since there was an intermediate region on each curve where the bed was partially fluidized. However, the minimum fluidization velocity, U_{mf}, at which fluidization of the bed begins, could be determined visually. Its magnitude varied from 0.2 to 2.4 cm/sec, in the order[2] of 212 μmsilica, 600 μm silica, 212 μm magnetite, and 600 μm hematite. As fluid velocity was further increased, channelling of the bed took place due to uneven fluid velocity distribution over the cross section of the column. Generally, fine gangue particles could reach a well-fluidized state more easily than coarser gangue particles could; a low density gangue bed was easier to fluidize and expand than with a higher

[1] The flowrate divided by the cross section area of the fluidization column.

[2] The lower size limit of the size fraction.

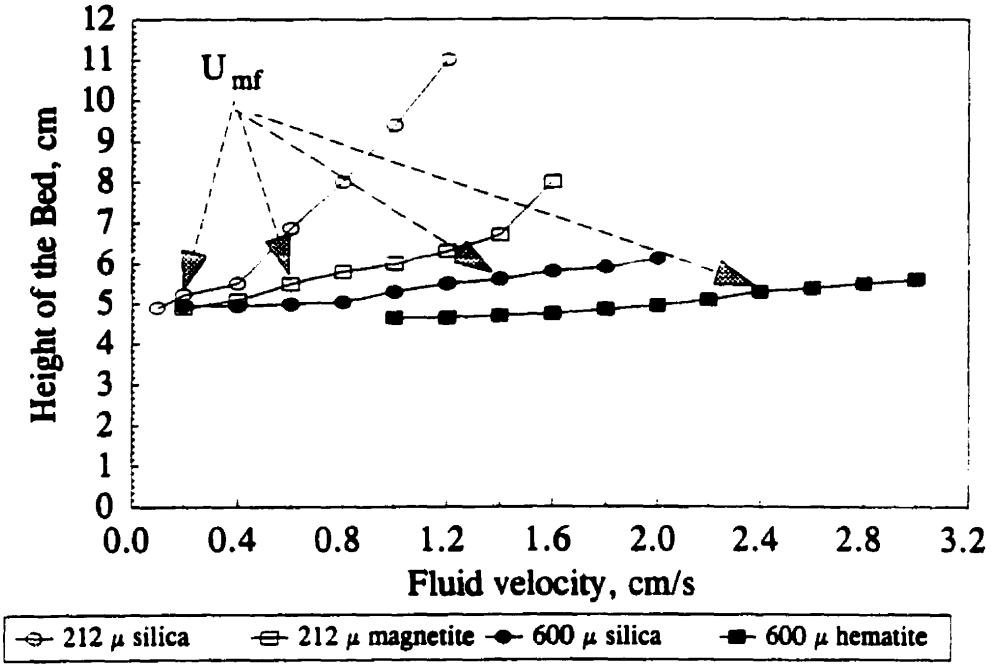

Figure 4-3 Height of the gangue bed as a function of fluid velocity

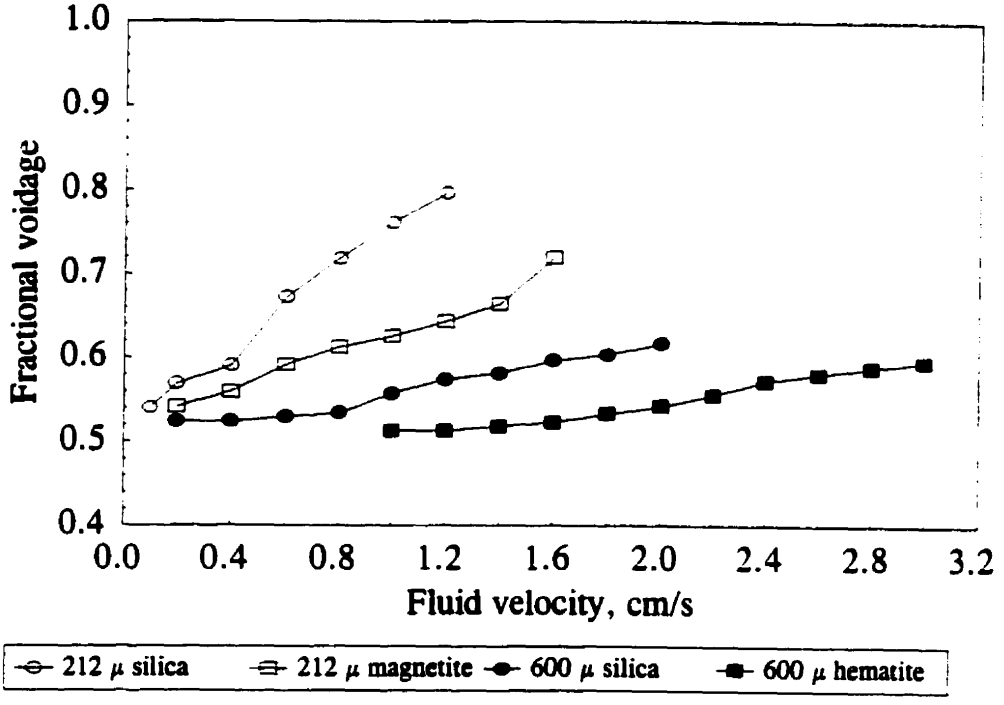

Figure 4-4 Fractional voidage of gangue bed as a function of fluid velocity

density gangue. This observation of particle behaviour was in a good agreement with the conclusions of the properties of the solid made by Richardson (1971).

As a particles bed expands, the voidage of a bed will change. The following equation can be used to calculate the fractional voidage (ϵ) of a particle bed.

$$\epsilon = \frac{V_l}{V_b} = \frac{V_b - V_s}{V_b} \qquad (4.1)$$

where V_l is the volume of the bed not occupied by solid material, V_s the volume of solid material, and V_b the volume of the bed.

Figure 4-4 shows the fractional voidage of these four types of gangue beds, calculated from Equation 4.1, as a function of superficial fluid velocity. The fractional voidage of the fine or low density gangue bed was more easily increased than that of the coarser or higher density gangue bed. For the 600 μm magnetite, the fractional voidage increased by only 0.09 at a fluid velocity of 3.0 cm/s compared to that measured at a zero fluid velocity, whereas for the 212 μm silica, a fluid velocity of 1.0 cm/s created an increase of a fractional voidage of 0.28.

4.3.2 Relation between tungsten recovery and the percolation (or migration) time

With a coarse silica (600-850 μm) bed at fluid velocities of 0.8 and 1.4 cm/s, the recovery of tungsten (106 μm and 600 μm) was measured as a function of time. Results are shown in Figure 4-5. As shown, tungsten recovery increased with increasing

percolation (or migration) time. Two observations can be made from Figure 4-5. The first is that at the same fluid velocity (0.8 cm/s), where the bed was partially fluidized, the recovery of 600 μm tungsten was higher than that of the 106 μm fraction. This indicated that under conditions of partial fluidization, the mass of a tungsten particle had a positive effect on the percolation rate. The second observation is that for the same size fraction (i.e., 106 μm) of tungsten, when the fluid velocity was as high as 1.4 cm/s (i.e., the minimum fluidizing velocity, U_{mf}, for 600 μm silica), recovery could quickly reach 78% within 5 seconds, while it took 60 seconds for the same tungsten particles to reach the same recovery at 0.8 cm/s of fluid velocity. The percolation (or migration) rate of tungsten at U_{mf} was higher than at a lower fluid velocity. This behaviour can be attributed to the increase of voidage of the bed when fluid velocity increased.

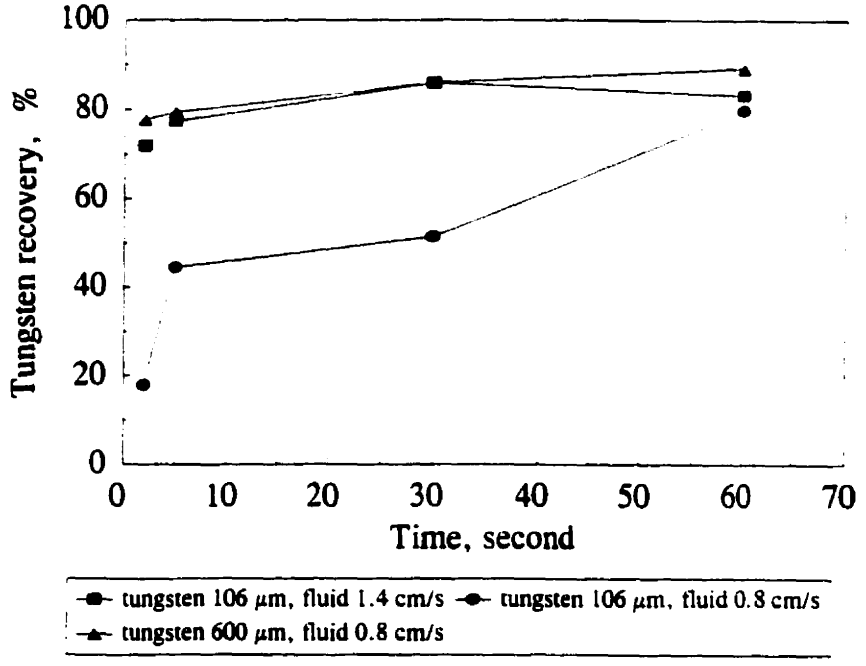

Figure 4-5 Tungsten recovery as a function of time (fluidized bed: 80 grams of 600-850 μm silica)

4.3.3 Effect of particle size and gangue density on percolation and migration of tungsten

(1) Percolation and migration in fine gangue beds

Figure 4-6 shows tungsten recovery as a function of tungsten particle diameter for 212-300 μm silica and magnetite beds. For silica, tungsten percolated quite well for all sizes even at a very low fluid velocity (0.1 cm/s), where the gangue bed was only partially fluidized. Since the fractional voidage of the bed at this low fluid velocity was as low as 0.54 (fractional voidage in the stagnant water was 0.52), the main reason for the high tungsten recovery may be related to the low density and small size of the silica, which resulted in a very low resistance to the motion of tungsten particles. It was

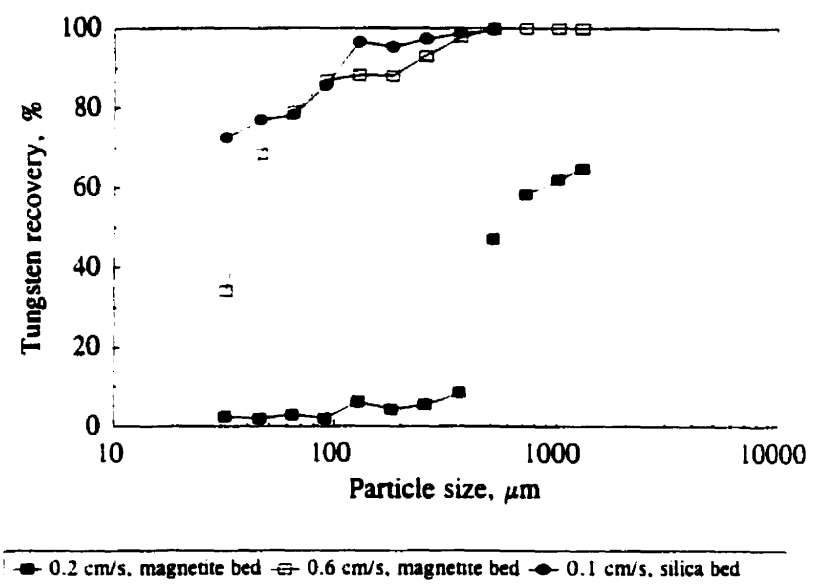

Figure 4-6 Tungsten recovery as a function of particle size for two types of fine gangue beds (212-300 μm silica and magnetite, time: 30 s)

observed during the measurement that most sizes of tungsten could pass through the fine silica bed easily. This indicates that the resistance or the dynamic friction force of the bulk particles to the movement of tungsten is not only a function of the bed voidage but also a function of the size and density of the bulk particles.

For the magnetite bed, at fluid velocity of 0.2 cm/s, tungsten particles below 425 μm could almost not percolate. Above 425 μm, the recovery increased up to 64% as tungsten particle size increased to 1180-1670 μm. It was observed during the testing that these very coarse tungsten particles pushed gangue particles aside and then buried themselves inside the partially fluidized gangue bed, rather than passing through the interstices of the bed. Therefore, it might be deduced that coarse tungsten migrated into the gangue bed in an intrusive manner, the result of high particle mass and settling velocity. When fluid velocity increased further to 0.6 cm/s, which was more than 5 times the flow rate for the silica bed on the same graph, the recovery increased significantly for all sizes of tungsten, as a result of the increased voidage of the gangue bed.

(2) Percolation and migration in coarse gangue beds

Figure 4-7 consists of two graphs presenting tungsten recovery as a function of particle size for two types of coarse gangue bed, 600-850 μm silica and hematite. For coarse silica, as seen in the upper graph, at a fluid velocity of 0.7 cm/s, the recovery of tungsten particles below 850 μm was almost nil, which means that they could not

percolate or migrate because at this low flow rate the bed was almost packed. However, tungsten recovery increased up to 87% for the 850-1670 μm size fraction, indicating that these particles were able to intrude into the gangue bed due to their very high mass or momentum. When the fluid velocity increased to 0.8 and 1.4 cm/s, where the silica bed was partially or well fluidized, tungsten recovery increased significantly, except for the -38 μm size fraction. As a reference, Table A2.1 of Appendix 2 lists the terminal free settling velocities of tungsten, magnetite and silica for different size fractions, calculated for the -106 μm size fractions in the Stoke's law region and the +106 μm size fractions in the intermediate region. It can be seen in Table A2.1 that the terminal free settling velocity for the 25-38 μm tungsten is 0.9 cm/s. Thus, the recovery of this very fine tungsten dropped as fluid velocity increased to 1.4 cm/s. Experimental observation also showed that there was some of the -38 μm tungsten lost in the overflow.

In the case of the hematite bed, as seen in the lower graph of Figure 4-7, at a superficial fluid velocity of 1.4 cm/s, where the bed was still highly fixed, the recovery of tungsten below 425 μm was almost nil for all sizes. As fluid velocity increased to 2.4 cm/s, where the hematite bed was well fluidized, tungsten particles above 75 μm percolated and migrated well. But those below 75 μm had a very low percolation velocity, especially for the -53 μm tungsten whose terminal free settling velocity is below 2.0 cm/s (as shown in Table A2.1). Comparing the results of the hematite bed with that of the silica bed, it can be expected that high density gangue, especially at coarse size, has a detrimental effect on the percolation of the fine dense particles.

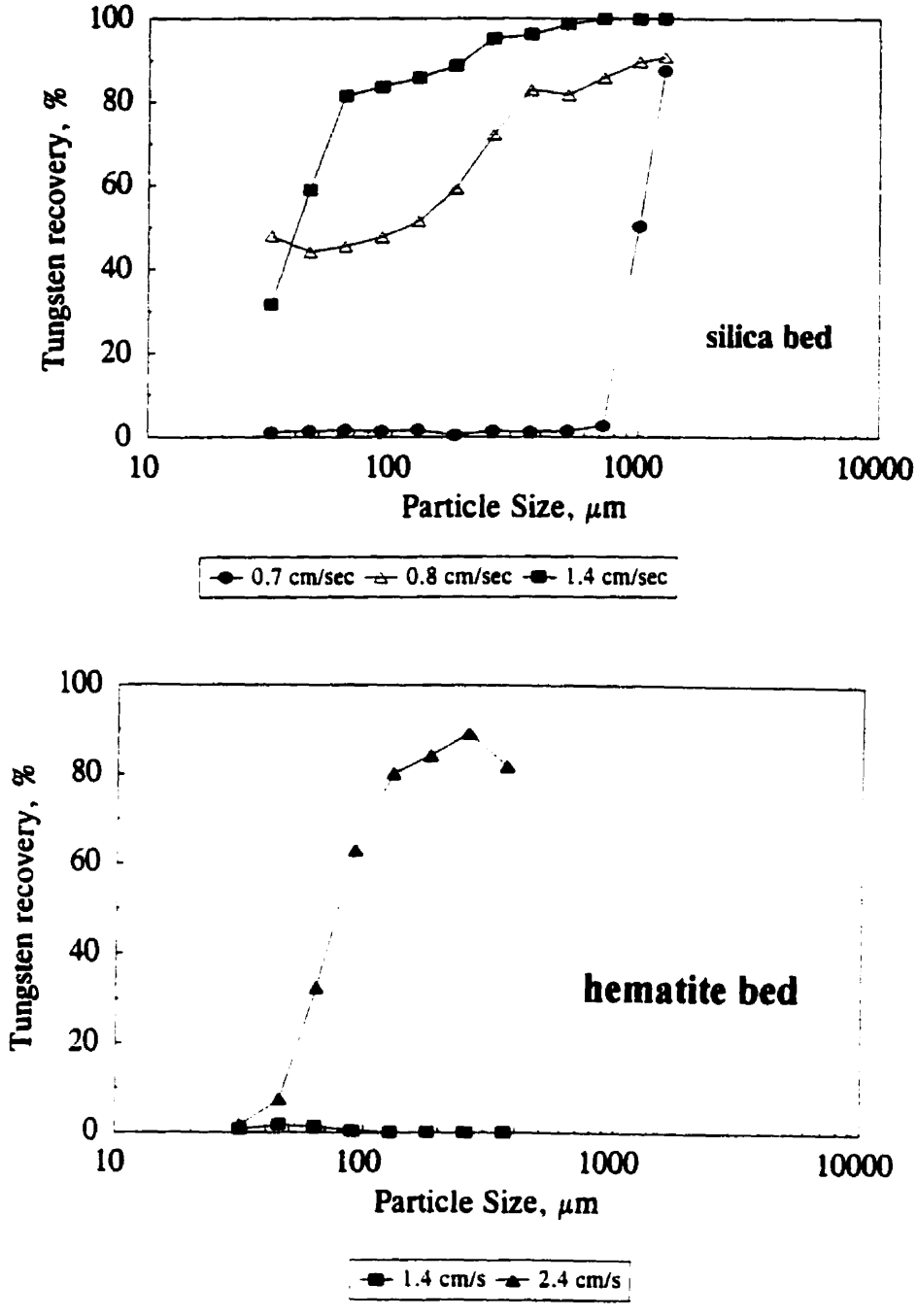

Figure 4-7 Tungsten recovery as a function of particle size in two types of coarse gangue beds (600-850 μm silica or hematite; time: 30 s)

4.3.4 Effect of particle size on percolation and migration of magnetite in a silica bed

This section deals with the third system, i.e. a system with a relatively lower s.g. differential than the two systems discussed above. Figure 4-8 illustrates magnetite recovery as a function of particle size for a coarse (600-850 μm) silica bed of three different fluidization velocities, 0.8, 1.4, and 2.0 cm/s (corresponding to the fractional voidages of 0.53, 0.58 and 0.61, as shown in Figure 4-4). Magnetite recovery increased considerably as fluid velocity increased from 0.8 to 1.4 cm/s, except for very fine magnetite, which, as shown in Table A2.1, has a terminal free settling velocity much lower than the fluid velocity of 1.4 cm/s. As fluid velocity increased to 2.0 cm/s, the recovery of magnetite below 150 μm was lower than at lower water flow rates (1.4 cm/s). This indicates that the reocvery of the -150 μm magnetite no longer increased with increasing fractional voidage when fluid velocity was up to 2.0 cm/s. In fact, it can be expected that there was a delicate balance between the percolation (or migration) velocity and the fluid velocity. In other words, if fluid velocity was too low, there was not enough voidage in the bed for tungsten to percolate or migrate, and if fluid velocity was too high, the settling and percolation (or migration) velocities of finer sizes of magnetite were dramatically reduced.

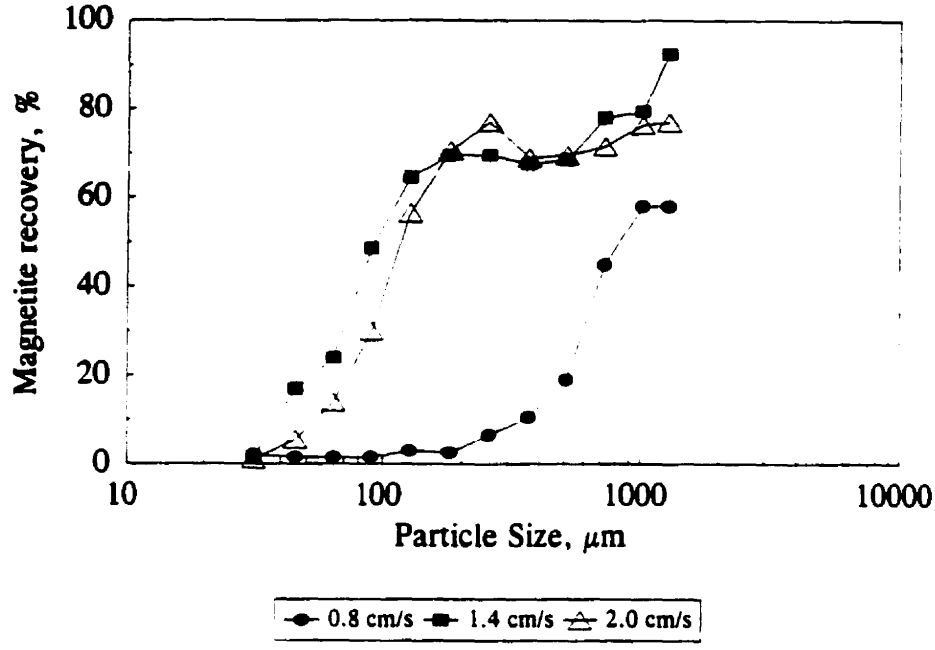

Figure 4-8 Mass of percolated magnetite as a function of particle size (fluidized bed: 80 grams of 600-850 μm silica; percolation time: 30 s)

Comparing Figures 4-7 (a) and 4-8, at a fluid flow of 1.4 cm/s, it can be seen that particles of lower density percolated more slowly than those of very high density. The difference in the recovery was small, since the percolation (or migration) time (30 seconds) was long enough to enable more magnetite particles to percolate when the bed was well fluidized.

It should be noted that there is a plateau between 106 and 425 μm for the recovery curve at fluidization flow rates of 1.4 and 2 cm/s. Experimental observation

showed that the fluidized bed under these conditions was channelling due to the uneven fluid velocity distribution in the column. According to the diffusion (i.e. dispersion) theory of particles, solid particles can disperse if the fluid is in a state of agitation or turbulence (Dallavalle,1948), and large particles can remain relatively undisturbed by turbulence due to their lower eddy diffusivities (Lyman, 1994). Particles finer than 106 μm have such a low terminal settling velocity (<1.7 cm/s) that they are washed out of the bed with decreasing particle size (despite a relatively high eddy diffusivity) by the drag of the fluidization flow. Between 106 and 425 μm, magnetite was relatively evenly dispersed in fluidized bed, and thus exhibited a recovery similar to that of the bed (approximately two thirds), hence the observed plateaus. The relatively even dispersion of 106-425 μm magnetite is an interesting phenomenon. Magnetite larger than 425 μm could migrate and stay near the bottom of the fluidized bed due to its higher migration velocity and lower eddy diffusivity, especially at a flow of 1.4 cm/s.

It was observed that at fluidization flow of 1.4 and 2 cm/s, channelling took place (although the full column was fluidized, some sections exhibited net upward motion, others net downward motion). It is theorized that this flow regime yielded relatively high eddy diffusivity which dominated in the 106 to 425 μm size range over whatever net downward or upward velocities magnetite particles might have had.

4.4 Tentative Expressions of Particle Percolation and Migration in the Gravitational Field

Considering the motion of a spherical dense particle percolating or migrating into a gangue bed in the gravitational field, the key forces acting on this particle, as illustrated in Figure 4-9, are the gravity, the buoyancy, the drag, and the dynamic friction force due to inter-particle collision in the gangue bed. It is also assumed that both fluid and the particle are moving only in the vertical direction (the Z-direction) and thus there is no velocity component in the X and Y directions. The expressions of the drag and the equations of motion of a dense spherical particle for different intervals

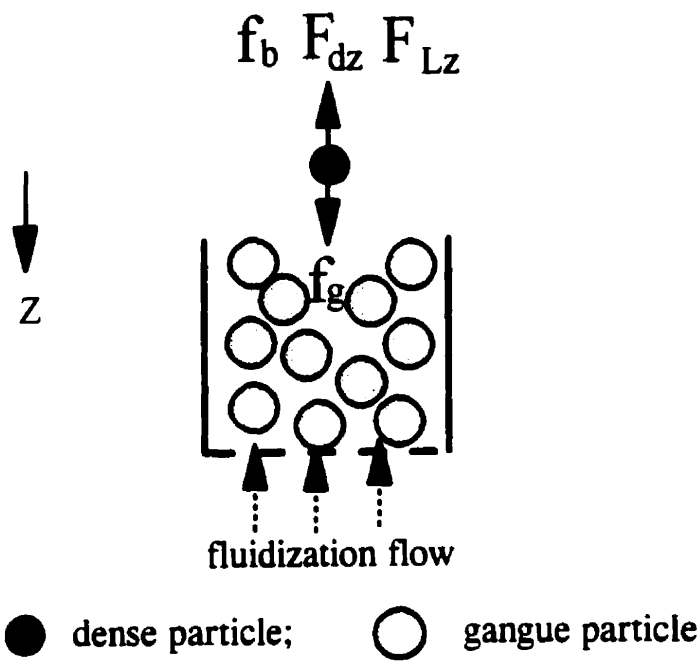

Figure 4-9 Forces on a percolating (or migrating) particle in the gravity field

of particle Reynolds number will be briefly presented in the following sections, whereas more details are presented in Appendix 2.

4.4.1 The drag force in different flow regions

Figure A2-4 (Clift et al, 1978) shows the drag coefficient of a sphere as a function of particle Reynolds number (standard drag curve). The standard drag curve may be divided into four regions, such as described by Coulson et al (1990). The subintervals of Re_p corresponding to these four regions are: the Stokes' Law region, or Region (a), 10^{-4} to 0.2, Region (b) 0.2 to 1000, Region (c) 1000 to 2×10^5, and Region (d) $> 2 \times 10^5$. In this section, only the drag forces in the first three regions of the graph will be considered as particles do not normally attain the extremely high Reynolds numbers of Region (d).

(1) The drag in the Stokes' Law region (Region a):

Similar to Equation 3.17, the drag on a spherical dense particle moving down in the fluidization column can be expressed as:

$$F_{dz} = 3\pi\mu d_p\left(\frac{dh}{dt} + u_i\right) \qquad (4.2)$$

where u_i is the interstitial velocity of fluidization flow with respect to the wall of the system.

(2) The drag in Region (b):

An approximate expression of the drag may be as follows:

$$F_{dz} = 0.055\pi d_p^2 \rho \left(\frac{dh}{dt}\right)^2 + (3\pi\mu d_p + 0.11\pi d_p^2 \rho u_i)\frac{dh}{dt} + (3\pi\mu d_p u_i + 0.055\pi d_p^2 \rho u_i^2) \quad (4.3)$$

(3) The drag in Region (c):

The drag force in this region can be expressed by Newton's Law (Coulson et al, 1990):

$$F_{dz} = 0.055\pi d_p^2 \rho[(dh/dt) + u_i]^2 \quad (4.4)$$

4.4.2 The equation of motion for the Stokes' Law region (Region a)

Assuming that the interstitial velocity of fluid, u_i, is constant, the equation of motion of a spherical dense particle in the Stokes' Law region is given by:

$$\frac{\pi}{6} d_p^3 (\rho_s - \rho) g - 3\pi\mu d_p \left(\frac{dh}{dt} + u_i\right) - C_p \left(\frac{dh}{dt}\right)^2 = \left(\frac{\pi}{6} d_p^3 \rho_s + \frac{\pi}{12} d_p^3 \rho\right)\frac{d^2h}{dt^2} \quad (4.5)$$

When the particle starts at $t = 0$, $h = h_1$, and $dh/dt = u_{pz0}$, using the same mathematic approach as in Section A1.2.3 to solve Equation 4.5 can result in the following solution, i.e. the instantaneous displacement of the particle, h:

$$h = \frac{k_5 + b_5}{2k_5a_5}\ln(1 - C_9e^{-k_5t}) - \frac{k_5 - b_5}{2k_5a_5}\ln\frac{1 - C_9e^{-k_5t}}{C_9e^{-k_5t}} + C_{10} \qquad (4.6)$$

$$\text{where} \quad a_5 = \frac{6C_P}{\pi d_p^3(\rho_s + \frac{\rho}{2})}, \quad b_5 = \frac{18\mu}{d_p^2(\rho_s + \frac{\rho}{2})}, \quad m_5 = \frac{-d_p^2 g(\rho_s - \rho) + 18\mu u_i}{d_p^2(\rho_s + \frac{\rho}{2})}$$

$$C_9 = \frac{2a_5u_{pz0} + b_5 - k_5}{2a_5u_{pz0} + b_5 + k_5}, \quad k_5 = \sqrt{b_5^2 - 4m_5a_5},$$

$$C_{10} = h_1 - \frac{b_5 + k_5}{2k_5a_5}\ln\frac{2k_5}{2a_5u_{pz0} + b_5 + k_5} - \frac{b_5 - k_5}{2k_5a_5}\ln\frac{2k_5}{2a_5u_{pz0} + b_5 - k_5}.$$

4.4.3 The equation of motion for Region (b)

Based on Equations 4.3, 3.36 and 3.13, the equation of motion of particle for Region (b) can be expressed by:

$$\frac{d^2h}{dt^2} + \frac{0.33\pi\rho d_p^2 + 6C_P}{\pi d_p^3(\rho_s + \frac{\rho}{2})}\left(\frac{dh}{dt}\right)^2 + \frac{18\mu + 0.66d_p\rho u_i}{d_p^2(\rho_s + \frac{\rho}{2})}\frac{dh}{dt} + \frac{(18\mu u_i + 0.33d_p\rho u_i^2) - d_p^2 g(\rho_s - \rho)}{d_p^2(\rho_s + \frac{\rho}{2})} = 0 \qquad (4.7)$$

When the particle starts at t = 0, h = h_1, and dh/dt = u_{pz0}, using the same mathematical approach as in Section A1.2.3 to solve Equation 4.7 results in the following solution:

$$h = \frac{k_6 + b_6}{2k_6a_6}\ln(1 - C_{11}e^{-k_6t}) - \frac{k_6 - b_6}{2k_6a_6}\ln\frac{1 - C_{11}e^{-k_6t}}{C_{11}e^{-k_6t}} + C_{12} \qquad (4.8)$$

where $C_{11} = \dfrac{2a_6u_{pz0} + b_6 - k_6}{2a_6u_{pz0} + b_6 + k_6}$, $k_6 = \sqrt{b_6^2 - 4m_6a_6}$

$$C_{12} = h_1 - \frac{b_6 + k_6}{2k_6a_6}\ln\frac{2k_6}{2a_6u_{pz0} + b_6 + k_6} - \frac{b_6 - k_6}{2k_6a_6}\ln\frac{2k_6}{2a_6u_{pz0} + b_6 - k_6}.$$

$$a_6 = \frac{0.33\pi\rho d_p^2 + 6C_P}{\pi d_p^3(\rho_s + \frac{\rho}{2})}, \quad b_6 = \frac{18\mu + 0.66d_p\rho u_i}{d_p^2(\rho_s + \frac{\rho}{2})}$$

$$m_6 = \frac{(18\mu u_i + 0.33d_p\rho u_i^2) - d_p^2g(\rho_s - \rho)}{d_p^2(\rho_s + \frac{\rho}{2})}$$

4.4.4 The equation of motion for Region (c)

The equation of motion for a spherical particle in Region (c) can be written by combining Equations 4.4, 3.36 and 3.13 and then rearranged, i.e.

$$\frac{\pi}{6}d_p^3g(\rho_s - \rho) - 0.055\pi d_p^2\rho\left(\frac{dh}{dt} + u_i\right)^2 - C_P\left(\frac{dh}{dt}\right)^2 = \frac{\pi}{6}D^3(\rho_s + \frac{\rho}{2})\frac{d^2h}{dt^2} \qquad (4.9)$$

When the particle starts at t = 0, h = h_1, and dh/dt = u_{pz0}, the solution of Equation 4.9 can be obtained with a mathematical approach similar to that used in Section A1.2.3:

$$h = \frac{k_7 + b_7}{2k_7a_7}\ln(1 - C_{13}e^{-k_7t}) - \frac{k_7 - b_7}{2k_7a_7}\ln\frac{1 - C_{13}e^{-k_7t}}{C_{13}e^{-k_7t}} + C_{14} \qquad (4.10)$$

$$\text{where } C_{13} = \frac{2a_7u_{pz0} + b_7 - k_7}{2a_7u_{pz0} + b_7 + k_7}, \quad k_7 = \sqrt{b_7^2 - 4m_7a_7}$$

$$C_{14} = h_1 - \frac{b_7 + k_7}{2k_7a_7}\ln\frac{2k_7}{2a_7u_{pz0} + b_7 + k_7} - \frac{b_7 - k_7}{2k_7a_7}\ln\frac{2k_7}{2a_7u_{pz0} + b_7 - k_7}.$$

$$a_7 = \frac{0.33\pi\rho d_p^2 + 6C_P}{\pi d_p^3(\rho_s + \frac{\rho}{2})}, \quad b_7 = \frac{0.66\rho u_i}{d_p(\rho_s + \frac{\rho}{2})}, \quad m_7 = \frac{0.33\rho u_i^2 - gd_p(\rho_s - \rho)}{d_p(\rho_s + \frac{\rho}{2})}.$$

4.5 Conclusion

(1) The fluidization properties of the four types of gangue beds have been studied in this work by determining the height and voidage of the bed at different fluid velocities and the minimum fluidizing velocity for each type of the gangue bed. The results have confirmed the conclusions made by Richardson (1971), that is, the minimum fluidizing velocity, U_{mf}, of fine or low density gangue bed was lower than that of coarser or higher density gangue bed.

(2) The percolation and migration behaviour of the two types of dense particles (tungsten and magnetite) was investigated by measuring the recovery of percolated or migrated dense particles under different conditions. It was found (such as from Figure 4-8) that in the gravitational field, percolation of dense particles was maximized at an intermediate fluidization flow, below which insufficient voidage would inhibit or limit the percolation of all but the coarsest dense particles, and above which fine dense particles would be prevented from percolating because of the drag force of the ascending fluidization flow. It was also observed that high density gangue, especially coarse size, had a detrimental effect on percolation and migration. Particles of high density percolated or migrated faster than those of lower density. When the gangue bed was well fluidized, the migration rate of coarse particles was higher than that of finer size.

(3) Tentative expressions of particle percolation and migration in a fluidization column was made for the gravitational field. The equations of motion of a spherical dense particle included the effect of inter-particle collision and were derived for three different particle Reynolds number regions.

CHAPTER 5 EXPERIMENTAL AND MACHINE CHARACTERISTICS OF THE CENTRIFUGE

5.1 Experimental Set-up for the Knelson Concentrator

The centrifuge used in the research work was a modified 3" (7.5 cm) Knelson Concentrator (KC), equipped with a variable speed control (a DC motor and a potentiometer). Figure 5-1 shows schematically the experimental set-up, and other details such as the position of the water pressure gauge are shown in Figure A3-3 (Appendix 3). Photographs of the set-up are shown in Figures A3-1 and A3-2. Figure 5-2 provides a schematic description of the fluidization water supply system.

As seen from the figures mentioned above, the KC is essentially comprised of a conical shaped and riffled inner bowl, which is made of polyurethane and installed concentrically within a cylindrical stainless steel outer bowl. Table 5-1 lists the distribution of surface area and number of water-injection holes of the five rings in the inner bowl . The definition of the ring in this work is the groove between the riffles, while a riffle is a rib of the inner bowl, as illustrated in Figure 5-2. The diameter of each hole is 0.79 mm or 1/32 inch. The designed concentrate volume of the inner bowl is approximately 65 ml (Knelson Gold Concentrator Inc., 1994).

The rotating speed of the drive motor can be varied by adjusting the potentiometer rotation. Motor velocity can reach 3967 rpm, corresponding to a bowl rotating velocity of 2024 rpm, and developing an acceleration at the ring surface varying from 58 Gs for the bottom ring to 115 Gs for the top ring. Table 5-2 shows a distribution of computed Gs in each ring of the inner bowl at 1040, 1465 and 2024 rpm of bowl rotating speeds. At a given rotating speed, centrifugal acceleration at the ring surface decreases from the top ring to the bottom ring due to the reduction in ring diameter. Since the diameter of the bottom ring (#1) is equal to a half of the diameter of the top ring, the acceleration at the bottom ring is half that at the top ring.

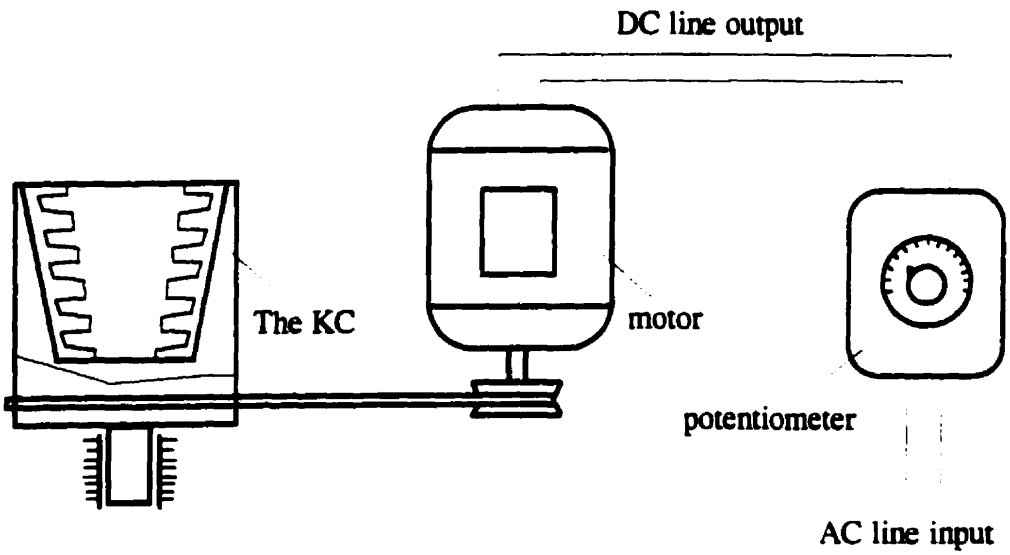

Figure 5-1 Experimental set-up of the KC

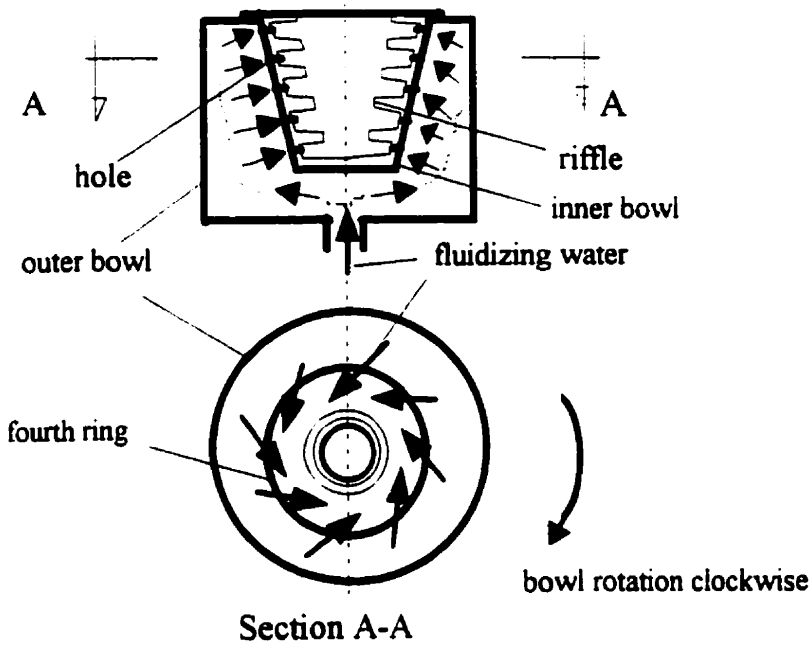

Figure 5-2 Fluidization water supply system of the KC

Table 5-1 Distributions of lateral area and injection holes of the inner bowl

Ring number	Ring diameter cm	Lateral area cm^2	Number of holes	
			Number	Density*, holes/cm^2
5	5.0	11.32	42	3.7
4	4.4	9.80	35	3.6
3	3.8	8.33	30	3.6
2	3.2	6.71	24	3.6
1	2.5	5.33	18	3.4
Sum.		41.49	149	3.6

* The density of holes is defined as the number of holes per unit ring area.

Table 5-2 Distribution of Gs in each ring at three rotating speeds

Ring number	Diameter cm	Gs		
		1040 rpm	1465 rpm	2024 rpm
5	5.0	30	60	115
4	4.4	27	53	100
3	3.8	23	46	87
2	3.2	19	38	73
1	2.5	15	30	58

5.2 Separation Principle of the Knelson Concentrator

The separation principle of the KC, for all models, is based on the difference in centrifugal forces exerted upon gold and gangue particles and on fluidization of the separation zone. As shown schematically in Figure 5-3, the feed is introduced to the base of the rotating inner bowl through the downcomer, and immediately mineral particles are centrifuged towards the conical wall of the concentrate bed at different rates depending on their size and specific gravity. At the same time, fluidization water enters tangentially opposite to the rotation into the concentrate bed, partially fluidizing it and preventing gangue particles settling in the separation zone. Under the effect of the centrifugal force and water fluidization, gold particles settle down and move (percolate or migrate) to the surface of the concentrate bed (some very fine concentrate may pass through the injection holes and accumulate on the base of the outer bowl); while gangue particles are washed out of the bowl due to their low specific gravity, thus completing the separation process.

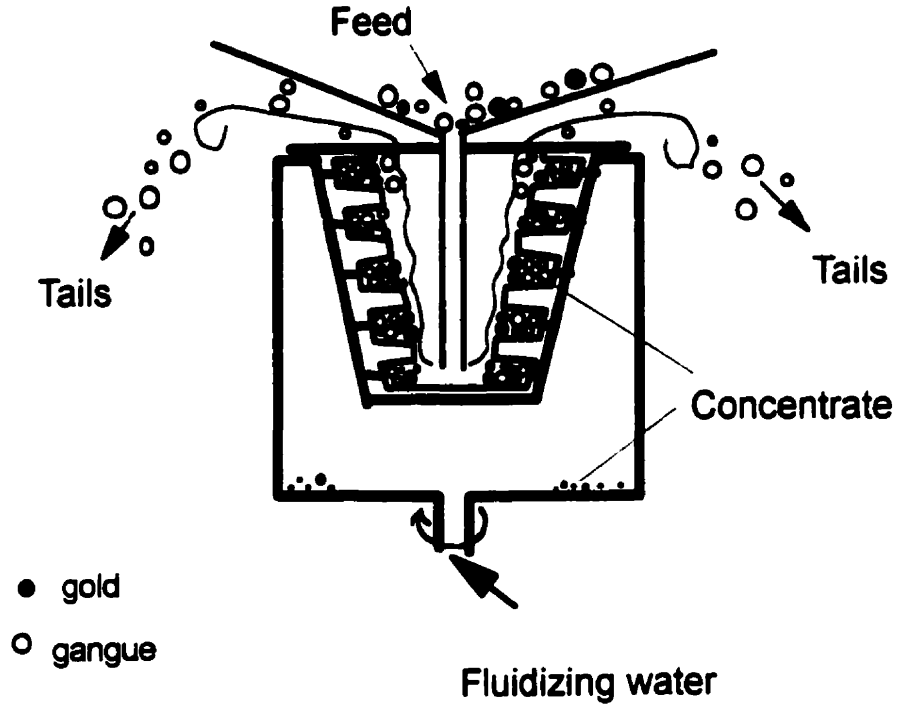

Figure 5-3 Separation principle of the KC

5.3 Relation between Centrifugal Acceleration and the Bowl Rotating Velocity

The rotating speed of the drive motor of the KC was measured at different potentiometer settings with a Cole-Parmer tachometer (model 8213-20, 5-digits), and each measurement was repeated once and the average rotating speed calculated. The rotating speed of the outer bowl was calculated from the ratio of the motor pulley to the

outer bowl diameters. The magnitude of centrifugal acceleration of the corresponding rotating speed was computed as follows:

$$Gs = \frac{\omega^2 R_t}{g} = \frac{(\pi n_d r_d)^2 R_t}{900 R_0^2 g} \qquad (5.1)$$

where Gs: the number of gravity accelerations (Svarovsky, 1990);

n_d: the rotating speed of the drive motor, rpm;

r_d: the radius of the motor pulley, cm;

R_t: the radius of the inner surface of the top rib, cm;

R_0: the radius of the outer bowl, cm;

g: gravitational acceleration, 981 cm/s^2.

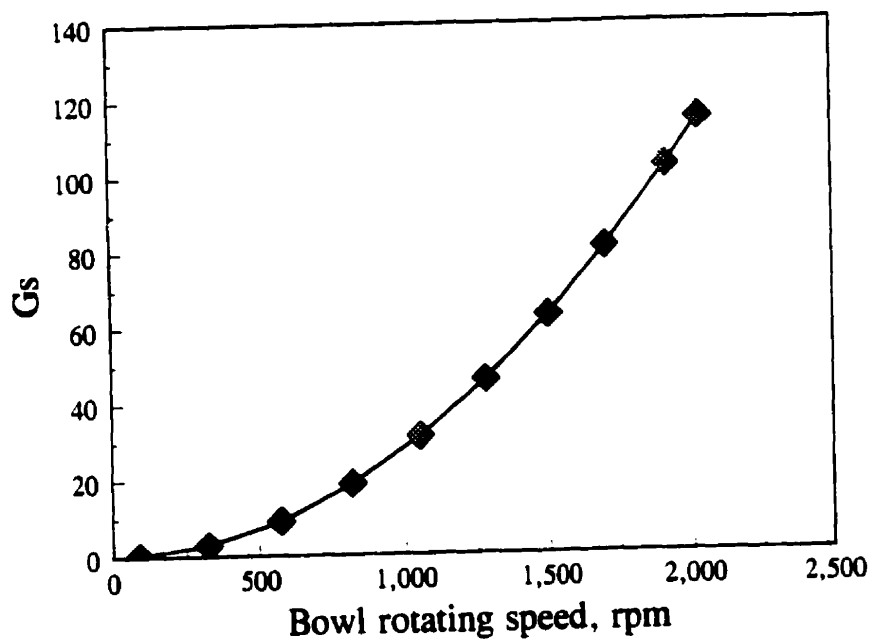

Figure 5-4 Centrifugal acceleration at the top ring as a function of bowl rotating speed

Figure 5-4 illustrates the relationship between the centrifugal acceleration (we use Gs as a dimensionless value) of the top ring and the bowl rotating velocity: it is a parabolic function and reaches 115 Gs for the top ring.

5.4 Effect of Rotating Speed on Fluidization Flow Rate

5.4.1 Methodology for measurement of fluidization flow rate

In the absence of any feed, the fluidization flow rate of the variable speed KC was determined at different rotating speeds and water pressures (read from an oil pressure gauge, 0 - 100 kPa or 0 - 15 PSIG). For given conditions (accelerations of 30, 60 and 115 Gs and water pressures of 8, 16, 24, 32, 40, and 46 kPa), flow rate was measured twice by extracting timed samples of fluidization water and measuring their volume. To measure ring-by-ring fluidization flow rate, the injection-holes in those rings not to be tested were sealed with removable glue. In addition, flow rate was determined when the inner bowl rotated reversely at 60 Gs so as to study the effect of the direction of the injection-holes on the fluidization. The reversal rotation was achieved by exchanging the electric poles of the DC motor.

5.4.2 Relationship between fluidization flow and centrifugal acceleration

5.4.2.1 Total fluidization flow of the inner bowl

Figure 5-5 shows fluidization flow rate as a function of water pressure and centrifugal acceleration. Water flow rate increased with increasing pressure. At a given

pressure, the water flow rate decreased as Gs increased from 30 to 115, indicating that the centrifugal force in the KC inner bowl had an ability to hinder the motion of fluidization water. This can be confirmed by comparing the result of normal rotation with that of reversal rotation at 60 Gs. As shown in Figure 5-5, at 60 Gs and a given pressure, the fluidization flow rate of reversal rotation is lower than that of normal rotation. Since the rotation of the injection-holes after reversing the bowl rotation was somewhat similar to the impeller rotation of a water pump, less fluidization water was able to enter the inner bowl. Owing to the centrifugal action of the flowing film, this pumping effect became stronger at a higher pressure.

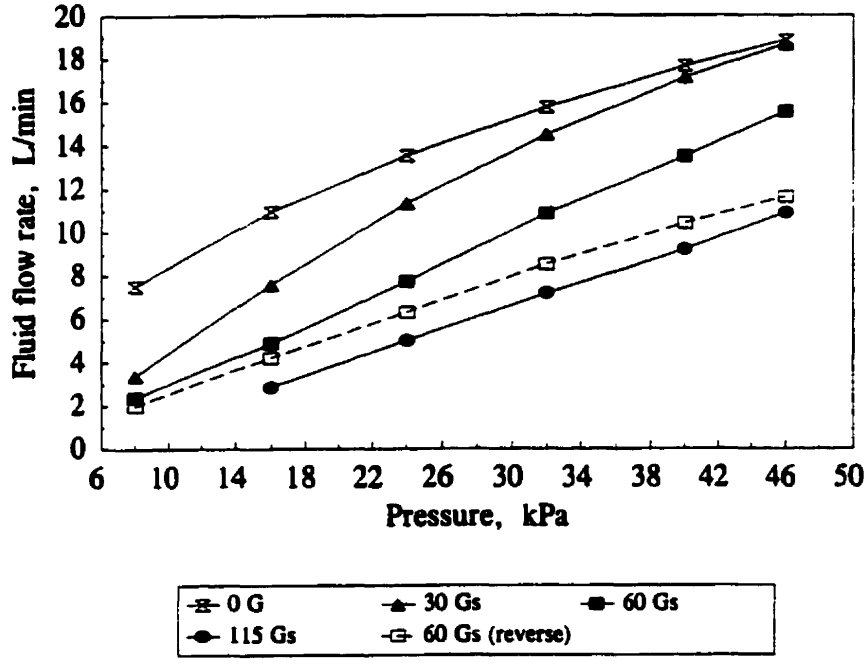

Figure 5-5 Total fluidization flow rate of the inner bowl as a function of water pressure and centrifugal acceleration

5.4.2.2 Ring-by-ring fluidization flow rate

Figure 5-6 shows ring-by-ring water flow rates under conditions of different water pressures and centrifugal accelerations in terms of superficial velocity vs ring number (lowest: #1; highest: #5, with the largest diameter). Superficial fluid velocities for lower rings (#1, #2 and #3) at 115 Gs could not be read because at very low flow rate and highest rotating speed, fluctuations of the pressure gauge reading were too large. The superficial fluid velocity at a given ring is equal to the fluidization flow rate of the ring divided by the ring surface area (Table 5-1). As seen from Figure 5-6, the superficial velocity tended to decrease with increasing ring diameter and acceleration. Since the density of holes, as seen in Table 5-1, is basically the same for all five rings, it is inferred that at the same rotating speed, the flow rate per hole decreases from Ring 1 to Ring 5 on account of the increasing Gs. This result is consistent with the observation that increasing rotating velocity decreases overall fluidization flowrate at constant pressure (Figure 5-5). For a given ring and at constant Gs, the superficial velocity increased gradually as water pressure increased from 24 to 46 kPa, which also confirms the effect of pressure on fluidization flow rate shown in Figure 5-5.

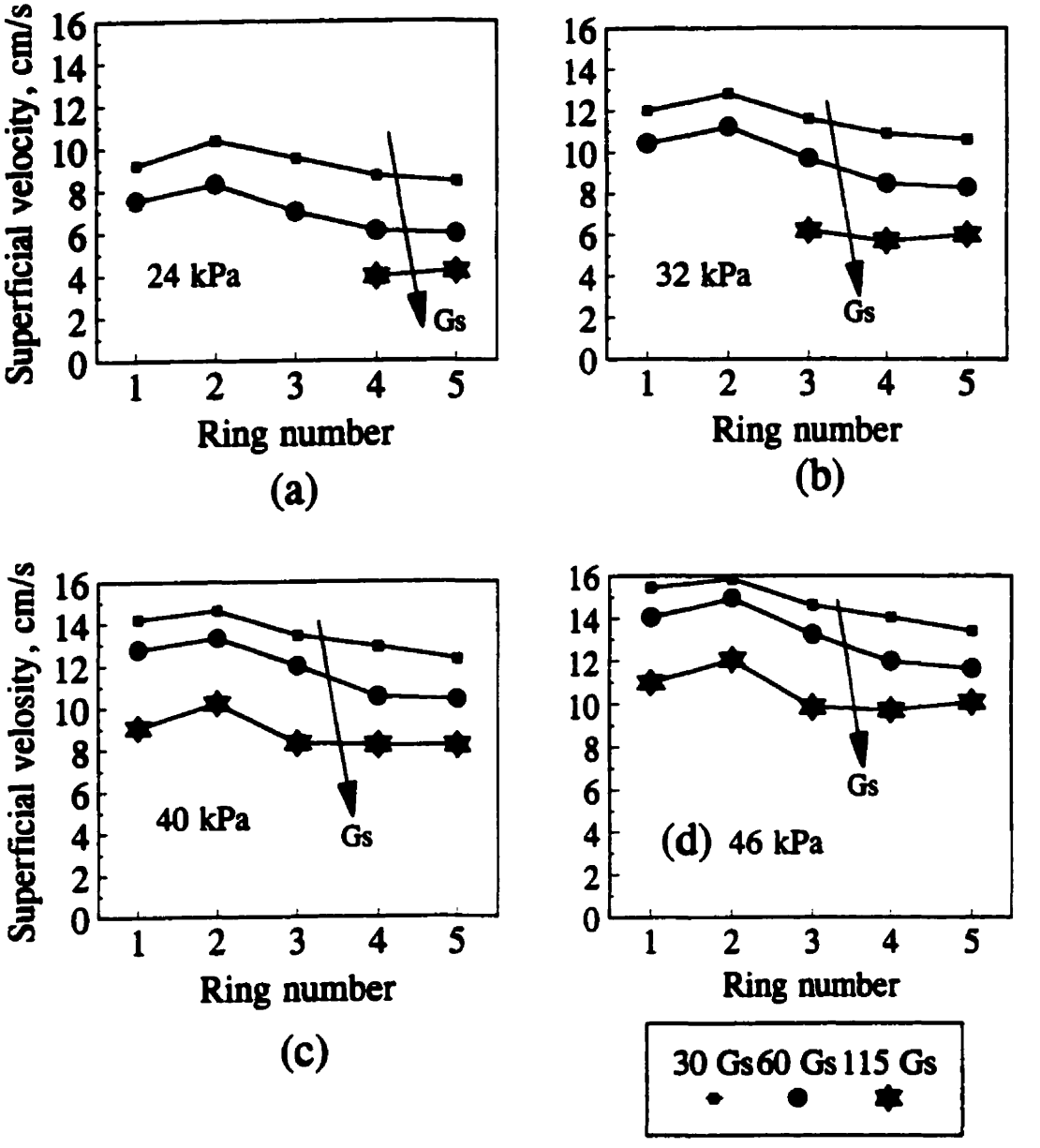

Figure 5-6 Superficial velocity of fluidization flow as a function of the ring number and Gs at different pressures: (a) 24 kPa; (b) 32 kPa; (c) 40 kPa; (d) 46 kPa.

5.5 Effect of Rotating Speed on the Thickness, Reynolds Number and Retention Time of the Flowing Film in the Inner Bowl

5.5.1 Methodology for measurement of the thickness of the flowing film

The measurement was taken while the KC was running, by removing its feeding funnel. For most tests, no solid particles and slurrying water were fed into the KC during the measurement. Before measuring, fluidization flow rate was adjusted between 2 and 14 L/min, and the bowl rotating speed was kept at 790, 1040, 1465 and 2024 rpm, corresponding to accelerations of 18, 30, 60 and 114 Gs, respectively. The internal diameter of the conical flowing film over the inner bowl was measured with an inside callipers under strong illumination. An outside measuring Vernier callipers with an accuracy of 0.02 mm was then used to determine the previous callipers setting. For each condition, the internal diameter of the flowing film was measured at five positions, located at the surface of each riffle and the top rib, and each measurement was repeated three times. Finally, the thickness of the flowing film at a given riffle was obtained by halving of the difference between the inner diameter of the riffle and the average internal diameter of the flowing film cone.

For measurement in the presence of a gangue bed, 200 grams of 212-300 μm silica particles were first fed into the rotating inner bowl to form a fluidized bed. The KC was kept running at 115 Gs acceleration and 8 L/min fluidization flow for two

minutes in order to obtain a constant mass of silica inside the bowl. Then, the thickness of the flowing film was measured as per the procedure mentioned above.

The standard deviation of each measurement ranged from 0.08 to 0.6 mm. The high deviation of readings happened on measuring a thicker water film due to oscillations of the flowing film when the KC was running. This accuracy was considered acceptable for a preliminary characterisation of the flowing film in the KC.

5.5.2 Effect of rotating speed and fluidization on the thickness of the flowing film

5.5.2.1 Thickness of the flowing film as a function of riffle number

Figure 5-7 shows how fluidization flow rate affected the thickness of the flowing film in the inner bowl at 18, 30, 60 and 115 Gs, for all five riffles. The thickness of the flowing film varied from 0.10 to 4.42 mm, depending on the flow position (the riffle number), flow rate, and rotating speed. Generally, the highest thickness was observed at the lowest Gs (18 Gs) and the highest flow rate; the lowest thickness was observed at the highest Gs (115 Gs) and the lowest flow rate. It can be seen that the thickness at 30 Gs was about twice the thickness at 115 Gs at any given position of the bowl, which might lead to an inference that the retention time of particles at 30 Gs will be longer than that at 115 Gs. Some characteristics of the flowing film can be summarized by comparing and contrasting the data in Figure 5-7. That is:

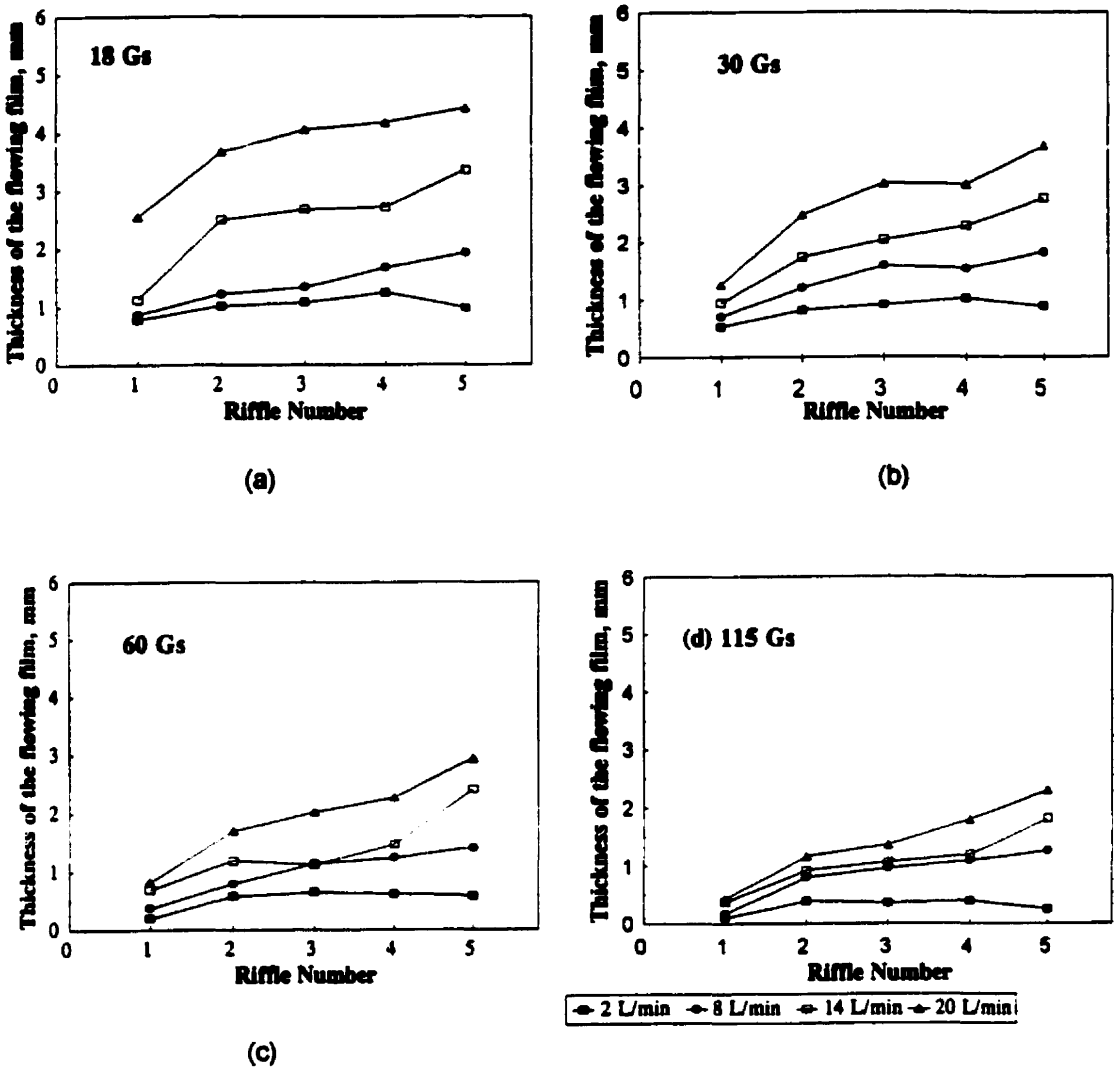

Figure 5-7 Thickness of the flowing film as a function of riffle number and fluidization flow rate at (a) 18 Gs,(b) 30 Gs, (c) 60 Gs, and (d) 115 Gs.

1) At a given Gs, the thickness of flowing film increased with increasing fluidization flow rate.

2) At a given flow rate, the film thickness decreased with increasing Gs. This was due to the higher driving force (or higher tangential fluid velocity).

3) At given Gs and flow rate, the film thickness increased gradually as the flowing film moved from the bottom to the top of the inner bowl. This effect was clearly more significant at high fluid flow. This could be attributed to the confluence of the fluidization flow ring-by-ring.

5.5.2.2 The weir model of fluid flow

As illustrated in Figure 5-8, the top rib of the inner bowl may function as a horizontal weir, over which the water film flows vertically out of the inner bowl. It is considered that the thickness (δ) of the flowing film at the top riffle is approximately equal to the head. Hence, the relationship between the total fluid flowrate (i.e. the water discharge) and the thickness of the flowing film may be expressed by a classical weir model (Streeter, 1971), which, in this work, is modified by substituting the centrifugal acceleration for the gravitational acceleration. That is:

$$Q = k_w \frac{2}{3} \sqrt{2Gsg} L \delta^{3/2} \qquad (5.2)$$

where Q is the fluid flowrate, ml/s; K_w is a dimensionless correction factor; L is the width of weir, in cm, which is equal to the circumference of the top rib.

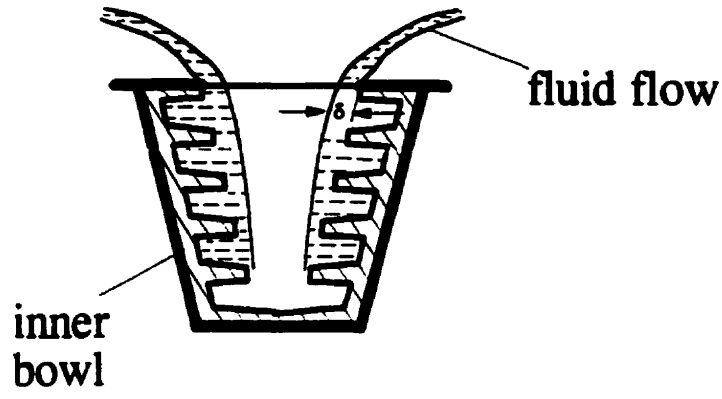

Figure 5-8 The weir phenomenon in the KC

Equation 5.2 can take the form:

$$Q = k_w \frac{2}{3}\sqrt{2g}\,2\pi\,(RGs^{1/2}\delta^{3/2}) \qquad (5.3)$$

In order to find the value of k_w, the values of the group $RGs^{1/2}\delta^{3/2}$ were calculated for the fifth ring at different Gs and fluid flow rates and then plotted against the water flow rates, as shown in Figure 5-9. The curves in the figure show basically linear. Therefore, it is appropriate to use Streeter's (1971) weir model to describe the relation between the flow rate and the thickness of the flowing film over the inner bowl. It can be found by regression that the magnitude of the all coefficients of the group $RGs^{1/2}\delta^{3/2}$ is equal to 107.5. Thus,

$$k_w = \frac{107.5}{\frac{2}{3}\sqrt{2g}2\pi} = \frac{107.5}{\frac{2}{3}*\sqrt{2*981}*2\pi} = 0.58$$

This k_w value is very close to the empirical value (0.6) measured by Streeter (1971), thus confirming the weir model.

From Equation 5.3, the thickness of a flowing film at the fifth riffle can be calculated by:

$$\delta = \left(\frac{Q}{1.09\sqrt{Gsg}\pi R}\right)^{\frac{2}{3}} \qquad (5.4)$$

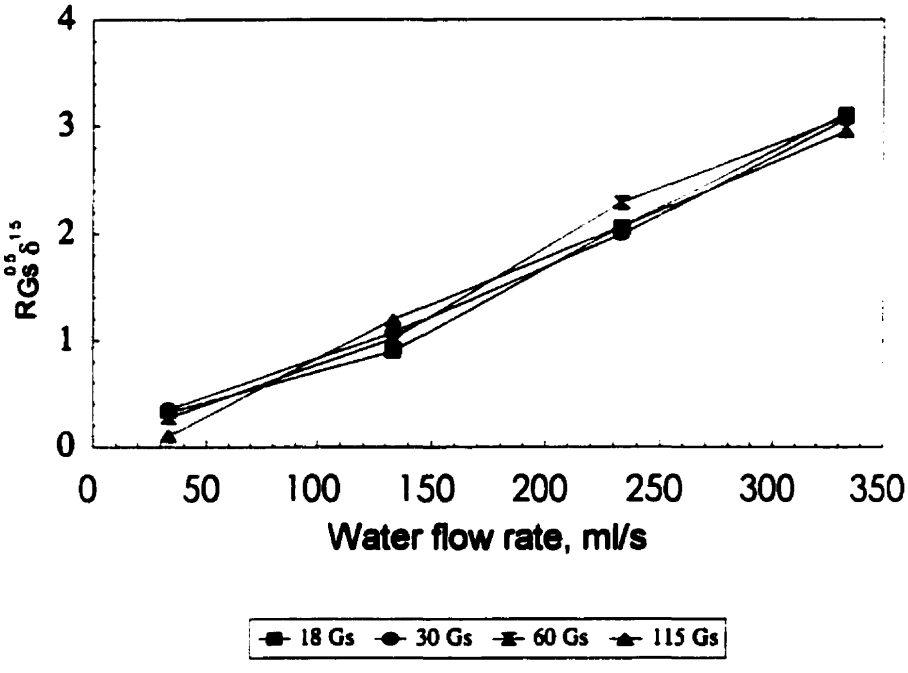

Figure 5-9 Relationship between $RGs^{1/2}\delta^{3/2}$ and fluid flowrate for different Gs

5.5.3 Effect of rotating speed and fluidization on the Reynolds number of the flowing film

Based on the results of the thickness measurement, the average Reynolds number of flowing film in the inner bowl, Re, was calculated according to the following formulation (Sun, 1982):

$$Re = \frac{\rho \bar{u}_f \delta_a}{\mu} \qquad (5.5)$$

where $\bar{u}_f$: the average fluid velocity, cm/s.

δ_a: the average thickness of the flowing film, cm.

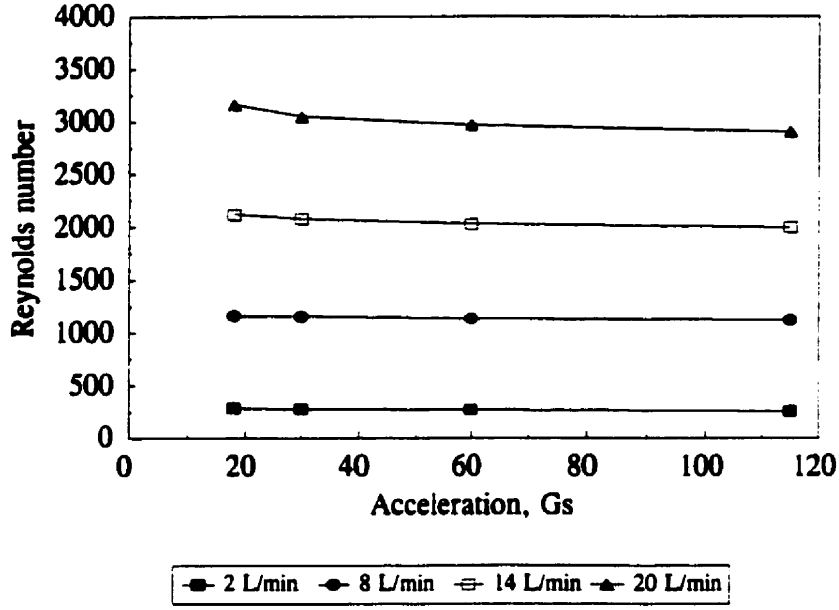

Figure 5-10 Reynolds number of flowing film as a function of rotating speed and fluid flow rate

Figure 5-10 illustrates the relationship between the average Reynolds number of the flowing film in the inner bowl and rotating speed of the KC at different fluid flow rates. The Reynolds number varied from 254 to 3164, as fluid flow increased from 2 to 20 L/min, with very little dependence on Gs between values of 18 and 115 Gs.

In mineral processing practice, it is generally stated that the critical Reynolds number for inclined flow marks the transition from laminar to turbulent flow, and varies between 300 and 1000 (Sun, 1982). Since the flowing film in the inner bowl not only moves in the axial direction but also moves radially and tangentially, it is postulated that the regime of the inner bowl flowing film is transitional, i.e. at intermediate Reynolds number (between 200 and 4000), where there may be a slight breakdown of laminar motion, or sharp bursts of turbulent fluctuation, or even partial (or local) turbulence. Although there was little effect of rotating speed on the Reynolds number, it is very plausible that higher rotating speeds will require more fluid flow, leading to higher Reynolds numbers and an increase in turbulence.

5.5.4 Effect of fluidization on the thickness of the flowing film in the presence of a silica bed

Figure 5-11 shows how the thickness of the flowing film varied from the bottom (Riffle 1) to the top (Riffle 5) of the bowl at 115 Gs and a fluidization flow rate of 8 L/min with and without a silica (212-300 μm) bed in the inner bowl. The profile of the

film thickness remained almost unchanged in the presence of a silica bed. This might indicate that the solids in each of the rings do not affect the flowing film significantly, and that some of the hydrodynamic characteristics of the flowing film free of solid particles can be applied to the study of the actual flowing film in the KC.

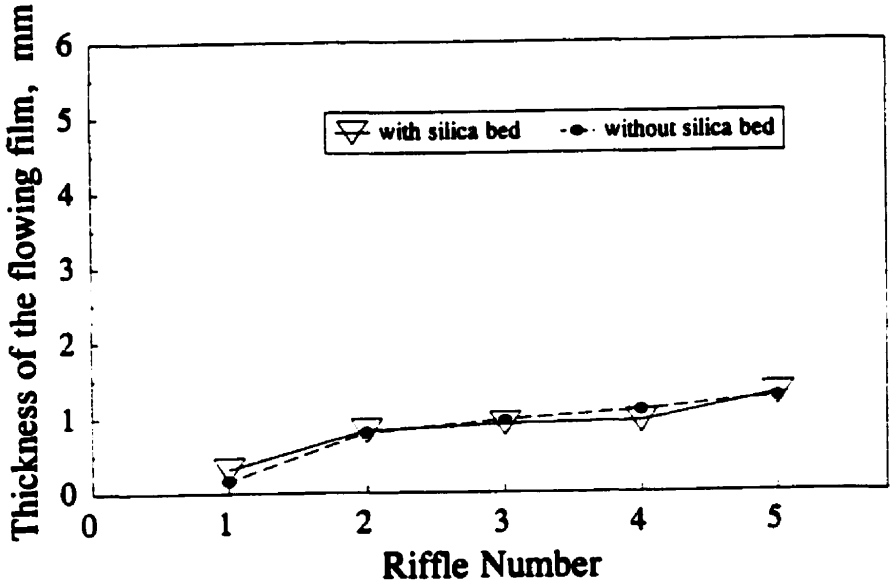

Figure 5-11 Thickness of flowing film as a function of riffle number at 115 Gs and a fluidization flowrate of 8 L/min with and without a silica (212-300 μm) bed

5.5.5 Effect of rotating speed and fluidization on the retention time of the flowing film

Based on the measured thickness of the flowing film, the retention time of the flowing film was calculated with following formulation for different rotating speeds and fluidization flows:

$$\tau = \frac{V}{Q} = \frac{V_0 - \frac{1}{3}\pi H(R_1^2 + R_5^2 + R_1 R_5)}{Q} \qquad (5.6)$$

where Q: the fluid flow rate of the flowing film, cm^3/s;

V: the volumetric holdup of flow in the inner bowl, cm^3;

V_0: the volume of the air cone of the inner bowl without fluidization water, 57.43 cm^3.

H: the height of the inner bowl, 5.69 cm;

R_1: the radius of the air cone at the bottom ring with fluidization water, cm;

R_5: the radius of the air cone at the top ring with fluidization water, cm.

Figure 5-12 illustrates the results of the calculation. It is shown that the retention time of the flowing film basically decreases with increasing Gs at a given fluidization flow. At a flow rate of 2 L/min, for instance, the retention time of the flowing film decreased from 0.19 to 0.05 second as Gs increased from 18 to 115. This indicates that increasing the rotating speed of the KC will accelerate the axial motion of the flowing film. At a given Gs, the retention time decreased as fluid flow rate increased from 2

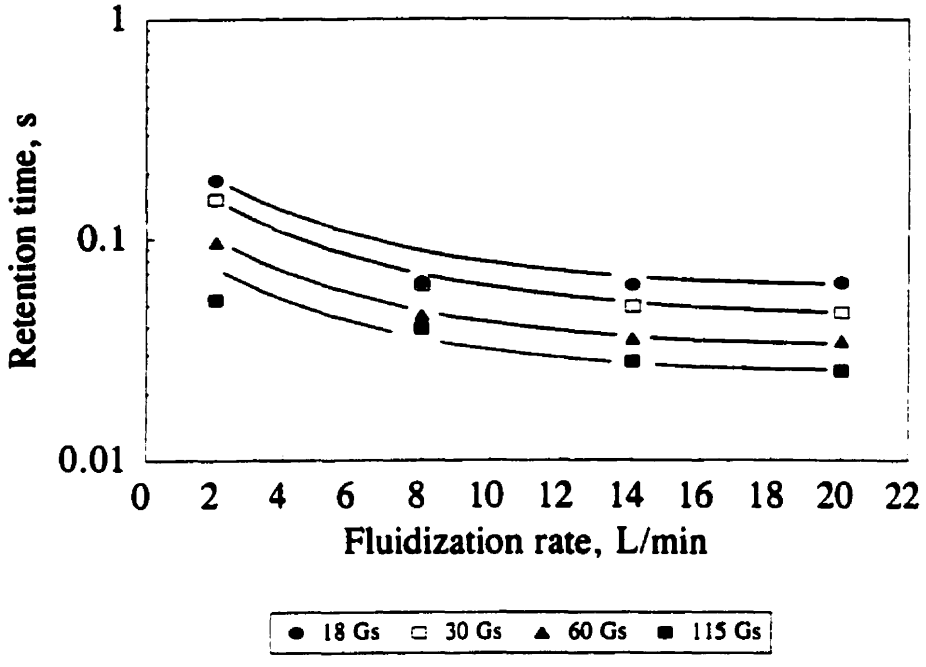

Figure 5-12 Retention time of flowing film as a function of rotating speed and fluid flow rate

to 8 L/min, which is the range of fluidization flow rate for normal operation of the 3-in KC at 60 Gs. Then, the retention time remained almost unchanged as flow rate increased from 8 to 20 L/min, since the volumes of both the fluid holdup and the flow rate increased almost at same rates. Increased fluidization flow is seen to decrease retention time for standard Knelson operating conditions, and increase the thickness of the flowing film. This would suggest that recovery will be more difficult, especially at high feed rates.

The data of Figure 5-12 were obtained using the thickness of the flowing film, a relatively noisy measurement. The resulting error clearly shows in the scatter, and second order polynomial fit of the data yields a lack-of-fit of 20% (error bars are not shown on the graph for the sake of clarity). Nevertheless, the trends are extremely clear, and the retention time of liquid phase was below 0.1 s for normal operating conditions.

5.6 Conclusions

A modified 3" (7.5 cm) variable speed Knelson Concentrator was set up for the research work. A number of machine characteristics relevant to unit performance, including the relation between rotating speed and centrifugal acceleration at the ring surface, the ring-by-ring fluidization flow at different rotating speeds and water pressures, and the thickness and retention time of the flowing film, were measured and discussed. It was shown that the relationship between the fluid flow rate and the thickness of the flowing film at the top rib well observed the classical weir model, modified for high Gs. Some of the results in this chapter will be used to provide the following gravity test work with a quantitative reference, and others will be used to explain some experimental phenomena and separation mechanisms of the Knelson Concentrator.

CHAPTER 6 SEPARATION OF TUNGSTEN FROM MAGNETITE AND SILICA GANGUES

6.1 Methodology for Gravity Concentration Tests

6.1.1 Materials and devices

6.1.1.1 Synthetic ores

Synthetic ores were used throughout this work. As shown by Laplante et al (1995), the use of synthetic ores with a substitute for gold is not only expedient, but it can also lead to an increased understanding of separation mechanisms, because of the more accurate results and controlled particle shape. In test work conducted in this chapter, four types of synthetic feeds were used and prepared by combining a heavy metal (tungsten, 2.5% of the feed for all tests) with a gangue (magnetite or silica) with two size distributions (coarse and fine). These distributions were chosen to mimic those which can be reasonably achieved with industrial static and vibrated screens, as well as flash flotation concentrates. The physical properties and preparation (or purification) of tungsten, magnetite, and silica have been described in Section 4.2.1 of Chapter 4. Table 6-1 shows the size distributions of the coarse and fine materials for the gravity tests.

Table 6-1 Size distributions of tungsten and gangue (% Mass)

Size μm	Mass (%)	
	Coarse	Fine
1180-1670	3.8	
850-1180	6.1	
600-850	10.8	
425-600	9.9	
300-425	13.7	3.2
212-300	12.9	5.9
150-212	15.3	11.6
106-150	11.3	17.0
75-106	7.9	21.5
53-75	4.5	18.1
38-53	3.0	13.8
25-38	0.5	6.1
-25	0.3	2.9
Total	100.0	100.0

6.1.1.2. Devices

The Variable Speed Knelson Concentrator used for test work has been described in Chapter 5. A Mozley laboratory separator (MLS) was used to determine the tungsten content in the sized fractions of the KC concentrate. With proper MLS operation (and magnetic separation in the presence of magnetite gangue), the concentrate obtained can be considered to be pure tungsten. This method had been successfully used by Laplante et al (1995a) in their research work.

In this work, the accuracy of the MLS analysis has been confirmed by conducting a series of repeated MLS gravity tests on different sizes of synthetic feeds (five repeats for each size fraction). In each test, 10 grams of tungsten and 50 grams of silica or magnetite were mixed before feeding onto the tray of the MLS. If a mixture was coarser than 106 μm, a "V" profile tray was used, otherwise a flat tray was used. Before each test, the speed, amplitude and slope of the MLS were set accordingly, and the flow rate of wash water was adjusted at 0.5 L/min for the "V" profile tray and 2.5 L/min for the flat tray. The standard deviations (STD) of five repeated MLS tests are given in Table A4-1 of Appendix 4 for mixtures of tungsten and silica, and in Table A4-2 for mixtures of tungsten and magnetite, respectively. In most tests the tungsten recoveries were very high, above 98%, with a low standard deviation less than 0.5% for silica gangue and a higher but still acceptable standard deviation for magnetite gangue. The minus 25 μm fraction gave slightly lower recoveries.

6.1.2 Methodology for the gravity concentration tests

The tests were conducted using procedures analogous to those developed at McGill University (Huang, 1996; Laplante et al, 1995, 1996a). Figure 6-1 demonstrates the key procedures.

(1) For each test, a 2 kg synthetic ore sample was prepared carefully by weighing each component material size-by-size with a AD Electronic scale according to the size distributions shown in Table 6-1. It was fed at a rate of 400 g/min with 0.5 L/min slurrying water to the KC. Fluidizing water flow rate was adjusted between 2 and 14

L/min; inner bowl rotating speed at 1040, 1465 or 2024 rpm (corresponding to 30, 60 or 115 Gs at the top ring).

(2) At the end of each test, the KC concentrate was recovered, dried and screened using a Tyler progression. Each size class was processed with the MLS (the Mozley Laboratory Separator), and in the case of magnetite gangue, residual magnetite was removed with a hand magnet (Model SP-90, made by Gilson Company, Inc., USA). Recovery was calculated from the mass of tungsten recovered by the MLS and that of the feed.

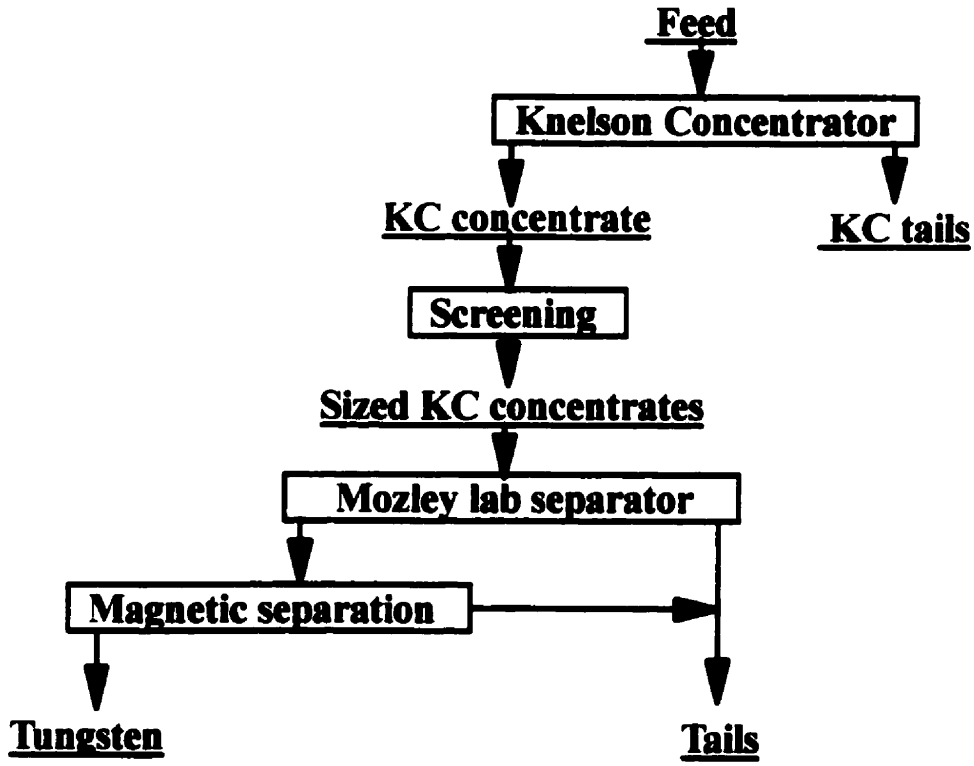

Figure 6-1 Methodology for tungsten-gangues separation

6.2 Experimental Results

6.2.1 Separation of tungsten from fine magnetite

Figure 6.2 shows how the fluidizing water flow rate and rotating speed of the KC affects total tungsten recovery. The highest recovery, 96.5%, was achieved at the lowest rotating speed and a fluidization flow rate of 5 L/min. On the other hand, the lowest recoveries were achieved at the highest rotating speed, especially at fluidization flow rates below the optimum (a recovery of 64% at 2 L/min). Each rotating velocity had an optimum fluidization flow rate, which increased from 5 L/min at 1040 rpm (30 Gs) to 14 L/min or more at 2024 rpm (115 Gs).

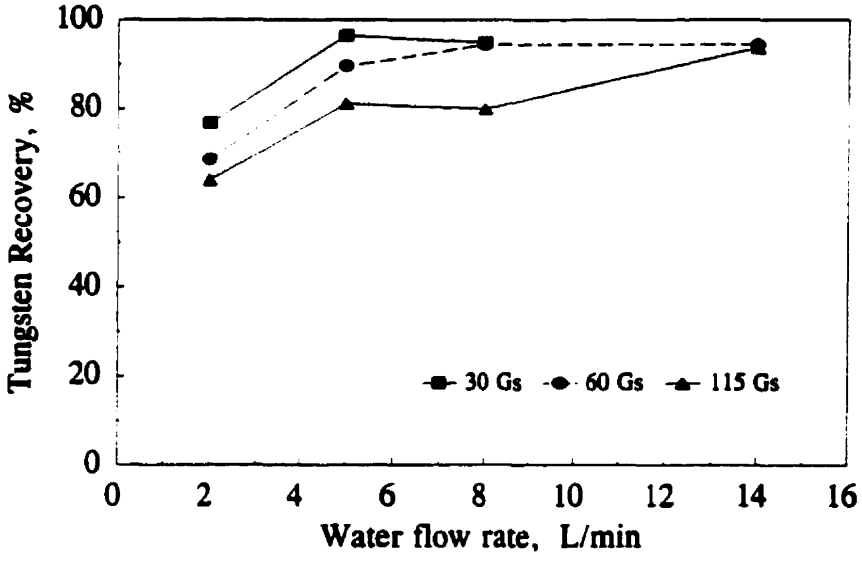

Figure 6-2 Tungsten recovery as a function of centrifuge acceleration and fluidization flow rate (gangue: -425 μm magnetite)

Figure 6-3 illustrates how fluidization flow rate affected the mass of concentrate corresponding to the tests in Figure 6-2. It can be seen that fluidization flow rate had an opposite effect on concentrate mass than recovery. At a given Gs, the concentrate mass decreased and the recovery increased as fluidization flow increased from 2 to 8 L/min. This indicates that the separation zone became more active since more gangue particles were flushed out of this zone. The largest concentrate mass, 369 grams, was obtained at the lowest recovery, under conditions of highest rotating speed and lowest fluidization velocity. This may imply that the separation zone became more compact with increasing rotating speed and decreasing fluidization flow rate. In the study of the

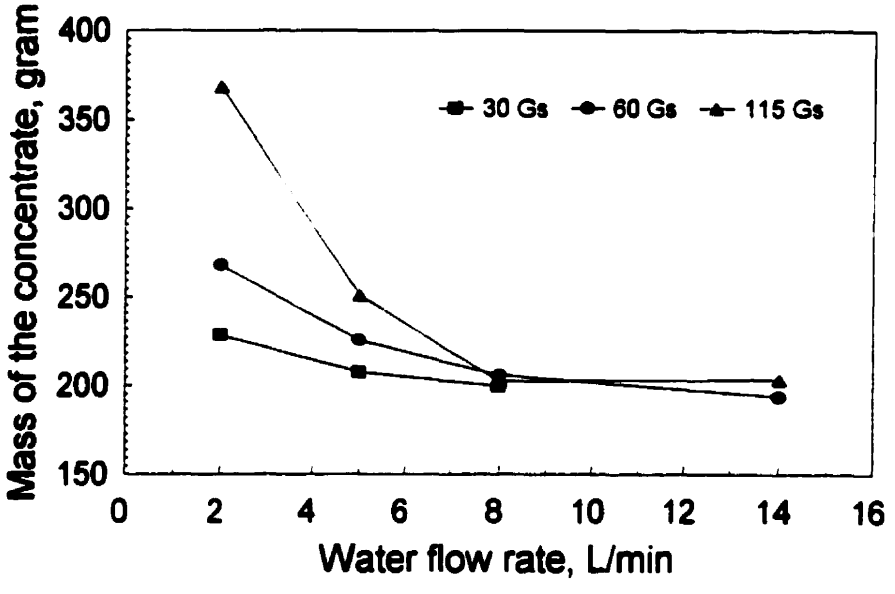

Figure 6-3 The mass of the KC concentrate as a function of centrifugal acceleration and fluidization flow rate (gangue type: -425 μm magnetite)

relationship between the voidage of the gangue bed and fluidization flow rate at one G in Chapter 4, it was shown (Figure 4-4) that the fractional voidage decreased with decreasing fluidization flow rate. Tungsten recovery then dropped because its percolation was impeded, as shown in Figure 4.7. A similar phenomenon has been reproduced in Figure 6-2, but at higher accelerations.

It should be noted that the recovery process in the KC is not an example of simple centrifugal settling of dense particles but also sizing of the gangue. Under the influence of water fluidization, a hydro classification process for gangue particles takes place within the separation zone. As a result of this process, large gangue particles survive and stay in the separation zone, whereas small ones are washed out of the zone, being replaced by oncoming larger gangue or dense particles. This classification process may operate during part or all of the recovering cycle. Meanwhile, high density particles are able to overcome the resistance and percolate or migrate to the concentrate bed under normal operating condition. Most of them are hardly affected by the classification action unless the fluidization flow rate is exceptionally high. Therefore, it may be hypothesized that at a given Gs, the presence of much gangue of a size typical of the feed (say the D_{80}) in the concentrate is an indication of inadequate fluidization, as the fine size of this material, if properly fluidized, should not report to the concentrate. Figure A4-1 shows the D_{80} of gangue in the concentrate as a function of fluidization flow rate and centrifuge acceleration, analyzed for the tests mentioned above. It increased with increasing fluidization flow rate and decreasing rotating speed,

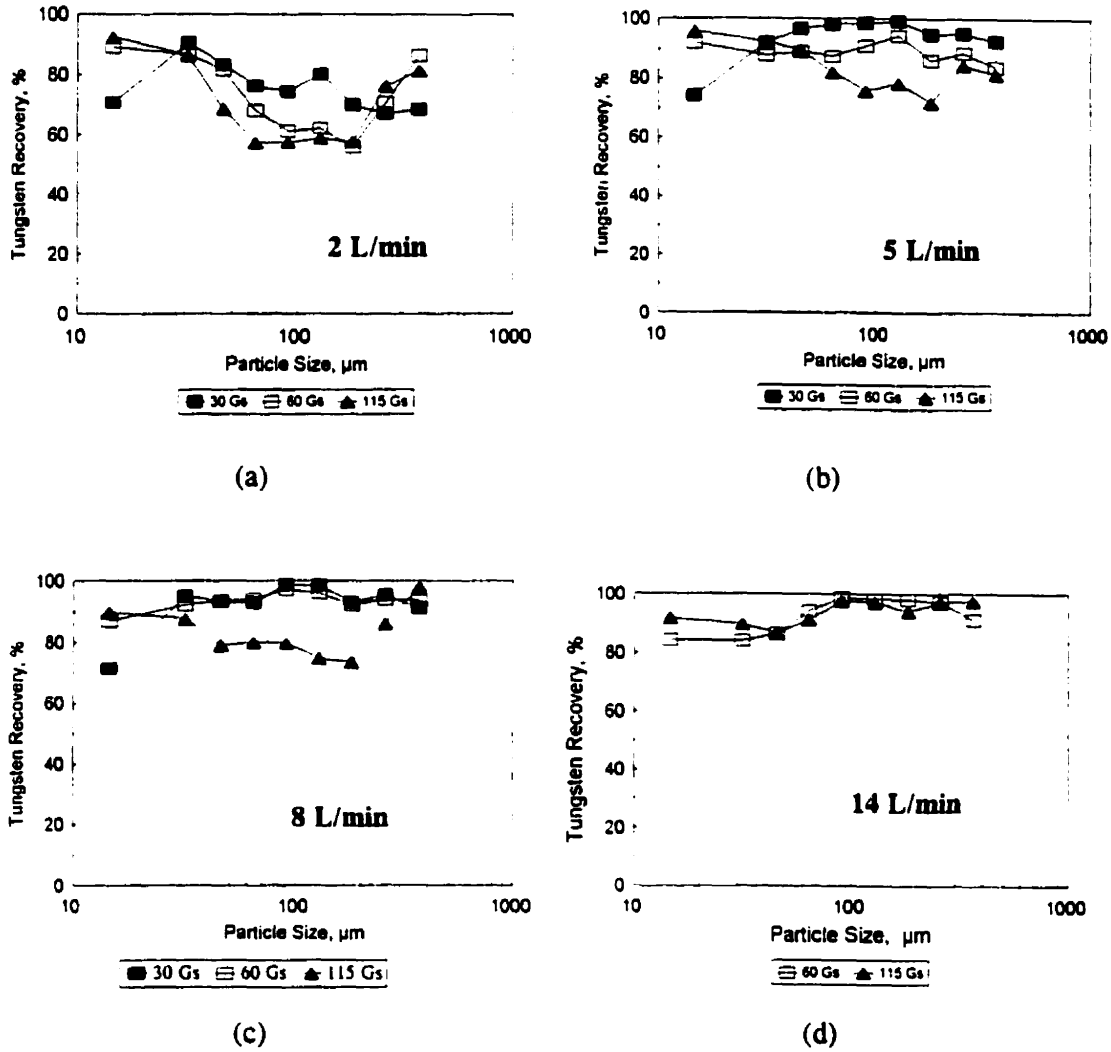

Figure 6-4 Tungsten recovery as a function of particle size and centrifuge acceleration at different fluidization flow rates (gangue type: -425 μm magnetite)

indicating that the size distribution of gangue in the bed became increasingly coarser than that of the feed (the D_{80} of gangue in the feed was 130 μm). It is observed that operating conditions yielding lower recoveries do correspond to D_{80}s in the concentrate close to that of the feed.

Size-by-size tungsten recoveries at fluidization flow rates of 2, 5, 8, and 14 L/min are shown in Figure 6-4 for different Gs. Results at 2 L/min (Graph a) confirm what could be hypothesized from the known effect of fluidization water: at flows below the optimum, the recovery drop was most significant at the intermediate size range, as reported for the unfluidized batch Falcon (Laplante et al, 1994), and it became more significant with increasing rotating speed. In fact, even at the lowest rotating speed, 30 Gs, 2 L/min was an inadequate fluidization flow rate. There was also evidence that at this low flow rate, even the coarsest tungsten lacked the momentum to migrate through the flowing slurry to the concentrate bed surface. This problem was corrected at higher rotation speeds, and the recovery of the +300 μm fraction increased to more than 80%. Recovery of the finest tungsten, -25 μm, also benefited from the higher rotating speed.

At 5 L/min (Graph b), where fluidization became better than at 2 L/min, the best overall size-by-size recoveries were obtained at 30 Gs, with only a slight drop in the recovery of the 25-38 μm fraction, and a more substantial drop in the -25 μm recovery. The recovery improvement from 2 L/min at intermediate size range was more significant at 60 Gs than 115 Gs, resulting in a relatively constant recovery above 80% over the full

size range. This may be attributed to an improvement of fluidization, which was lost again at 115 Gs.

Graph (c) shows that as fluidization flow rate increased further to 8 L/min, the overall size-by-size recoveries began to decrease at 30 Gs due to the increasing radial drag of fluidization water, which hindered tungsten particle migration and percolation. This graph indicates that the drop is limited to tungsten finer than 106 μm, which would be more susceptible to the drag (i.e. of lower terminal settling velocity). Only at 60 Gs the recovery of most sizes reaches an optimum because of a sufficient acceleration to resist the drag and a suitable voidage to percolate and migrate. Still, at 115 Gs, the recovery problems experienced at 5 L/min persisted. Figure A4-1 shows that the gangue D_{80} at 115 Gs and 8 L/min, 145 μm, was still close to that of the feed (130 μm), indicating that fluidization of the separation zone was not yet sufficient. As a result, there was little improvement in tungsten percolation (or migration) and overall recovery under these conditions.

At 14 L/min, as seen in Graph (d), the recovery at the intermediate size range was the highest for 115 Gs. This again was linked to improved fluidization, as suggested by Figure A4-1, which shows that the high recovery was achieved at a fluidization flow rate high enough to increase the D_{80} of the recovered gangue to reach values similar to those of the optimum recovery at lower Gs. At 60 Gs, the recovery

of the -53 μm tungsten started to decrease, as it had at 30 Gs at a lower fluidization flow.

6.2.2 Separation of tungsten from coarse magnetite

Figure 6-5 shows how the fluidization flow rate and rotating speed of the KC affected overall tungsten recovery from coarse magnetite gangue. As expected, overall recovery was below that of the fine magnetite gangue, and varied from 58 to 83%. The lowest rotating speed achieved the highest recovery at a fluidization flow rate of 5 L/min, as had been the case with the finer magnetite gangue.

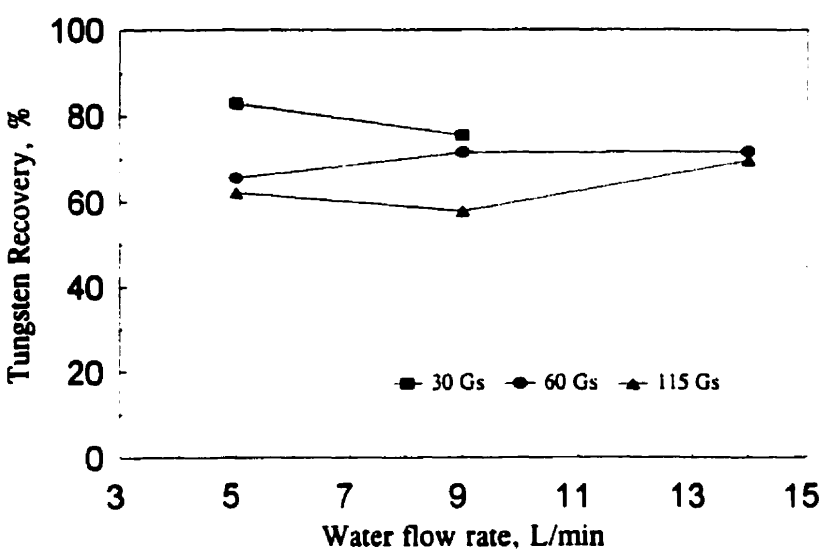

Figure 6-5 Tungsten recovery as a function of centrifuge acceleration and fluidization flow rate (gangue: -1670 μm magnetite)

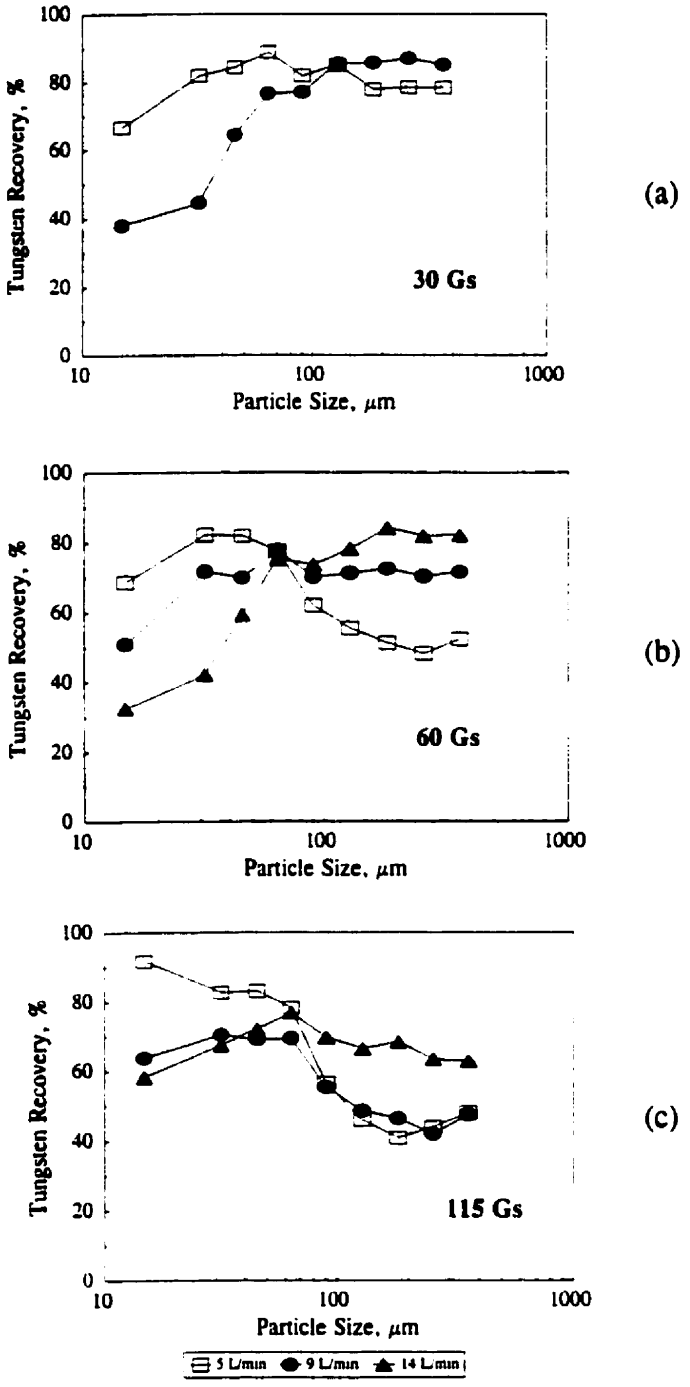

Figure 6-6 Tungsten recovery as a function of particle size and fluidization flow rate at different centrifuge accelerations (gangue type: - 1670 μm magnetite)

The effect of tungsten particle size was very significant, and is detailed in Figure 6-6 for accelerations of 30, 60 and 115 Gs, respectively. It was clear that high recoveries over the full size range could not be achieved within the range of operating conditions tested. The highest recoveries below 38 μm were achieved at 115 Gs and the lowest fluidization water, whereas the +212 μm fraction was best recovered at 30 Gs and a high fluidization flow rate of 9 L/min. These are diametrically opposed operating conditions, and also correspond roughly to the minimum recovery of particles at the opposite end of the size spectrum. None of the curves showed the restoration of recovery at tungsten sizes equivalent to the coarsest gangue particles, but this was simply because coarse (>425 μm) tungsten was not used. Curves such as the one at 14 L/min and 60 Gs strongly suggest that this restoration would indeed take place.

All recovery versus size curves indicate that recovery in the 50 to 100 μm size range was relatively independent of both of fluidization flow and rotating speed (i.e. when the results in Figure 6-6 are compared). Interestingly enough, this corresponds to the dominating size range for gold accumulating in most grinding circuits (Banisi et al. 1991; Zhang, 1997; Vincent, 1997).

One final observation should be made: Figure 6-6 suggests that a wider range of fluidization flows should be tested. For example, recovery of the +100 μm fraction at 115 Gs could undoubtedly be boosted with a flow above 14 L/min, whereas the -37 μm fraction recovery would probably be slightly boosted with a flow below 5 L/min. In

both cases, this would be at the cost of recovery at the other end of the size distribution; flows exceeding 14 L/min would also result in a very high water consumption, more than threefold that of the Knelsons in present industrial applications.

The effect of fluidization flow rate and rotating speed on the mass of the concentrate is presented in Figure A4-2, and the relationship between the D_{80} of gangue in the concentrate and fluidization flow at different Gs is shown in Figure A4-3 of Appendix 4. It can be seen from these two figures that the variation of both the concentrate mass and the D_{80} of gangue in the concentrate were not as significant as for fine magnetite gangue (comparing with Figure 6-3 and Figure A4-1). This is a good indication that the separation zone dominated by coarse dense gangue had a very low voidage and was not well fluidized even at the highest fluidization flow tested. Figure 4-3 had shown that the coarse (600-850 μm) hematite bed was the most difficult to fluidize at one G. Furthermore, Figure 4-7 had shown that the percolation or migration velocity of tungsten in the coarse hematite bed was much lower than those in other three types of gangue bed. Results in this chapter suggest that similar problems plague the Knelson over a relatively high range of Gs. They also suggest that there is a limit to the top size that a centrifuge such as a Knelson can treat when gangue density is extremely high. This limit is located somewhere between the coarse and fine magnetite feeds tested in this work.

6.2.3 Separation of tungsten from fine silica

Figure 6-7 shows how the fluidizing water flow rate and rotating speed of the KC affected tungsten recovery from fine silica gangue. Tungsten recovery was high (well above 95%) for all cases, except for the lowest water flow rate (2 L/min) at the highest Gs, where fluidization was obviously inadequate. There was also a modest drop in recovery at the highest water flow rate (6 L/min) and the lowest Gs, where fluidizing water flushed some of the fine tungsten out of the concentrate.

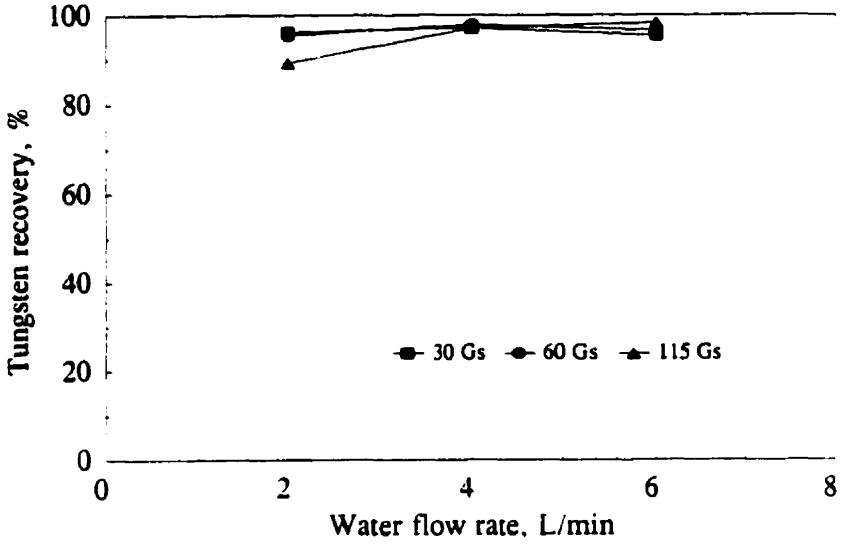

Figure 6-7 Tungsten recovery as a function of centrifuge acceleration and fluidization rate (gangue type: -425 μm silica)

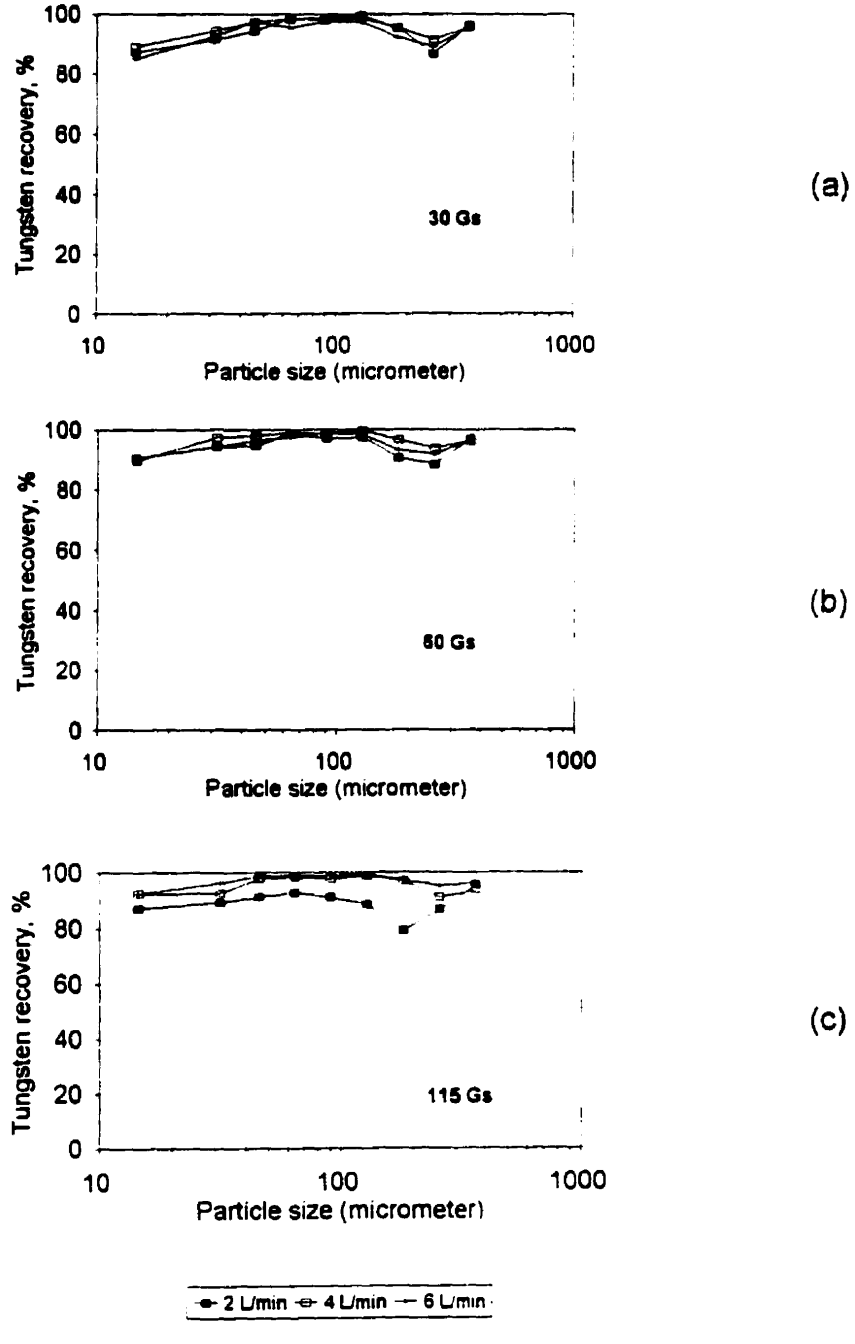

Figure 6-8 Tungsten recovery as a function of particle size and fluidization flow rate at centrifuge accelerations of 30, 60 and 115 Gs (gangue: -425 μm silica)

Size-by-size tungsten recoveries at 30, 60 and 115 Gs are shown in Figure 6-8 for conditions of three different fluidizing water flow rates. Common for these three centrifuge accelerations was a small dip in recovery between particle sizes of the 106 and 300 μm, which was exacerbated by reducing fluidization flow rate and increasing Gs.

The effect of fluidization flow and rotating speed on the mass of concentrate and the D_{80} of gangue in the concentrate was significant, and is detailed in Figures A4-5 and A4-4 of Appendix 4, respectively. As a whole, the concentrate mass decreased with increasing fluidization flow rate and decreasing Gs, whereas the D_{80} of gangue in the concentrate increased with increasing fluidization flow rate and decreasing Gs. Although tungsten recovery was very high over the full range of operating conditions Figure A4-5 shows that the dip in tungsten recovery in the 150-300 μm fraction is most pronounced where the D_{80} in the concentrate is closest to that of the feed --- in the 130-150 μm range.

Comparing the results in Figure 6-7 with those in Figure 6-2 for separation of tungsten from magnetite, the fluidizing water flow rate where the maximum recovery occurred at a certain rotating speed was much lower for the silica gangue, even at the highest Gs. We suggest that the fine low density gangue (silica) tended to form a more fluidized separation zone in the inner bowl, thus requiring a lower fluidization flow rate.

The fundamental study of fluidization behaviour of different types of gangue bed in Chapter 4 has already illustrated this observation.

6.2.4 Separation of coarse tungsten from coarse silica

Figure 6-9 is a plot of tungsten recovery versus fluidization flow rate at different Gs. As for Figure 6-7, the most serious drop in recovery was due to an inadequate fluidization flow at high Gs. Figure 6-10 shows that the extent of the problem was limited to a relatively narrow size range, 150-600 μm, thus, again the intermediate coarse size range. Increasing fluidization flow to 7 L/min fully restored recovery above the 95% range, except for the -37 μm fraction, whose recovery remained high ($>80\%$) even though it had a relatively low percolation rate at high fluidization flow rate. These data suggest that tungsten (or gold) could be effectively separated from silica over a wide size range with Knelson-like centrifuge units, at accelerations which need not exceed 60 Gs. This is consistent with observed industrial performance.

The concentrate mass varied from 131 to 146 grams, increasing with decreasing fluidization flow rate and increasing Gs. This variation was consistent with others analyzed above, thus confirming the inferred fluidization behaviour of the concentrate bed.

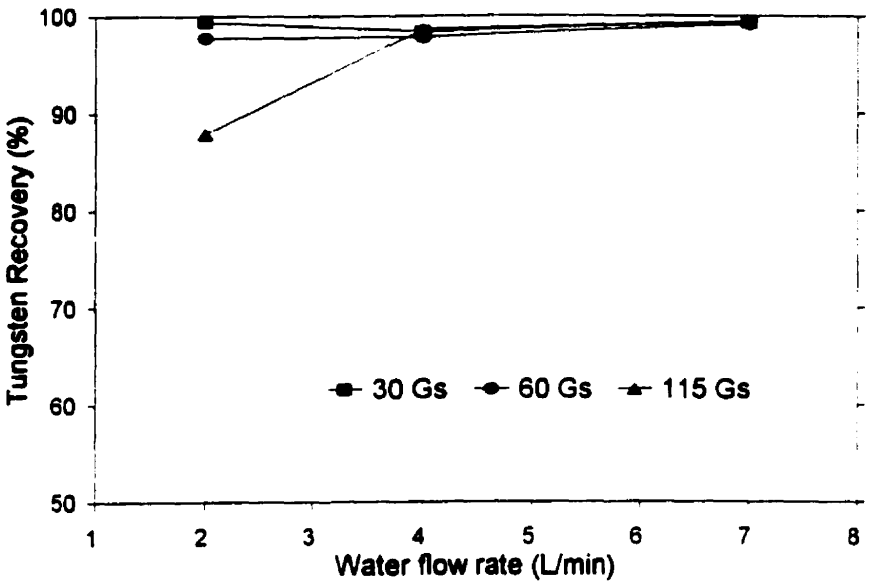

Figure 6-9 Tungsten recovery as a function of rotating speed and fluidization flow rate (gangue type: -1670 μm silica)

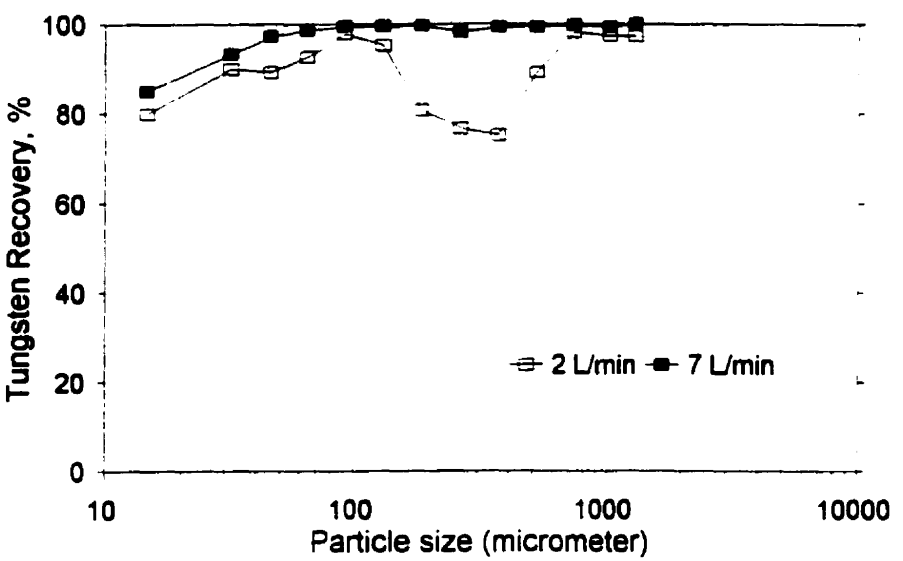

Figure 6-10 Tungsten recovery as a function of particle size (centrifugal acceleration: 115 Gs, gangue type: -1670 μm silica)

6.3 Discussion

6.3.1 Modelling the optimum fluidization for tungsten (gold) recovery

The optimum fluidization velocity (at which the maximum recovery can be reached) is an important parameter for the KC performance and depends upon variables such as the acceleration of the separation system and physical properties of the feed. The effect of acceleration on the optimum fluidization for fine (-425 μm) magnetite and silica gangues is plotted in Figure 6-11. The minimum fluidizing velocities of 212-300 μm magnetite and silica at one G (in the gravitational field), determined in Figure 4-3 of Chapter 4, are included as a reference in order to develop a more comprehensive relationship between the optimum fluidization and acceleration.

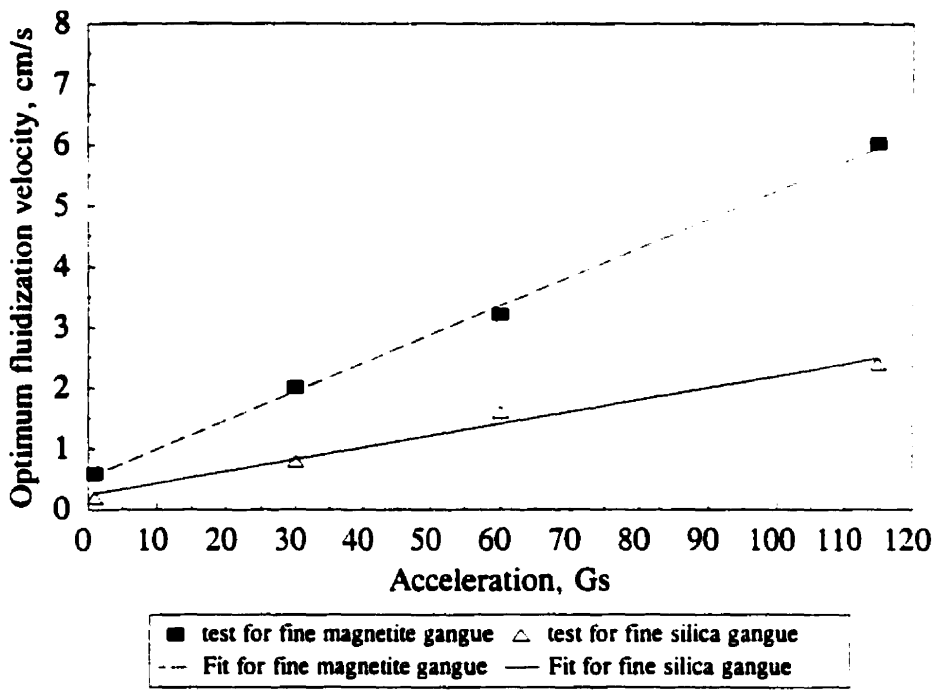

Figure 6-11 Optimum fluidization velocity for tungsten recovery as a function of acceleration for magnetite and silica gangues

Figure 6-11 shows a good linear fit for the test data for both magnetite and silica gangues, despite the obvious difficulty of estimating U_{max}, especially for the -425 μm silica gangue (tungsten recoveries were very high for most tests, and varied only in a very narrow range). The optimum fluidization velocity U_{max} for the tungsten size distribution used may be given by the following equations.

For the feed of the -425 μm magnetite gangue:

$$U_{max} = 0.59 + 0.05*Gs \qquad (6.1)$$

For the feed of the -425 μm silica gangue:

$$U_{max} = 0.25 + 0.02*Gs \qquad (6.2)$$

6.3.2 Relation between the ratio of D_{80}s of the gangue to tungsten in the concentrate and acceleration

Figure 6-12 shows the ratio of the D_{80} of the gangue and tungsten in the concentrate as a function of acceleration at the optimum fluidization for magnetite and silica gangues. The figure also shows how the concentrate mass varies for the corresponding optimum condition. In the graph (a), the D_{80} ratio is basically constant (between 1.3 and 1.4) over an acceleration range of 30 to 115 Gs. The concentrate mass remains almost constant at 203 - 208 grams. For fine silica (Graph b), the effect of acceleration on the D_{80} ratio and concentrate mass for silica gangue is comparable with that for magnetite gangue (Graph a), though the magnitude of the optimum concentrate mass is different due to different types of gangue.

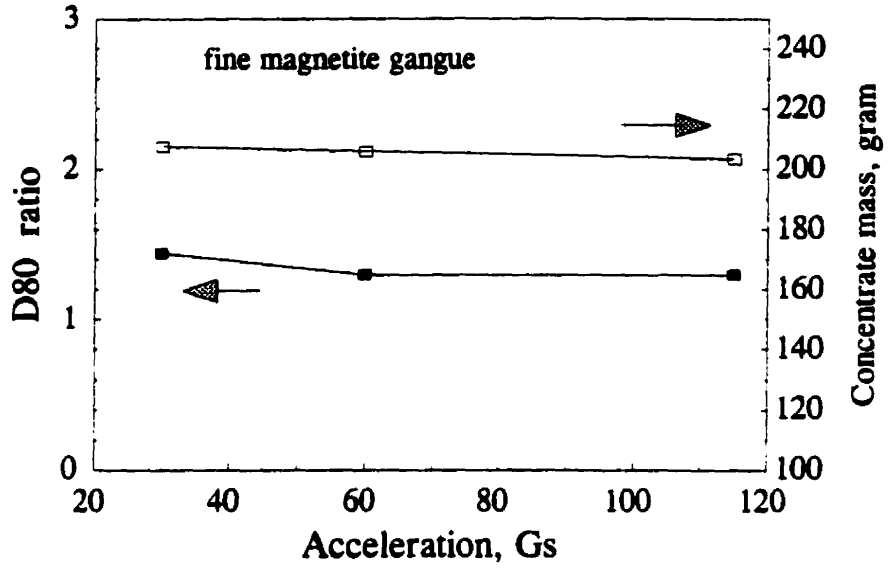

(a)

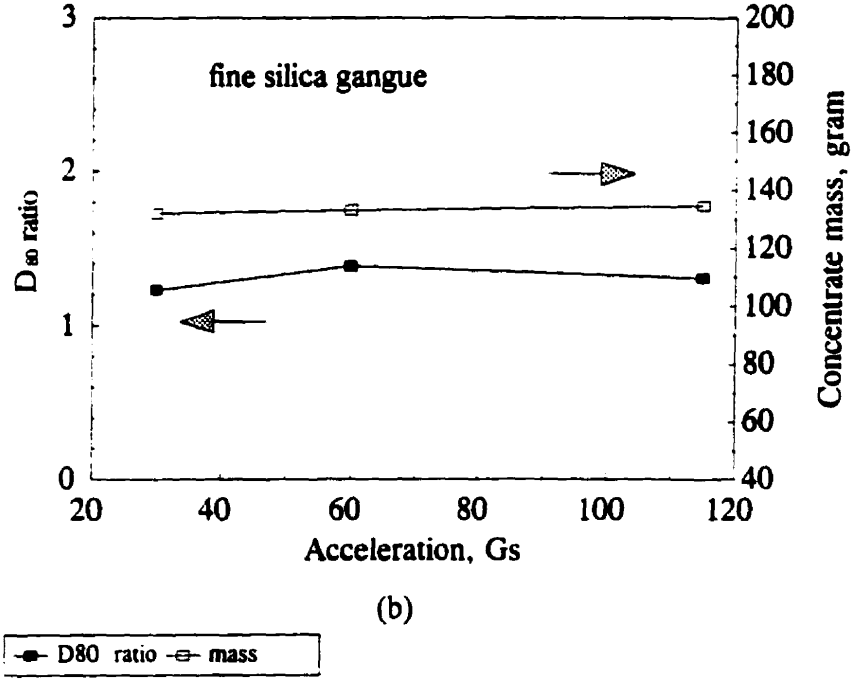

(b)

Figure 6-12 D_{80} ratio and concentrate mass as a function of centrifuge acceleration at the optimum fluidization flow rate

This interesting analogy demonstrates that neither the D_{80} ratio nor concentrate mass varies significantly as a function of acceleration, provided fluidization flow is adjusted to its optimum.

6.3.3 The behaviour of the intermediate size tungsten

In this work, the meaning of the intermediate size is a range of size fractions between the fine and the coarse size fractions for any type of ore used in the experiments. For instance, the 53-212 μm range is an intermediate size for the -425 μm feed (D_{80} of 135 μm), and the 150-425 μm range is an intermediate size for the -1670 μm feed (D_{80} of 600 μm).

It was shown in this chapter that there was a dip in recovery whenever fluidization flow rate was below the optimum, especially for the condition of the highest Gs (115 Gs). This may be attributed to the percolation or migration problem of tungsten particles of the intermediate size moving in a relatively compact separation zone. Since in the separation zone the ratio of the diameters of intermediate size tungsten to gangue particles is relatively higher than the ratio of the diameters of finer tungsten to gangue particles, the intermediate size tungsten has a lower ability to percolate through the small void of the relatively compact separation zone. Intermediate size tungsten, unlike coarser tungsten, does not have a mass large enough to intrude forcefully and firmly into the separation zone (i.e. "migrate").

It should be pointed out that the recovery "dip" observed in this work is quite similar to those in the previous work conducted by other workers. Laplante et al (1996 b) observed a dip in recovery in the 100-300 μm range of the Knelson gold concentrates with two different densities gangues (-1000 μm) and under a condition of insufficient fluidization water pressure. Zhang (1997) also found a recovery "trough" in a Knelson gold concentrate recovered from a high density Gemeni table tails with a D_{80} of 160 μm. Even in other gravity devices, such as jigs, a smaller recovery dip has been reported (Burt, 1984). Different explanations for this phenomenon were proposed by these authors. In the hypothesis presented by Laplante et al (1996 b), the recovery "trough" was attributed to a particle shape effect, i. e. gold became increasingly flakier with increasing particle size, and they were too coarse to percolate and not large enough to displace other particles in the settling toward the separation zone. Another typical interpretation was based on the velocity difference in particle movement which resulted from a transition from hindered settling to interstitial tricking (Burt, 1984). Obviously, both the explanations above should be proved experimentally. In this work, the feed rate was low enough to maximise recovery, less than 500 g/min of solids (Laplante et al, 1996b); tungsten particles in each size class of the feed were of irregular, rather than a flaky shape. Thus, the observation of the similar recovery dips in this work clearly negates the major effect of particle shape on tungsten (gold) recovery, and recognizes particle size as the main cause of the recovery trough. On the other hand, based on the fact that coarse tungsten particles could be partially recovered even though the separation zone was compact, where the hindered settling was impossible due to the inadequate

voidage, it is inferred that coarse tungsten was recovered mainly by the migration mechanism rather than by the "hindered settling" mechanism proposed by Burt.

6.4 Conclusions

Rotating speed and fluidization flow have a significant effect on the performance of the Knelson Concentrator. They affect both the percolation or migration of tungsten and the fluidization of the flowing slurry and the concentrate bed, which in turn affects how large tungsten particles can percolate or migrate to the concentrate bed. At high rotating speed (115 Gs), tungsten particles are imparted a high centrifugal force and tend to reach a high percolation or migration velocity; at the same time, however, the flowing slurry tends to collapse rapidly, which lowers the recovery of tungsten in the coarse intermediate size range, i.e. particles slightly finer than the D_{80} of the feed, especially in the presence of high density gangue.

Coarse size distribution (-1670 μm) of high density gangue (magnetite) has a markedly detrimental effect upon the tungsten recovery. No single combination of centrifuge acceleration and fluidization flow can achieve a totally satisfactory performance in the presence of coarse high density gangue. The detrimental effect of coarse magnetite on tungsten recovery might be due to three mechanisms: a) increasing the intensity of interparticle collision, which would cause the oncoming tungsten particles to be "bumped" off the inner bowl, b) building up in the separation zone and

then making the zone more compact, and c) eroding the captured tungsten away of the surface of the concentrate bed.

The existing Knelson rotating velocity (corresponding to an acceleration of 60 Gs) and suggested flows, however, are a reasonable compromise for most recovery application. For more difficult applications, i.e. finer gravity recoverable material, higher accelerations can theoretically achieve a better overall recovery.

For the -425 μm feeds with magnetite or silica gangue, it was found that the optimum fluidization velocity was directly proportional to acceleration of the concentrator, with a slope that increased with increasing gangue density.

CHAPTER 7 SEPARATION OF MAGNETITE FROM SILICA GANGUE

As reviewed in Chapter 2, industrial applications of the KC are essentially limited to gold recovery. Since most dense minerals which are traditionally recovered by gravity concentration, such as hematite, pyrite, wolframite and cassiterite, have a density between 4 and 7.5 g/cm^3, it is worthwhile to investigate how well the performance of the KC would be in the recovery of a lower high density mineral from gangue. In this chapter, testwork was conducted on separation of magnetite (with a density of 4.78 g/cm^3) from silica gangue and the discussion will focus on an assessment of the performance and recovery mechanisms of the KC.

7.1 Experimental Methodology

7.1.1 Materials and devices

Two types of synthetic ores were used, composed of magnetite and silica sized to below 425 μm. The first type, low grade, contained 1.25% magnetite, to ensure that even a full magnetite recovery (25 grams) from a 2 kg sample would not cause an overload in the separation zone. The second, high grade, contained 2.5% magnetite, to investigate the effect of feed grade on the performance of the KC. It also yielded slightly lower experimental errors (because of the increased magnetite mass). Both

types of feeds were prepared with the procedures given in Chapter 6 and with the same size distribution as that of fine tungsten and gangue shown in Table 6.1.

As for test work of Chapter 6, the gravity tests were conducted with the variable speed 3-in Knelson Concentrator, and the KC concentrate was analyzed with the Mozley Laboratory Separator (MSL). The standard deviations (STD) of five repeated MLS tests are given in Table A5-1 of Appendix 5 for mixtures of magnetite and silica. In most tests the magnetite particles were nearly completely recovered (generally 99%) with a standard deviation $\leq 0.3\%$ in recovery. For the -25 μm mixture the standard deviation was higher, 0.5%, and recovery slightly lower, 98-99%, but still acceptable.

7.1.2 Methodology

(1) For each test, a 2 kg synthetic feed was prepared by carefully weighing each component mineral size-by-size with an AD Electronic scale (precision: 0.01 g) according to the given size distribution in Table 6.1, and then split equally and loaded into five plastic trays after mixing thoroughly.

(2) At the beginning of each test, the 2 kg feed was fed manually at the rate of 400 g/min (one tray of feed/min) with 0.5 L/min slurrying water to the KC. Fluidizing water flowrate was given in the range between 1 and 14 L/min; rotating speed was conditioned from four options corresponding to 18, 30, 60 and 115 Gs.

(3) At the end of each test, the KC concentrate was recovered, dried and screened. Each size was analyzed for the magnetite content and then the total recovery calculated.

Figure 7-1 illustrates the methodology for the magnetite-silica tests, which was similar to that of Chapter 6. For the analysis of magnetite content in the sized concentrate, a two-step procedure was used: each size class of the concentrate was first separated magnetically (with a hand magnet), with a cleaning stage, to produce a pure

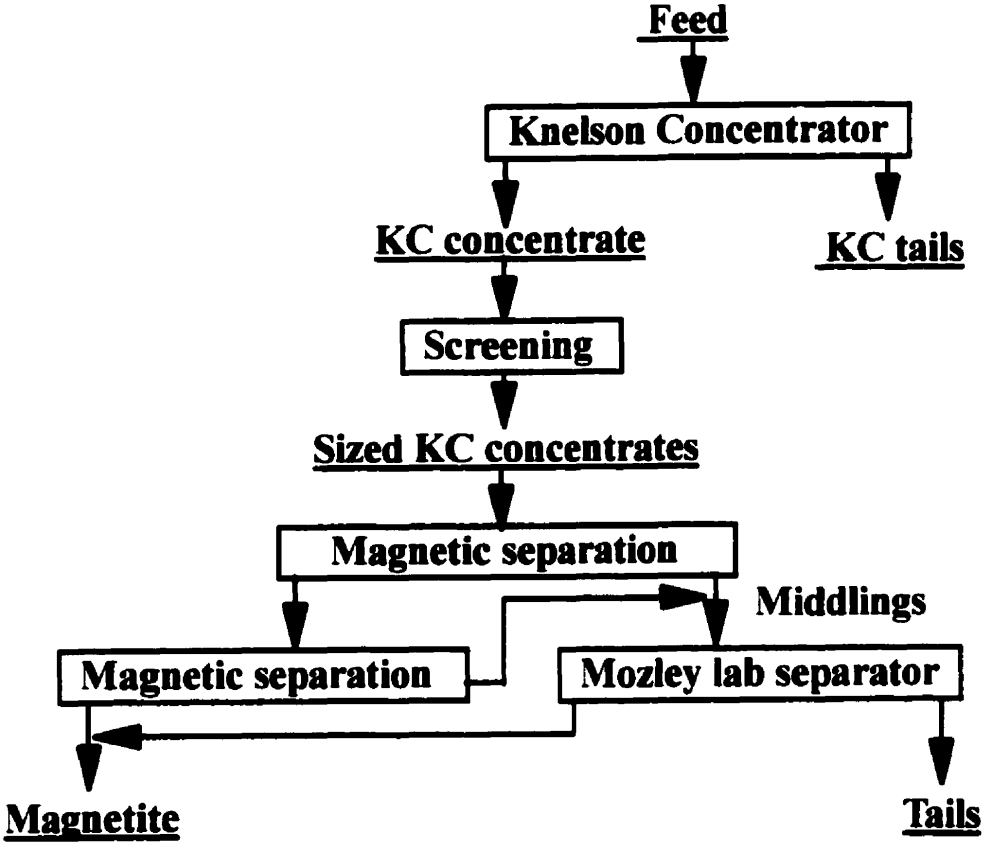

Figure 7-1 Methodology for magnetite-silica separation

magnetite concentrate, and then the middlings were treated with the MLS to recover residual magnetite. Recovery was calculated from the mass of magnetite recovered by magnetic separation and the MLS and that of the feed (i.e. the tail stream was not analyzed).

7.2 Experimental Results

7.2.1 Separation for the feed of 1.25% magnetite

Figure 7-2 shows how the rotating speed and fluidization velocity affected total magnetite recovery for the 1.25% magnetite feed. To test the reproducibility of the gravity experiments, two repeats were carried out for two conditions of 2 and 5 L/min at 115 Gs. Table 7-1 lists the experimental data of the repeated Knelson gravity tests, showing that the recovery difference of two repeated tests was 0.9 and 1.9%, respectively.

Table 7-1 Magnetite recovery of repeated Knelson gravity tests at 115 Gs

Fluidization	2 L/min		5 L/min	
Test No.	Test 1	Test 2	Test 1	Test 2
Recovery, %	61.1	59.3	66.6	64.7

Figure 7-2 shows that magnetite recovery varied from 35% to 89%, depending on both the rotating speed and fluidization velocity. Two features of the three recovery curves in Figure 7-2 can be observed. The first is that total magnetite recovery passed

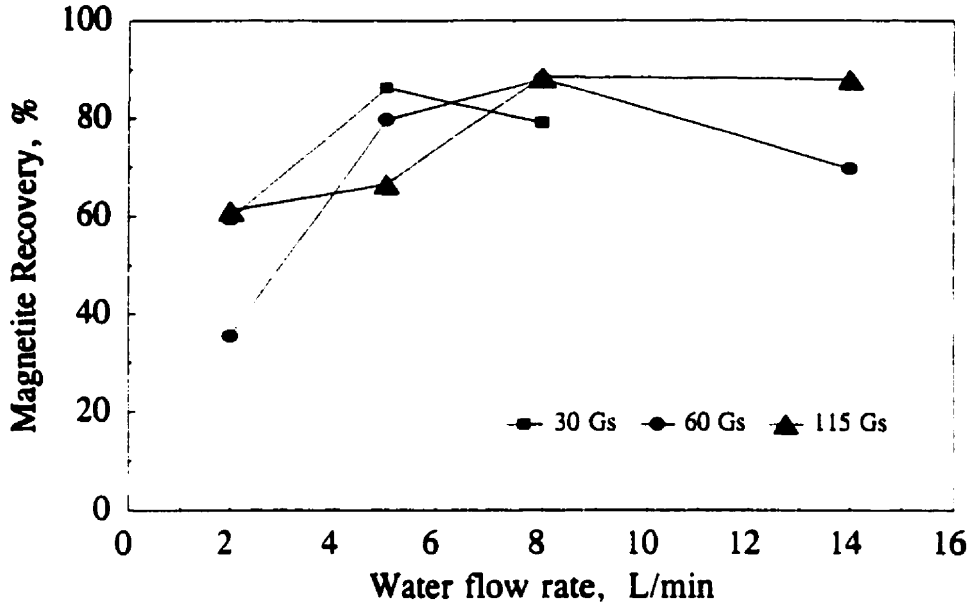

Figure 7-2 Magnetite recovery as a function of centrifuge acceleration and fluidization rate (feed grade: 1.25% magnetite)

a maximum at a given rotating speed. The maximum had also been observed with tungsten as the dense phase in the previous chapter. The second feature is that the peak shifted and increased slowly to a higher fluidization velocity as Gs increased. This could be attributed to the following two factors. First, since the separation zone tends to be more compact as rotating speed increases, the fluidization velocity has to be increased so as to keep the separation zone effectively fluidized. Second, since the centrifugal force applied on gangue particles also increases with increasing Gs, the fluidization velocity must be increased to maintain a water drag high enough to keep them from settling and moving on to the concentrate bed.

The effect of fluidization velocity and centrifuge acceleration on the mass of the concentrate corresponding to the tests in Figure 7-2 is shown in Figure A5-1 of Appendix 5. Except for the test at highest Gs and lowest fluidization flow, concentrate mass varied little. At a given Gs, the concentrate mass decreased with increasing fluidization velocity. At a given fluidization velocity, the highest Gs (115 Gs) resulted in the largest mass of concentrate, especially at the lowest fluidization velocity (2 L/min). The significant increase in concentrate mass at 115 Gs, as fluidization flow rate is reduced from 5 to 2 L/min, corresponds to a severe collapse of the flowing film, with less of fluidization and voidage between particles. As a result, magnetite recovery dropped markedly, although this drop is partly compensated by a large increase in yield (Figure A5-1), and as a result is not as significant as the corresponding loss at 60 or 30 Gs .

Figure A5-2 in Appendix 5 shows the D_{80} of the gangue in the concentrate as a function of fluidization velocity and centrifuge acceleration. Similar to the results shown in Chapter 6, the D_{80} of gangue in the concentrate increased with increasing fluidization velocity and decreasing acceleration (Gs), indicating that the size distribution of gangue in the separation zone became increasingly coarser than that of the feed (the D_{80} of the gangue in the feed was 130 μm). The lowest magnetite recoveries corresponded to D_{80}s in the concentrate closest to that of the feed.

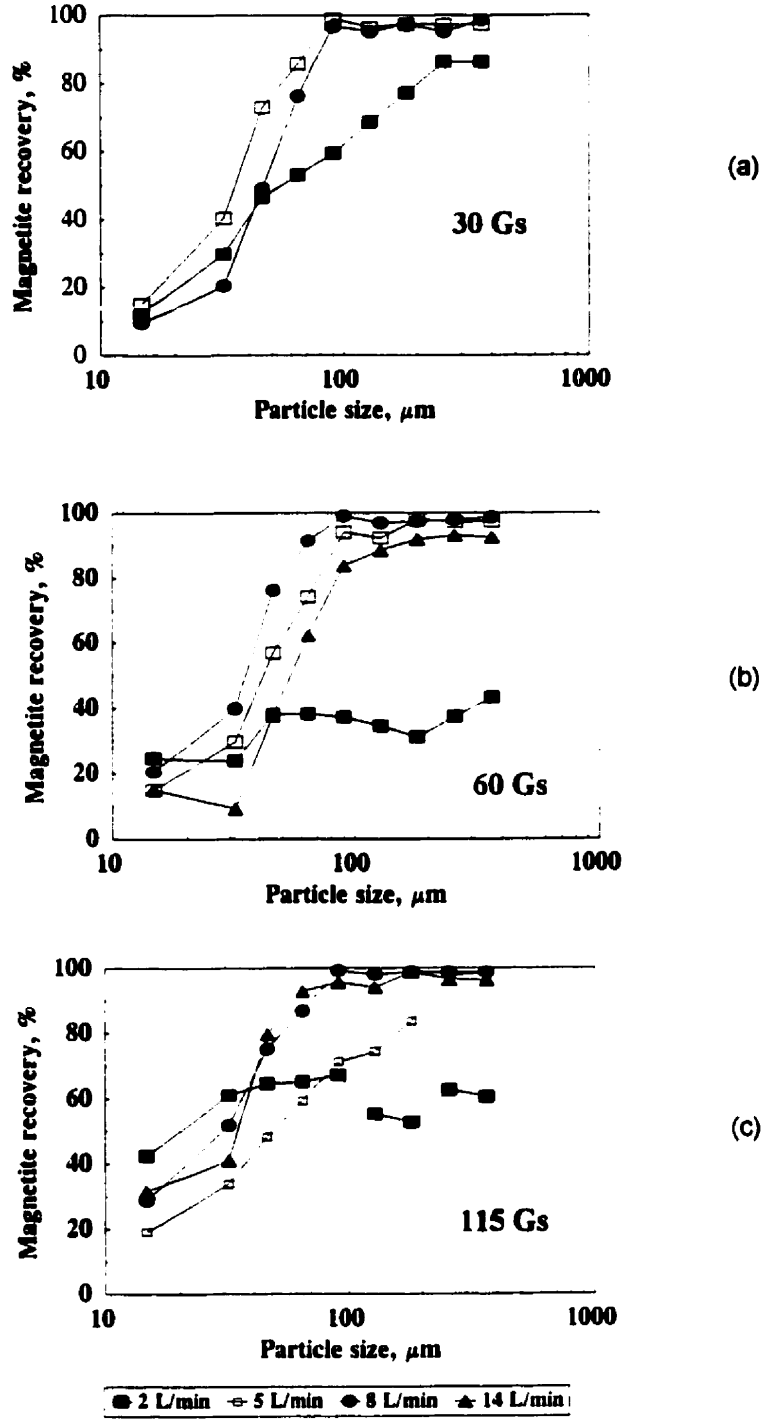

Figure 7-3 Magnetite recovery as a function of particle size and fluidization rate at different centrifuge acceleration (feed grade: 1.25% magnetite)

Size-by-size magnetite recoveries at different fluidization velocities are shown in Figures 7-3 for accelerations of 30, 60 and 115 Gs, respectively. In most cases the recovery of the finest magnetite particles (-38 μm) was very low. This observation is in good agreement with the percolation behaviour of fine magnetite observed in Figure 4-8 of Chapter 4. Thus, the low recovery of very fine magnetite particles is without doubt because of its low terminal settling velocity, too low to settle and percolate into the separation zone against the strong drag of fluidization flow, even in centrifugal field of 30 to 115 Gs. As a result, the recovery of the -38 μm magnetite fraction is highest at the highest Gs and lowest fluidization velocity. However, a penalty of this result is a low recovery of coarse magnetite fractions due to high compaction of separation zone.

For the +38 μm fraction, the size-by-size recovery was strongly dependent of both fluidization velocity and centrifuge acceleration. At a given Gs, low recoveries over almost the full size range took place at the lowest fluidization, 2 L/min; a gradual restoration of recovery of coarse magnetite then took place with increasing fluidization velocity, until the recovery dropped again at an over-fluidization velocity.

7.2.2 Separation for the feed of 2.5% magnetite

Figure 7-4 illustrates the effect of fluidization velocity and centrifuge acceleration on total magnetite recovery for the feed of 2.5% magnetite. These tests were performed to test the effect of feed grade, i.e. the possibility that too much magnetite in the feed could lead to a drop in recovery because of overload in the recovery zones. Thus, 50

grams of magnetite were fed, rather than 25 grams. Results are similar to those obtained with a 1.25% magnetite feed, and a small loss did indeed take place because of overload. However, the effect of rotating speed and fluidization flow is similar. For example, the maximum recovery at a given Gs is obtained at a similar fluidization flow, e.g. 5 L/min at 30 Gs and 8-9 L/min at 60 Gs.

Figure 7-5 shows that the size-by-size behaviour of magnetite is similar to that of the lower feed grade (Figure 7-3). Again, most curves assume the typical "S" curve of classifiers, except at high Gs (60 and 115) and low fluidization flow (2-4 L/min). Fine magnetite recovery is clearly much lower than with the 1.25% magnetite feed, an indication of possible erosion of these lighter particles from the concentrate bed.

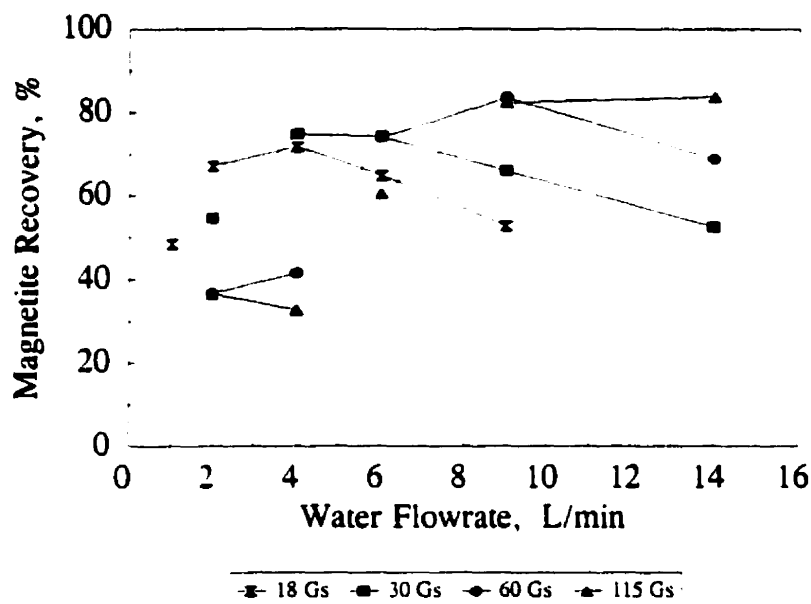

Figure 7-4 Magnetite recovery as a function of centrifuge acceleration and fluidization rate (feed grade: 2.5% magnetite)

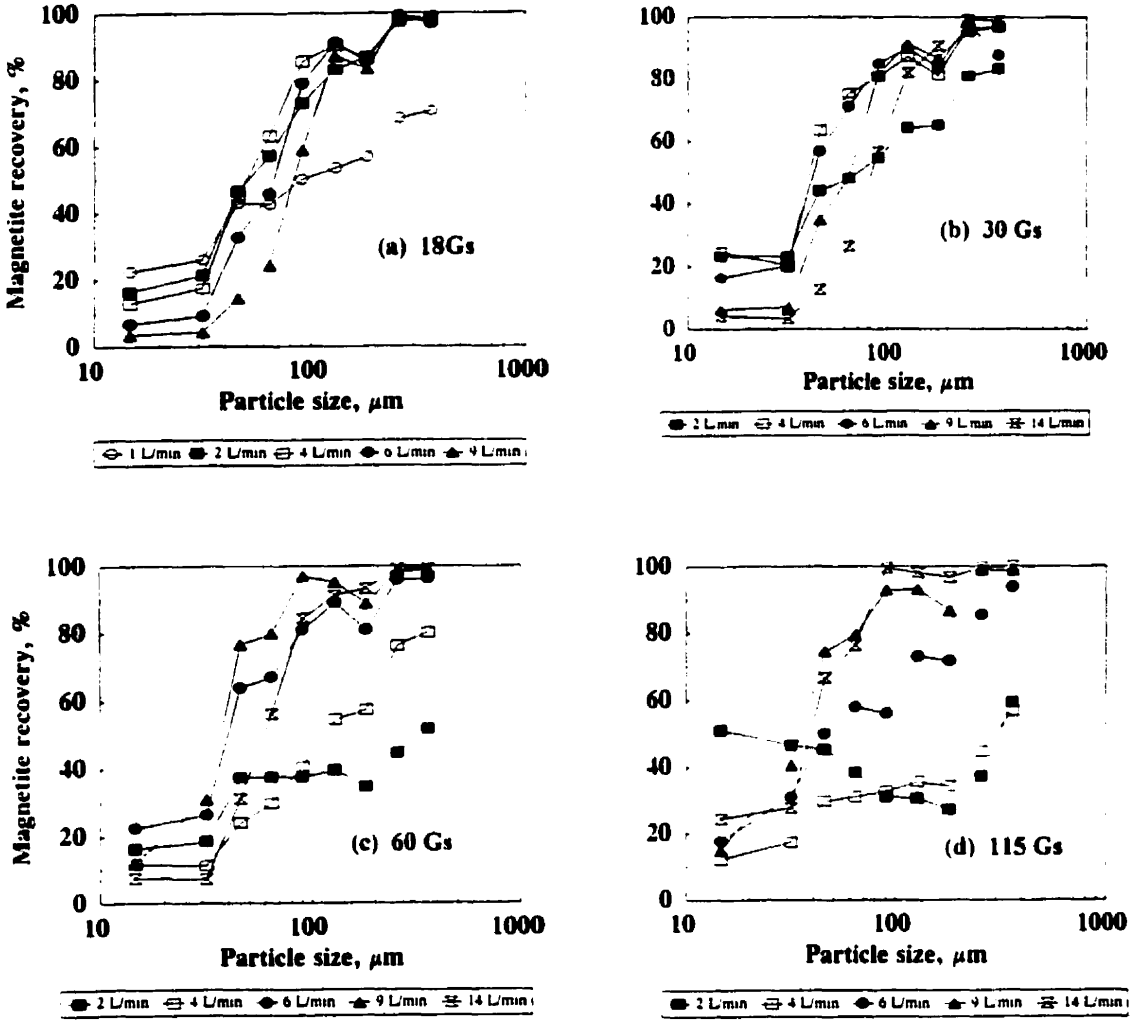

Figure 7-5 Magnetite recovery as a function of particle size and fluidization rate at different centrifuge acceleration (feed grade: 2.5% magnetite)

7.3 Discussion

7.3.1 Modelling the Optimum fluidization

The effect of acceleration on the optimum fluidization which was averaged from the data for the feeds of 1.25% and 2.5% magnetite is plotted in Figure 7-6. The minimum fluidizing velocity of 212-300 μm silica at one G (in the gravitational field), determined in Figure 4-3 of Chapter 4, is included as a reference.

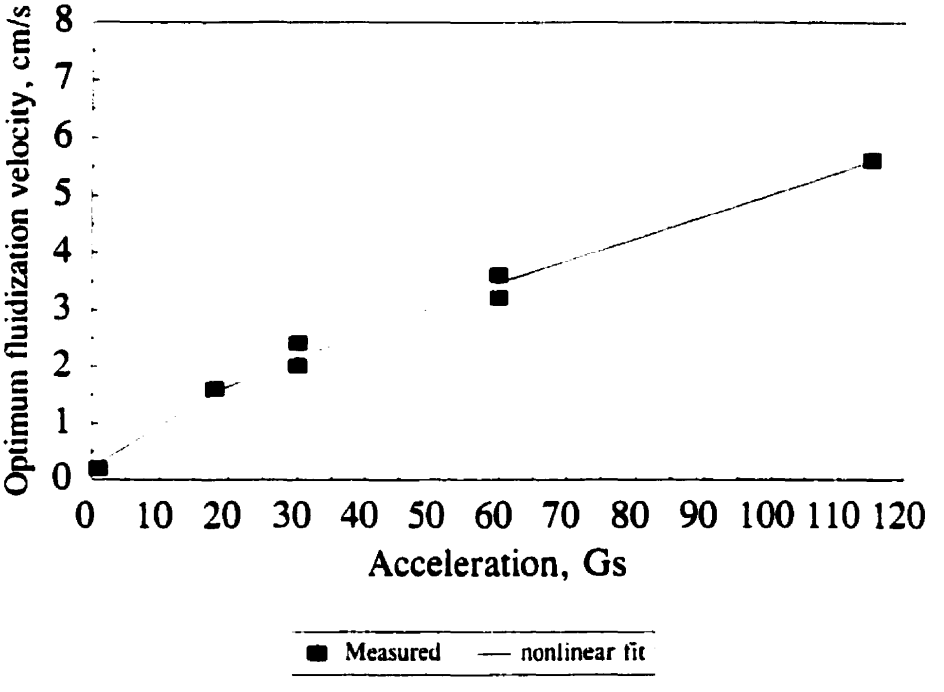

Figure 7-6 Optimum fluidization velocity as a function of acceleration for magnetite recovery

As shown in the figure, the optimum fluidization velocity increases with increasing acceleration of the concentrator, which is similar to the observation for tungsten recovery in Figure 6-11 of Chapter 6. Figure 7-6 shows a good nonlinear fit for the test data, hence the estimation of the optimum fluidization velocity for magnetite concentration may be given by the following equation:

$$U_{max} = 0.26\sqrt{Gs} + 0.02Gs \qquad (7.1)$$

where U_{max} is the optimum fluidization velocity, cm/s. The validity of this empirical relationship is restricted to the feed size distribution tested.

7.3.2 Relation between the D_{80} of the gangue and acceleration

Figure 7-7 shows the ratio of the D_{80}s of the gangue and magnetite in the concentrate and the concentrate mass as a function of acceleration at the optimum fluidization for the feeds of 1.25% and 2.5% magnetite. The curves of the D_{80} ratio versus acceleration are basically level at ratios of 1.9 for the feed of 1.25% magnetite and 1.8 for the feed of 2.5% magnetite. The curves of the optimum concentrate mass remain almost horizontal at a position of 87 grams for the feed of 1.25% magnetite and 95 grams for the feed of 2.5% magnetite, indicating that higher feed grade yields a higher concentrate mass. These phenomena are similar to those observed in Figure 6-12 for tungsten recovery. Hence, it is clear now why the optimum fluidization velocity had to increase with increasing acceleration: to prevent gangue particles moving into the separation zone and keep the fractional voidage of the separation zone at a constant and optimum value.

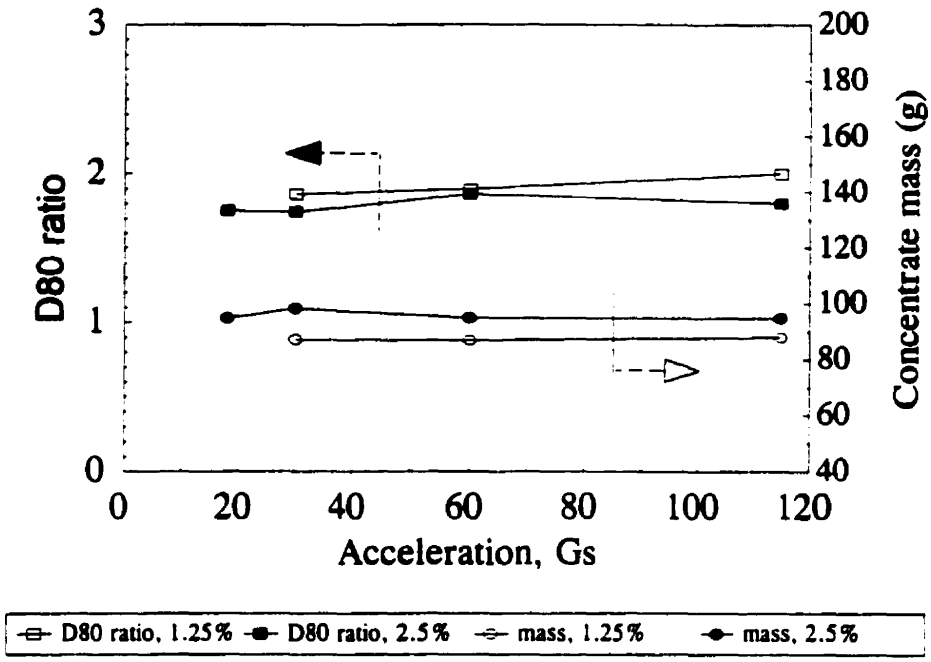

Figure 7-7 D_{80} ratio of the concentrate and the optimum concentrate mass as a function of centrifuge acceleration for magnetite recovery

7.3.3 Characterizing Knelson separation

Since the shapes of the size-by-size recovery curves of the magnetite - silica system are essentially similar to the typical "S" curves of classifiers, except under poor fluidization, the classifier-mixer model described by Plitt et al (1990, 1980, and 1976) according to a Rosin-Rammler's equation can be used to express this type of Knelson separation. That is

$$p_i = \{1 - \exp[-0.693(d_i/d_{50c})^m]\}(1 - r_i) + r_i \qquad (7.2)$$

where p_i is the mass fraction of particles of a given size and density which will be directed to the concentrate as a result of the classifying action; m is the sharpness of

separation coefficient; d_i is the characteristic size of particle size class i; d_{50c} is the corrected cut size; r_i is the fraction of particle i in the concentrator feed which reports to the concentrate by short circuit.

For the Knelson gravity separation, the values of the three variables (d_{50c}, m and r_i) can be estimated by optimizing (i.e. minimizing the lack-of-fit) some combination of variables in Plitt's model (Equation 7.2). Table 7.2 lists the values of m and d_{50c} which correspond to those gravity separation tests with recoveries around the optimum in Figure 7-5. The corresponding values of r_i are almost zero and not included in the table. Figure 7-8 shows the cut-size, d_{50c}, as a function of centrifuge acceleration (Gs) of the concentrator in the optimum fluidization range.

Table 7.2 Estimation of m and d_{50c} for gravity separation tests

Test conditions	Variables	
	m	d_{50c}, μm
18 Gs & 2 L/min	1.13	55
18 Gs & 4 L/min	1.63	51
30 Gs & 4 L/min	1.05	41
30 Gs & 6 L/min	1.44	45
60 Gs & 6 L/min	1.00	41
60 Gs & 9 L/min	1.66	32
115 Gs & 9 L/min	1.60	34
115 Gs & 14 L/min	2.30	45

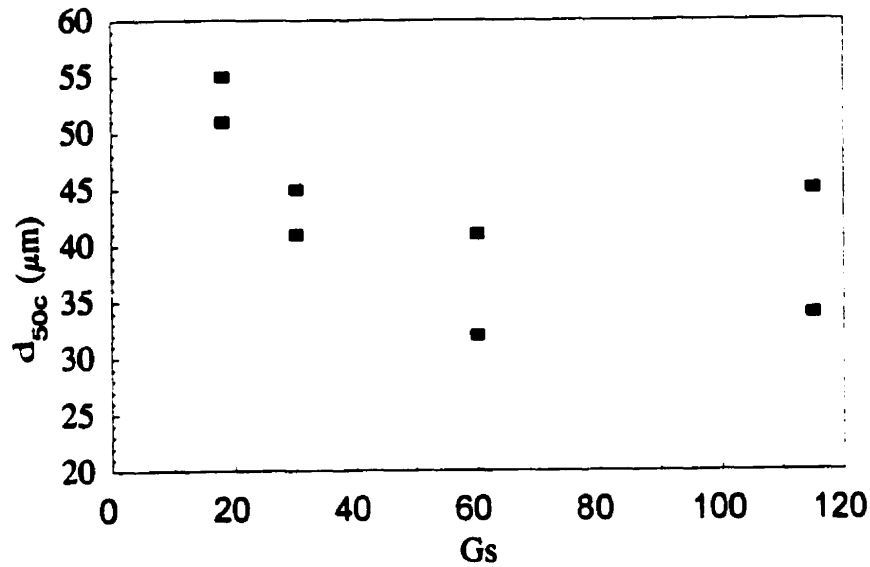

Figure 7-8 The cut-size, d_{50c}, as a function of centrifugal acceleration in the optimum fluidization range

Separation sharpness, except for one measurement at 115 Gs, is in the 1 - 1.7 range with no obvious trend. The d_{50c} clearly decreases as acceleration increases from 18 to 60 Gs, but the trend is lost between 60 and 115 Gs (possibly because of experimental error). Because the d_{50c} represents the size with a recovery of only 50%, the potential for adequate recovery below 40 μm is clearly limited. Above 40 μm, there is no need to increases acceleration above 60 Gs.

7.4 Conclusions

(1) At a given rotating speed, total magnetite recovery passed a maximum as fluidization rate increased from 1 to 14 L/min, and the peak of the recovery curve shifted gradually to a higher fluidization rate as rotating speed increased.

(2) Under the conditions studied in this work, the recovery of magnetite from silica was lower than that of tungsten from silica because of low solid-liquid density difference for magnetite.

(3) The loss of fine magnetite (-38 μm) was significant for all conditions studied in this work. Recovery of fine magnetite was maximized at 115 Gs and a fluidization rate of 2 L/min, where fine magnetite could be imparted high centrifugal force and while exposed to a small fluid drag, and the lowest overall magnetite recovery.

(4) Due to the moderate classification of the KC, there was a tendency for the size distribution of gangue particles in the concentrate to shift to a coarser size range with increasing fluidization rate and decreasing rotating speed. At the optimum fluidization velocity, the ratio of D_{80}s of the gangue and magnetite particles in the concentrate was approximately constant to 1.9 or 1.8 for all rotating speeds studied.

(5) At any acceleration, the shape of the recovery vs particle size curve shifted to that of a classifier as fluidization flow increased. The effect of acceleration on the sharpness of this classification showed no clear trend, and only a limited decrease in the classification cut-size with increasing acceleration.

CHAPTER 8 THE EFFECT OF FEED RATE ON SEPARATION OF TUNGSTEN FROM SILICA GANGUE

This test series was designed to study how the rotating speed and the feed rate affect the performance of the Knelson concentrator under conditions of optimum fluidization, and investigate the mass and size distributions of the concentrate in each ring of the inner bowl, which is an indirect measure of capture kinetics.

8.1 Methodology

The 9-test design consisted of three levels of feed rates (0.5, 1.5 and 5 kg/min) and three levels of rotating speeds corresponding to 30 Gs, 60 Gs and 115 Gs. The lowest feed rate, 0.5 kg/min, yields the highest recovery with the 3-in KC (Laplante et al, 1996a), whereas the highest, 5 kg/min, is equivalent to a loading of 36 t/h[1] for a 30-in unit, which has 100 times the bowl surface of the 3-in unit. The experimental procedure was as follows:

(1) For each test, a 4 kg coarse synthetic feed containing 1% tungsten and 99% silica was prepared by weighing each component size-by-size to achieve the size

---

[1] The manufacturer gives a nominal capacity of 36 t/h for a 30-in Knelson.

distribution shown in Table 8.1. It was fed manually at the chosen rate with proper slurrying water to the KC running at the chosen rotating speed matched with the optimum fluidization rate (i. e., 3 L/min for 30 Gs, 4 L/min for 60 Gs, and 6 L/min for 115 Gs). For the high feed rate tests (1.5 and 5 kg/min), the downcomer was replaced with one of a larger diameter (Laplante et al, 1996a).

Table 8-1 Size distributions of tungsten and silica (% Mass)

Size (μm)	Mass (%)
850-1180	3.06
600-850	4.80
425-600	10.63
300-425	10.98
212-300	11.66
150-212	11.89
106-150	13.46
75-106	11.63
53-75	10.46
38-53	7.13
25-38	2.32
-25	1.96
Total	100.00

(2) At the end of each test, the KC concentrate was recovered and screened into four size ranges (300-1180 μm, 106-300 μm, 38-106 μm, and -38 μm). Each size range was processed with a Mozley laboratory separator to analyze tungsten recovery.

(3) For the four Knelson gravity tests under extreme conditions, i.e., at 30 and 115 Gs and the feed rates of 0.5 and 5 kg/min, the concentrate was analyzed ring-by-ring. A set of rubber stoppers of different diameters and suitable thickness was used to block the rings of the inner bowl in order to remove the concentrate from

each individual ring as soon as the KC test was finished, starting with Ring 5. Figure 8-1 shows the schematic arrangement of the stoppers in the inner bowl. By turning the inner bowl upside down and removing each stopper, the concentrate in each ring could be flushed completely into a container.

8.2 Results and Discussion

8.2.1 Total tungsten recovery

Figure 8-2 shows how the feed rate and rotating speed of the KC affects total tungsten recovery. At the lowest feed rate (0.5 kg/min), total tungsten recoveries were very high (around 97.5%) for all three rotating speeds studied. However, the recoveries decreased gradually and almost linearly as the feed rate was increased to 5 kg/min. This trend was obviously caused by the reduced retention time of the feed in the inner bowl. Recovery decreased at an increasing rate with decreasing Gs. Thus, the difference in the slopes of the recovery curves can be attributed to the difference in the centrifuge acceleration of the feed slurry. At higher rotating speed, more tungsten particles imparted higher centrifugal force and were able to percolate or migrate to the concentrate bed, thereby causing a lower loss of tungsten at high feed rate.

Since tungsten recovery decreased almost linearly with increasing feed rate, a general model for the recovery curves in Figure 8-2 can be expressed by

$$R_W = - k_r * f(Q_s) \qquad (8.1)$$

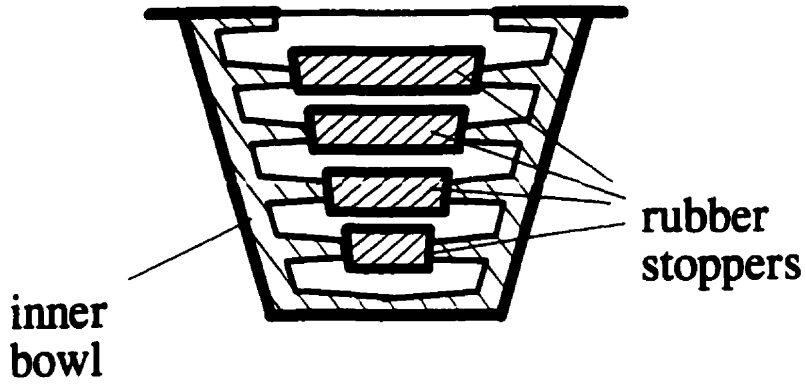

Figure 8-1 Methodology for analysis of ring-by-ring recovery

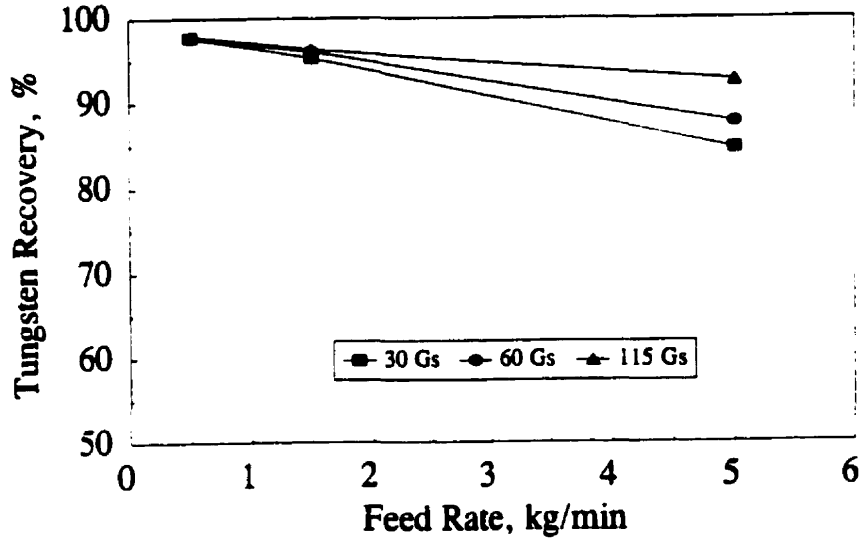

Figure 8-2 Tungsten recovery as a function of feed rate (fluidization rate: 3 L/min for 30 Gs, 4 L/min for 60 Gs, and 6 L/min for 115 Gs)

where R_W is the percentage tungsten recovery; Q_s is the feed rate, kg/min; k_r is a constant that depends on the rotating speed of the KC (and probably depends on the size distribution and density of gangue), which is the slope of the recovery curve, min/kg.

8.2.2 Size range-by-size range analysis

Figure 8-3 shows size range-by-size range tungsten recovery for the nine tests. For all rotating speeds, tungsten losses below -106 μm increased with increasing feed rate and decreasing rotating speed. Percolation velocity in this system clearly decreased with decreasing tungsten particle size.

8.2.3 Ring-by-ring analysis

Figure 8-4 presents tungsten recovery as a function of the ring number at 30 and 115 Gs and the feed rates of 0.5 and 5 kg/min, which represent the extreme operating conditions of the test series. Recoveries of the lower three rings (Rings 1, 2 and 3) were higher than those of the two upper rings, as most tungsten was recovered into the lower part of the inner bowl. This phenomenon was much more pronounced at the lowest feed rate, at both rotating speeds (recovery in Ring 5 was almost negligible).

It should be noted that tungsten recovery at the top ring (Ring 5) for the highest feed rate was still significant (about 8% at both 30 and 115 Gs). This suggests that extending the length of the inner bowl (i.e. increasing the number of rings could be an

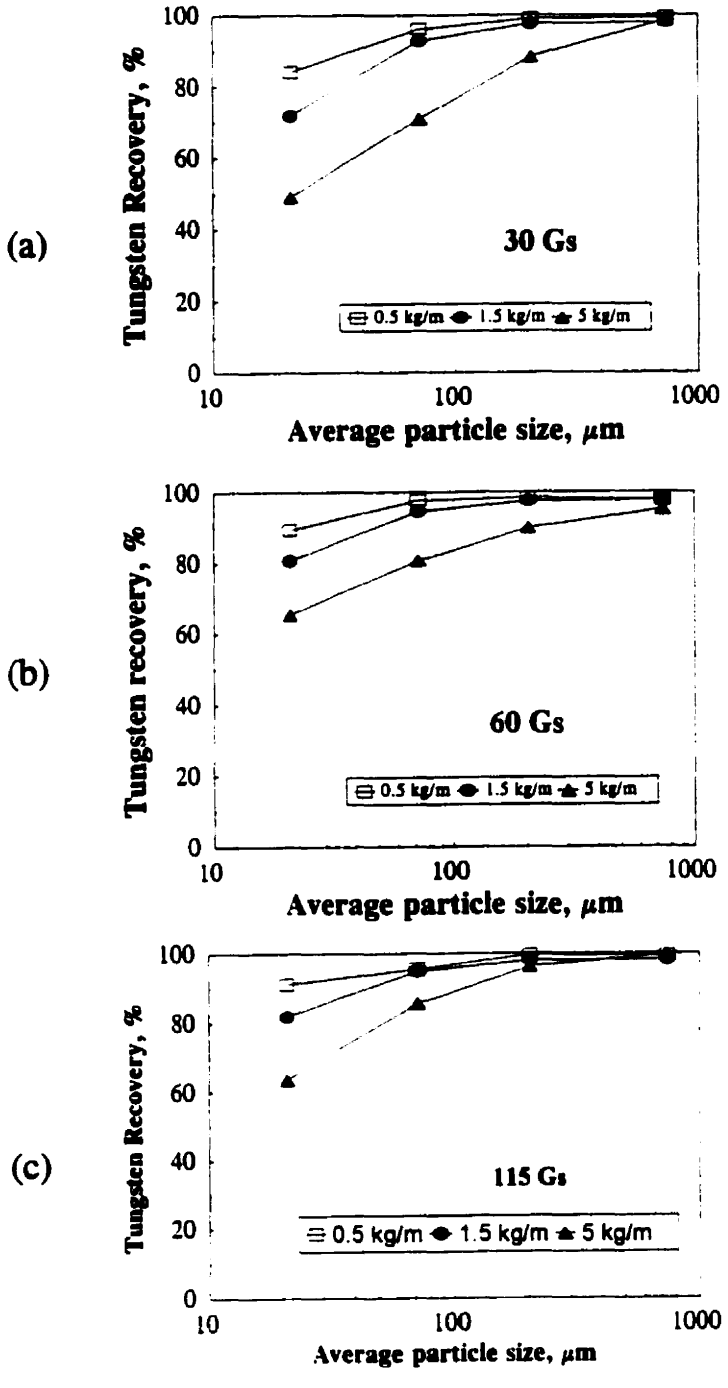

Figure 8-3 Tungsten recovery as a function of particle size and feed rate at different centrifuge accelerations (gangue type: -1180 μm silica)

effective approach to maximize the overall recovery at the high feed rate. In a closed-loop application, most of the lost fine gold would be recycled back to the unit feed.

At the low feed rate, there is little difference in overall recovery between 30 and 115 Gs, and virtually all of the tungsten has been recovered after four rings. At the high feed rate, recovery is highest in Ring 1, and drops to level at around 10% for each of Rings 3, 4 and 5, whereas it drops more steadily at 115 Gs. Because recovery is so size dependent, only size-by-size data can yield additional insight into the mechanisms which yield such results. This will now be presented.

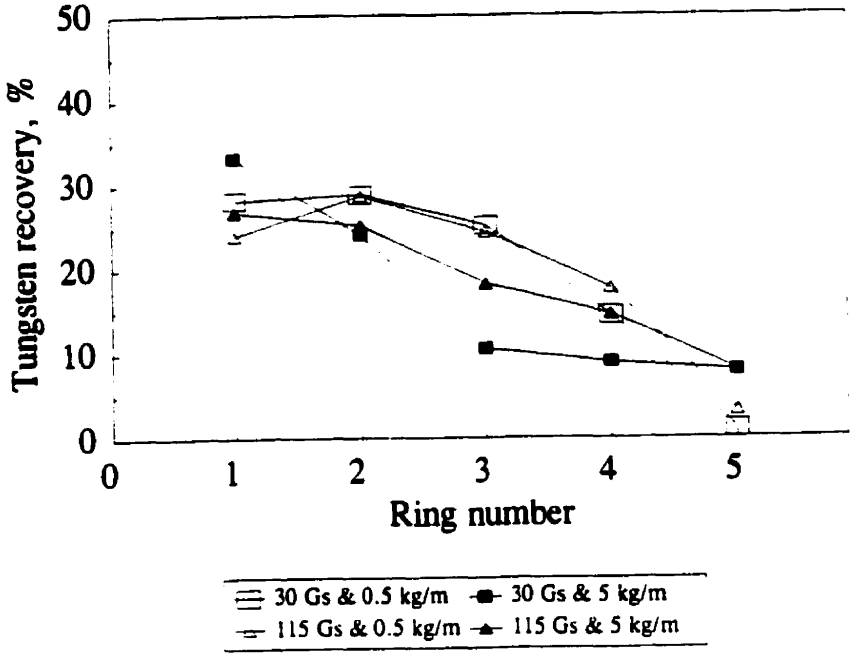

Figure 8-4 Tungsten recovery as a function of the number of ring at 30 and 115 Gs and the feed rates of 0.5 and 5 kg/min (gangue: -1180 μm silica)

8.2.4 Analysis of ring-by-ring and size-by-size

Figure 8-5 shows tungsten recovery as a function of the ring number and average particle size at accelerations of 30 and 115 Gs and feed rates of 0.5 and 5 kg/min, respectively. Figure 8-5(a) shows that at low Gs and feed rate, the relatively small differences in the recovery of each size class (Figure 8-3a) are amplified when ring-by-ring recovery is examined. Ring 5 is only recovering the finest tungsten fraction. Ring 1, which can only recover fast percolating and migrating tungsten, or that which is close to the concentrate bed upon feeding, shows a steadily decreasing recovery with decreasing particle size. The three intermediate rings recover all size classes equally, or with no detectable pattern.

Still at 30 Gs but a feed rate of 5 kg/min, as seen in Figure 8-5(b), ring-by-ring recovery has dramatically changed. The much shorter retention time requires very high migration velocity for recovery in Ring 1; consequently, recovery drops dramatically from 58% for the coarsest fraction down to a mere 6% for the -38 μm fraction. In the second ring, the higher percolation or migration velocity of the coarser particles is still apparent, especially for the 106-300 μm size class. The last three rings recover much less of the two coarsest size classes, and about equal amounts of the two finest size classes. Obviously, a sixth ring would recover significant amount of tungsten from all size range but the coarsest one (i.e. retention time is only adequate for the coarsest (+300 μm) material).

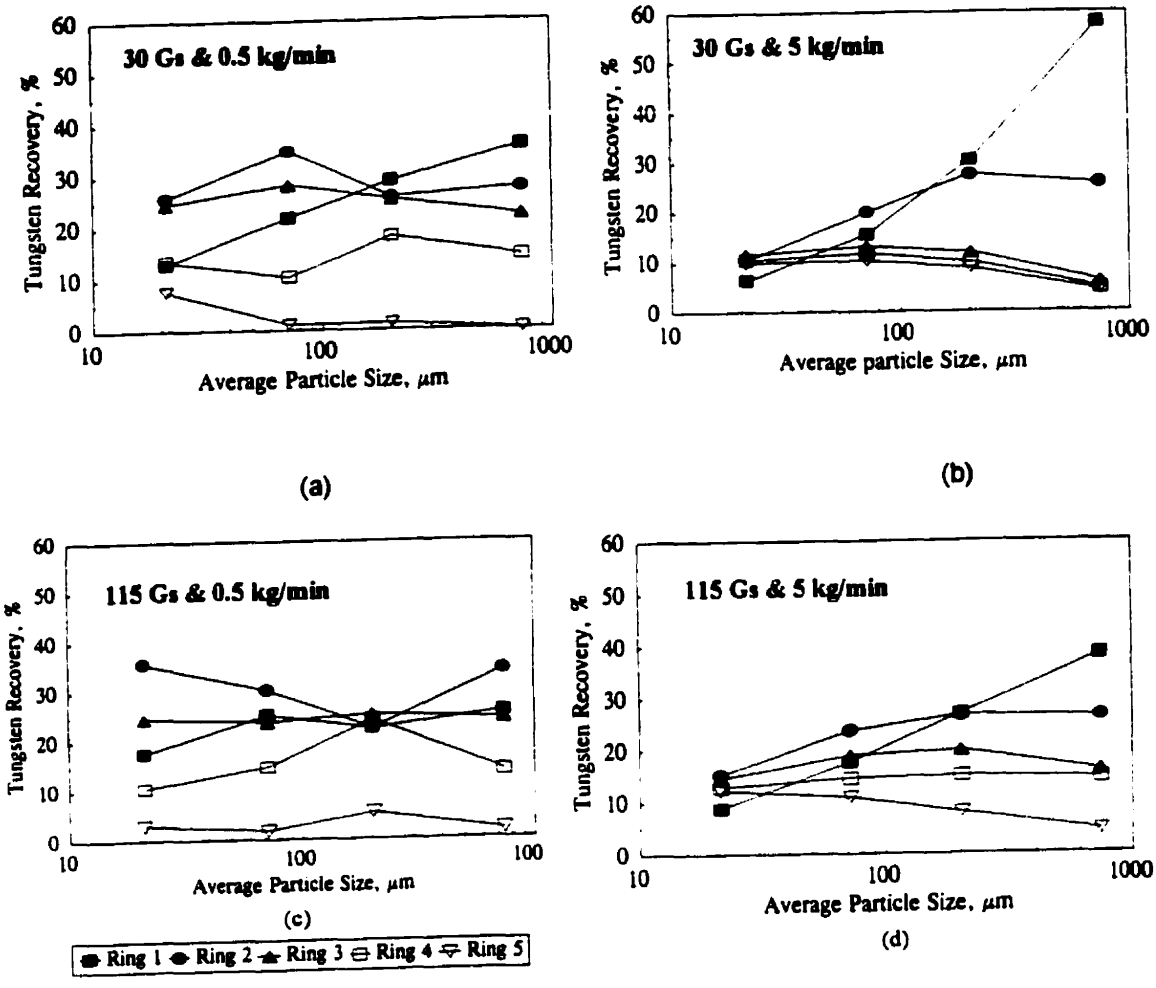

Figure 8-5 Tungsten recovery as a function of particle size and the ring number at accelerations of 30 and 115 Gs and the feed rates of 0.5 and 5 kg/min: (a) 30 Gs and 0.5 kg/min; (b) 30 Gs and 5 kg/min; (c) 115 Gs and 0.5 kg/min: and (d) 115 Gs and 5 kg/min

Figure 8-5(c), at high Gs but low feed rate, is very similar to 8-5 (a), but a revealing difference appears: the last ring serves more to recover the 106-300 μm material (recovery: 6%) than the -38 μm material (recovery: 3%). This observation is in good agreement with the dip in recovery in the 106-300 μm size range observed in Figure 6-10 for the same system (coarse silica gangue), and repeated in many other systems (e.g. Figures 6-8 and 6-4). Partial collapse of the flowing slurry due to the higher Gs hinders percolation and migration in the intermediate size range.

Figure 8-5 (d) confirms the rather surprising observation that recovery in Ring 1 for the coarsest size class went up from 36 to 58% at 30 Gs when feed rate increased from 0.5 to 5.0 kg/min. At 115 Gs, the corresponding increase is lower, 26 to 38% (still above the experimental error, an estimated 2%). Other trends of Figure 8-5 (c) are also confirmed, such as the decreasing recovery of Ring 1 with decreasing particle size. Recoveries of the two finest fractions are generally below those of Figure 8-5 (c) for each ring, thus resulting in a lower total recovery (92.7%, as shown in Figure 8-2) than that of Figure 8-5 (c) (97.9%). It is extremely likely that the increase in recovery of Ring 1 (as feed rate increases from 0.5 to 5 kg/min) is due to the inability of the KC to accelerate the slurry to its theoretical acceleration (i.e. 30 or 115 Gs) before the feed passes over Ring 1 at the higher feed rate. The lower acceleration had been found to increase recovery in Chapter 6 (Figure 6-9). The lower effective rotating velocities,

hence lower Gs, fail to collapse the feed slurry to any significant extent, resulting in a high voidage and very high migration velocity for the coarsest size fraction.

8.2.5 Kinetics of separation

Since kinetics for most mineral processes is first-order (Kelly et al, 1982; Laplante, 1989), the rate of separation of mineral particles with identical size, density and shape in the KC can be described by the following equation (Hu et al, 1991):

$$dR/dt = K'(1-R) \qquad (8.2)$$

where R is recovery fraction at time t, and (1 - R) is the loss of mineral particle at time t, or the fraction unrecovered; K' is the rate constant.

When t = 0, R = 0. Then, integrating Equation 8.2 gives (Hu et al, 1991):

$$\ln\frac{1}{1-R} = K' * t \qquad (8.3)$$

For the Knelson Concentrator, each ring of the inner bowl can be considered a stage of separation with (approximately) an equi-retention time. Hence, the relationship between the fraction unrecovered and ring location actually represents the kinetics of the Knelson separation. That is:

$$\ln\frac{1}{1-R} = K*i \qquad (8.4)$$

where i is the number of a ring, and K a dimensionless rate constant (proportional to K').

Figure 8-6 shows the semi-log value of (1/(1-R)) as a function of the number of the ring for the four conditions used in Figure 8-5, which can be used to estimate the rate constant. As a first approximation, capture kinetics for each tungsten size fraction is essentially first-order, although the linearity may tailor off when only small masses of tungsten are left unrecovered. Estimation of the rate constant, K, for each size fraction of tungsten was made from the slope of each curve in Figure 8-6 and listed in Table 8.2.

Inspection of Figure 8-6 suggests that first order can represent capture kinetics for the two finest fractions, for all four conditions tested, and for the test at 30 Gs and 5 kg/min. However, for the two coarsest size classes, particularly at 115 Gs and a feed rate of 5 kg/min, there is a clear indication that the rate constant (i.e. the slope of the curve) increases with increasing ring number. (Although it could also be claimed that the kinetic order is higher than unity, this is a very unlikely possibility.) This result is consistent with the hypothesis that coarser particles are accelerated more slowly because of their higher inertia. As a result, their rotation velocity (and the centrifuge

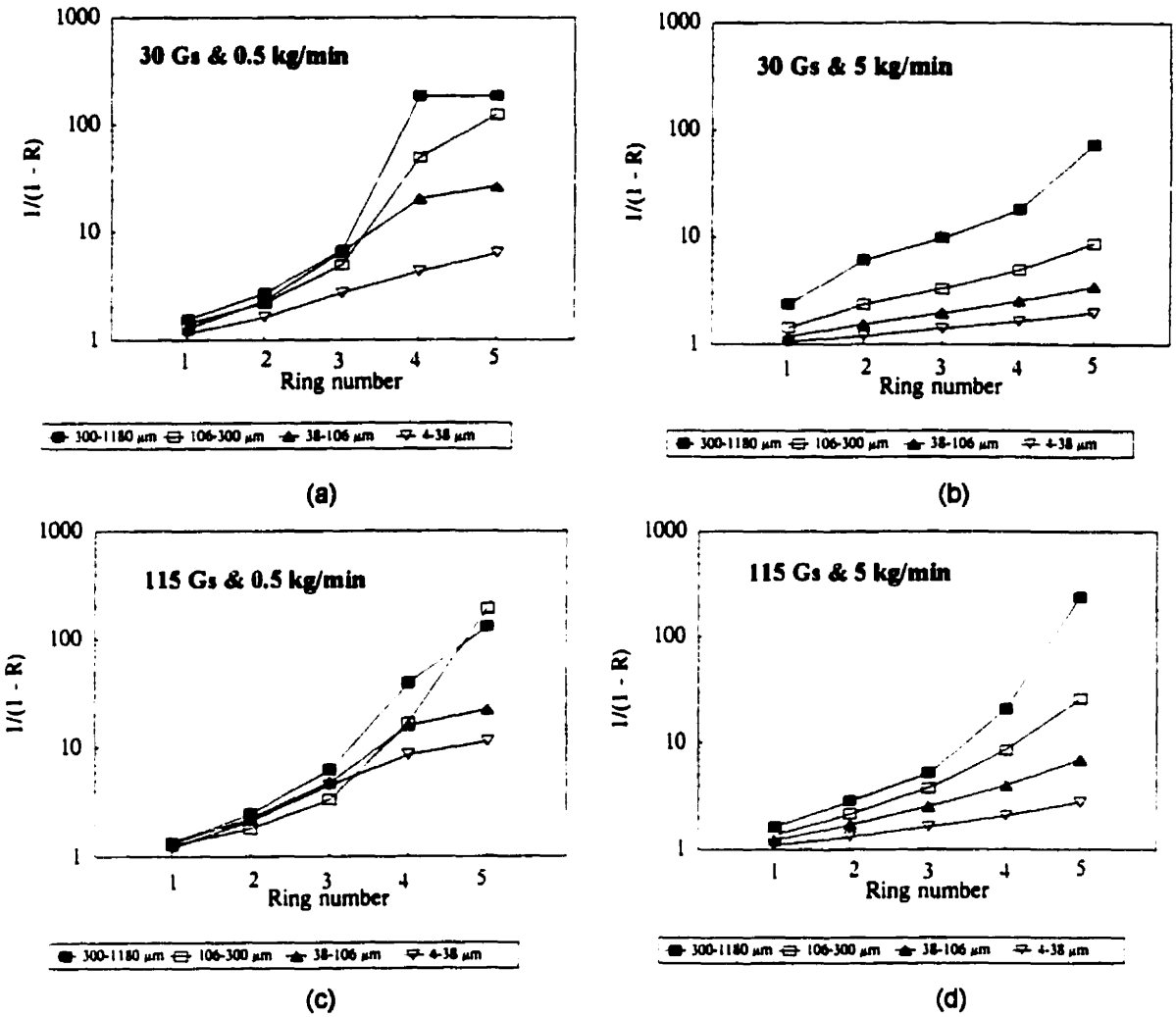

Figure 8-6 1/(1-R) as a function of particle size and the ring number at accelerations of 30 and 115 Gs and the feed rates of 0.5 and 5 kg/min: (a) 30 Gs and 0.5 kg/min; (b) 30 Gs and 5 kg/min; (c) 115 Gs and 0.5 kg/min; and (d) 115 Gs and 5 kg/min

Table 8.2 The rate constant K for different size fractions of tungsten

Rotation & feed rate	300-1180 μm	106-300 μm	38-106 μm	4-38 μm
30 Gs & 0.5 kg/min	0.37-0.81	0.32-0.81	0.74	0.39
30 Gs & 5 kg/min	0.80	0.42	0.25	0.14
115 Gs & 0.5 kg/min	0.38-0.76	0.24-1.22	0.68	0.54
115 Gs & 5 kg/min	0.29-1.22	0.25-0.56	0.39	0.21

force they are subjected to) increases from Ring 1 to 5, in such a way that capture rate constant also increases. Table 8.2 suggests that increases can be significant, especially at 115 Gs and a feed rate of 5 kg/min.

Table 8.2 shows that the capture rate constant decreases with decreasing particle size, particularly below 300 μm (i.e. for the three finest size fractions). Increasing rotation velocity increases the capture rate constant most significantly below 106 μm at high feed rate.

Comparing rate constants at 0.5 and 5 kg/min is extremely informative: since retention time is not explicitly included in Equation 8.4, one would expect the rate constant at the higher feed rate to be one tenth of that at the lower feed rate. In fact, the rate constants of the two coarsest size classes hardly drop at 5 kg/min, whereas the

drop for the two finest size classes is generally between twofold to three fold. This suggests that the recovery drop for the coarsest size classes at very high feed rate is minor, whereas for finer (<106 μm) material, the drop is more significant but easily compensated by the significantly higher feed rate. Thus, for typical applications where the KC feed is a bleed of the grinding circulating load, it would be beneficial to run plant units at very high feed rates (and higher Gs), to maximize the mass of gold recovered (as opposed to stage recovery). For alluvial operations with many KCs, series operation may be preferable to the more classical parallel circuits.

That increasing feed rate tenfold only reduces the recovery of coarse (>106 μm) tungsten slightly strongly suggests a retention time very different from that of the liquid phase, or even other mineral particles. This is likely to make the phenomenological modelling of Knelson Concentrators and similar units very difficult.

For gold recovery from grinding circuits, fine gold is always present, whereas coarse gold will be absent from the cyclone if it is absent from the ore itself. The benefits of a higher rotation speed are limited to finer gold (<106 μm) recovery, and may be negated by higher wear and water consumption (although the latter can be initiated with the use of a water saving cone). It is suggested that when GRG is predominantly below 106 μm, a higher rotation speed should be used, or at least tested.

8.3 Conclusions

1. For all the three rotating speeds studied, tungsten recovery decreased gradually and almost linearly as the feed rate increased from 0.5 to 5 kg/min, and the slope of the recovery curve became smaller with increasing Gs. This suggests that reductions of both the retention time of the feed and rotating speed have a negative effect on the performance of the Knelson.

2. Under the conditions studied in this work, most of the tungsten was recovered and built up in the lower rings of the inner bowl. The coarsest tungsten particles tended to be recovered in the lowest ring (Ring 1).

3. The rate constant of capture basically increased with increasing particle size at constant rotation speed and feed rate. At constant rotating speed, the rate constant (with ring number used as a measure of retention time) of the finer (< 106 μm) size fraction was lower at high feed rate than at lower feed rate. For a lower feed rate, the rate constant of a given size fraction was almost similar for both high and lower Gs.

4. The effect of a tenfold variation in feed rate was small for coarse (> 106 μm) tungsten and moderate for fine (< 106 μm) tungsten, suggesting that feed rate should be maximized in typical grinding circuit applications.

CHAPTER 9 GENERAL CONCLUSIONS

9.1 General Summary

The main findings of this thesis may be summarized as follows:

(1) The percolation and migration of dense particles in a fluidized gangue bed at one G (i.e. in the gravitational field) was found to be dependent of the density and size of both dense and gangue particles, and fluidization velocity. There was an intermediate fluidization flow rate which maximized recovery. High density gangue, especially when coarse, had a detrimental effect on percolation and migration. Particles of higher density percolated or migrated faster than those of lower density. When the gangue bed was well fluidized, the migration velocity of coarse particles was higher than the percolation velocity of fines. These fundamental findings can be used to explain some of the recovery mechanisms of fluidized semi-batch centrifuge concentrators.

(2) At constant fluidization pressure, the fluidization flow rate in the inner bowl decreased with increasing rotating speed. The superficial fluidization velocity was found to decrease slightly with increasing ring diameter. This is consistent with the above finding, as hole density is constant from ring to ring, and the centrifuge force increases with increasing ring diameter (i. e. from Ring 1 to 5). The thickness of the flowing film was measured and found to increase with decreasing rotating speed. At a given rotating speed and fluidization flow, the film thickness increased gradually from the bottom to the top of the inner bowl due to the confluence of fluidization flow from each of the

rings. The relationship between the fluid flow rate and the thickness of the flowing film at the top rib followed the classical weir model well, i.e. the fluid flow rate is directly proportional to 1.5 exponents of the thickness of the flowing film, with an empirical coefficient equal to 0.6.

Under normal operation conditions, the retention time of the flowing film decreases with increasing rotating speed and increasing fluidization flow rate. The decrease in retention time at high Gs is offset by a decrease in film thickness, which lowers the average travelling distance from the flowing slurry to the concentrate bed. The Reynolds number of the flowing film was also determined, varying from 250 to 3200 as fluidization flow increased from 2 to 20 L/min. This intermediate Reynolds number suggests that the regime of the flowing film in the KC is transitional, probably moving with a slight breakdown of laminar or partial turbulence. In addition, it was found that rotating speed has little effect on the Reynolds number of the flowing film at constant fluidization flow.

(3) Rotating speed and fluidization flow were found to have a significant effect on the performance of the KC. In general, they affect both the movement of solid particles and fluidization of the flowing film and the top layer of the concentrate bed, which in turn affects KC performance. In this work, the peak of the recovery curves generally shifted to a higher fluidization flow rate as rotating speed increased, though the peaks of tungsten recovery curves were not as evident as those of magnetite recovery curves.

This indicates that the maximum recovery of dense particles is achieved at an optimum dynamic balance between the centrifugal force and the drag of fluidization flow, which maximises the amount of dense particles capable of migrating or percolating to the concentrate bed. In addition, it was found that the size distribution of gangue particles in the concentrate shifted to a coarser size range with increasing fluidization rate and decreasing rotating speed. This finding might imply that a classification process takes place in the first stage of or during the separation process. At the optimum fluidization velocity, the ratio of D_{80}s of the gangue and dense particles in the concentrate was approximately constant for all rotating speeds studied.

(4) When separating magnetite from silica, the loss of fine magnetite (-53 μm) from the KC was found to be significant for all conditions studied in this work, except for the highest Gs (115 Gs) and the lowest fluidization rate (2 L/min). For the magnetite silica system (top size: 425 μm), most of recovery vs size curves exhibited the type S-shape of hydro classifiers, thus confirming the classifying action of the KC. Under optimum separation conditions, the classification curve had a sharpness of separation coefficient (of Plitt's model) between 1.0 and 1.7. Increasing rotating velocity had only a modest effect on the cut size, suggesting that higher rotating velocity will only have a limited success in recovering finer particles. Although such a behaviour has never been reported for gold, it likely takes place below 25 μm (a size range which does not lead itself well to size-by-size characterization). At high rotating speed and low fluidization flow, the unit exhibited a very different behaviour not unlike that of a non-fluidized

centrifuge. Whilst this can be attractive for fines recovery, previous studies at McGill University have shown that such a performance is not very selective and cannot be sustained over long recovery cycles.

(5) The effect of feed rate on tungsten recovery from silica was investigated at three rotating speeds. It was found that tungsten recovery decreased gradually and almost linearly as the feed rate increased from 0.5 to 5 kg/min, and the slope of this decrease became smaller with increasing Gs. However, the effect of a tenfold variation in feed rate was small for coarse (>106 μm) tungsten and moderate for fine (<106 μm) tungsten, suggesting that for normal plant operations, feed rate should be maximized. The study of kinetics of separation shows that the rate constant of capture increased with increasing particle size at constant rotation speed and feed rate. At the same rotating speed, the rate constant of the finer (<106 μm) size fraction was lower at high feed rate than at lower feed rate. For a lower feed rate, the rate constant of a given size fraction was almost similar for both high and lower Gs.

(6) Equations for determining the instantaneous radial settling velocity of particles in the dilute zone of the inner bowl have been derived for the Stokes' Law region based on Newton's second law of motion. Also, equations for determining the instantaneous percolation or migration velocity of particles in the separation zone were tentatively derived, but with an unknown dynamic coefficient of friction. It can be expected from the equations of motion for a spherical particle in the radial direction that the

instantaneous radial settling velocity and percolation (or migration) velocity of the particle moving in the inner bowl of the KC depend not only on the centrifugal acceleration, particle size and density, but also on the radial fluidization fluid velocity.

9.2 Claims for Original Contributions

To the best of our knowledge the work in this thesis represents the first published study of the effect of rotating speed on the performance of the Knelson Concentrator. To obtain a more fundamental understanding of the recovery mechanisms of the Knelson Concentrator, the present study has also examined the percolation or migration behaviour of dense particles in a gangue bed in the gravitational field. Specific contributions are:

(1) A comprehensive experimental study of the performance of a 3-in Knelson centrifugal concentrator for different types of synthetic ores at three rotating speeds, and the effects of fluidizing water, gangue density, size distribution and the feed rate.

(2) The establishment of the relationship between the optimum fluidization velocity and rotating speed of the KC.

(3) The observation of a typical dip in tungsten recovery whenever fluidization flow was below the optimum, which resulted essentially from particle size instead of particle shape.

(4) A study of percolation and migration behaviour of dense particles in a vertical upward water flow and in the gravitational field, and the use of the experimental results to relate and explain recovery mechanisms of the Knelson Concentrator.

(5) The development of a simple and rapid method (i.e. the use of a set of rubber stoppers) to obtain the concentrate ring-by-ring, which helped effectively the author analyze the mass and size distributions of the concentrate in the inner bowl. Unlike a previous method developed at McGill University, a conventional (rather than split) inner bowl can be used, and experimental results can be directly compared to those of conventional tests.

(6) The examination of the effect of rotating speed and fluidization flow on the size distribution of gangue particles in the concentrate, which unfolds a hydro classification process which might have been carrying on in the first stage of or during centrifuge concentration.

(7) The determination of the thickness of flowing film in the inner bowl at four rotating speeds, thereby giving the relationship between the rotating speed and the retention time of the flowing film, and confirming that the relationship between the fluid flow rate and the thickness of the flowing film at the top rib obeys the classical weir model.

(8) A study of the kinetics of separation under conditions of different feed rates and Gs, using ring number as a measure of retention time, and the estimation of the rate constants of capture of different sizes of tungsten.

(9) An extension to the theory describing centrifugal separation of dense particles from gangue particles by deriving the equations of motion of a spherical solid particle in a fluidized centrifuge concentrator.

9.3 Suggestions for Future Work

There are many aspects of this relatively new field that warrant further study both from theoretical and experimental standpoints, which could have short-term industrial applications. Some specific points are:

(1) Experimental and theoretical exploration of the possibility of using air or pneumatic for part of the fluidization of the Knelson Concentrator. It is likely that the consumption of water for the KC would greatly decrease due to the use of air as an abundant (and free) substance for fluidization water. This should also improve the efficiency of recovering very fine dense particles since extreme high rotating speeds (higher than 200 Gs) would be possible and the thickness of the flowing film would decrease.

(2) The development of a new type of laboratory centrifuge that can achieve a higher recovery by means of periodical alternation of positive and negative fluidization. Since the existing Knelson Concentrator uses merely positive fluidization flow (positive means opposite to the settling of particles), the loss of very fine (-38 μm) of dense particles is significant, especially for separation of lower high density particles (i. g. magnetite) from silica gangue. To solve this problem, a periodically negative flow should also be applied to the slurry. The mechanism of alternating positive and negative fluidization flow would likely enhance the differential acceleration and interstitial trickling of particles and increase the recovery of very fine dense particles.

(3) Experimental study of oil-sands separation by high-temperature Knelson centrifugation. There is a huge source of oil-sands deposits in Canada; thus, it would be interesting to explore the possibility of using a high speed Knelson Concentrator to separate crude oil from sands at high temperature and compare technically and economically this gravity approach with conventional flotation. In addition, testing a flowsheet such as flotation followed by Knelson concentration or Knelson concentration followed by flocculation of fine sands in crude oil is also recommended.

(4) Experimental and theoretical studies of the percolation of fine dense particles in centrifugal fields with a fluorescent tracer technique. This would provide insight in the difference in percolation behaviour of fine dense particles between the gravitational and centrifugal fields.

(5) Experimental investigation of the recovery process of fine and extra fine dense particles from a narrow size feed with a very high rotating speed (300 Gs or higher) centrifuges. As noted in the gravity experiments of this work, the recovery of very fine (-38 μm) dense particles (either tungsten or magnetite) at the highest speed (115 Gs) and at the lowest fluidization flow (2 L/min) was higher than those of any other conditions, especially for low density gangue (silica). It would be interesting to further increase the rotating speed of the KC and decrease the fluidization flow to enhance the recovery.

(6) Experimental study of the separation of ores of intermediate density difference (i.e. between those tungsten-silica and magnetite-silica, such as cassiterite-silica) to complete the data bank for simulation.

REFERENCES

Altair International, 1996, The Centrifugal Jig, 1996 Annual Report, or from Internet: http://www.ctaonline.com/ir/centjig.htm.

Anonymous, 1983, New separator for fine gold recovery, Mining Journal, London, January, pp. 40-41.

Banisi, S., Laplante, A.R., and Marois, J., 1991, The Behaviour of Gold in Hemlo Mines Ltd. Grinding Circuit, CIM Bull., Vol. 84 (955), pp.72-78.

Beer, G., 1991, Gravity Circuit of the Darlot Gold Project Sundowner - Australia, a report of Technical Papers and Performance Reports, edited by Knelson Gold Concentrators Inc.

Beniuk, V.G., Vadeikis, C.A., and Enraght-Moony, J.N., 1994, Centrifugal jigging of gravity concentrate and tailing at Renison Limited, Minerals Engineering, Vol. 7, Nos. 5/6, pp. 577-589.

Brewis, T., 1995, Gravity separation, Mining Magazine, May, pp. 279-292.

Bridgwater, J., Cooke, M.H., and Scott, A.M., 1978, Inter-particle percolation: Equipment development and mean percolation velocities, Trans. Instn. Chem. Engrs., Vol. 56, pp. 157-167.

Bridgwater, J., and Ingram, N.D., 1971, Rate of spontaneous inter-particle percolation, Trans. Instn. Chem. Engrs, Vol. 49, 163-169.

Bridgwater, J., Sharpe, N.W., and Stocker, D.C., 1969, Particle mixing by percolation, Trans. Instn. Chem. Engrs., Vol. 47, T114-119.

Buonvino, M., 1993, A Study of the Falcon Concentrator, M.Eng. Thesis, McGill University, Canada, 195 pp.

Burt, R.O., and assisted by Mills, C., 1984, Miscellaneous methods of concentration, Gravity Concentration Technology, Elsevier Science Publishers B.V., pp. 373-385; Interstitial trickling, pp. 88-89.

Burt, R.O., Korinek, G., Young, S.R., and Deveau, C., 1995, Ultrafine Tantalum Recovery Strategies, Minerals Engineering, Vol. 8, No. 8, pp. 859-870.

Chan, B.S.k., Mozley, R.H., and Childs, G.J.C., 1991, Extended trials with the high tonnage Multi-Gravity Separator, Minerals Engineering, Vol. 4, No. 3/4, pp. 489-496.

Clift, R., Grace, J.R., Weber, M.E., 1978, Bubbles, Drops, and particles, Academic Press, 380 pp.

Clifton, H.E., Hunter, R.E., Swanson, F.J., and Phillips, R.L., 1969, Sample size and meaningful gold analysis, United States Geological Survey Professional Paper 625-C, pp. C1-C17.

Cloutt, B., 1995, Gravity concentration at W.M.C.'s St Ives Gold Mines, Randol Gold Forum Perth '95 Proceedings, Australia, March.

Couderc, J.-P., 1985, Incipient Fluidization and Particulate Systems, Fluidization, second edition, edited by J.F.Davidson, R.Clift, and D.Harrison, Academic Press, London, Chapter 1, pp. 1-30.

Coulson, J.M., Richardson, J.F., 1990, Chemical Engineering, fourth edition, Pregamon Press, Vol. 2, pp. 174-177.

Dallavalle, J.M., 1948, Micromeritics (The Technology of Fine Particles), Pitman Publishing Corporation, New York, p. 23.

Darnton, B., Lloyd, S., and Antonioli, M.A., 1992. Gravity concentration: research, design and circuit performance at Montana Tunnels, Randol Gold Forum Vancouver '92 Proceeding, Canada, March.

Darnton, B.T., Lloyd, S., and Antonioli, M.A., 1995. Gravity circuit improvements at the Montana Tunnels Mine, Randol Gold Forum Perth '95 Proceeding, Australia, March.

Donsi, G., and Ferrari, G., 1988, On the segregation mechanism of percolating fines in coarse-particle fluidized beds, Powder Technology, Vol. 55, June, No. 2, pp. 153-158.

Environmental Management (EM) of the U.S., 1995, Schematic of the Campbell Centrifugal Jig, from Internet: http://www.em.doe.goc/rainplum/fig310b.html.

Falcon Concentrators Inc., 1997a, Product line information, from Internet: http://www.icafe.com/falcon/products.

Falcon Concentrators Inc., 1997b, Research and development, from Internet: http://www.icafe.com/falcon/rd/index.html.

Falcon Concentrators Inc., 1996, Model SB4 operating guide.

Ferrara, G., 1960, A process of centrifugal separation using a rotating tube, Proceedings of (5th Inter. Miner. Proc. Cong., London, pp. 173-184.

Ferrara, G., 1974, Discussion on others' paper, Proceedings of Inter. Miner. Proc. Cong., London, pp. 313-316.

Folinsbee, J.A., and Hewitt, B., 1997. Gravity concentration at Placer Dome's Campbell gold mill, Mining Engineering, October, pp. 44-47.

Forssberg, E., and Nordquist, T., 1987. Pilot plant trials of new gravity concentration equipment, Minerals and Metallurgical Processing, May, pp. 87-89.

Gaudin, A.M., 1939, Principles of Mineral Dressing, McGraw-Hill, New york, Chapter XII (Jigging), pp. 250-279.

Giusti, L., 1986, The morphology, mineralogy, and behaviour of "fine-grained" gold from placer deposits of Alberta: sampling and implications for mineral exploration, Canadian Journal of Earth Science, Vol. 23, pp.1662-1672.

Graham, P.R., 1989. 'Following the gold, through Mamhattan's gravity circuit by size distribution and a flotation method of processing gravity concentrates', SME Ann. Meet., Las Vegas, Feb.

Griffith, S.V., 1960, Alluvial prospecting and mining, Pergamon Press, pp. 33-99.

Hart, S.D., and Hill, G., 1995. Gravity separation development at Boddington Gold Nine, Randol Gold Forum Perth'95 Proceedings, Perth, Australia, March, pp. 53-59.

Hoberg, H., 1993, Applications of mineral processing in waste treatment and scrap recycling, 18th International Mineral Processing Congress , Vol. 1, pp. 27-37.

Honaker, R.Q., Paul,B.C., Wang, D., and Huang, M., 1995, Application of centrifugal washing for fine-coal cleaning, Minerals and Metallurgical Processing, Vol. 12, No. 2, May, pp. 80-84.

Honaker, R.Q., Wang, D., and Ho, K., 1996. Application of the Falcon Concentrator

for fine coal cleaning, Minerals Engineering, Vol. 9, No. 11, pp.1143-1156.

Honan, S.G., and Luinstra, W.F., 1996. Gravity gold concentration at Hemlo Gold Mines Inc. Golden Giant Mine, Proceedings of 28th Ann. Meet. Canadian Mineral Processors, Ottawa, January, Paper #7, pp. 83-96.

Hope, G.H., Mcmullen, J., and Green, D., 1993. Process advances at Lac Minerals Ltd. - Est Malartic Division, Proceedings of 25th Ann. Meet. of Canadian Mineral Processors, Ottawa, January, 13 pages.

Hou, Z.S., 1983. Rotatable Spiral, Non-ferrous, No. 2, pp. 17-20 (in Chinese).

Hu, X., Huang, H., and Mao, J., 1991. Theory and Technology of Flotation, Publishing House of the Central-South University of Technology, Hunan, pp. 97-101 (in Chinese).

Huang, L., 1996. Upgrading of gold gravity concentrates: A study of the Knelson Concentrator. Ph.D. thesis, McGill University, Chapter 6, pp. 94-117.

Kelly, E.G., and Spottiswood, D.J., 1982. Introduction to Mineral Processing, John Wiley & Sons, New York, pp. 50-55.

Knelson, B., 1992. The Knelson Concentrator. Metamorphosis from crude beginning to sophisticated world wide acceptance. Minerals Engineering, Vol. 5, Nos. 10-12, pp. 1091-1097.

Knelson, B., 1985. Centrifugal concentration and separation of precious ores. 17th Ann. Meet. of Canadian Mineral Processors, Ottawa, January.

Knelson, B., and Edwards, R., 1990. Development and economic application of Knelson Concentrators in low grade alluvial gold deposits, a presentation in The AusIMM

1990 Annual Conference, Rotorua, New Zealand.

Knelson, B., and Jones, R., 1994, "A New Generation of Knelson Concentrators" A Totally Secure System Goes on Line, Minerals Engineering, Vol. 7, Nos. 2/3, pp. 201-207.

Knelson Gold Concentrators Inc., 1994, Operator's manual for Knelson 3" Concentrator, pp. 1-19.

Kusakabe, K., Yamaki, T., Morooka, S., and Matsuyama, H., 1991, Percolating velocity of fine particles through packed bed of coarse particles, Tetsu to Hagane - Journal of the Iron & Steel Institute of Japan, Vol. 77, No. 9, Sept., pp. 1407 - 1402. (in Japanese)

Madhav, G.V., Chhabra, R.P., 1995, Drag on non-spherical particles in viscous fluids, Int. Journal of Mineral Processing, Vol. 43, pp. 15-29.

Laplante, A.R., 1989, Modelling and control of mineral processing systems, Course notes, McGill University, pp.4-7.

Laplante, A.R., 1993, A comparative study of two centrifugal concentrators, 25th Ann. Meet. of Canadian Mineral Processors, Ottawa, January, Paper 5, 18 pages.

Laplante, A.R., Buonvino, M., Veltmeyer, A., Robitaille, J., and Naud, G., 1994, A study of the Falcon Concentrator, Canadian Metallurgical Quarterly, Vol. 33, No. 4, pp. 279-288.

Laplante, A.R., Huang, H., Knelson, B., and Harris, B., 1998, The search for the optimum batch concentration centrifuge: modifications to the bowl geometry and fluidization water distribution for a 3-in Knelson concentrator, submitted for

publication in Transactions IMM, Section C, England.

Laplante, A.R., Liu, L., and Cauchon, A., 1990, Gold gravity recovery at the Mill of Les Mines Camchib Inc., Chibougama, Quebec, Intern.Symp. of Gold Recovery, Salt Lake City, February.

Laplante, A.R., and Shu, Y., 1992, The Use of a Laboratory Centrifugal Separator to Study Gravity Recovery in Industrial Circuits, Proceedings of 24th Ann. Meet. of the Canadian Mineral Processors, Ottawa, Jan.

Laplante, A.R., Shu, Y., and Marois, J., 1996a, Experimental Characterization of a Laboratory Centrifugal Separator, Canadian Metallurgical Quarterly, Vol. 35, No. 1, pp. 23-29.

Laplante, A.R., Putz, A., and Huang, L., 1993b, Sampling and Sample Processing for Gravity Circuits, Presented at The McGill University Professional Development Seminar on Gold Recovery by Gravity, May.

Laplante, A.R., Vincent, F., and Luinstra, W.F., 1996b, A laboratory procedure to determine the amount of gravity recoverable gold - a case study at Hemlo Gold Mines, Proceedings of 28th Ann. Meet. Canadian Mineral Processors, Ottawa, January, Paper #6, pp. 69-82.

Laplante, A.R., Woodcock, F., and Noaparast, M., 1995, Predicting Gold Recovery by Gravity, Minerals and Metallurgical Processing, Vol. 12, No. 2, May, pp. 74-79.

Laplante, A.R., Zhang, B., Huang, L., Ling, J., Cousin, P., and Racine, L., 1997, Difficult gold gravity separations, Proc. of 29th Ann. Meet. of Canadian Mineral

Processors, Ottawa, January, Paper 31, pp. 421-434.

Lazarkiewicz, S., and Troskolanski, A.T., 1965, Impeller pumps, Pergamon press, Oxford, New York, pp. 7-9.

Lepekhin, V.M., Borzov, V.L., and Yaramenko, V.N., 1995, The centrifugal separation of fine minerals, Magnetic and Electrical Separation, Vol. 6, pp. 235-242.

Li, S., Li, G., and Du, T., 1984, Gravity concentration of complex tin slimes, Mineral processing and extractive metallurgy, proceedings of the international conference "Mineral precessing and extractive metallurgy", Kunming, Yunnan, China, Edited by M.J.Jones and P. Gill, pp. 491-507.

Lins, F.F., Veiga, M.M., Stewart, J.A., Papalia, A., and Papalia, R., 1992, Performance of a new centrifuge (Falcon) in concentrating a gold ore from Texada Island, B.C., Canada, Minerals Engineering, Vol. 5, Nos 10-12, pp. 1113-1121.

Liu, P., and Wang, D., 1984, Combined centrifugal separation-flotation-magnetic concentration flowsheet for treatment of wolframite slimes, Mineral Processing and Extractive Metallurgy, proceedings of the international conference "Mineral precessing and extractive metallurgy", Kunming, Yunnan, China, Edited by M.J.Jones and P. Gill, pp. 607-613.

Lloyd, S., 1991, a report of Technical Papers and Performance Reports, edited by Knelson Gold Concentrators Inc.

Loggio, T., and Letki, A., 1994, New directions in centrifuging, Chemical

Engineering, January, pp. 70-76.

Louis, H., 1894, A Handbook of Gold Milling, London: Macmillan and Co., pp. 319-320.

Lu, Y., 1985, The Chinese Patent, CN 85 1 02837 B, Int.Cl⁴. B03B 5/00.

Lyman, G.J., and Davis, J.J., 1994, Water based processes (Cleaning coarse and small coal), Advanced Coal Preparation Monograph Series, Volume III, Part 7, p. 12.

Meia, F., 1993, A brief performance report of Technical Papers and Performance Reports, edited by Knelson Gold Concentrators Inc.

Meza S., L.A., Hartmann, W., and Escobar, C.A., 1994, Recovery of placer gold using the Knelson Concentrator, Innovations in Mineral Processing, Proceedings, Edited by Turgut Yaçin, Sudbury, Canada, June 6-8, pp. 339-347.

Morooka, S., Kusakabe, K, Ohnishi, N., Gujima, F., and Matsuyama, H., 1989, Measurement of local fines movement in a fluidized bed of coarse particles by a fluorescent tracer technique, Powder Technology, Vol. 58, pp. 271-277.

Napier-Munn, T.J., 1997, Invention and innovation in mineral processing, Minerals Engineering, Vol. 10, No. 8, pp. 757-773.

Odar, F., and Hamilton, W.S., 1964, Forces on a sphere accelerating in a viscous fluid, Journal of Fluid Mechanics, Vol. 18, Part 2, February, pp. 302-314.

Ounpuu, M., 1992, Gravity Concentration of Gold from Base Metal Flotation Mills, Proceedings, Proceedings of 24th Ann. Meet. of Canadian Mineral Processors, Ottawa, Jan., Paper 10, 10 pp.

Owen, T.A., 1991, Knelson Concentrator installation Paddington Gold Mine, Australia,

a report of Technical Papers and Performance Reports, edited by Knelson Gold Concentrators Inc.

Özdag, H., UçbasY., and Koca, S., 1994, Recovery of chromate from slime and table tailings by multi-gravity separation, Innovations in Mineral Processing, Proceedings of the innovations in Mineral Processing Conference, Editor: Turgut Yalçin, Sudbury, Canada, June 6-8, pp. 267-278.

Patchejreff, B., Gaidarjiev, St., and Lazarov, D., 1994, Technical Note Opportunities of fine gold recovery from a copper flotation circuit using a Knelson Concentrator, Minerals Engineering, Vol. 7, Nos. 2/3, pp. 404-409.

Penney, B., 1996, An integrated approach to iron ore recovery at the Iron Ore Company of Canada, Proceedings of 28th Ann. Meet. Canadian Mineral Processors, Ottawa, January, Paper #15, pp. 213-225.

Phillips, J.A., 1867, The Mining and Metallurgy of Gold and Silver, London: R. Clay, Son, and Taylor Printers, p. 196.

Plitt, L.R., 1976, A mathematical model of the hydrocyclone classifier, CIM Bulletin, Vol. 69, pp. 114-123.

Plitt, L.R., Conil, P., and Broussaud, A., 1990, An improved method of calculating the water-split in hydrocyclones (technical note), Minerals Engineering, Vol. 3, pp. 533-535.

Plitt, L.R., Finch, J.A., and Flintoff, B.C., 1980, Modelling the hydrocyclone classifier, Proc. Eur. Symp. Particle. Tech., Amsterdam, pp. 790-804.

Plummer T., 1995, 'Superbowls' enhance fine gold recovery, Mining Magazine,

September, p. 159.

Poulter, S., Fitzmaurice, C., and Steward, G., 1994, The Knelson Concentrator: Application and operation at Rosebery, Proc. of Fifth Mill Operators' Conference, Roxby Downs, October, pp. 227-233.

Putz, A.L., 1994, An investigation of the gravity recovery of gold, M.Eng. Thesis, McGill University, Canada, 230 pp.

Putz, A.L., Laplante, A.R., and Ladouceur, G., 1993, Evaluation of a Gravity Circuit in a Canadian Gold Operation, Proceedings, Randol Gold Forum, Beaver Creek, Sept., pp. 145-149.

Ren, X., Li, Q., Zhang, Y., and Liu, D., 1994a, A new centrifugal separator for recovering minerals from fine and ultrafine sizes, Innovations in Mineral Processing, Proceedings of the Innovations in Mineral Processing Conference, Laurention University, Sudbury, Canada, June 6-8, Editor: Turgut Yalçin.

Ren, X., Li, Y., and Li, Q., 1994b, Study and Practice of SL-type Continuous Discharge Jet Centrifugal Separator, Metal Mine, Series No. 212, February, pp. 33-36 (in Chinese).

Richard Mozley Limited, 1998, Multi-gravity separator, from Internet: http: //www. mozley.co.uk.

Richardson, J.F., 1971, Incipient Fluidization and Particulate Systems, Fluidization, edited by J.F.Davidson, and D.Harrison, Academic Press, London, Chapter 2, pp. 32-34.

Rose, T.K., 1898, The Metallurgy of Gold, London: Charles Griffin and Company,

Limited, pp. 183-184.

Serway, B. A., 1996, The kinetic theory of gases, Physics, Fourth edition, Vol. 1, pp.586-614.

Stephens, D.J., and Bridgwater, J., 1978a. The mixing and segregation of cohesionless particulate materials Part I: Failure zone formation, Powder Technology, Vol. 21, pp. 17-28.

Stephens, D.J., and Bridgwater, J., 1978b. The mixing and segregation of cohesionless particulate materials Part II: Microscopic mechanisms for particles differing in size, Powder Technology, Vol. 21, pp. 29-44.

Streeter, V.L., 1971, Fluid mechanics, fifth edition. McGraw-hill Book Company, New York, pp. 474-482.

Sun, S., Chen, Q., and Yang, Y., 1984, New techniques in processing tungsten ore slimes, Mineral processing and extractive metallurgy, proceedings of the international conference "Mineral precessing and extractive metallurgy", Kunming, Yunnan, China, Edited by M.J.Jones and P. Gill, pp. 521-530.

Sun, Y., 1982, Gravity Concentration. China Publication House of Metallurgical Industry, pp. 256-265 (Yunxi Centrifuge); pp. 61-88 (Theoretical fundamentals of inclined flowing-film concentration); (in Chinese).

Sutter, J., 1997a. SuperBowl nominal specifications, from internet: http://www.rmsross.com/sb_spec.htm

Sutter, J., 1997b. A list of SuperBowls that are in operation throughout the world today, from internet: http://www.rmsross.com sbinst.htm.

Suttill, K.R., 1990. Merro De Ouro --- Brazil's hill of gold. E/MJ, June, pp. 25-28.

Svarovsky, L., 1990. Solid - Liquid Separation. 3rd edition, Butterworths, pp. 687-692.

Svoboda, J., 1996. A contribution to the theory of separation in a rotating ferrofluid, Minerals Engineering, Vol. 9, No. 7, pp. 743-752.

Taggart, A.F., 1945, Handbook of Mineral Processing, p. 11-136.

Teaching and Research Divisions of Mineral Processing, 1978. The separation principles of the Yunxi Centrifuge and its practice in iron ore processing, Journal of North-east Institute of Technology, No. 3, pp. 1-30 (in Chinese).

Traore, A., Conil, P., Houot, R., and Save, M., 1995. An evaluation of the Mozley MGS for fine particle gravity separation, Minerals Engineering, Vol. 8, No. 7, pp. 767-778.

Truscott, S.J., 1923. A text-book of ore dressing, Macmillan and Co., Limited, London, pp. 583-590.

Tucker, P., 1995. Technical Note: Modelling the Kelsey Centrifugal Jig, Minerals Engineering, Vol. 8, No. 3, pp. 333-336.

Ungarish, M., 1993, Hydrodynamics of Suspensions: Fundamentals of Centrifugal and Gravity Separation, Springer-Verlag, Berlin, pp. 37-60.

Ungarish, M., 1995. On the modelling and investigation of polydispersed rotating suspensions, International Journal of Multiphase Flow, Vol. 21, No. 2, pp. 267-284.

Weber, M.E., 1998, A private communication at McGill University, June 16, 3 pp.

Witteveen, H.J., 1995. The response of a uniform jig bed in terms of the porosity

distribution, Ph.D. thesis, Delft University of Technology, The Netherlands.

Wong, N., 1988, Mineral Processing Design Handbook, China Publication House of Metallurgical Industry, p. 979 (in Chinese).

Woodcock, F., 1994, Use of a Knelson unit to quantify gravity recoverable gold in an ore sample, M.Eng. Thesis, McGill University, Canada, 114 pp.

Woodcock, F., and Laplante, A.R., 1993, A Laboratory Method for Determining the amount of Gravity Recovery Gold, Randol gold Seminar, Beaver Creek, Sept.

Wyslouzil, H.E., 1990, Evaluation of the Kelsey Centrifugal Jig at Rio Kemptville Tin, Proceedings, 22nd Ann. Meet. Canadian Minerals Processors, Jan., Ottawa, Paper No. 23, pp. 461-472.

Zhang, B., 1998, Recovering gold from high density gangues with Knelson Concentrator, M. E. thesis, McGill University, Canada.

Appendix 1 Derivation of General Equations of Motion for a Particle in the KC

A1.1 The equations of motion for a particle in the dilute zone

A1.1.1 The equation of motion in the radial direction

As described in the section 3.2.2.1 of Chapter 3, the equation of motion is given by:

$$\frac{\pi}{6}d_p^3(\rho_s-\rho)r\omega^2-3\pi\mu d_p\left(\frac{dr}{dt}+u_{fx}\right)=\left(\frac{\pi}{6}d_p^3\rho_s+\frac{\pi}{12}d_p^3\rho\right)\frac{d^2r}{dt^2} \qquad (A1.1)$$

or

$$\frac{\pi}{6}d_p^3(\rho_s-\rho)r\omega^2-3\pi\mu d_p\left(\frac{dr}{dt}+u_{fx}\right)=\frac{\pi}{6}d_p^3(\rho_s+\frac{\rho}{2})\frac{d^2r}{dt^2} \qquad (A1.2)$$

Equation (A1.2) can be further expressed as follows.

$$\frac{d^2r}{dt^2}+\frac{18\mu}{d_p^2(\rho_s+\frac{\rho}{2})}\frac{dr}{dt}-\frac{(\rho_s-\rho)\omega^2r}{(\rho_s+\frac{\rho}{2})}+\frac{18\mu u_{fx}}{d_p^2(\rho_s+\rho)}=0 \qquad (A1.3)$$

or

$$\frac{d^2r}{dt^2}+a_1\frac{dr}{dt}-n_1r=m_1 \qquad (A1.4)$$

$$\text{where} \quad a_1 = \frac{18\mu}{d_p^2(\rho_s + \frac{\rho}{2})}, \quad n_1 = \frac{(\rho_s - \rho)\omega^2}{(\rho_s + \frac{\rho}{2})}, \quad m_1 = -\frac{18\mu u_{fx}}{d_p^2(\rho_s + \frac{\rho}{2})}$$

The solution of Equation A1.4, which is a nonhomogeneous linear differential equation with constant coefficients, takes the form:

$$r = C_1 e^{-[a_1/2 + \sqrt{a_1^2/4 + n_1}]t} + C_2 e^{-[a_1/2 - \sqrt{a_1^2/4 + n_1}]t} + q_1 \qquad (A1.5)$$

$$= e^{-a_1 t/2}\left(C_1 e^{-k_1 t} + C_2 e^{k_1 t}\right) + q_1 \qquad (A1.6)$$

$$\text{where} \quad k_1 = \sqrt{\frac{a_1^2}{4} + n_1}, \qquad q_1 = \frac{18\mu u_{fx}}{d_p^2 \omega^2 (\rho_s - \rho)}$$

If the particle starts (t=0) at a radius r_1 with zero velocity (dr/dt =0), then from Equation A1.6:

$$\frac{dr}{dt} = e^{-a_1 t/2}\left(-k_1 C_1 e^{-k_1 t} + k_1 C_2 e^{k_1 t}\right) - \frac{a_1}{2} e^{-a_1 t/2}\left(C_1 e^{-k_1 t} + C_2 e^{k_1 t}\right)$$

$$= e^{-a_1 t/2}\left[\left(k_1 - \frac{a_1}{2}\right) C_2 e^{k_1 t} - \left(k_1 + \frac{a_1}{2}\right) C_1 e^{-k_1 t}\right] \qquad (A1.7)$$

Substituting the boundary condition into Equations A1.6 and A1.7:

$$r_1 = C_1 + C_2 + q_1 \qquad (A1.8)$$

$$0 = C_2(k_1 - a_1/2) - C_1(k_1 + a_1/2) \qquad (A1.9)$$

Solving the equations set of A1.8 and A1.9 gives:

$$C_1 = \frac{(r_1 - q_1)\ (2k_1 - a_1)}{4k_1}; \qquad C_2 = \frac{(r_1 - q_1)\ (2k_1 + a_1)}{4k_1}$$

Thus, Equation A1.6 becomes:

$$r = e^{-a_1 t/2}\left(\frac{(r_1 - q_1)(2k_1 - a_1)}{4k_1}e^{-k_1 t} + \frac{(r_1 - q_1)(2k_1 + a_1)}{4k_1}e^{k_1 t}\right) + q_1 \qquad (A1.10)$$

i.e.

$$r = e^{-a_1 t/2}\frac{(r_1 - q_1)}{4k_1}\left[2k_1\left(e^{k_1 t} + e^{-k_1 t}\right) + a_1\left(e^{k_1 t} - e^{-k_1 t}\right)\right] + q_1$$

$$= e^{-a_1 t/2}(r_1 - q_1)\left[\cosh k_1 t + \frac{a}{2k_1}\sinh k_1 t\right] + q_1 \qquad (A1.11)$$

If the inertial term on the right-hand side of Equation A1.2 can be neglected (or when the instantaneous velocity is close to the terminal velocity), then

$$\frac{\pi}{6}d_p^3(\rho_s - \rho)r\omega^2 - 3\pi\mu d_p\left(\frac{dr}{dt} + u_{fx}\right) = 0 \qquad (A1.12)$$

or

$$\frac{d_p^2(\rho_s - \rho)r\omega^2}{18\mu} = \frac{dr}{dt} + u_{fx}$$

Therefore, the expression of the instantaneous velocity of the particle is:

$$\frac{dr}{dt} = \frac{d_p^2(\rho_s - \rho)r\omega^2}{18\mu} - u_{fr} \qquad (A1.13)$$

A1.1.2 The equations of motion in the axial direction

Substituting Equations 3.8, 3.9 and 3.21 in Equation 3.13 and rearranging yields the equation of motion in the axial direction::

$$\frac{d^2h}{dt^2} + \frac{18\mu}{d_p^2(\rho_s + \frac{\rho}{2})}\frac{dh}{dt} - \frac{18\mu u_{fz} - d_p^2 g(\rho_s - \rho)}{d_p^2(\rho_s + \frac{\rho}{2})} = 0 \qquad (A1.14)$$

or

$$\frac{d^2h}{dt^2} + a_2\frac{dh}{dt} - m_2 = 0 \qquad (A1.15)$$

$$where \quad a_2 = \frac{18\mu}{d_p^2(\rho_s + \frac{\rho}{2})}; \quad m_2 = \frac{18\mu u_{fz} - d_p^2 g(\rho_s - \rho)}{d_p^2(\rho_s + \frac{\rho}{2})}$$

If the particle starts at t=0, h=h_1, and dh/dt=0, then the solution of Equation A1.32 is as follows.

$$h = h_1 e^{-a_2 t/2}\left[\cosh k_2 t + \frac{a_2}{2k_2}\sinh k_2 t\right] \qquad (A1.16)$$

where $k_2 = \sqrt{\frac{a_2^2}{4} + m_2}$

If d^2h/dt^2 on the left-hand side of Equation A1.14 is equal to zero, i.e., the particle stops vertical acceleration, then

$$\frac{18\mu}{d_p^2(\rho_s + \frac{\rho}{2})}\frac{dh}{dt} - \frac{18\mu u_{fz} - d_p^2 g(\rho_s - \rho)}{d_p^2(\rho_s + \frac{\rho}{2})} = 0 \qquad (A1.17)$$

Solving Equation A1.17, the axial velocity of the particle is expressed by:

$$\frac{dh}{dt} = u_{fz} - \frac{d^2 g(\rho_s - \rho)}{18\mu} \qquad (A1.18)$$

A1.2 The equations of motion for a particle in the separation zone

A1.2.1 Relation between the collision frequency and fractional voidage

The collision frequency of a moving spherical particle in the separation zone of the inner bowl can be expressed by a formulation similar to that of the collision frequency for a gas molecule (Serway, 1996), that is:

$$f = \pi d^2 \mid \bar{u}_p \mid n_v \qquad (A1.19)$$

where f is the collision frequency, or the number of collisions per second; d is the distance between the centres of the moving particle and bulk particle; n_v is the number of the bulk particles per unit volume.

The fractional voidage of the separation zone, ϵ, can be expressed by:

$$\epsilon = 1 - V_s/V_T \qquad \text{(A1.20)}$$

where V_s is the volume of solid particles; V_T is the volume of the separation zone.

or

$$\epsilon = 1 - \frac{V_T n_v \frac{\pi}{6} d_b^3}{V_T} \qquad (A1.21)$$

where d_b is the average diameter of the bulk particles in the separation zone.

Thus, solving Equation A1.21 gives:

$$n_v = \frac{6(1-\epsilon)}{\pi d_b^3} \qquad (A1.22)$$

Substituting Equation A1.22 in Equation A1.19 gives:

$$f = \frac{6|\vec{u}_p|d^2(1-\epsilon)}{d_b^3} \qquad (A1.23)$$

Since the centre line d is equal to $d_p/2 + d_b/2$, Equation 1.23 becomes:

$$f = \frac{3|\vec{u}_p|(d_p+d_b)^2(1-\epsilon)}{2d_b^3} \qquad (A1.24)$$

A1.2.2 The expression of the dynamic friction force

The dynamic friction force $\vec{F}_L$ proposed in this work may be a function of momentum of the percolating particle and the collision frequency:

$$\vec{F}_L = C_L f m \vec{u}_p \qquad (A1.25)$$

where C_L is the dynamic coefficient of friction between the bulk and percolating particles, a concept proposed in this work based on the hypothesis that percolation velocity is a function of the ratio of percolating to bulk particle diameters (Bridgwater, 1983), and takes the form:

$$C_L = \frac{k_p \rho_b}{\epsilon \rho_s} \qquad (A1.26)$$

where k_p is a dimensionless correction factor; ρ_b is the density of bulk particles.

If C_P is used to stand for all the constants in Equation A1.25 (the fractional voidage e is supposed to be constant), the dynamic friction force $\vec{F}_L$ can be expressed by:

$$\vec{F}_L = C_P |\vec{u}_p| \vec{u}_p \qquad (A1.27)$$

$$where \quad C_P = \frac{3 k_p \rho_b (d_p + d_b)^2 (1 - \epsilon)}{2 \epsilon \rho_s d_b^3} \qquad (A1.28)$$

The X-component of $\vec{F}_L$ can be expressed by:

$$F_{Lx} = C_P \left|\frac{d\vec{r}}{dt}\right| \frac{dr}{dt} \qquad (A1.29)$$

The Z-component of $\vec{F}_L$ can be expressed by:

$$F_{Lz} = C_D \left|\frac{d\vec{h}}{dt}\right| \frac{dh}{dt} \qquad (A1.30)$$

A1.2.3 The equation of motion in the radial direction in the Stokes' Law region

Since the action of fluidization flow is more significant in the separation zone than in the dilute zone, it is assumed that the X-component of fluid velocity is approximately equal to the interstitial velocity of fluidization flow with respect to the wall of the system, denoted by u_i. This interstitial velocity of fluidization flow is a function of the fractional voidage and can be expressed by (Witteveen, 1995, p.129):

$$u_i = \frac{U_F}{\epsilon} \qquad (A1.31)$$

where U_F is the superficial fluid velocity.

The equation of motion in radial direction in the separation zone is given by:

$$\frac{\pi}{6} d_p^3 (\rho_s - \rho) r\omega^2 - 3\pi\mu d_p \left(\frac{dr}{dt} + u_i\right) - C_D \left(\frac{dr}{dt}\right)^2 = \left(\frac{\pi}{6} d_p^3 \rho_s + \frac{\pi}{12} d_p^3 \rho\right) \frac{d^2 r}{dt^2} \qquad (A1.32)$$

Assuming that the centrifugal acceleration of the particle, $r\omega^2$, is constant, the above nonhomogeneous nonlinear differential equation with constant coefficients becomes:

$$\frac{d^2r}{dt^2} + \frac{6C_P}{\pi d_p^3(\rho_s + \frac{\rho}{2})}\left(\frac{dr}{dt}\right)^2 + \frac{18\mu}{d_p^2(\rho_s + \rho)}\frac{dr}{dt} + \frac{-d_p^2(\rho_s - \rho)r\omega^2 + 18\mu u_i}{d_p^2(\rho_s + \frac{\rho}{2})} = 0 \qquad (A1.33)$$

or

$$\frac{d^2r}{dt^2} + a_3\left(\frac{dr}{dt}\right)^2 + b_3\frac{dr}{dt} + m_3 = 0 \qquad (A1.34)$$

where $a_3 = \dfrac{6C_P}{\pi d_p^3(\rho_s + \frac{\rho}{2})}$, $b_3 = \dfrac{18\mu}{d_p^2(\rho_s + \frac{\rho}{2})}$, $m_3 = \dfrac{-d_p^2(\rho_s - \rho)r\omega^2 + 18\mu u_i}{d_p^2(\rho_s + \frac{\rho}{2})}$

Let dr/dt = p, then

$$\frac{dp}{dt} + a_3p^2 + b_3p + m_3 = 0 \qquad (A1.35)$$

Separating the variables and integrating both sides gives

$$-\int \frac{dp}{m_3 + b_3p + a_3p^2} = \int dt + C_5 \qquad (A1.36)$$

Hence

$$p = \frac{dr}{dt} = \frac{C_5e^{-k_3t}(b_3 + k_3) - (b_3 - k_3)}{2a_3(1 - C_5e^{-k_3t})} \qquad (A1.37)$$

where $k_3 = (b_3^2 - 4m_3a_3)^{0.5}$.

or

$$\int dr = \int \frac{C_5 e^{-k_3 t}(b_3 + k_3) - (b_3 - k_3)}{2a_3(1 - C_5 e^{-k_3 t})} dt \qquad (A1.38)$$

Dividing the right side into two terms gives:

$$\int dr = \int \frac{C_5 e^{-k_3 t}(b_3 + k_3)}{2a_3(1 - C_5 e^{-k_3 t})} dt - \int \frac{b_3 - k_3}{2a_3(1 - C_5 e^{-k_3 t})} dt + C_6 \qquad (A1.39)$$

Integrating Equation A1.39 and then calculating the constants C_5 and C_6 when the particle starts at t = 0, r = r_1, and dr/dt = u_{px0}, the solution is given as follows:

$$r = \frac{b_3 + k_3}{2k_3 a_3} \ln(1 - C_5 e^{-k_3 t}) - \frac{b_3 - k_3}{2k_3 a_3} \ln \frac{1 - C_5 e^{-k_3 t}}{C_5 e^{-k_3 t}} + C_6 \qquad (A1.40)$$

$$\text{where } C_5 = \frac{2a_3 u_{px0} + b_3 - k_3}{2a_3 u_{px0} + b_3 + k_3}, \quad C_6 = r_1 - \frac{b_3 + k_3}{2k_3 a_3} \ln \frac{2k_3}{2a_3 u_{px0} + b_3 + k_3} - \frac{b_3 - k_3}{2k_3 a_3} \ln \frac{2k_3}{2a_3 u_{px0} + b_3 - k_3}$$

If the inertial term on the right-hand side of Equation A1.32 can be neglected (or when the instantaneous velocity is close to the terminal velocity), then

$$\frac{6C_P}{\pi d_p^3(\rho_s+\frac{\rho}{2})}\left(\frac{dr}{dt}\right)^2+\frac{18\mu}{d_p^2(\rho_s+\rho)}\frac{dr}{dt}-\frac{d_p^2(\rho_s-\rho)r\omega^2-18\mu u_l}{d_p^2(\rho_s+\frac{\rho}{2})}=0 \qquad (A1.41)$$

or

$$a_3\left(\frac{dr}{dt}\right)^2+b_3\frac{dr}{dt}-m_3=0 \qquad (A1.42)$$

Hence, solving this second-order equation with one unknown (dr/dt) gives

$$\frac{dr}{dt}=-\frac{3\pi\mu d_p}{2C_P}\pm\sqrt{\left(\frac{3\pi\mu d_p}{2C_P}\right)^2+\frac{\pi d_p^2(\rho_s-\rho)r\omega^2-18\pi\mu u_l}{6d_pC_P}} \qquad (A1.43)$$

Since the displacement of the particle is assumed to be positive (i.e. assuming that it always moves from the centre to the wall of the inner bowl), the instantaneous velocity of the particle should take this form:

$$\frac{dr}{dt}=\sqrt{\left(\frac{3\pi\mu d_p}{2C_p}\right)^2+\frac{\pi d_p^2(\rho_s-\rho)r\omega^2-18\pi\mu u_l}{6d_pC_P}}-\frac{3\pi\mu d_p}{2C_P} \qquad (A1.44)$$

A1.2.4 The equation of motion for a particle moving up the inner bowl along the separation zone in the Stokes' Law region

The equation of motion for the particle moving up alone the separation zone is expressed by:

$$\frac{\pi}{6}d_p^3\rho_s r\omega^2\sin\alpha - \frac{\pi}{6}d_p^3\rho_s g\cos\alpha + 3\pi\mu d_p\left(u_{fz}\cos\alpha - \frac{dh'}{dt}\right)$$

$$+\frac{\pi}{6}d_p^3\rho g\cos\alpha - \frac{C_P}{\cos\alpha}\left(\frac{dh'}{dt}\right)^2 = \frac{\pi}{6}d_p^3(\rho_s+\frac{\rho}{2})\frac{d^2h'}{dt^2} \qquad (A1.45)$$

Assuming that the centrifugal acceleration of the particle ($r\omega^2$) is constant and manipulating algebraically, we have:

$$\frac{d^2h'}{dt^2} + a_4\left(\frac{dh'}{dt}\right)^2 + b_4\frac{dr}{dt} + m_4 = 0 \qquad (A1.46)$$

$$\text{where} \quad a_4 = \frac{6\cos\alpha\, C_P}{\pi d_p^3(\rho_s+\frac{\rho}{2})}, \quad b_4 = \frac{18\mu}{d_p^2(\rho_s+\frac{\rho}{2})},$$

$$m_4 = \frac{-\sin\alpha d_p^2\rho_s r\omega^2 - 18\mu u_{fz}\cos\alpha + g d_p^2(\rho_s-\rho)\cos\alpha}{d_p^2(\rho_s+\rho/2)}$$

Under conditions of t = 0, h' = h'$_1$, and dh'/dt = u_{pz0} (the initial velocity larger than zero), the solution can be obtained using the same approach as for Equation A1.32 and is expressed by:

$$h' = \frac{b_4 + k_4}{2k_4a_4}\ln(1 - C_7e^{-k_4t}) - \frac{b_4 - k_4}{2k_4a_4}\ln\frac{1 - C_7e^{-k_4t}}{C_7e^{-k_4t}} + C_8 \qquad (A1.47)$$

where $C_7 = \dfrac{2a_4u_{pz0} + b_4 - k_4}{2a_4u_{pz0} + b_4 + k_4}$, $k_4 = \sqrt{b_4^2 - 4m_4a_4}$

$$C_8 = h_1' - \frac{b_4 + k_4}{2k_4a_4}\ln\frac{2k_4}{2a_4u_{pz0} + b_4 + k_4} - \frac{b_4 - k_4}{2k_4a_4}\ln\frac{2k_4}{2a_4u_{pz0} + b_4 - k_4} .$$

Appendix 2 Images and Settling Velocity of Particles and Derivation of Equations of Motion in a Fluidization Column

A2.1 Images of Tungsten Particles

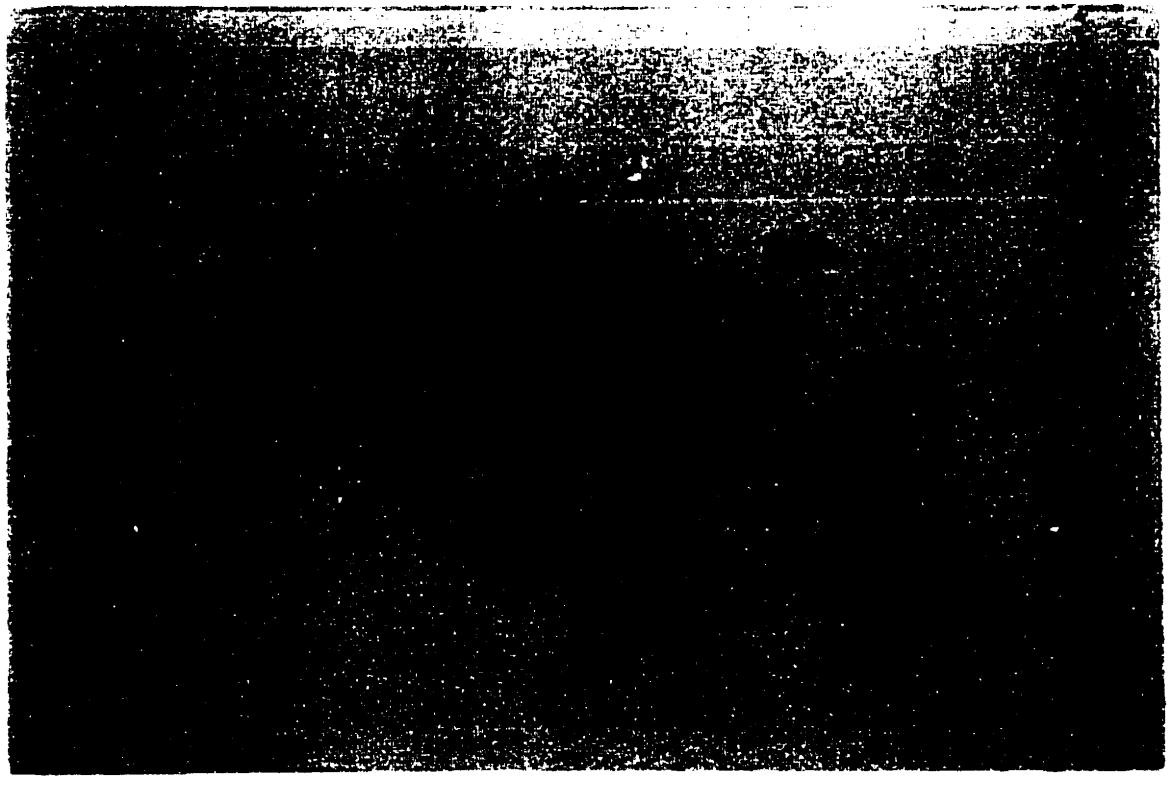

Figure A2-1 Natural appearance of 300-425 μm tungsten particles. The photograph was taken with an ordinary camera with a magnification of 3x.

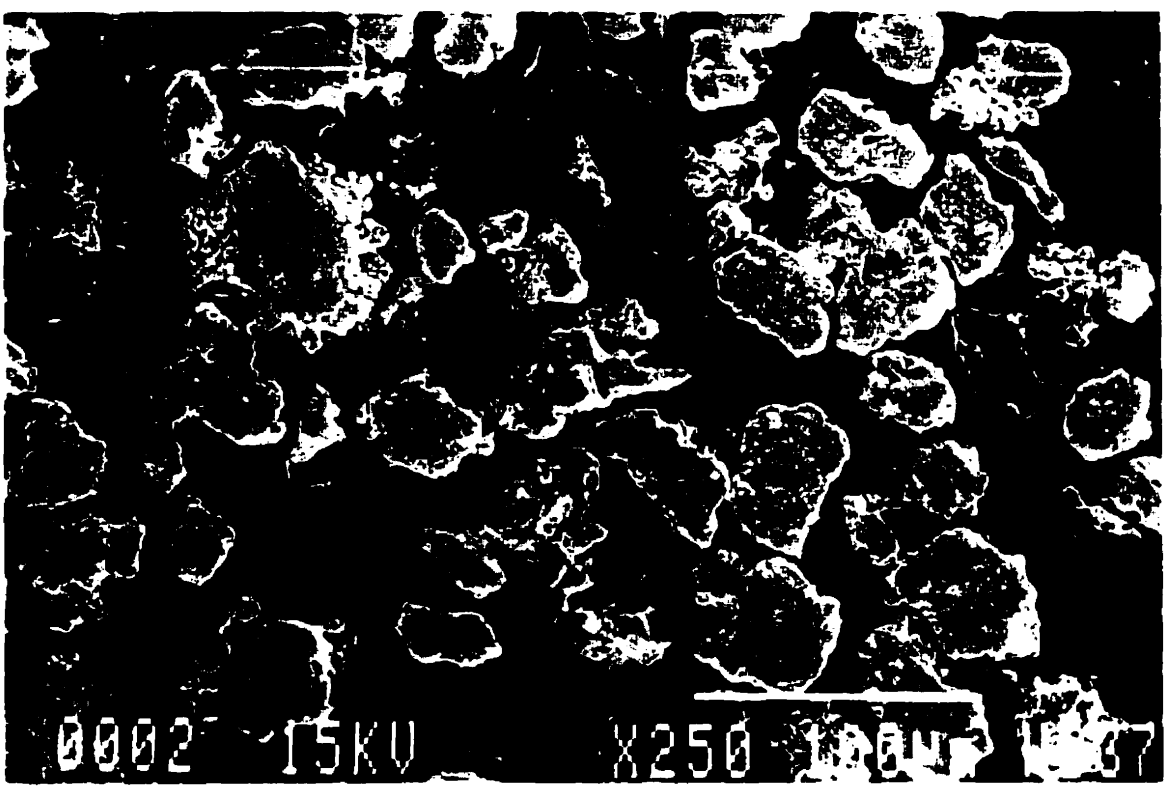

Figure A2-2 SEM back-scattered image of 25-38 μm tungsten particles from a polished surface of a sample (grey phase is tungsten; dark phase is mounting medium; the accelerating voltage was set at 15 keV; the magnification was set at 250x; the working distance was set at 37 mm.)

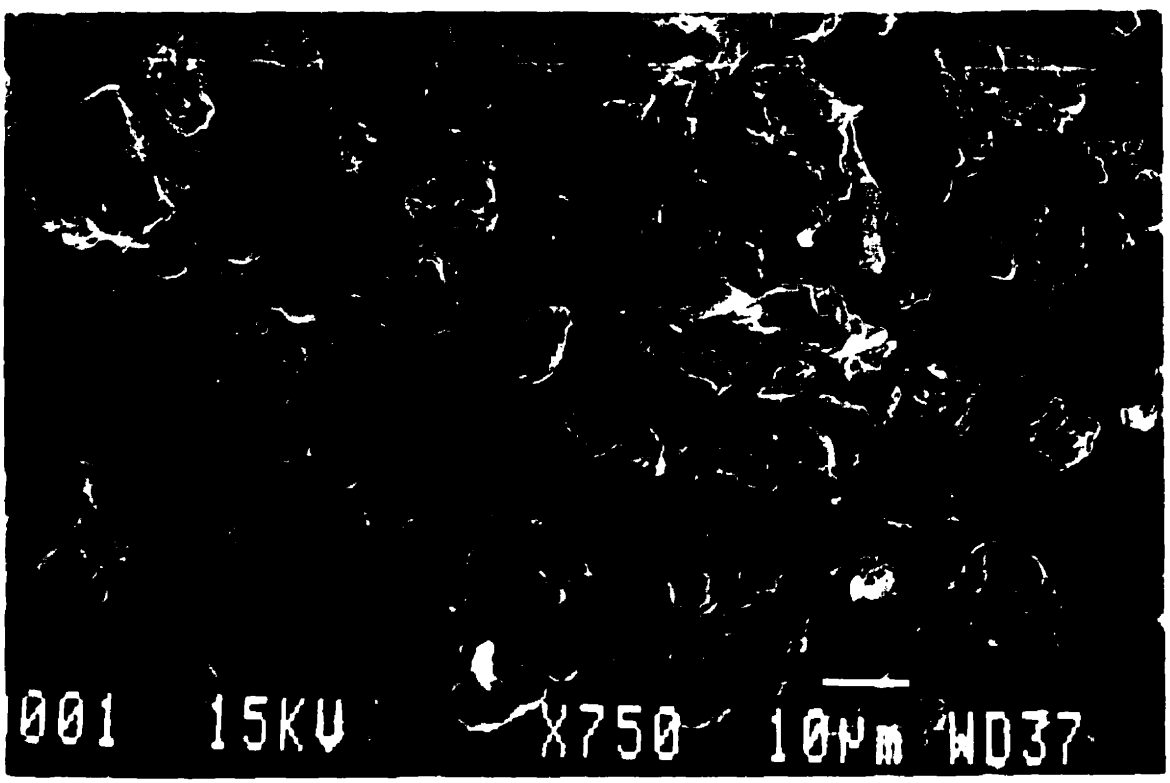

Figure A2-3 SEM back-scattered image of -25 μm tungsten particles from a polished surface of a sample (grey phase is tungsten; dark phase is mounting medium; the accelerating voltage was set at 15 keV; the magnification was set at 750x; the working distance was set at 37 mm.)

Table A2-1 Terminal free settling velocity of particle, cm/s

Size, μm	tungsten	magnetite	silica
1180-1670	96.1	35.3	20.3
850-1180	75.6	27.8	16.0
600-850	54.0	19.8	11.4
425-600	38.2	14.0	8.1
300-425	27.0	9.9	5.7
212-300	19.1	7.0	4.0
150-212	13.5	5.0	2.9
106-150	9.5	3.5	2.0
75-106	7.6	1.7	0.7
53-75	3.8	0.8	0.4
38-53	1.9	0.4	0.2
25-38	0.9	0.2	0.1
-25	0.2	0.04	0.02

The data for particles below 150 μm in Table A2-1 was calculated with the equation for the Stoke's Law region, i. e.

$$Terminal\ velocity = 5450 d_p^2 (\rho_p - 1) \qquad (A2.1)$$

The data for particles above 150 μm was calculated with an equation (Wong, 1988) for the intermediate region of the drag coefficient curve, i. e.

$$Terminal\ velocity = 112.8 d_p * \sqrt[3]{(\rho_p - 1)^2} \qquad (A2.2)$$

A2.3 Derivation of General Equations of Motion of a Particle in a Fluidization Column

A2.3.1 The drag force in different flow regions

Figure A2-4 (Clift et al, 1978) shows the drag coefficient of a sphere as a function of particle Reynolds number (standard drag curve). The standard drag curve may be divided into four regions, such as described by Coulson et al (1990). The subintervals of Re_p corresponding to these four regions are: Region (a) 10^{-4} to 0.2, Region (b) 0.2 to 1000, Region (c) 1000 to 2×10^5, and Region (d) $> 2 \times 10^5$. In this work, only the drag forces in the first three regions of the graph will be considered as particles do not attain the extremely high Reynolds numbers of Region (d).

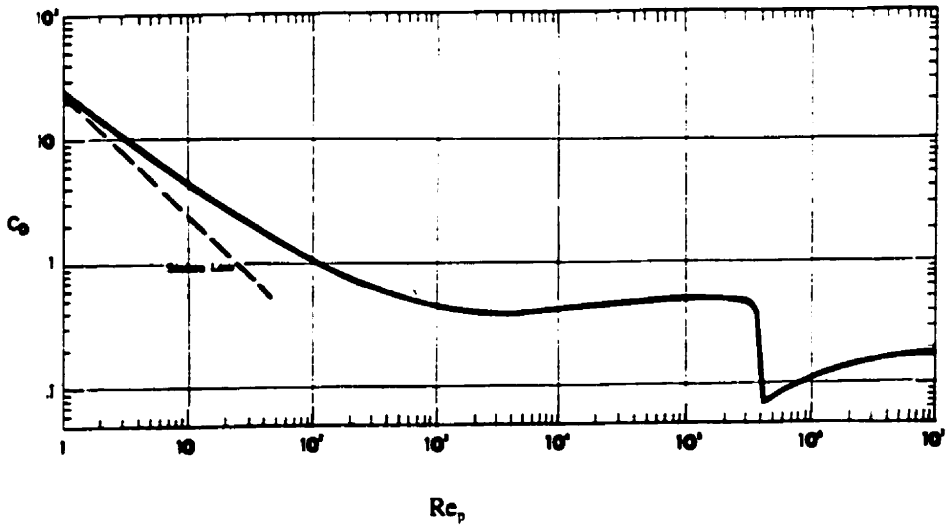

Figure A2-4 Drag coefficient of a sphere as a function of particle Reynolds number (after Clift et al, 1978, p.110)]

APPENDIX 2 IMAGES AND SETTLING VELOCITY OF PARTICLES AND DERIVATION OF EQUATIONS OF MOTION IN A FLUIDIZATION COLUMN

(1) The drag in the Stokes' Law region (Region a):

Similar to Equation 3.17, the drag on a spherical dense particle moving down in the fluidization column can be expressed as:

$$F_{dz} = 3\pi\mu d_p\left(\frac{dh}{dt} + u_i\right) \qquad (A2.3)$$

where u_i is the interstitial velocity of fluidization flow with respect to the wall of the system.

(2) The drag in Region (b):

For the drag coefficient in the intermediate region, an approximate expression suggested by Dallavelle (1948; Coulson et al, 1990) is used, i.e.

$$C_D = 0.44 + \frac{24}{Re_p} \qquad (A2.4)$$

Substituting Equation 3.7 in Equation A2.4 and rearranging gives:

$$C_D = 0.44 + \frac{24\mu}{d_p\rho\left|\frac{dh}{dt} + u_i\right|} \qquad (A2.4)$$

Assuming that the motion of both fluid and particle in the column is one dimensional, combining Equations 3.6 and A2.4 and then rearranging gives the expression of the drag force:

$$F_{dz} = 0.055\pi d_p^2\rho\left(\frac{dh}{dt}\right)^2 + (3\pi\mu d_p + 0.11\pi d_p^2\rho u_i)\frac{dh}{dt} + (3\pi\mu d_p u_i + 0.055\pi d_p^2\rho u_i^2) \qquad (A2.5)$$

(3) The drag in Region (c):

The drag force in this region can be expressed by Newton's Law (Coulson et al, 1990):

$$F_{dz} = 0.055\pi d_p^2\rho[(dh/dt) + u_i]^2 \qquad (A2.6)$$

A2.3.2 The equation of motion for the Stokes' Law region (Region a)

The equation of motion of a spherical dense particle in the Stokes' Law region is given by:

$$\frac{\pi}{6}d_p^3(\rho_s-\rho)g - 3\pi\mu d_p\left(\frac{dh}{dt}+u_i\right) - C_p\left(\frac{dh}{dt}\right)^2 = \left(\frac{\pi}{6}d_p^3\rho_s + \frac{\pi}{12}d_p^3\rho\right)\frac{d^2h}{dt^2} \qquad (A2.7)$$

Assuming that the interstitial velocity of fluid, u_i, is constant, Equation A2.7 becomes:

$$\frac{d^2h}{dt^2} + \frac{6C_p}{\pi d_p^3(\rho_s+\frac{\rho}{2})}\left(\frac{dh}{dt}\right)^2 + \frac{18\mu}{d_p^2(\rho_s+\rho)}\frac{dh}{dt} + \frac{-d_p^2(\rho_s-\rho)g + 18\mu u_i}{d_p^2(\rho_s+\frac{\rho}{2})} = 0 \qquad (A2.8)$$

or

$$\frac{d^2h}{dt^2} + a_5\left(\frac{dh}{dt}\right)^2 + b_5\frac{dh}{dt} + m_5 = 0 \qquad (A2.9)$$

$$\text{where } a_5 = \frac{6C_p}{\pi d_p^3(\rho_s + \frac{\rho}{2})}, \quad b_5 = \frac{18\mu}{d_p^2(\rho_s + \frac{\rho}{2})}, \quad m_5 = \frac{-d_p^2 g(\rho_s - \rho) + 18\mu u_i}{d_p^2(\rho_s + \frac{\rho}{2})}$$

When the particle starts at t = 0, h = h_1, and dh/dt = u_{pz0}, using the same mathematic approach as in Section A1.2.3 to solve Equation A2.9 can results in the following solution:

$$h = \frac{k_5 + b_5}{2k_5 a_5}\ln(1 - C_9 e^{-k_5 t}) - \frac{k_5 - b_5}{2k_5 a_5}\ln\frac{1 - C_9 e^{-k_5 t}}{C_9 e^{-k_5 t}} + C_{10} \qquad (A2.10)$$

$$\text{where } C_9 = \frac{2a_5 u_{pz0} + b_5 - k_5}{2a_5 u_{pz0} + b_5 + k_5}, \quad k_5 = \sqrt{b_5^2 - 4m_5 a_5}$$

$$C_{10} = h_1 - \frac{b_5 + k_5}{2k_5 a_5}\ln\frac{2k_5}{2a_5 u_{pz0} + b_5 + k_5} - \frac{b_5 - k_5}{2k_5 a_5}\ln\frac{2k_5}{2a_5 u_{pz0} + b_5 - k_5}.$$

A2.3.3 The equation of motion for Region (b)

Based on Equations A2.5, 3.36 and 3.13, the equation of motion of particle in Region (b) can be expressed by:

$$\frac{d^2h}{dt^2} + \frac{0.33\pi\rho d_p^2 + 6C_p\left(\frac{dh}{dt}\right)^2}{\pi d_p^3(\rho_s + \frac{\rho}{2})} + \frac{18\mu + 0.66 d_p \rho u_i}{d_p^2(\rho_s + \frac{\rho}{2})}\frac{dh}{dt} + \frac{(18\mu u_i + 0.33 d_p \rho u_i^2) - d_p^2 g(\rho_s - \rho)}{d_p^2(\rho_s + \frac{\rho}{2})} = 0$$

(A2.11)

or

$$\frac{d^2h}{dt^2} + a_6\left(\frac{dh}{dt}\right)^2 + b_6\left(\frac{dh}{dt}\right) + m_6 = 0 \qquad (A2.12)$$

where $a_6 = \dfrac{0.33\pi\rho d_p^2 + 6C_p}{\pi d_p^3(\rho_s + \frac{\rho}{2})}$, $b_6 = \dfrac{18\mu + 0.66 d_p \rho u_i}{d_p^2(\rho_s + \frac{\rho}{2})}$

$$m_6 = \frac{(18\mu u_i + 0.33 d_p \rho u_i^2) - d_p^2 g(\rho_s - \rho)}{d_p^2(\rho_s + \frac{\rho}{2})}$$

When the particle starts at t = 0, h = h_1, and dh/dt = u_{pz0}, using the same mathematical approach as in Section A1.2.3 to solve Equation A2.12 can results in the following solution:

$$h = \frac{k_6 + b_6}{2k_6a_6}\ln(1 - C_{11}e^{-k_6t}) - \frac{k_6 - b_6}{2k_6a_6}\ln\frac{1 - C_{11}e^{-k_6t}}{C_{11}e^{-k_6t}} + C_{12} \qquad (A2.13)$$

where $C_{11} = \dfrac{2a_6u_{pz0} + b_6 - k_6}{2a_6u_{pz0} + b_6 + k_6}$, $k_6 = \sqrt{b_6^2 - 4m_6a_6}$

$$C_{12} = h_1 - \frac{b_6 + k_6}{2k_6a_6}\ln\frac{2k_6}{2a_6u_{pz0} + b_6 + k_6} - \frac{b_6 - k_6}{2k_6a_6}\ln\frac{2k_6}{2a_6u_{pz0} + b_6 - k_6}.$$

A2.3.4 The equation of motion for Region (c)

The equation of motion for a spherical particle in Region (c) can be written by combining Equations A2.6, 3.36 and 3.13 and then rearranged, i.e.

$$\frac{\pi}{6}d_p^3 g(\rho_s-\rho)-0.055\pi d_p^2\rho\left(\frac{dh}{dt}+u_i\right)^2-C_p\left(\frac{dh}{dt}\right)^2=\frac{\pi}{6}D^3(\rho_s+\frac{\rho}{2})\frac{d^2h}{dt^2} \qquad (A2.14)$$

or

$$\frac{d^2h}{dt^2}+\frac{0.33\pi\rho d_p^2+6C_p}{\pi d_p^3(\rho_s+\frac{\rho}{2})}\left(\frac{dh}{dt}\right)^2+\frac{0.66\rho u_i}{d_p(\rho_s+\frac{\rho}{2})}\frac{dh}{dt}+\frac{0.33\rho u_i^2-2gd_p(\rho_s-\rho)}{d_p\rho_s}=0 \qquad (A2.15)$$

or

$$\frac{d^2h}{dt^2}-a_7\left(\frac{dh}{dt}\right)^2+b_7\frac{dh}{dt}+m_7=0 \qquad (A2.16)$$

$$\text{where}\quad a_7=\frac{0.33\pi\rho d_p^2+6C_p}{\pi d_p^3(\rho_s+\frac{\rho}{2})},\quad b_7=\frac{0.66\rho u_i}{d_p(\rho_s+\frac{\rho}{2})},\quad m_7=\frac{0.33\rho u_i^2-gd_p(\rho_s-\rho)}{d_p(\rho_s+\frac{\rho}{2})}$$

When the particle starts at t = 0, h = h_1, and dh/dt = u_{pz0}, the solution of Equation A2.15 can be obtained with a mathematical approach similar to that used in Section A1.2.3:

$$h = \frac{k_7 + b_7}{2k_7a_7}\ln(1 - C_{13}e^{-k_7t}) - \frac{k_7 - b_7}{2k_7a_7}\ln\frac{1 - C_{13}e^{-k_7t}}{C_{13}e^{-k_7t}} + C_{14} \qquad (A2.17)$$

$$\text{where } C_{13} = \frac{2a_7u_{pz0} + b_7 - k_7}{2a_7u_{pz0} + b_7 + k_7}, \quad k_7 = \sqrt{b_7^2 - 4m_7a_7}$$

$$C_{14} = h_1 - \frac{b_7 + k_7}{2k_7a_7}\ln\frac{2k_7}{2a_7u_{pz0} + b_7 + k_7} - \frac{b_7 - k_7}{2k_7a_7}\ln\frac{2k_7}{2a_7u_{pz0} + b_7 - k_7}.$$

APPENDIX 3 Photos and Drawing of the Variable Speed KC

Figure A3-1 The 3" (7.5 cm) variable speed Knelson Concentrator (side view)

Figure A3-2 The 3" variable speed Knelson Concentrator (front view)

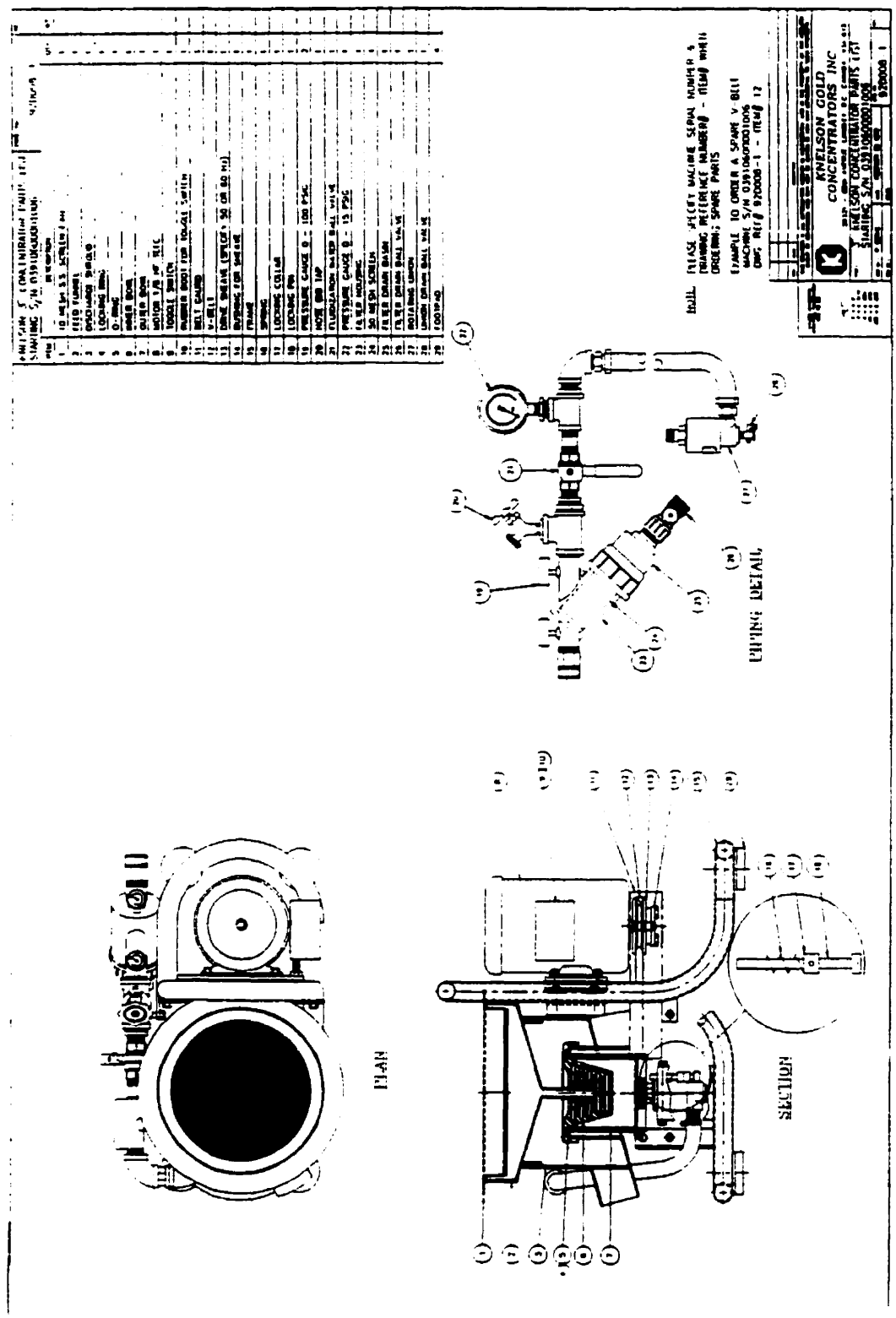

Figure A3-3 General drawing of the 3-in Knelson Concentrator (Knelson Gold Concentrator Inc., 1994)

Appendix 4 Supplementary Data and Figures for Chapter 6

Table A4-1 Standard deviation of tungsten recovery from silica analyzed by MLS and magnetic separation

Size ->	300 μm		106 μm		75 μm		38 μm		-25 μm	
Repeated test No.	Conc. grams	Recovery %	Conc. grams	Recovery %	Conc. grams	Recovery %	Conc. grams	Recovery %	Conc. grams	Recovery %
1	9.97	99.7	9.94	99.4	9.98	99.8	9.95	99.5	9.66	96.6
2	9.98	99.8	9.99	99.9	9.95	99.5	9.92	99.2	9.73	97.3
3	9.92	99.2	9.91	99.1	9.96	99.6	9.93	99.3	9.73	97.3
4	9.99	99.9	9.97	99.7	9.92	99.2	9.96	99.6	9.68	96.8
5	9.96	99.6	9.97	99.7	9.99	99.9	9.96	99.6	9.79	97.9
STD		0.27		0.31		0.27		0.18		0.51

Table A4-2 Standard deviation of tungsten recovery from magnetite analyzed by MLS and magnetic separation

Size ->	212 μm		106 μm		75 μm		38 μm		-25 μm	
Repeated test No.	Conc. grams	Recovery %	Conc. grams	Recovery %	Conc. grams	Recovery %	Conc. grams	Recovery %	Conc. grams	Recovery %
1	9.95	99.5	9.97	99.7	9.76	97.6	9.67	96.7	9.21	92.1
2	9.96	99.6	9.65	96.5	9.85	98.5	9.48	94.8	9.25	92.5
3	9.95	99.5	9.80	98.0	9.68	96.8	9.66	96.6	9.28	92.8
4	9.89	98.9	9.91	99.1	9.86	98.6	9.54	95.4	9.20	92.0
5	9.96	99.6	9.72	97.2	9.87	98.7	9.67	96.7	9.34	93.4
STD		0.29		1.32		0.82		0.88		0.57

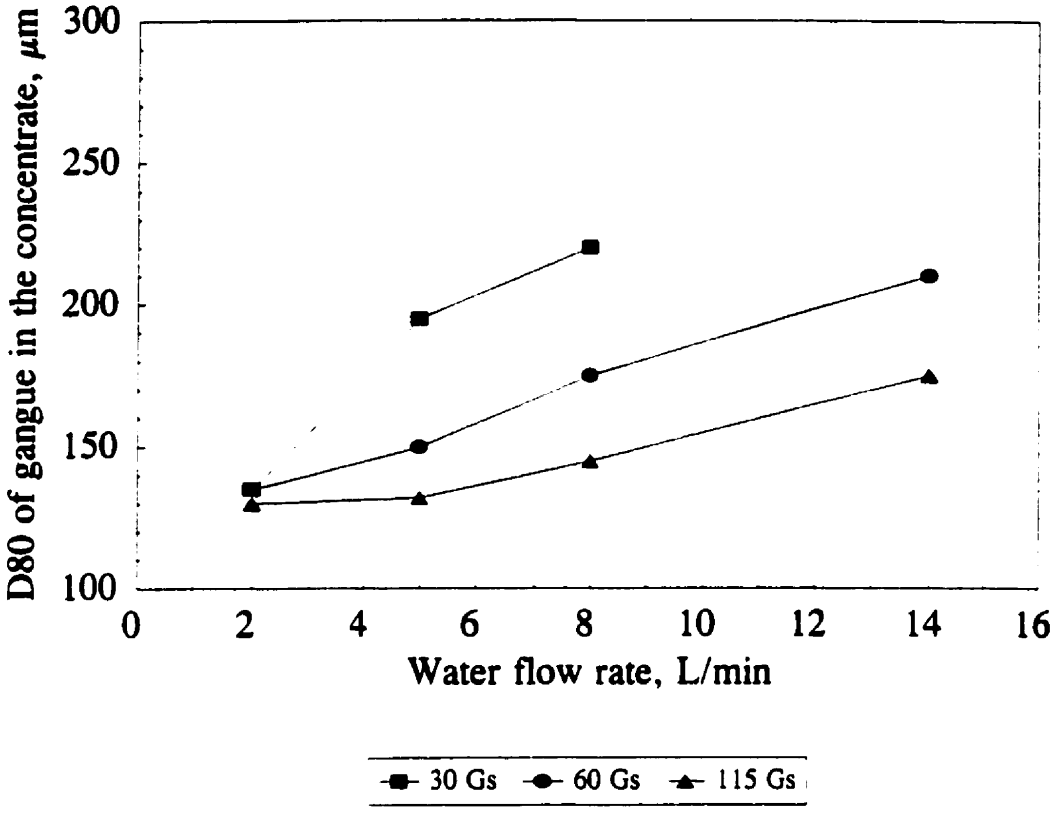

Figure A4-1 D_{80} of gangue in the concentrate as a function of fluidization rate and centrifuge acceleration (gangue type: -425 μm magnetite)

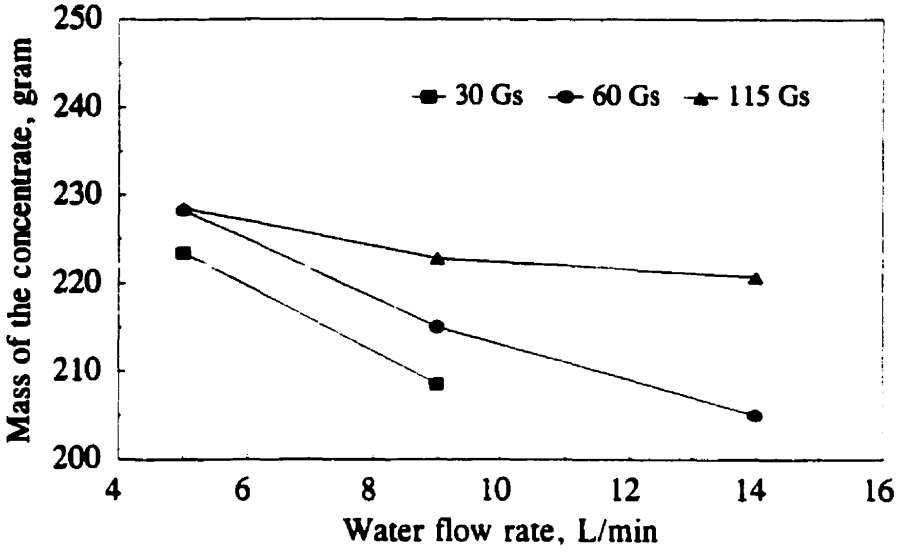

Figure A4-2 Mass of the concentrate as a function of centrifuge acceleration and fluidization rate (gangue type: -1670 μm magnetite)

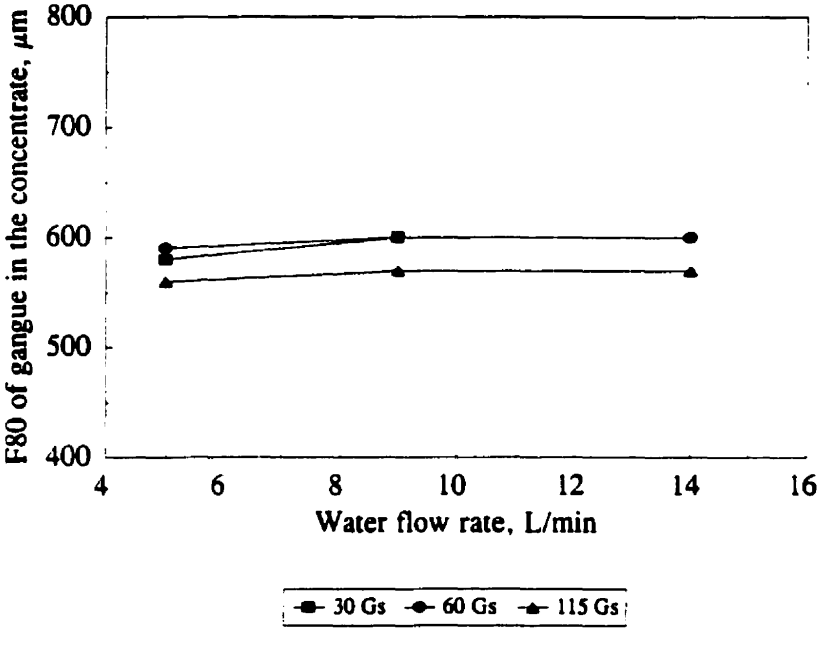

Figure A4-3 D_{80} of gangue in the concentrate as a function of fluidization rate and centrifuge acceleration (gangue type: -1670 μm magnetite)

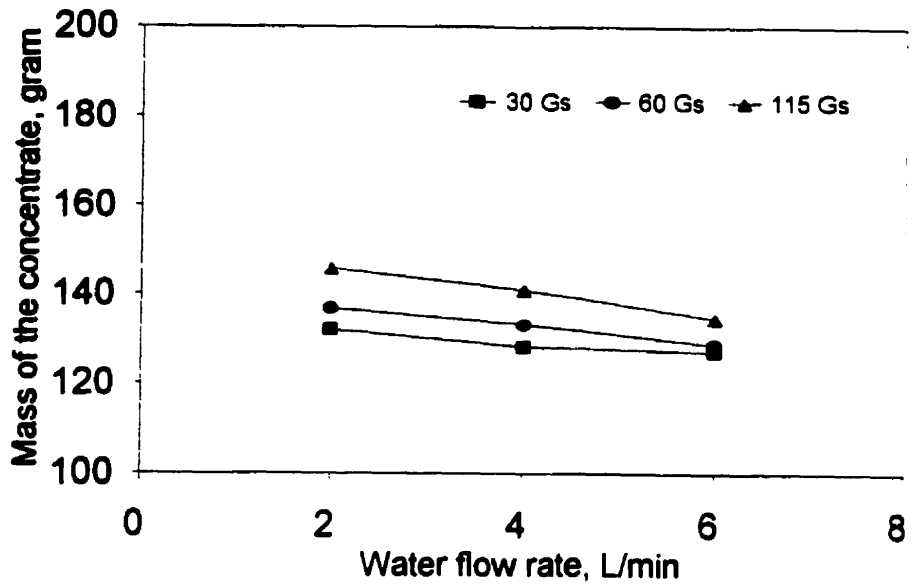

Figure A4-4 Mass of the concentrate as a function of centrifuge acceleration and fluidization rate (gangue type: -425 μm silica)

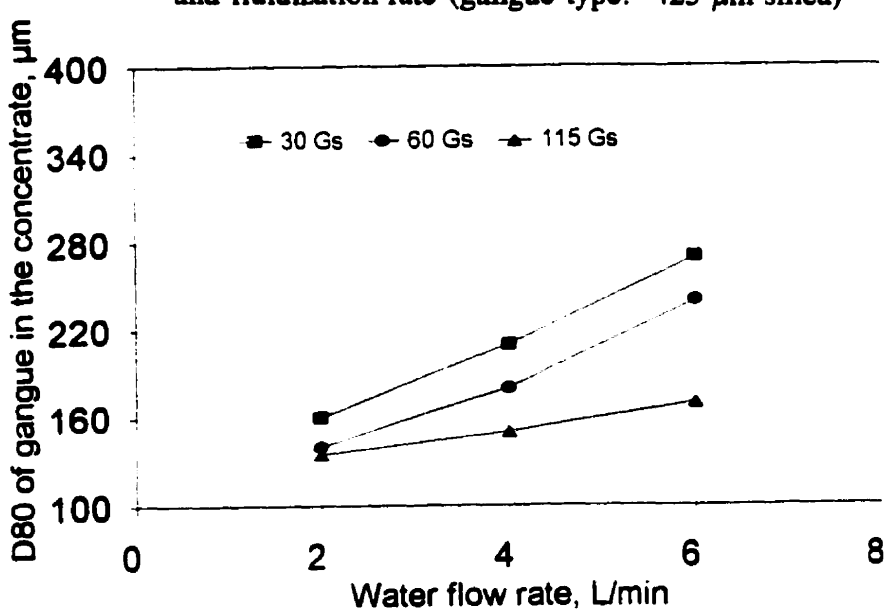

Figure A4-5 D_{80} of gangue in the concentrate as a function of fluidization rate and centrifuge acceleration (gangue type: -425 μm silica)

Appendix 5 Supplementary Data and Figures for Chapter 7

Table A5-1 Standard deviation of magnetite recovery from silica analyzed by magnetic and MLS separation

Size ->	300 μm		106 μm		75 μm		38 μm		-25 μm	
Repeated test No.	Conc. grams	Recovery %	Conc. grams	Recovery %	Conc. grams	Recovery %	Conc. grams	Recovery %	Conc. grams	Recovery %
1	9.87	98.70	9.94	99.40	9.86	98.60	9.92	99.20	9.86	98.60
2	9.94	99.40	9.96	99.60	9.90	99.00	9.89	98.90	9.82	98.20
3	9.95	99.50	9.93	99.30	9.91	99.10	9.93	99.30	9.89	98.90
4	9.97	99.70	9.94	99.40	9.90	99.00	9.91	99.10	9.83	98.30
5	9.91	99.10	9.90	99.00	9.93	99.30	9.88	98.80	9.76	97.60
STD	0.04	0.39	0.02	0.22	0.03	0.25	0.02	0.21	0.05	0.49

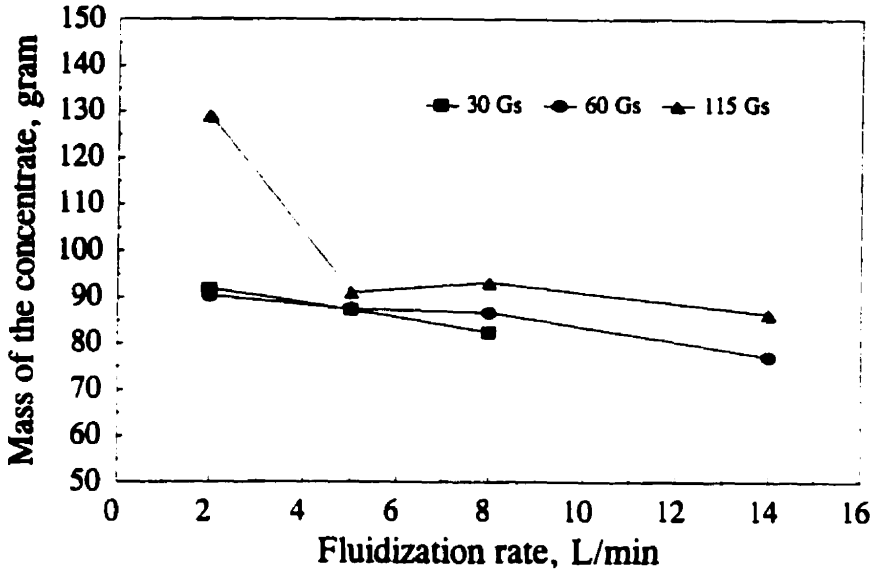

Figure A5-1 Mass of the KC concentrate as a function of centrifuge acceleration and fluidization rate (feed: 1.25% magnetite)

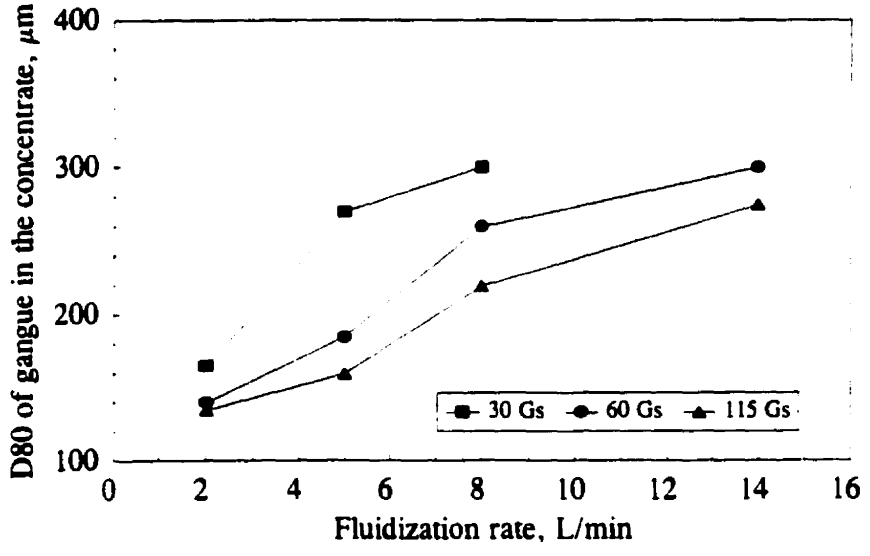

Figure A5-2 D_{80} of gangue in the concentrate as a function of fluidization rate and centrifuge acceleration (feed: 1.25% magnetite)

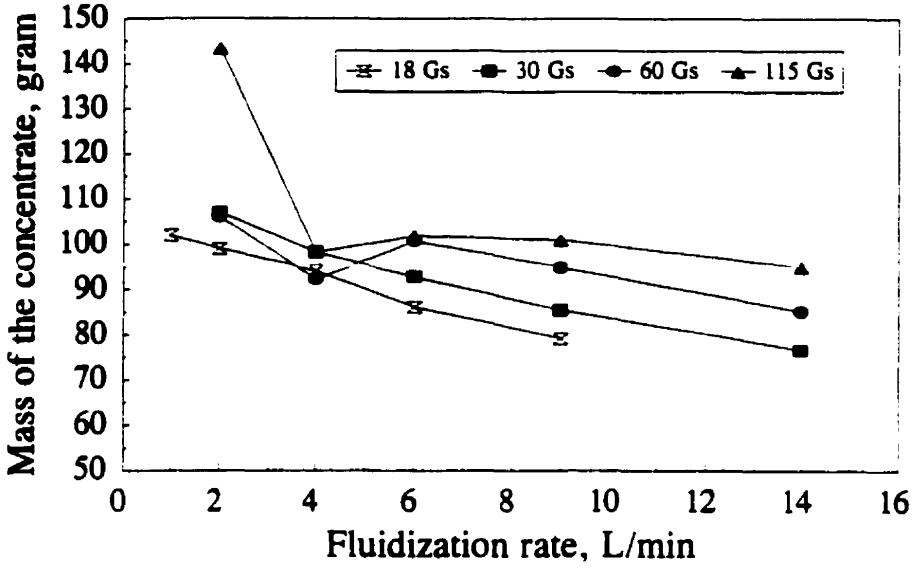

Figure A5-3 Mass of the KC concentrate as a function of centrifuge acceleration and fluidization rate (feed: 2.5% magnetite)

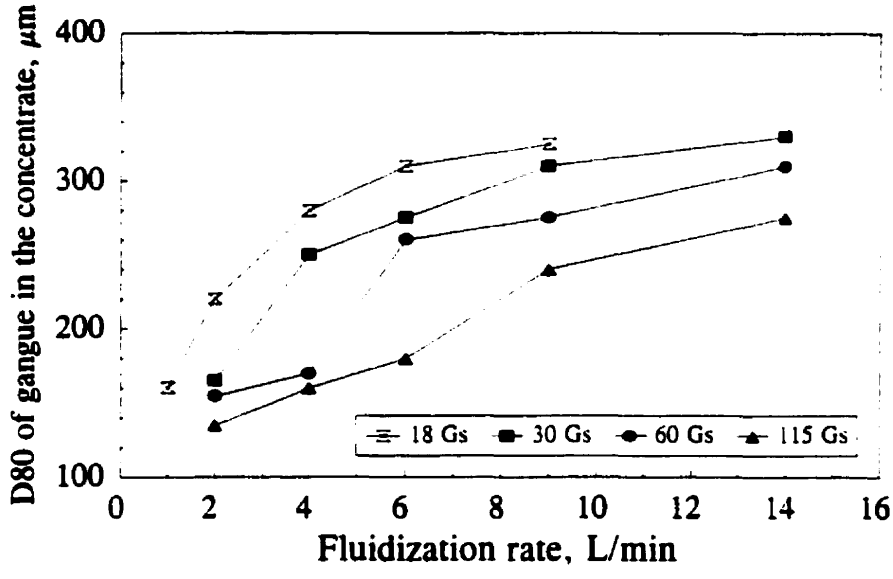

Figure A5-4 D_{80} of gangue in the concentrate as a function of fluidization rate and centrifuge acceleration (feed: 2.5% magnetite)